Dissertation

submitted to the

Combined Faculty of Natural Sciences and Mathematics of the
Ruperto-Carola University Heidelberg, Germany

for the degree of

Doctor of Natural Sciences

presented by

M.Sc. Marleen Büchler-Schäff

born in Mosbach, Germany

Oral examination: 19th May 2021

Investigation into hematopoietic stem cell function in the context of developmental specification and stress hematopoiesis

Faculty supervisor: Prof. Dr. Ursula Klingmüller

Supervisor: Dr. Michael Milsom

The investigations of the following dissertation were performed from January 2017 to March 2021 under the supervision of Dr. Michael Milsom in the Division of Experimental Hematology at the German Cancer Research Center (DKFZ) and the Heidelberg Institute for Stem Cell Technology and Experimental Medicine (HI-STEM) in Heidelberg, Germany.

I herewith declare (according to § 8 (3) b) and c) of the Doctoral Degree Regulations) that the thesis I have submitted is my own work and all the used sources are indicated. I have not made unauthorized use of figures, tables, etc. of a third person and the source is always indicated.

_____

Marleen Büchler-Schäff

Table of contents

Publications

Parts of this work have been published in:

Ruzhica Bogeska, Paul Kaschutnig, Malak Fawaz, Ana-Matea Mikecin, **Marleen Büchler-Schäff**, …, Michael D. Milsom (2020). Hematopoietic stem cells fail to regenerate following inflammatory challenge. bioRxiv preprint

Manuscript in preparation:

Marleen Büchler-Schäff, Paul Kaschutnig, Roshana Thambyrajah, Wiebke Nadler, Sabrina Hanke, Stella Paffenholz, Milena Block, Julius Gräsel, Jakob Kremer, Irem Bayindir-Buchhalter, Wenjun Chang, David Hills, Richard Harbottle, Christoph Rösli, Alexander Medvinsky, Michèle Souyri, Georges Lacaud and Michael D. Milsom (presumablz 2021). Identification and characterization of novel functional markers during the hematopoietic stem cell specification process

Parts of this work have been presented at:

GSCN 2019 - poster presentation:

Marleen Büchler-Schäff, Ruzhica Bogeska, Ana-Matea Mikecin, Julia Knoch, Melanie Ball, Michael Milsom. Thrombopoietin-induced HSC proliferation and potential adverse effects of chronic activation

DKFZ 2019 - poster presentation:

Marleen Büchler-Schäff, Ruzhica Bogeska, Ana-Matea Mikecin, Julia Knoch, Melanie Ball, Michael Milsom. Thrombopoietin-induced HSC proliferation and potential adverse effects of chronic activation

ISEH 2020 - poster presentation:

Marleen Büchler-Schäff, Paul Kaschutnig, ..., Michael D. Milsom. Identification and characterization of novel functional markers during the hematopoietic stem cell specification process

I Summary

Hematopoietic stem cells (HSCs) derive from an endothelial precursor during embryonic development and undergo endothelial to hematopoietic transition (EHT). EHT is a highly dynamic process that is challenging to study *in vivo* and problematic to model *in vitro*, partly due to an inability to identify biologically relevant intermediate cell states. However, a previous study conducted in our group identified Evi2a as a crucial protein in hematopoietic specification. In this PhD thesis we aimed to investigate the role of Evi2a during hematopoietic specification. We performed differential gene expression analysis on differentiated wildtype and Evi2a KO cells to decipher differences in signaling processes and identify the downstream pathways of Evi2a. Furthermore, we developed an Evi2a KO mouse model to identify hematopoietic defects *in vivo*. Our results suggested that Evi2a KO delayed hematopoietic differentiation and a homozygous Evi2a KO might be embryonically lethal.

Adult hematopoietic stem cells are at the peak of the hematopoietic hierarchy and responsible for the lifelong production of all differentiated peripheral blood cells to ensure a healthy and balanced blood composition. In order to avoid DNA damages induced by e.g., stress, it is crucial for HSCs to remain in a quiescent state. Only when desired HSCs proliferate to replenish the need for blood cells. However, during severe infections, chronic inflammation, injury trauma as well as other challenging events HSCs are pushed to proliferate and to actively contribute to the increased cellular demand of differentiated blood cells. Repetitive activation of HSCs, as it happens during a lifetime, has been shown to lead to HSC attrition and in the worst case to aberrant blood production often coming along with a myeloid bias.

In this study we investigated the changes in HSC function and their ability to produce all downstream cells after repeated stimulation. HSC attrition has been extensively studied before using inflammatory agents. However, we were interested in HSC activation beyond inflammatory stimuli and used Thrombopoietin (TPO) and the clinically used TPO mimetic Romiplostim to induce HSC cycling. TPO stimulates megakaryocyte and platelet production and has been shown to be required for HSC maintenance and self-renewal divisions. However, we hypothesize that any cell division can induce DNA damages and consequently lead to loss of HSC function indicated by a decrease in reconstitution potential.

After repetitive TPO and Romiplostim treatment we observed an increase in the phenotypic long-term HSC pool. Performing competitive repopulation assays showed that no change in donor chimerism between control and treated group was detected. We could neither note loss of HSC function nor a myeloid bias that usually arises from exhausted HSCs. By using a label-retention mouse model we were able to track the proliferative history of HSCs and again, did not observe any reduced repopulation capacity between cells that cycled and cells that remained dormant during TPO treatment. Concluding, repetitive activation of HSCs using TPO did not lead to HSC

exhaustion. However, transcriptome and methylome analysis will be carried out next to examine potential changes on molecular level.

II Zusammenfassung

Hämatopoetische Stammzellen (HSZ) entstehen während der Embryonalentwicklung aus einem endothelialen Vorläufer und durchlaufen den so genannten endothelialen-zu-hämatopoetischen Übergang (EHT). Der EHT ist ein hochdynamischer Prozess, der *in vivo* nur schwer zu untersuchen und *in vitro* nur schwer zu modellieren ist. Das liegt unter anderem an der Unfähigkeit, biologisch relevante Zellzwischenzustände zu identifizieren. Eine frühere Studie aus unserer Gruppe, identifizierte jedoch Evi2a als ein entscheidendes Protein in der hämatopoetischen Spezifikation. In dieser Doktorarbeit galt es, die Rolle von Evi2a während der hämatopoetischen Spezifikation zu untersuchen. Wir führten differentielle Genexpressionsanalysen an differenzierten Wildtyp- und Evi2a KO-Zellen durch, um Unterschiede in den Signalprozessen zu entschlüsseln und die nachgeschalteten Signalwege von Evi2a zu ermitteln. Darüber hinaus entwickelten wir ein Evi2a KO-Mausmodell, um hämatopoetische Defekte *in vivo* zu identifizieren. Unsere Ergebnisse legten nahe, dass der Evi2a KO die hämatopoetische Differenzierung verzögert und ein homozygoter Evi2a KO embryonal letal sein könnte.

Adulte hämatopoetische Stammzellen stehen an der Spitze der hämatopoetischen Hierarchie und sind für die lebenslange Produktion aller differenzierten peripheren Blutzellen verantwortlich, damit eine gesunde und ausgewogene Blutzusammensetzung gewährleistet ist. Es ist entscheidend, dass HSZ in einem Ruhezustand verbleiben, um DNA-Schäden zu vermeiden, die durch z.B. Stress induziert werden. Nur bei Bedarf proliferieren HSZ, um die benötigte Menge an Blutzellen wieder aufzufüllen. Bei schweren Infektionen, chronischen Entzündungen, traumatischen Verletzungen und anderen einschneidenden Ereignissen werden HSZ jedoch zur Zellteilung gedrängt und tragen aktiv zum erhöhten Bedarf an differenzierten Blutzellen bei. Die wiederholte Aktivierung von HSZ, wie sie auch im Laufe des Lebens stattfindet, führt nachweislich zu einer HSZ-Erschöpfung und im schlimmsten Fall zu einer anormalen Blutbildung, die oft mit einer myeloischen Tendenz einhergeht.

In dieser Studie untersuchten wir die Veränderungen der HSZ-Funktion und der HSZ-Fähigkeit, nach wiederholter Stimulation, alle nachgeschalteten Zellen zu produzieren. Die HSZ-Erschöpfung wurde in anderen Studien ausgiebig mit Agenzien untersucht, die zu Entzündungen führen. Wir waren jedoch an der HSZ Aktivierung jenseits von Entzündungsreizen interessiert und verwendeten daraufhin Thrombopoietin (TPO) und das klinisch verabreichte TPO-Mimetikum Romiplostim, um die HSZ Zellteilung zu induzieren. Thrombopoietin stimuliert die Megakaryozyten- und Thrombozytenproduktion und ist nachweislich für die Erhaltung und selbsterneuernde Teilung der HSZ erforderlich. Wir stellen jedoch die Hypothese auf, dass jede Zellteilung DNA-Schäden induzieren kann und folglich zu einem Verlust der HSZ-Funktion führt, der durch eine Abnahme des Rekonstitutionspotenzials angezeigt wird.

Nach wiederholter TPO- und Romiplostim-Behandlung beobachteten wir eine Zunahme des phänotypischen HSZ-Vorkommens. Nach kompetitiven Repopulationstests wurde keine Veränderung des Spenderchimärismus zwischen der Kontroll- und der behandelten Gruppe festgestellt. Wir konnten weder einen Verlust der HSZ-Funktion noch eine myeloischen Tendenz feststellen, wie sie bei erschöpften HSZ auftritt. Durch die Verwendung eines Label-Retention-Mausmodells konnten wir den Teilungshintergrund der HSZ nachverfolgen. Dabei wurde wiederum keine reduzierte Repopulationskapazität zwischen Zellen, die sich teilten, und Zellen, die während der TPO-Behandlung in einem Ruhezustand verblieben, beobachtet. Abschließend lässt sich sagen, dass die wiederholte Aktivierung von HSZ mit TPO nicht zu einer Erschöpfung der HSZ führte. Jedoch werden weitere Transkriptom- und Methylomanalysen durchgeführt, um eventuelle Veränderungen auf molekularer Ebene zu untersuchen.

1 Introduction

In this thesis we are interested in the study of hematopoietic stem cells (HSCs) starting from their developmental origin to their behavior upon induced stress. Hematopoietic stem cells are one of the best described and most studied adult stem cell population. However, there are still a lot of unknown and uncharacterized processes during embryonic development with regards to when exactly the first hematopoietic cell arises and how it can be identified. During adulthood it is still not fully understood how HSCs respond to different stressors and/or which long-term consequences this entails.

1.1 Hematopoietic development

Hematopoietic development is largely conserved between mouse and human even though the time differs by about 259 days (Figure 1)[1]. Mouse pups are born approximately 21 days after fertilization of the egg whereas human development takes approximately 280 days until birth. In this study, we focused on murine development.

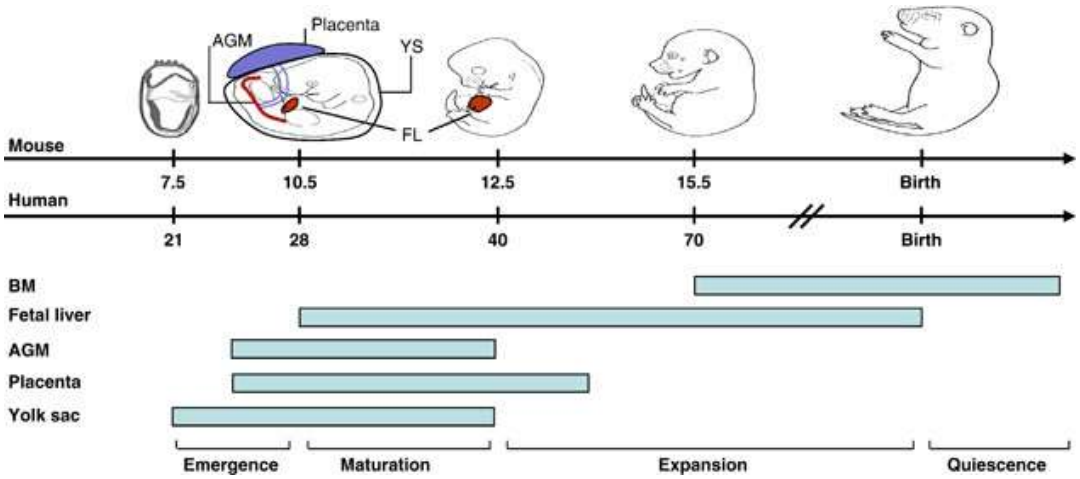

Figure 1: **Hematopoietic development in mouse and human**. This figure highlights relevant hematopoietic structures and organs during embryonic development, starting with the emergence of immature erythroid cells in the yolk sac at E7.5 and ending with the mature, quiescent HSCs in the BM upon birth. Horizontal bars represent where each developmental step of the hematopoietic processes takes place AGM = aorta-gonad-mesonephros region, YS = yolk sac, FL = fetal liver, BM = bone marrow. Figure was taken from Luis et al. 2012. *Signal transduction pathways regulating hematopoietic stem cell biology: Introduction to a series of spotlight reviews*. Leukemia.

The development of the hematopoietic system occurs already very early during embryonic development. Figure 1 summarizes the hematopoietic development which is organized in a temporal manner occurring in several consecutive waves and involving different embryonic and maternal structures. Starting with the first wave generating immature hematopoietic cells, which are primitive erythrocytes. These primitive red blood cells are required to transport oxygen through the developing body to support survival until mature red blood cells (RBCs) are formed[2]. The second and/or third wave creates transplantable stem cells, defined as giving rise to peripheral blood chimerism, in the aorta-gonad-mesonephros region AGM[3]. It is still unknown whether definitive hematopoiesis giving rise to mature, transplantable hematopoietic cells takes place at unique or at multiple defined time points throughout development. Likewise, it is still not fully understood which role several fetal structures and organs like yolk sac (YS), AGM comprising the dorsal aorta (DA) and fetal liver (FL) but also the maternal placenta play, since it has been observed that a small subset of adult hematopoietic stem and progenitor cells (HSPCs) is already initiated in the yolk sac[4] as well as in the dorsal aorta[5]. Of note, proliferation and cellular expansion of hematopoietic (stem) cells during hematopoietic development and fetal liver maturation are crucial to obtain enough cells for future, healthy blood production. Of note, proliferation and active cycling are avoided in adult HSCs being a predominantly dormant and quiescent population.

1.1.1 Emergence of hematopoietic stem cells

Due to the limited number of cells during development and the lack of precise fetal hematopoietic markers the exact details and molecular mechanisms of hematopoietic development are still ambiguous. As an example, the hemangioblast has been described in one study[6] as Flk1^{+}brachyury^{+} whereas in a second study[7] it was suggested to define hemangioblast as Ve-cadherin^{+}. However, remarkable progress has been made in developing microscopy techniques as well as highly sensitive single cell isolation and sequencing methods which help to examine and understand the developing embryo. Nevertheless, a general consensus of how and in which fetal organs HSCs develop exists. The primitive streak forms and initiates gastrulation leading to the formation of all three germ layers: endoderm, ectoderm and mesoderm. Of interest for hematopoietic development is the mesoderm[8]. In this structure a so-called hemangioblast forms which is described as a cell or a cell cluster that harbors endothelial and hematopoietic characteristics[9] but it has not yet been uniformly defined. The hemangioblast emerges in the yolk sac, around the time when the primitive streak if fully formed. On the one hand it contributes to the formation of blood islands in the yolk sac to initiate production of primitive red blood cells (RBCs)[10] and on the other hand precedes the development of the well described common endothelial and hematopoietic precursor: the hemogenic endothelium (HE)[6]. Different transcriptional programs leading to asymmetric cell divisions have been shown to be active in HE[11] resulting in budding off a daughter cell which then forms so-called aortic clusters in the dorsal

aorta (DA). In these aortic clusters true, definitive hematopoietic cells are found. Since the precise space plays a relevant role during hematopoietic development these clusters are only found on the ventral side of the DA[12]. The process of transitioning from aortic clusters to definitive hematopoietic cells is described as endothelial to hematopoietic transition (EHT) and will be elaborated in more detail in the next section.

Regarding the temporal organization of hematopoietic stem cell development, it is suggested that hematopoietic development takes place in three waves[13]. However, some studies also describe hematopoietic development in two waves[14]. Overall, most studies agree that mesodermal formation at the end of the primitive streak around embryonic day (E) E7 is the first important step for hematopoietic development; and that the first wave generates very primitive erythroid cells in the YS at around E7/E7.5 in mice. The second wave, is considered to take place at around E8.5 giving rise to more differentiated, potent myeloid and megakaryocytic biased hematopoietic cells in the YS. However, at the same time the formation of hematopoietic cells has also been observed in the placenta. The third and last wave is considered to appear at E10/E10.5 giving rise to definitive and fully potent hematopoietic cells in the AGM. From E11.5 onwards hematopoietic stem cells colonize the fetal liver and undergo maturation and a 100-fold expansion within four days. Upon birth or at early neonatal stages HSCs migrate to the BM and acquire their quiescent state[1,13,15,16].

1.1.2 Endothelial to hematopoietic transition

A critical step in the generation of hematopoietic cells is the endothelial to hematopoietic transition. During this transition phase transcriptional programs are changed in favor of hematopoietic specification. Up to date, EHT has been best studied in zebrafish and mouse in cells that emerge from the hemogenic endothelium within the aortic clusters or sometimes referred to as intra-aortic clusters (IACs). IACs typically bud off from the ventral site of the DA. However, since hematopoietic cells also emerge *de novo* in YS and placenta EHT is hypothesized to take place in these structures, too[17]. Many structural changes which occur during EHT, have already been observed microscopically *in vitro*[18] and *in vivo*[5]; thus, the underlying molecular changes have been of great interest in recent years. Subsequently, it was discovered that brachyury, a mesodermal marker, can be used in combination with Flk1 (Kdr) to define hemangioblasts an immature precursor of HE. HE derived from YS or AGM is defined by the expression of c-Kit and the absence of the pan-hematopoietic marker CD45. Additionally, it was shown that the cell surface marker (CSM) CD31/PECAM1 (platelet endothelial cell adhesion molecule 1) was present on IACs[5] and marked cells that were able to engraft upon transplantation[11]. Ultimately, cells that undergo EHT already express both endothelial (Cdh5) and hematopoietic (Runx1 and Gata2) markers[17,19]. However, many cells with different combinations of endothelial (such as Flk1 or CD31) and

hematopoietic cell surface marker or transcription factor (such as Gata2 or Runx1) expressions have been identified as potential first emerging hematopoietic cell[6,17]. Defining the first hematopoietic cell on phenotypic and molecular level during development is still a matter of debate. However, since molecular analysis is preferably performed on only a single cell type rather than a diverse mixture of cell types reporter mouse models were developed to specifically isolate and sort for certain cell populations. The aim of many studies was to find a marker that can be traced throughout hematopoietic specification to create a potential map of the different steps that are required for successful EHT. As an example, the development of Lyve-1 reporter mouse can be described. Even though Lyve1-GFP expression was prevalent in YS, flow cytometric analysis revealed that Ter119$^+$ erythroid cells did not express Lyve1. Concluding, Lyve1 does not mark all emerging hematopoietic cells[4]. Development of Gata2 reporter mice[20] or Runx1 reporter mice[21] were also of immense use to decipher signaling processes in certain cell types before, during and after EHT. Most promising for identifying the first hematopoietic cell are cells with the combined expression of Runx1 and Ly6a[22]. Hoxb4 expression has also been shown to be a reliable marker to identify early, emerging hematopoietic cells. Hoxb4 is a homeobox gene encoding for a transcription factor that is active during early hematopoietic specification. Hoxb4 operates downstream of mesoderm formation but upstream of hematopoietic specification and induces Runx1 expression[23]. Furthermore, Hoxb4 expression was also present in cells with endothelial (VE-Cadherin/Cdh5) and hematopoietic (CD45) potential[24]. A Hoxb4-YFP reporter mouse model showed that Hoxb4 expression is upregulated from fetal liver HSCs up to adult HSCs. Concluding, that Hoxb4 identifies prospective mature HSCs.

Not many studies have been performed with human samples, however, a study published last year investigated hematopoietic development in human embryos. The group of Alexander Medvinsky focused on spatial organization of the dorsal aorta and concluded that also in humans the ventral part of the dorsal aorta plays a major role in promoting hematopoietic specification. In contrast to Cdh5$^+$ CD45$^+$ cells derived from the dorsal side of the DA, Cdh5$^+$ CD45$^+$ cells from the ventral side of the DA showed upregulation of both endothelial/vascular and hematopoietic signatures (e.g. Hey2/Smad6 and Runx1/Myb, respectively) and characteristic EHT signatures such as inhibition of Notch signaling[25].

1.1.3 Evi2a – a novel marker to study HSC emergence

A study previously conducted in the DKFZ Division of Experimental Hematology addressed the questions of which markers to use (i) to identify emerging hematopoietic cells during development and (ii) to identify cells undergoing EHT, specifically in the context of *in vitro* specification of blood stem/progenitor cells from pluripotent cell lines *in vitro*. In brief, Hoxb4-YFP ESCs were *in vitro* differentiated and three subpopulations were defined representing different stages of

hematopoietic development: immature Hoxb4^{-}Flk1^{+} cells, transitional Hoxb4^{+}Aa4.1^{+} cells and mature Hoxb4^{-}CD41^{+}. Differential gene expression analysis revealed that Evi2a and Lyve1 are highly upregulated on the transient Hoxb4^{+}Aa4.1^{+} cell population. Functional validation of identified markers demonstrated that Lyve1 and Evi2a are crucial markers for hematopoietic development *in vitro* (Figure 2)[26].

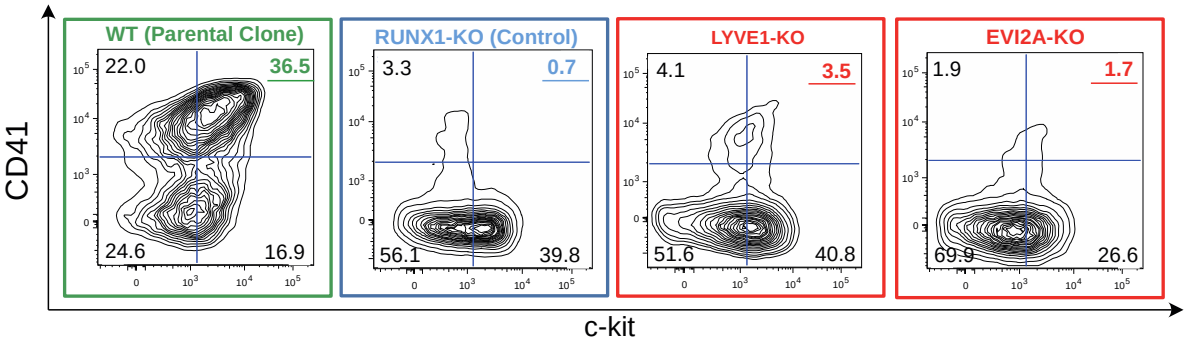

Figure 2: **Hoxb4-YFP reporter ESCs were differentiated to hematopoietic cells using a six-day *in vitro* embryoid body differentiation protocol**. Runx1, Evi2a and Lyve1 KO Hoxb4-YFP reporter ESCs were impaired in their *in vitro* hematopoietic specification and did not generate CD41^{+} c-Kit^{+} cells after six days of *in vitro* differentiation. Figure taken from the PhD thesis of Dr. Paul Kaschutnig 2018: "*HSCs – A journey from development to aging*".

Consistent with the study described above, Hannah Mikkola and her group developed a Lyve1 reporter model and verified the expression of Lyve1 in YS derived endothelial cells as early as E9.5. Lyve1 expression was maintained throughout hematopoietic stem and progenitor cell development in the fetal liver[4]. Conversely, Evi2a, ecotropic viral integration site 2a, has been first identified in viral integration experiments with BXH-2 mice. These mice were prone to develop leukemia due to spontaneous retroviral integrations and Evi2a, located in an Nf1 intron, was frequently targeted. NF1 is a tumor suppressor and after viral integration into Evi2a, NF1 expression was abrogated leading to the onset of leukemia[27,28]. Apart from this, Evi2a is a largely uncharacterized protein. The function of Evi2a, interaction partners or signaling processes that Evi2a might be involved in have not been described so far. Structural predictions suggested that Evi2a is a transmembrane protein with receptor tyrosine kinase characteristics. In a study of Zeng et. al Evi2a has been ranked as one out of the ten most upregulated genes during lymphoid specification of hematopoietic cells lacking erythroid characteristics (CD235^{-}CD45^{+}CD34^{+} cells)[29]. In a study from Gentles *et al*. Evi2a was listed as a leukemic stem cell signature gene in acute myeloid leukemias (AML) with normal karyotypes and linked to an unfavorable outcome[30]. Additionally, Rücker *et al*. found that Evi2a was highly expressed in AML cell lines indicating that aberrantly high Evi2a expression leads to malignant transformation of cells[31]. Concluding, Evi2a might play a role in both hematopoietic development and the onset of leukemia.

1.1.4 *In vitro* protocols to recapitulate hematopoietic development

One of the major aims in the hematopoietic developmental field is to robustly generate functional HSCs *in vitro*. The potential to find reliable protocols lies in identifying and characterizing all relevant and crucial signaling molecules, transcription factors and cellular interactions that an embryonic stem cell (ESC) has to undergo during hematopoietic specification. Since the hematopoietic specification depends on the maturation in different organs, this is still a major obstacle in developing *in vitro* protocols. Huge effort has been undertaken to optimize culture conditions and direct ESCs to differentiate to hematopoietic cells. Vitamin C (ascorbic acid) has been shown to induce embryoid body (EB) formation in ESCs. Factors such as Bmp4 were added to induce mesoderm formation, growth factors like FGF and VEGF were used to induce endothelial and vascular development and to promote proliferation. Combining Activin A with the previously named factors led to the formation of hematopoietic cells in cell culture[32]. Similar protocols have been further developed and advanced and suggested to use co-culture conditions of ESCs together with OP9 cells and/or to transduce cells with endothelial and hematopoietic transcription factors such as Etv2 and Tal1[33].

In 2017, two studies (Lis *et al*. and Sugimura *et al*., Nature) were presented on how to efficiently generate HSCs from human iPSCs. The approaches in the two studies were slightly different. Lis *et al*. took murine endothelial cells for viral transduction of four transcription factors whereas Sugimura *et al*. used *in vitro* differentiated $CD34^+$ hemogenic endothelial cells for viral transduction with seven transcription factors. In both approaches the *in vitro* generated cells were successfully transplanted and peripheral blood lineage contribution was achieved. Both studies discussed the issue of viral transductions to re-program cells and the impaired response of the immune system upon stimulation. Both studies showed that the transcriptome of the *in vitro* generated HSCs resembled the transcriptome of adult HSCs (List *et al*.) and adult HSPCs (Sugimura *et al*.). However, DNA methylation patterns and epigenetic marks have not been compared between the populations derived from adult mice and the *in vitro* culture[34,35]. However, the efficiency of these protocols is extremely low and is a limiting factor in the application of these approaches for further biological studies or translational applications.

1.1.5 Therapeutic potential of isolating emerging hematopoietic cells

Generating hematopoietic (stem) cells *in vitro* harbors great therapeutic potential. The future of medical treatment strategies aims to use personalized and individualized medicine against diseases like leukemia[36]. A putative approach could be to isolate patient derived fibroblasts reprogram these to pluripotent stem cells (iPSCs), subsequently differentiate these to hematopoietic stem cells or, for example T-cells. Before the *in vitro* differentiated and modified

cells are transplanted back into the patients, the cells have to be sufficiently expanded in number to be able to achieve successful engraftment[37]. It is already possible to reprogram somatic fibroblasts into iPSCs using the Yamanaka factors Oct3/4, Sox2, c-Myc and Klf4[38]. Even though there have been many approaches to generate HSCs from ESCs or iPSCs *in vitro* the generated hematopoietic cells showed impaired long-term engraftment and were not able to generate fully functional differentiated blood cells. Since cells are often transduced using viral particles to deliver genes, these approaches come along with an increased oncogenic risk[39,40].

However, not only developing the isolation and development of emerging HSCs and subsequent propagation *in vitro* has great therapeutic potential but also the cultivation and propagation of adult HSCs to their differentiated progeny.

1.2 Adult hematopoietic system

The adult HSCs in the bone marrow (BM) can be further defined as long-term (LT) and short-term (ST). LT-HSCs are at the top of the hematopoietic hierarchy, residing in specialized niches in the BM and are responsible for the lifelong supply and production of all differentiated peripheral blood cells. This process is defined as adult hematopoiesis[41]. Figure 3 shows the classical hematopoietic hierarchy[42]. The classical hierarchy displays cells that can be defined and described by a certain set of transcription factors or cell surface marker expression[41]. LT-HSCs reside at the top as they are capable to long-term engraft upon transplantation whereas ST-HSCs are situated further downstream since they exhibit slightly reduced potential and only give rise to short-term engraftment post-transplantation. ST-HSCs are followed by multipotent progenitors (MPPs) which are already primed towards a certain lineage specification and can clearly be identified by their cell surface marker (CSM) expression. The MPPs comprise also oligopotent progenitors such as common myeloid progenitors, megakaryocyte/erythroid progenitor, granulocyte/macrophage progenitor (CMP, MEP, GMP), which subsequently give rise to more committed precursors that produce differentiated hematopoietic cells. These different differentiated cells make up the cellular compartment of the peripheral blood (PB), as well as secondary hematopoietic organs such as spleen, thymus and lymph nodes. White blood cells (leukocytes), including components of the adaptive immune system, such as B-, and T-cells and the innate immune system, such as natural killer cells and myeloid cells such as neutrophils, are required for a functional immune system to combat a diverse range of pathogens. By secreting inflammatory cytokines, immune cells are activated and begin to proliferate and mature into fully functional and specified cells in order to combat bacteria, viruses or parasites at the site of infection. Red blood cells (erythrocytes) are required for oxygen (O_2) transport from the lungs to all other body parts and return carbon dioxide (CO_2) from the body to the lungs. Platelets (thrombocytes) originate from megakaryocytes

and are required to contain bleedings by forming blood clots at the site of the injured blood vessels[42,43].

To ensure a healthy and balanced blood production it is crucial to maintain some HSC in a quiescent state, as every cell division comes along with a risk of acquiring DNA mutations or other damages. Hence, under homeostatic conditions, a subset of HSCs divide very rarely and are termed as being “dormant”. However, during challenging conditions, such as infections, chronic inflammation or injury trauma, HSCs are pushed into cell cycle and actively proliferate in order to meet the increased cellular demand and replace lost blood cells[44,45,46]. These stress agonists that force HSCs to divide lead to an increase in the risk of accumulating DNA mutations, which can potentially cause an adverse outcome during a lifetime. The increase in DNA mutations and genomic instability are only two examples of age-associated attrition in the HSC compartment, which can ultimately lead to formation of leukemia in the hematopoietic system[47]. Leukemias are most often observed in older people and it is speculated that the underlying cause are exhausted and dysfunctional HSCs that give rise to a disproportionate hematopoietic system with an increase of a certain hematopoietic population[48].

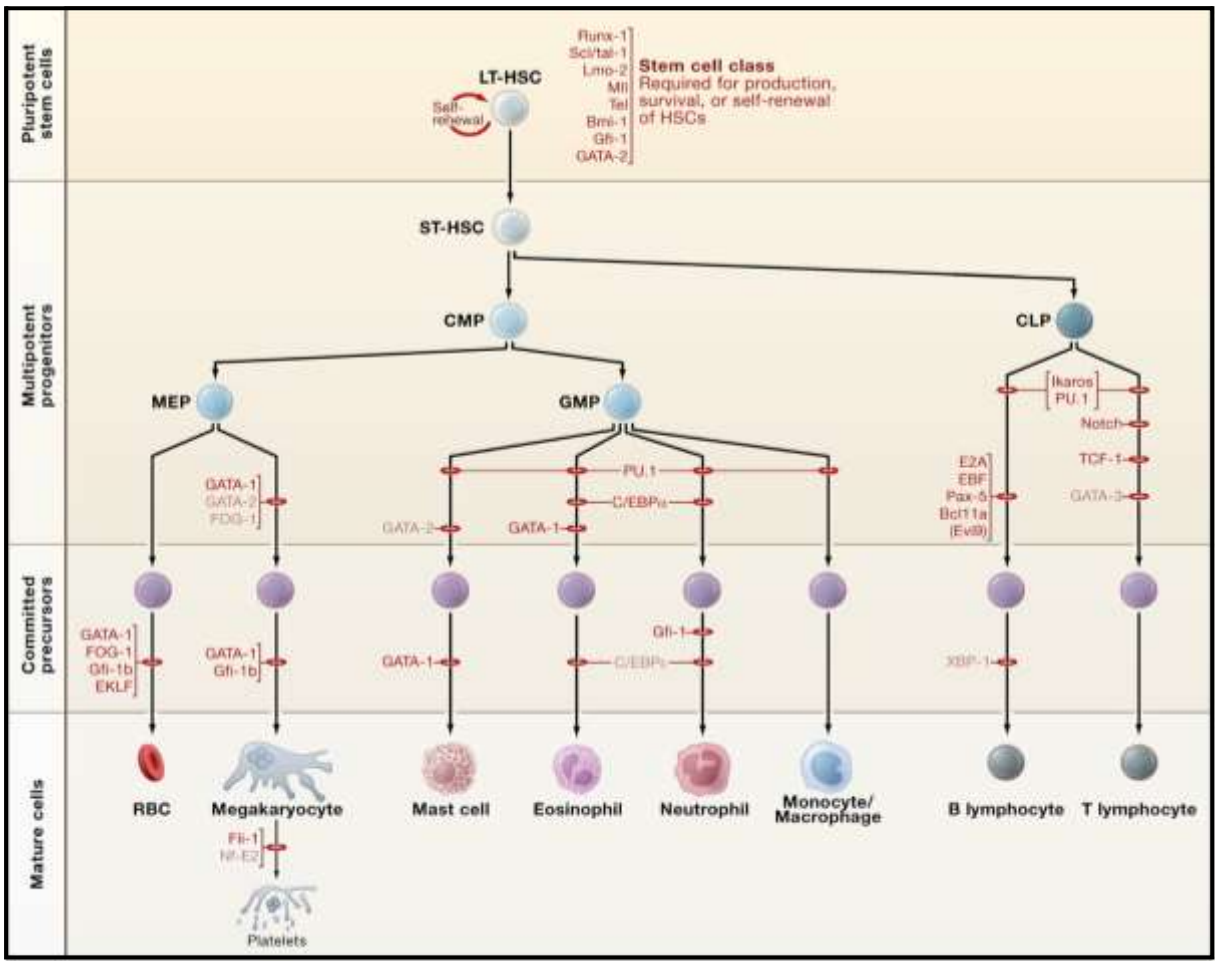

Figure 3: **Classical hematopoietic hierarchy with multipotent long-term-HSCs at the top**. LT-HSCs are, amongst certain transcription and cell surface marker expression defined by their competence to self-renew. LT-HSCs give rise to ST-HSCs and other defined multipotent progenitors (MEP, CMP, CLP) which then give rise to more committed oligopotent progenitors that generate all differentiated cells found in the peripheral blood. Every cell population is defined by expression of a specific set of cell surface markers and transcription factors. Figure was taken from Stuart H. Orkin, Leonard I. Zon, Hematopoiesis: *An Evolving Paradigm for Stem Cell Biology*. Cell, 2008.

1.2.1 Hematopoietic hierarchy

In recent years, single cell sequencing studies have challenged the classical hematopoietic hierarchy model. It has been shown that adult hematopoiesis is a continuous and highly dynamic process rather than a sequential step wise differentiation process consisting of defined homogeneous cell types. This finding led to the development of new hematopoietic hierarchy models (Figure 4). However, a similarity of the different hematopoietic hierarchy models is that HSCs are defined as a mainly quiescent population with the capacity to self-renew, which is underpinned by their ability to divide both asymmetrically (one HSC daughter cell and one differentiated daughter cell) and symmetrically (two HSC daughter cells). Another common feature of the different hierarchy models is the gradual decreased in potential of generating all hematopoietic cells with increased specificity of the progenitor cells. This continuous loss of multilineage potential can already be observed at the level of the HSCs, where LT- and ST-HSCs differ in their potential to give rise to long-term reconstitution of hematopoietic system after lethal irradiation[49,50].

Camargo *et al*. performed single cell transplantation experiments and revealed that not every HSC exhibits the full potential to engraft and give rise to all differentiated blood cells[51]. In a different study he and his colleagues confirmed that most of the HSCs are already biased, some towards megakaryocytic lineage and some towards myeloid/lymphoid lineages[52]. Velten *et al*. depicted this heterogeneity within the HSC population as a continuous model and proposed to display hematopoietic hierarchy in a similar fashion to the classical Waddington landscape that had been devised to represent epigenetic programming (Figure 4 C). Velten *et al*. performed single cell sequencing on more than 1000 human HSCs and MPPs from two young, healthy donors and showed that a classical hematopoietic hierarchical tree could not be established from this data. They rather identified a multitude of intermediate cell states, with lineage-specific trajectories already present within the HSPC compartment, suggesting that lineage fate or lineage decision begins already quite early during differentiation[50].

An unpublished study of our group also addressed the question of HSC heterogeneity by performing single cell transplantations. We used EPCR, also known as CD201 or Procr to define potent HSCs since it has been shown to be expressed only on a specific subset of LT-HSCs ($CD34^-$

HSCs). Upon transplantation EPCR-positivity conferred an increased engraftment compared to the EPCR-negative control HSCs. Moreover, EPCR has been shown to be already expressed on immature and highly potent fetal liver HSCs[53]. Along those lines, Laurenti and Göttgens surmised that LSK CD48$^-$Flt3$^-$CD150$^+$CD34$^-$EPCR$^+$ cells likely possess the highest self-renewing potential[54]. Excluding Flt3$^+$ (CD135/Flk2) cells from the HSC pool might be crucial to avoid choosing lymphoid biased HSCs[55,56]. The results from our group showed that most of the single transplanted EPCR$^+$LT-HSCs were already bias towards a specific lineage. Of note, our unpublished data from single cell transplantation experiments shows that LT-HSCs that give rise to a high platelet chimerism also contributed to a high total BM chimerism. Supporting previous studies stating that even though the HSC pool seems to be phenotypically uniform with regards to CSM expression, differentiation output and engraftment potential can vary significantly. In line with our unpublished study, the Nerlov group identified the van Willebrand factor (vWf) as a promising factor to define potent HSCs, since the vWF$^+$ cells gave rise to high BM engraftment and often showed a platelet biased reconstitution potential[57].

Even though HSC heterogeneity is a highly studied field, accurate definition of the HSC at the top of the hierarchy, harboring the highest potential still remains to be elusive. Figure 4 summarizes the different hematopoietic hierarchy models[49].

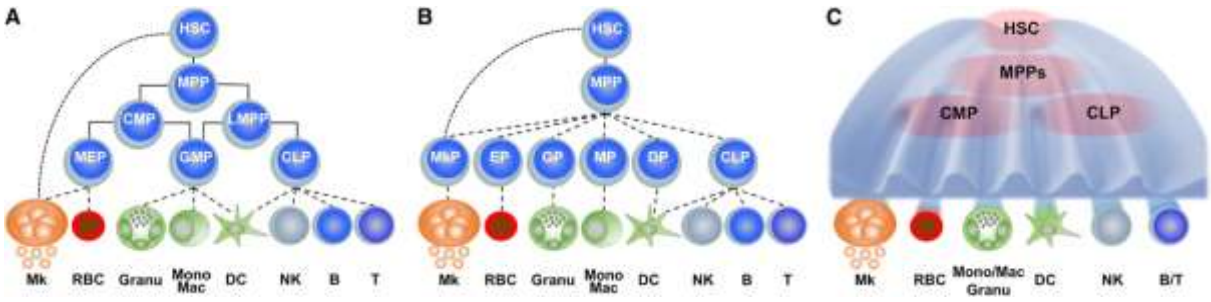

Figure 4: **Different models of hematopoietic hierarchy**. A) Describes the classical hematopoietic hierarchy with the exception that HSCs have the potential to directly differentiate to megakaryocytes (MKs). B) Describes a less stringent hematopoietic hierarchy model showing that all committed progenitors retain the same potential. Cell populations in A and B can be phenotypically defined by their CSM expression. C) Displays a very heterogeneous and highly dynamic hematopoietic hierarchy that lacks defined downstream populations and rather represents a continuous differentiation process. Figure is taken from Haas *et al*. 2018. *Causes and Consequences of Hematopoietic Stem Cell Heterogeneity*. Cell Stem Cell Review.

1.2.2 HSCs are dormant under homeostatic conditions

Even though cell surface markers for the most potent and least biased HSCs are not fully defined yet, it is clear that keeping HSCs in a quiescent, or so-called dormant state, is crucial for maintaining their potential. Quiescence is defined as cells being in G0 cell cycle phase, meaning these cells do not show signs of active cell cycle which would correspond to G1, S or G2-M phases

as depicted in Figure 5. Of note, Figure 5 highlights the ability of cells to switch from a quiescent state in G0-phase to an active cell cycle phase[58]. Dormancy however, is defined as a prolonged state of HSCs being quiescent and metabolically inactive[59]. It has been demonstrated that dormancy not only protects HSCs but also other stem cells from accumulating DNA damage[59], which can be acquired during proliferation.

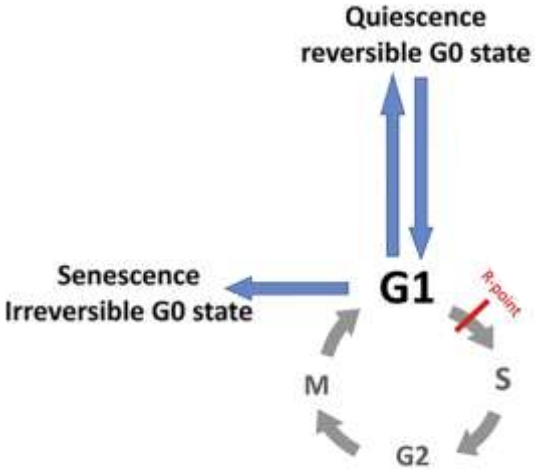

Figure 5: **Quiescence is reversible.** HSCs can reversibly switch from a quiescent state also referred to the G0 phase of the cell cycle to an active state which allows them to undergo cell cycle. The R-point (restriction point) marks the point where the cell decides to actively proliferate and progress through all phases of the cell cycle including S, G2, and M phase. Figure was modified from Cho *et al*. 2019. *Mechanisms, Hallmarks, and Implications of Stem Cell Quiescence*. Stem Cell Reports.

However, examination of the quiescent or even dormant status of a given cell, poses a challenge, since most cell cycle markers require intracellular staining, after which functional potential cannot be assessed. The most useful tool in identifying dormant HSCs which allows further functional analysis, is the Scl-tTA-H2B-GFP mouse model, also referred to as label-retaining mouse model (LRC mouse model)[60,61]. This model is advantageous over the previously used BrdU labeling method, as BrdU has the disadvantage that during the labeling phase, BrdU is only incorporated into the DNA of actively cycling cells, meaning that true dormant HSCs will not be labelled and cannot be subsequently distinguished from cells that subsequently dilute label during the chase period. BrdU also cannot be administered to mice for more than 14 days due to its toxicity. Additionally, cells have to be fixed in order to stain for BrdU and cannot be used for further *in vitro* or *in vivo* functional studies.

The LRC mouse model expresses a Histone 2B (H2B) GFP molecule in the HSPC compartment under the scl promoter. The promoter is regulated by a transactivator protein (tTA) according to a tet-off system, meaning when mice are treated with doxycycline GFP expression is stopped. Subsequently, with each cell division the GFP label of a cell is diluted until GFP detection is within the background. Label and non-label retaining LT-HSCs (LR and non-LR LT-HSCs) from the same mouse can be sorted and used for functional analysis[60,61]. Interestingly, researchers previously

observed that even though LRC mice were challenged with a pro-inflammatory stimuli, LR HSCs remained in the BM and showed the same *in vitro* repopulation capacity as the LR HSCs from control treated mice[62]. Using BrdU these cells would not have been detected, since they were not actively dividing. The LRC model has also been used to study HSC dormancy during aging. When aged label retaining HSCs, from LRC mice older than 1.5 years were examined, it was found that they resided predominantly in the surroundings of the sinusoidal niche[63]. As such, it was further hypothesized that a few remaining HSCs in the BM retain their full potential over a lifetime and suggested that the HSC niche in the BM plays a major role in keeping HSCs in a quiescent state. It can be said that dormancy slows down functional aging of a sub-set of HSCs. Additionally, it was also surmised that the BM niche protects LR LT-HSCs from harmful environmental influences. The BM niche is a complex organization of different types of stromal and endothelial cells that provide HSCs an anchor to the niche by expressing cadherins and adhesion molecules. HSCs reside mainly in two niches, the sinusoidal, which is in proximity to blood vessels, and the endosteal, which is close to the bone lining. Moreover, other hematopoietic cells such as megakaryocytes can also be found in the niche and have been shown to provide appropriate signaling to keep HSCs in a quiescent state[64,41,65].

1.2.3 Stress hematopoiesis

As mentioned above, HSCs are usually in a dormant state and avoid entry into cell cycle to prevent damages induced by proliferation and active metabolism. However, during severe infections, injury trauma or other adverse events that require a dramatic increase in the amount of either lymphoid or myeloid cells or platelets, HSCs are pushed into cell cycle. Only loss of erythroid cells can probably be compensated by progenitor cells and does not induce HSCs cycling[66]. These challenging events occur repeatedly during an individual´s lifetime and may have a cumulative effect that can lead to an aging phenotype, indicated by decreased potential of HSCs and by a loss of balanced and healthy contribution to the differentiated blood cell lineages. A frequently underlying mechanistic cause of loss of functional potential, may be the acquisition of mutations. This sometimes results in the uncontrolled proliferation and expansion of only a certain lineage primed cell[67,68]. Older people often show signs of dysbalanced peripheral blood composition or an increase of a specific HSC clone in the bone marrow, which is called clonal hematopoiesis. Both, dysbalanced peripheral blood composition as well as clonal hematopoiesis, may indicate preliminary stages of bone marrow failure or hematopoietic malignancies and are more prevalent in elderly individuals. These can, in the worst case, lead to leukemia which is most prevalent in people above the age of 70 years[69].

To better understand the above-mentioned processes during stress hematopoiesis, many studies have been performed where HSCs are activated using different agonists and subsequently

examined their function. However, most agents used to study stress hematopoiesis, induced a pro-inflammatory immune reaction and a common phenotype of exhausted and/or artificially aged HSCs was observed. Upon transplantation these repeatedly stimulated HSCs showed a low BM engraftment as well as a myeloid bias in their PB contribution. When injecting the chemotherapeutic Fluorouracil (5-FU), the bacterial cell wall component lipopolysaccharide (LPS)[70] or the inflammatory cytokine interferon (IFN) alpha into mice, researchers could observe the same phenomena[44,45]. Interestingly, when G-CSF was used to stimulate HSCs, they were also sufficiently activated to proliferate but also mobilized and an accumulation of HSCs could be observed in the spleen[61]. This demonstrates that extramedullary organs play a major role during stress hematopoiesis. One of the most often used molecule to study stress hematopoiesis is the dsRNA mimetic polyinosinic:polycytidylic acid (polyI:C). It activates HSCs indirectly by binding and activating the toll-like receptor 3 (TLR3) to induce an immune response and a cytokine storm. After repetitive polyI:C injections Walter *et al*. observed that HSCs accumulated DNA damage and, when treating a DNA damage repair deficient mouse model with polyI:C this repeated activation led to a severe BM failure phenotype[44].

In another study by Haas *et al*., an interesting observation was made after a single polyI:C injection when the frequency of megakaryocytic progenitors in the BM significantly increased. It was demonstrated that upon polyI:C treatment, HSCs were able to directly differentiate to megakaryocytes (MKs) and a strong increase in both MKs and platelets could be observed. The so-called emergency megakaryopoiesis program was activated to protect the body from a life-threatening decrease in thrombocytes that would result from ineffective clotting. In addition, during acute infection platelets generate the so-called neutrophil extracellular traps (NETs) together with neutrophils, which help to capture and combat pathogens. In order to meet this high need of platelets, HSCs can directly respond and start a separate differentiation program[71]. This was surprising since it was thought that thrombopoietin (TPO)-induced MK and platelet production. Of note, the TPO receptor Mpl has also been shown to be specifically present on dormant HSCs and it is known that HSCs can also directly respond to TPO signaling. Remarkably, it was shown that Mpl is expressed as early as around E11.5 in fetal liver HSCs[72]. However, TPO-induced activation showed ambiguous results which will be explained in detail in the next section[73].

1.2.4 The role of TPO in HSC maintenance, self-renewal and cycling

TPO is an interesting molecule to look at in the context of hematopoiesis since it acts on many levels and several cell types are involved in its regulation and generation. The main source of TPO production in the body is the liver. TPO mRNA transcripts have been detected in MKs and BM stromal cells, but presence of the TPO protein could not be verified[74]. Interestingly, even though

Mpl is expressed on HSCs, TPO is not required for the HSC development since TPO knock out (KO) pups are viable and show a normal BM composition. In contrast, adult TPO KO mice cannot form a quiescent HSC pool in the BM and HSCs from these TPO KO mice show increased cell cycling. Hence, it was suggested that TPO is required to maintain and establish a quiescent HSC pool in adult animals. The fact that TPO KO mice show decreased MK and platelet counts has not further been examined[75].

Along these lines, studies by Qian *et al*. and Yoshihara *et al*. showed the importance of TPO in keeping HSCs in a quiescent state. Qian *et al*. used TPO KO and Mpl KO mice in order to study the effects of a lack of TPO and TPO signaling on HSCs. They concluded that TPO keeps HSCs in a quiescent state[76]. Yoshihara *et al*. supported these findings in *in vitro* studies in which TPO/Mpl signaling blockade, led to impaired HSCs proliferation and differentiation potential. In addition, inhibition of the TPO/Mpl signaling axis decreased the adhesion of HSCs to the co-cultured feeder cells[77]. This suggests that TPO signaling is also required for keeping HSCs attached to their BM niche. This hypothesis is further strengthened by a study of Umemoto *et al*., where it was observed that TPO signaling induced a change of the ß3 integrin receptor, which enhanced the interaction of HSCs with cells of the BM niche[78].

In a strong contrast to the above-mentioned studies which highlighted TPO as crucial component for maintaining HSC quiescence, it was also shown that TPO leads to the expansion of the HSC pool. In transplantation experiments Fox *et al*. showed that HSCs would not engraft in TPO KO mice. Only upon exogenously applied TPO, the transplanted HSCs showed donor chimerism in TPO KO recipients[79]. In line with these transplantation experiments, Kovtonyuk *et al*. observed that TPO-induced cycling did not result in impaired engraftment potential. They stated that TPO induces HSC expansion by self-renewal divisions[80]. Based on the findings that TPO leads to the self-renewal of HSCs, Porteu and her group examined the underlying properties of this effect and showed that DNA repair is increased in wt mice compared to Mpl KO counterparts. Additionally, they observed that TPO treatment of mice prior to irradiation increased their ability to repair irradiation-induced DNA damages[81]. In a second study they showed that TPO signaling results in phosphorylation and activation of Erk, a protein that can complex with Iex-1 and lead to specific activation of the DNA-PK dependent non-homologous DNA (NHEJ) repair pathway[82]. Of the two DNA repair pathways (homologous recombination (HR) and NHEJ) that have been studies in cells, NHEJ repair pathways is the preferred pathway in quiescent HSCs[83].

To sum up the above-mentioned studies, TPO signaling is required for: (i) keeping HSCs in a quiescent state, (ii) expansion and self-renewal of HSCs and (iii) NHEJ repair in HSCs.

1.2.5 TPO signaling pathway

TPO binds to the receptor Mpl which can be found on various different cell types, including platelets, HSCs and megakaryocytes. Upon Mpl binding, TPO is internalized and degraded and in the case of MK binding, these cells are stimulated to mature and produce platelets. A feedback loop between TPO levels and platelets was observed, as an increased number of platelets also lead to a faster decrease of TPO levels in the blood serum.

The effects of TPO are so diverse due to the fact that TPO/Mpl signaling activating more than one downstream pathway, all of which are summarized in Figure 6[73]. Upon TPO binding, dimerization of the Mpl receptor is induced which leads to activation of three different downstream signaling pathways: 1) JAK/STAT pathway, 2) MAPK pathway and 3) PI3K pathway. After dimerization of Mpl, Janus kinase 2 (JAK2) is phosphorylated (-p), which in turn leads to phosphorylation and activation of signal transducer and activator of transcription molecules 3 and 5 (STAT3 and STAT5). STAT3-p and STAT5-p migrate to the nucleus and activate transcription of pathways involved in proliferation and cell survival. Interestingly, STAT5 signaling has also been associated with self-renewal divisions of hematopoietic and leukemic stem cells[84].

As previously noted, TPO additionally activates the Erk1/2 mitogen-activated-protein-kinase (MAPK) pathway, which is known to play a role in cell cycle regulation, development and proliferation[85]. Activation of this pathway can explain the findings from de Laval *et al*. who reported that TPO leads to upregulation of the DNA-PK which is activated through Erk signaling[81]. Another pathway that is activated is the phosphoinositide 3-kinase (PI3K)/AKT pathway. This pathway is mainly involved in regulation of cell cycle since activation of AKT leads to expression of the cell cycle inhibitor p27. These findings explain the involvement of TPO in the regulation of the cell cycle activity and proliferation properties of HSCs. However, all signaling processes that respond to the TPO/Mpl signaling axes were recently examined and it turned out that TPO activation involves far more downstream processes than presented in this section[86]. In summary, TPO/Mpl signaling is also involved in the regulation of extracellular matrix components, in apoptosis as well as in the onset of cancer.

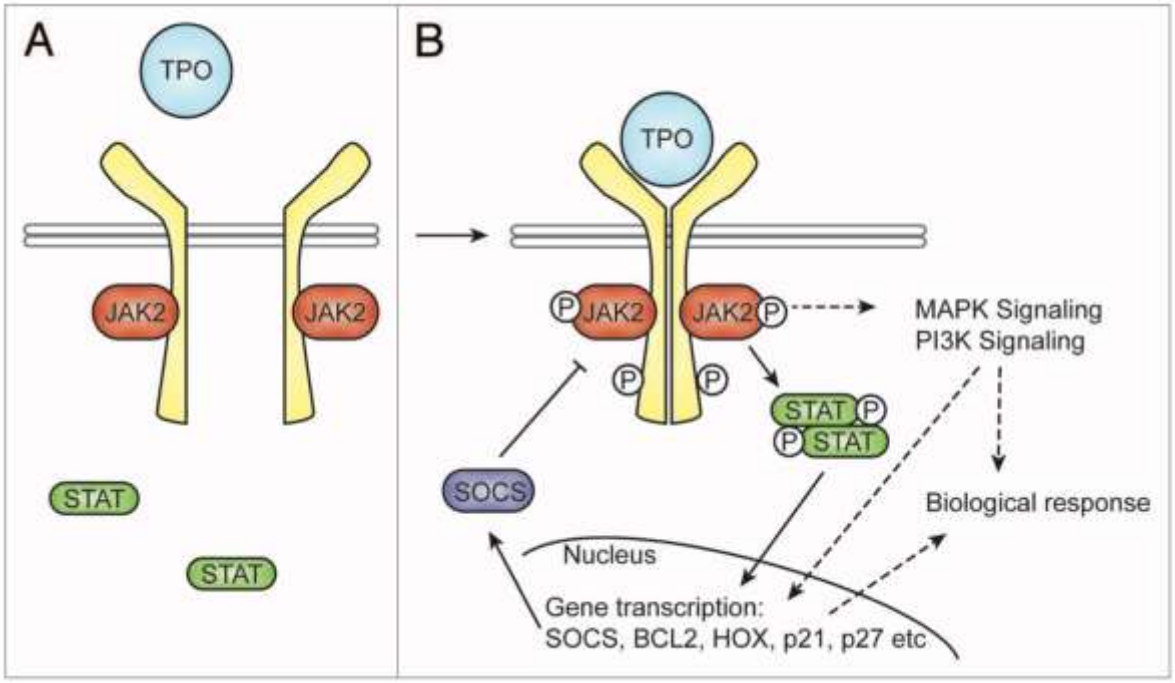

Figure 6: **TPO signaling via the receptor Mpl activates the JAK2/STAT5, Erk/MAPK and PI3K/AKT pathways**. A) The TPO receptor Mpl dimerizes upon TPO binding and activates downstream signaling processes, shown in B) Three different downstream signaling pathways are activated via the TPO/Mpl signaling axis: 1) JAK2/STAT3/5 pathway 2) Erk1/2 and Ras/MAPK signaling pathway and 3) PI3K /AKT signaling pathway, leading to various biological responses such as cell cycle regulation and cell differentiation. Figure is taken from a review by de Graaf and Metcalf 2011. *Thrombopoietin and hematopoietic stem cells*. Cell Cycle.

Aberrations in TPO regulation and signaling are the underlying cause of diseases such as myeloproliferative neoplasms (MPNs), congenital amegakaryocytic thrombocytopenia (CAMT) and idiopathic thrombocytopenic purpura (ITP). Defects in Mpl signaling as observed in CAMT lead to reduced MK and platelet numbers. Since these patients do not respond to TPO treatment the only curative option is an allogenic stem cell transplantation as early as possible[87]. MPN is a generic term summarizing different diseases that refer to an excessive proliferation of a specific myeloid cell type to which some can be related to constitutive TPO signaling. The $JAK2^{V617F}$ mutation is the most prevalent mutation of MPNs leading to constitutive signaling via JAK2/STAT5. Common Mpl mutations leading to constitutive activation of the TPO/Mpl signaling axis occur at the amino acid 515. Furthermore, mutations in the endoplasmic reticulum protein calreticulin can result in calreticulin binding to the Mpl receptor. This false binding of mutated calreticulin to the Mpl receptor leads to constitutive activation and signaling[88,89]. The above-described mutations all result in an increase in MK numbers and are accompanied by an increased risk of thrombosis and leukemia development[90]. In contrast to essential thrombocythemia, where too many platelets are generated, immune thrombocytopenias represent a situation where the body develops antibodies against platelets, resulting in patients developing thrombocytopenia. Even though patients usually show normal levels of TPO, it is often not enough to produce a sufficient number of platelets.

Therefore, patients need to be treated with recombinant human (rh) TPO or other drugs that additionally stimulate platelet production[91,92].

Of note, the studies described in the previous section examined the effects of TPO using only a single or a few TPO treatments and highlighted the beneficial effects of TPO. However, as deregulated TPO signaling plays a major role in disease onset, one aim of this thesis was to examine the effects of repeated TPO stimulation on HSCs. Up to now, consequences of repetitive TPO signaling have not been studied in an experimental setting.

1.2.6 Use of TPO mimetics in the clinic

Recombinant human TPO has been used in the clinics to treat thrombocytopenic patients, such as those with ITP, as well as and cancer patients to increase their platelet counts. However, after long-term rhTPO treatment it was observed that patients stopped responding to the rhTPO therapy. Enzyme-linked immunosorbent assays (ELISA) showed that patients developed antibodies not only against the rhTPO but also against the endogenous TPO. In order to prevent such immunogenic reactions, the TPO mimetics Eltrombopag and Romiplostim were developed[93]. Eltombopag is a small chemical molecule that binds to the intermembrane section of the Mpl receptor and induces activation. In contrast, Romiplostim (Rom) is a peptibody (peptide-antibody) consisting of a peptide sequence, in this case the Mpl receptor binding sequence, coupled to an antibody, here a human Fc receptor part. Peptibodies prevent immune reactions and stabilize the protein *in vivo*[91].

Both agonists were approved in 2008 by the US Food and Drug Administration (FDA) and patients initially responded well to the treatment[94]. However, adverse side effects developed after long-term treatment with the TPO mimetics, which were observed by increased reticulin in the BM and bone marrow fibrosis. Even though this returned back to normal upon discontinued treatment, high reticulin levels are considered as a detrimental prognostic factor of MPNs. These observations suggested that repeated Rom treatment might negatively impact on BM cells and when looking at TPO signaling in more detail it is not surprising that adverse side effects were observed. As TPO/Mpl signaling leads to proliferation and differentiation of cells. However, these side effects occur only in rare cases and hence, TPO mimetics are still regularly administered[95].

1.3 Studying HSCs *in vitro* and *in vivo*

In science, researchers try to avoid animal experiments along the lines of the "3Rs" recommendation: reduce, refine and replace[96]. A lot of effort is put into developing 3D culture models and organs-on-a-chip techniques[97]. However, until now it remains difficult to maintain functional, dormant HSCs in *in vitro* cell culture for extended periods and for this reason mouse models are still commonly used to study HSCs. For short term experiments *in vitro* techniques are available and are used, for example when examining the repopulation or the differentiation potential of HSCs. However, these assays only allow examination of a specific characteristic and do not allow the appreciation of the full HSC differentiation and functional potential. For these particular experiments mouse models are still necessary.

1.3.1 Hematopoietic stem cells in cell culture

The possibility of propagating, maintaining and modifying functional HSCs *in vitro* such that a specific lineage can be generated, is not only scientifically interesting but holds great therapeutic potential. Despite the high risk of the patient's body to reject the allogenic stem cell transplant and develop graft versus host disease, these transplantations are still the only curative treatment for a range of diseases [98]. To avoid both, allogenic transplantation and the risk of rejection, healthy patient-derived HSCs could be expanded and/or modified *in vitro* and then transplanted back into the patients. This could potentially solve the issue of identifying a suitable HLA matched transplant donor.

Recent protocols from Kobayashi *et al*. and Wilkinson *et al*. showed that it is possible to maintain murine HSCs in culture for up to 28 days and 57 days, respectively[99,100]. Despite this progress, there is still much to be done in order to establish a standardized protocol. Both protocols successfully maintained transplantable HSCs but the two suggested protocols are completely different in terms of medium composition and medium supplements. Although the *in vitro* maintained HSCs display a similar transcriptome compared with *in vivo* HSCs, both studies mention that the low donor chimerism, which gradually decreases over time has to be overcome. Additionally, the variability within the generated HSC pool is still too high and reproducibility is weak. However, these protocols open up possibilities of the long-term maintenance and expansion of functional HSCs.

Until now, most *in vitro* protocols have been used to analyze the function of HSPCs. These protocols are often referred to as colony forming assays and have been developed to *in vitro* facilitate and enumerate the clonal production of differentiated progeny from primary isolated HSPCs into for example, oligopotent progenitors. In order to assess a potential lineage bias or a loss of function. One caveat of these protocols is that only a certain cell lineage can be examined

as every differentiated cell type needs different culture conditions. For example, to *in vitro* differentiate HSCs into B-cells, co-culture with OP9 stromal cells and interleukin 7 (IL-7) is required. Whereas myeloid cells need to be differentiated in medium containing erythropoietin, thrombopoietin (TPO) and IL-3[56]. Therefore, to assess the full differentiation potential of a HSC pool or a single HSC, *in vivo* transplantation assays are still considered the gold standard.

1.3.2 Reporter mouse models

For transplantation assays three different mouse strains are required: (i) a donor whose cells should be tested for engraftment and lineage contribution, (ii) a supporter or competitor and (iii) a recipient. In order to distinguish cells derived from donor, competitor and recipient mice, C57BL/6J wild type (wt) strains with different CD45 isoform expression (CD45.1 and CD45.2) are used which can be separately identified using isoform specific monoclonal antibodies. CD45, known as the common leukocyte antigen, is a pan-hematopoietic marker that is expressed on every hematopoietic cell except for platelets and red blood cells[101]. Therefore, one disadvantage of using wt mice as donors and this CD45 isoform system is, that platelet and RBC engraftment cannot be monitored following transplantation. Another downside of using transplantation assays is that recipient mice have to be myeloablated prior to transplantation by either lethal irradiation or chemotherapeutic treatment, which poses a severe burden for the recipient mice[102]. To solve the issue of not being able to detect platelet and RBC chimerism, the UBC-GFP mouse model was developed. It expresses the green fluorescent protein (GFP) under the constitutive human ubiquitin C (UBC) promoter leading to GFP expression in hematopoietic cells including RBCs and platelets. However, when using the UBC-GFP mouse model it has been observed that engraftment efficacy is somewhat lower than when compared to non-transgenic wt mice[103].

Of particular interest for this study, was the assessment of the divisional history of the transplanted HSCs. It has been observed before, that the phenotypical HSC or LT-HSCs pool displays a great heterogeneity in terms of functional potential following transplantation. As mentioned before, dormant HSCs comprise a sub-set of the HSC pool that harbors the greatest functional potential. To experimentally monitor the divisional history of the phenotypic LT-HSC pool, we made use of the Scl-tTA-H2B-GFP mouse model. In brief, these mice express a H2B-GFP reporter downstream of the Scl gene, which is only expressed in HSPCs. Additionally, the expression of the Scl-H2B-GFP is controlled by a tTA element. When dox binds to the tTA element, H2B-GFP expression will be stopped. Subsequently, when this cell divides it will distribute the remaining H2B-GFP amongst the resulting cells leading to a GFP-dilution of divided cells. This allows us to differentiate between cells within the phenotypic HSC pool with higher potential into those who have undergone numerous divisions, resulting in a low GFP intensity, and those who have undergone none or only a few divisions and therefore retain a high GFP intensity[61,60].

1.3.3 Disease mouse models

In the study represented here, we were mainly interested in the effects of TPO signaling. Since TPO mimetics are also used to treat aplastic anemia patients to enhance their overall blood cells counts, we performed experiments using a diseased mouse model of bone marrow failure. In three clinical trials (ClinicalTrials.gov Identifier: NCT03957694, NCT04095936 and NCT03206086) patients with the Fanconi anemia disease are also considered for a treatment with the TPO mimetics Romiplostim and Eltrombopag. Fanconi anemia is a protein complex, consisting of 16 currently known Fanc proteins, that are crucial for homologous recombination (HR) DNA repair. In the case of the Fanconi anemia syndrome one of the Fanc proteins is mutated and hence, functional HR DNA repair is disrupted leading to bone marrow failure and myeloid leukemias[104,105]. We made use of the Fanc A KO mouse model ($Fanca^{-/-}$) to examine effects of repeated TPO treatment within a disease setting. Previous studies using TPO treatment reported an increase in the HSC pool after TPO treatment and supported the hypothesis that TPO leads to self-renewal divisions with an increase in NHEJ DNA repair. In contrast, previous studies conducted with polyI:C to challenge $Fanca^{-/-}$ mice showed that this led to a decrease in HSC potency with a severe BM failure phenotype[44]. Therefore, we were interested in whether TPO can not only increase the overall peripheral blood counts but also increase the phenotypic HSC pool in $Fanca^{-/-}$ mice.

In this study, we furthermore used the Rag2 KO mouse model. These mice do not express the protein Rag2 that is responsible for the maturation of the B- and T-cell receptor via mediating DNA recombination at these loci[106]. By using this model, the effects on the hematopoietic system can be observed without interference of the immune system. This is particularly relevant to our study, as we were also interested in HSC exhaustion in a non-inflammatory setting.

1.4 Aims of this thesis

The results and discussion part of this thesis were each divided into two parts.

The aims of the first part were based on the still incomplete information regarding essential markers of EHT. Evi2a was found to be crucial for hematopoietic specification *in vitro* and we wished to interrogate this phenomenon further. Thus, the specific aims of this section of the thesis are:

1) To define signaling pathways that Evi2a is involved in: Identification of signaling pathways that are inhibited/altered during hematopoietic specification of Evi2a KO cells.

2) To study the importance of Evi2a in hematopoiesis *in vivo* via the generation and validation of a conditional Evi2a KO mouse model.

3) To characterize heterozygous and homozygous Evi2a KO mice in terms of their hematologic parameters.

The aim of the second part was based on studies reporting HSC attrition and myeloid bias upon extensive HSC stimulation as well as on reports communicating that TPO leads to self-renewal divisions and increased DNA repair in HSCs. We aimed to investigate HSC function after serial stimulation with TPO and the TPO mimetic Romiplostim to examine HSC loss-of-function in a non-inflammatory setting. We hypothesized that any proliferation (also TPO-induced) would lead to HSC attrition in the long-term. The specific aims of this second part are:

1) To examine HSC exhaustion after repetitive TPO and TPO mimetic stimulation by assessing reconstitution potential and lineage contribution of HSCs.

2) To interrogate the proliferative history of HSCs following TPO challenge and assess HSC potency between cells that cycled frequently and cells that remained in a dormant state.

3) To investigate the impact of TPO treatment in a diseased setting and determine if deleterious or beneficial effects are observed after TPO treatment.

2 Results – part one

In our group, we were interested in hematopoietic development and the early emergence of the first hematopoietic cells. We wanted to understand which markers were expressed early on in development and could subsequently be used to isolate and propagate original and highly potent hematopoietic cells *in vitro*. In this part, results will be presented where we specifically investigated the role of Evi2a during hematopoietic development and hematopoietic specification.

2.1 Evi2a as novel functional marker during hematopoietic stem cell specification *in vitro*

Previous *in vitro* studies performed in our laboratory by Dr. Paul Kaschutnig revealed that Evi2a, a relatively uncharacterized cell surface protein with transmembrane and intracellular characteristics, was crucial for the proper differentiation of murine embryonic stem cells into hematopoietic cells. He showed that Evi2a was differentially expressed during the endothelial to hematopoietic transition (EHT), an essential step during hematopoietic specification. To validate its importance during EHT, functional KO studies were performed. Evi2a was knocked out in ESCs using CRISPR/Cas9 and multiple single Evi2a KO ESC were expanded to establish stable Evi2a KO cell lines. Subsequently, Evi2a KO ESCs were *in vitro* differentiated and the Evi2a knock out resulted in the block of formation of hematopoietic cell formation, which suggested a crucial role for Evi2a during EHT (Figure 2).

Since we already have functional data showing that Evi2a is crucial during hematopoietic specification, we wanted to understand which processes were altered upon Evi2a KO. Transcriptome analysis helped us to identify differentially expressed genes (DEGs) between wt and Evi2a KO cells and to understand deregulated pathways after Evi2a KO during development. Our aim was to decipher the signaling networks that Evi2a was involved in.

2.1.1 RNA seq analysis reveals delayed differentiation kinetics of Evi2a KO cells

We took advantage of a Hoxb4-YFP reporter ESC line previously generated at the DKFZ where ESCs were isolated from a blastocyst stage of the Hoxb4-YFP reporter mouse model (Hills *et al*., Blood 2011[24]). It was known that Hoxb4 was already present early on during development and sustained expression until HSC expansion within the fetal liver and beyond. Overexpression studies showed that Hoxb4 promoted and activated hemogenic endothelium (HE), a progenitor of hematopoietic cells and probably the initial site of endothelial to hematopoietic transition. In the previous

experiment, sorting for Hoxb4-YFP$^+$ and Hoxb4-YFP$^-$ cells facilitated the analysis of differences in early hematopoietic cells, especially during the endothelial to hematopoietic transition. By analyzing differentially expressed genes using microarray it was found out that Evi2a was exclusively upregulated in the EHT population. Interestingly, even though Evi2a KO led to an impaired hematopoietic potential (see Figure 2), Evi2a KO cells were still able to express Hoxb4 after six days of *in vitro* differentiation (Figure 7).

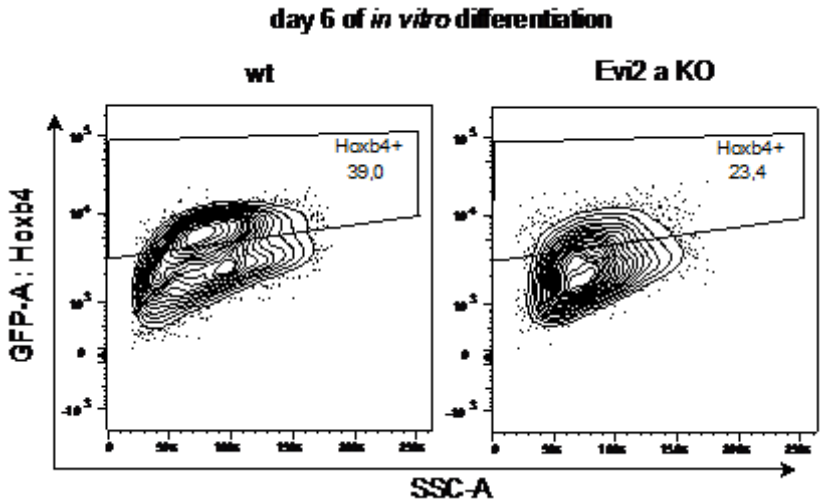

Figure 7: **Hoxb4-YFP expression on day 6 of *in vitro* differentiated wt and Evi2a KO Hoxb4-YFP reporter ESCs**. Wt and Evi2a KO cells were *in vitro* differentiated to hematopoietic stem cells. On day 6 of the *in vitro* embryoid body differentiation protocol, cells were FACS analyzed for their YFP expression. Exemplary FACS plots show expression of the Hoxb4-YFP reporter (recorded in the GFP channel) plotted against side scatter area (SSC-A).

The *in vitro* differentiation protocol was established in our laboratory according to Pearson *et al*. 2008[32]. In brief, ESCs were cultivated in embryoid body (EB) differentiation medium, 60h later cytokines which induce mesodermal and hematopoietic formation (BMP4, VEGF, FGF and Activin A) were added and another four days later EBs were dissociated. We performed transcriptome analysis in triplicate on Hoxb4+ cells of three *in vitro* differentiated wt ESC lines and three Evi2a KO ESC lines (Figure 8 A). We sorted Hoxb4-YFP$^+$ cells from differentiated wt and Evi2a KO cells on day 4, day 5 and day 6 of *in vitro* differentiation, isolated RNA and submitted prepared cDNA library samples for sequencing (see bioanalyzer results in appendix: section 10.1, Figure 37 and Figure 38). Principal component (PC) analysis was performed on the RNA seq data to visualize differences and similarities in gene expression between Evi2a KO and wt cells from day 4, 5 and 6 of the *in vitro* culture.

PC1 accounted for 79% of the variance in gene expression and seemed to separate samples by their differentiation dynamics ranging from early undifferentiated cells isolated on day 4 to more differentiated hematopoietic cells on day 6. PC2 seemed to be associated with minor differences between the different analysis days of the Evi2a KO cells (Figure 8 B). Notably, the gene expression

of Evi2a KO cells on day 6 resembled that of wt cells on day 5 suggesting that differentiation is delayed in Evi2a KO cells. Additionally, wt cells of day 4 and Evi2a KO cells of day 5 were also in close proximity supporting the assumption of Evi2a KO cells being delayed in their differentiation kinetics. PC3 is dominated by differences between wt and Evi2a KO cells (Figure 8 C). However, these differences only explain 4% of the variance indicating that only little differences can be explained since 90% of the variability in gene expression is already covered by PC1 and PC2. Of note, we could observe that Cdh3, also known as placental cadherin[107], was highly expressed on day 4 of wt cells and day 5 of Evi2a KO cells, but expression was reduced on wt cells of day 5 (Figure 8 D). Moreover, c-Kit is required for the onset of hemogenic endothelium formation[108] and was already highly expressed on day 4 of wt cells but not on day 4 of Evi2a KO cells. c-Kit expression increased on day 5 of Evi2a KO cells supporting the hypothesis that Evi2a KO delayed embryonic development.

In summary, PC analysis led us to hypothesize that Evi2a KO delayed the normal embryonic development. As we aimed to differentiate ESCs to hematopoietic cells, this resulted in impaired hematopoietic specification.

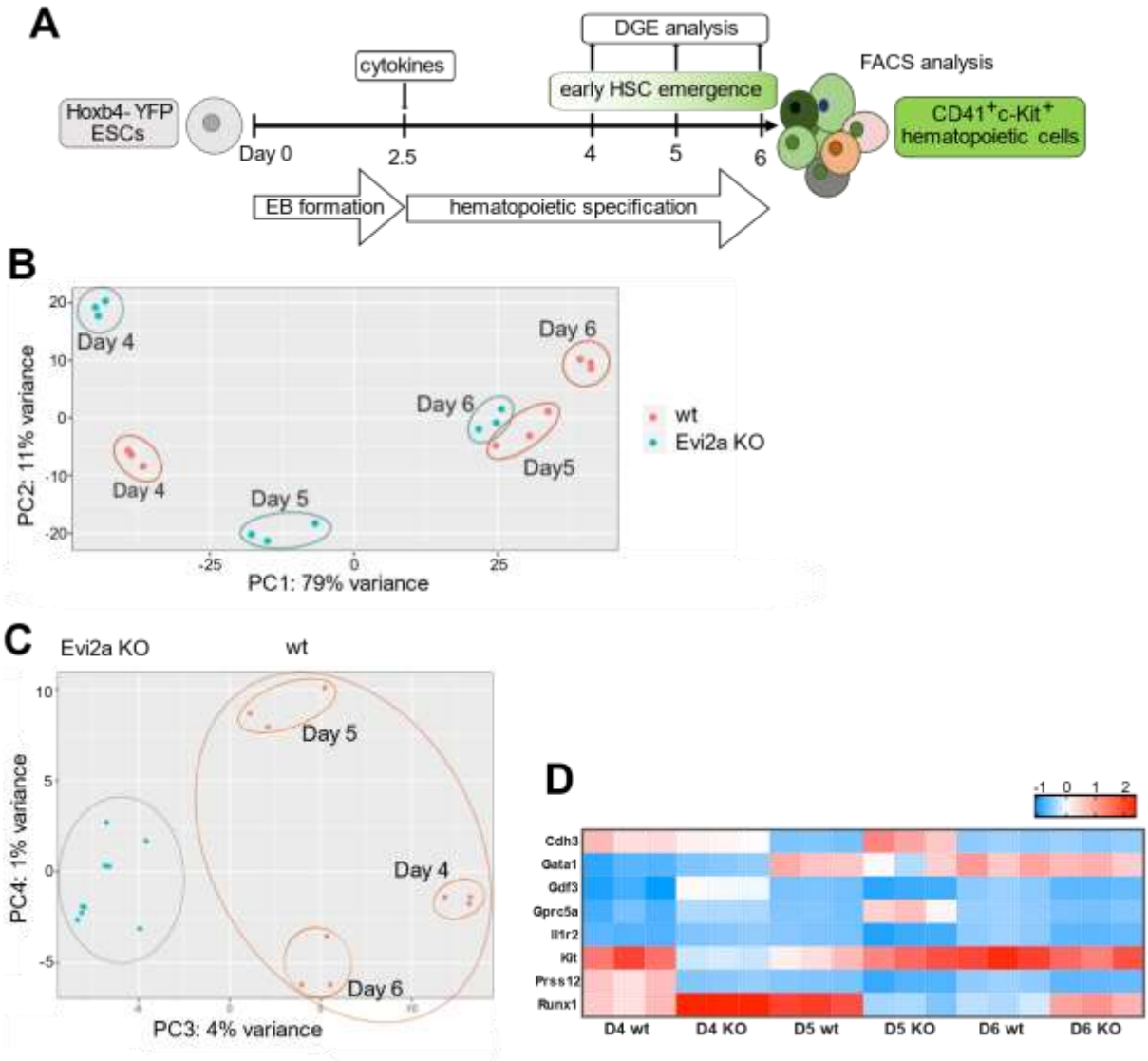

Figure 8: **Differentiated wt cells of day 5 and Evi2a KO cells of day 6 clustered together.** A) Schematic workflow of *in vitro* embryoid body (EB) differentiation. On day 0 Hoxb4-YFP reporter ESCs were transferred into ultra-low attachment flasks containing EB differentiation medium, supporting EB formation and differentiation. On day 2.5 cytokines (BMP4, FGF2, VEGF and Activin A) were added to activate mesoderm formation and induce hematopoietic specification. Samples for differential gene expression (DGE) analysis were taken on day 4, day 5 and day 6. Hoxb4-YFP$^+$ cells were FACS sorted, RNA isolated and prepared for sequencing to analyze differentially expressed genes (DEGs). B-C) Principal component (PC) analysis was performed and plots comparing PC1 vs PC2 and PC3 vs PC4 are displayed. D) Heatmap of a selection of genes contributing to the variation represented by PC3.

2.1.2 The hematopoietic cell lineage pathway is enriched in differentiated wt cells

Delineating mechanisms leading to impaired hematopoietic differentiation is of importance to understand how a lack of Evi2a signaling might alter or block differentiation pathways. Volcano plots were used to display and capture the most significantly differentially expressed genes (Figure 9 A). Remarkably, many genes were differentially expressed between wt and KO cells which stressed the importance of Evi2a during the developmental process.

Cdh2 and Cdh11 are already expressed during mesoderm formation. Additionally, Cdh11 plays a role in neuronal development[109]. The fact that Cdh2 and Cdh11 were highly upregulated in wt cells of day 4 suggested that Cdh2 and Cdh11 were downregulated in Evi2a KO cells. This indicated that Evi2a signaling is crucial for early mesodermal development. Of note, Foxf1, Kdr, Bmper and Bmp2[7] were highly upregulated in wt cells of day 4 verifying the onset of endothelial development during our *in vitro* differentiation. In contrast, Foxf1 was downregulated on day 5 in wt cells meaning that it was highly expressed in Evi2a KO cells, confirming our previously formed hypothesis that Evi2a KO cells were delayed in their differentiation kinetics. On day 6 Evi2a KO cells showed an upregulation of Cdh1 and Wnt5a which are known to be involved in early cell differentiation of the blastocyst stage and mesodermal specification[110]. This hinted that Evi2a KO cells were still at a mesodermal stage and had not differentiated further.

To understand the impact of the up and downregulation of genes we performed gene set enrichment analysis (GSEA) between wt and Evi2a KO cells of each differentiation time point (Figure 9 B). wt cells from day 4 compared to Evi2a KO cells from day 4 cells were enriched in epithelial to mesenchymal transition (EMT) and hedgehog signaling, which are pathways relating to early development and early endothelial and hematopoietic specification, respectively[111]. Wt cells on day 5 and 6 of differentiation were highly enriched in early blood cell developmental processes involving the hematopoietic cell lineage pathway, heme metabolism and platelet activation. In contrast, pathways regarding hematopoietic development were lacking in Evi2a KO cells. Instead, pathways that were enriched in Evi2a KO cells were linked to basic developmental signaling processes such wnt/beta catenin signaling pathway which is crucial already early on for cell fate decisions and EMT formation[112,113,114].

In summary, we could verify the previous *in vitro* findings[26] that Evi2a KO led to impairment of hematopoietic development on a transcriptional level by showing enrichment of hematopoiesis related pathways in wt differentiated cells, whereas differentiated Evi2a KO cells only showed enrichment in basic developmental processes but lacked hematopoietic specification.

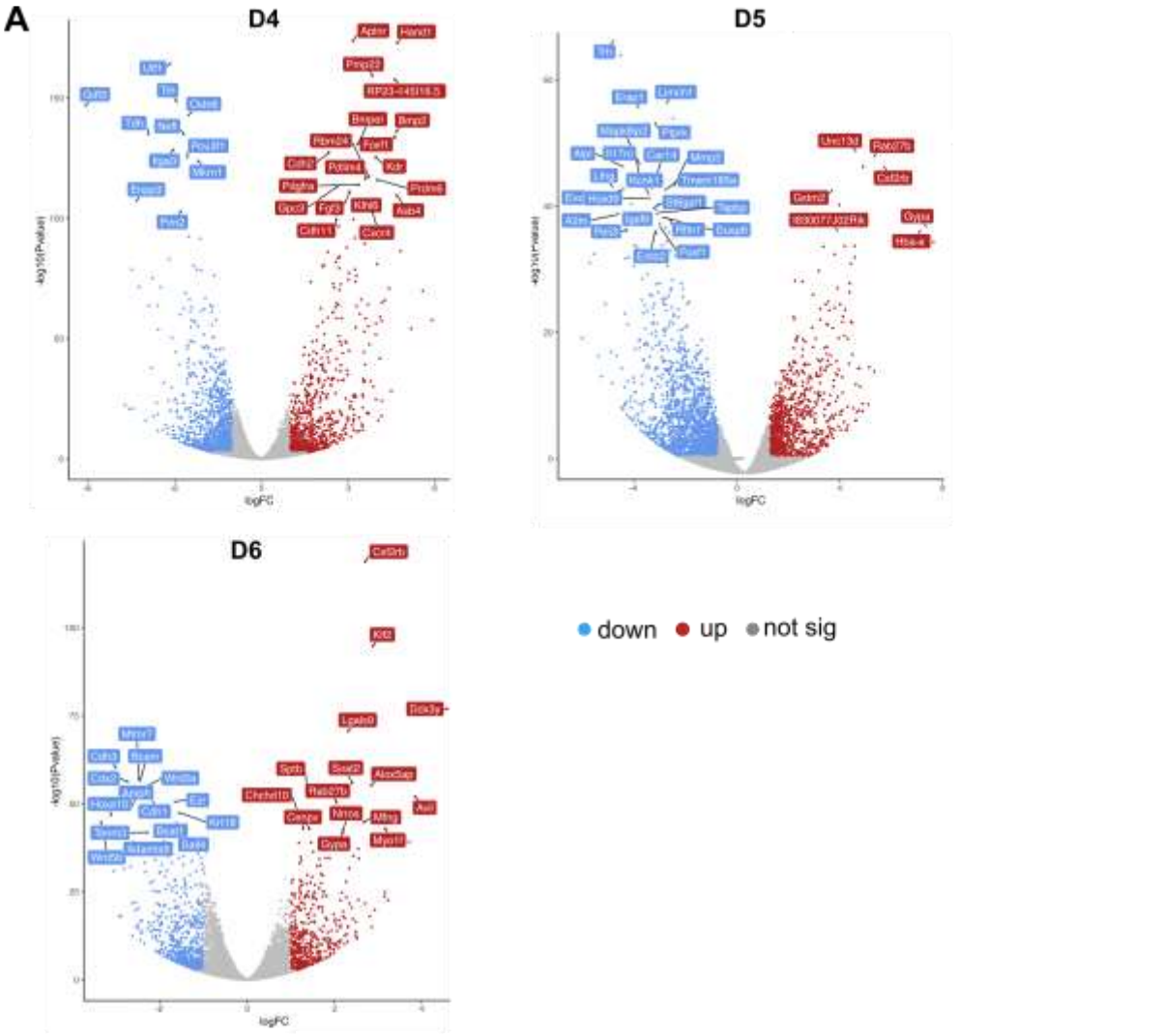
A
D4
D5
D6
down
up
not sig
B
enriched in wt
enriched in Evi2a KO
D4
D5
D6
NES: 1.91 FDR: 0.06
NES: 2.0 FDR: 0.20
NES: -1.92 FDR: 0.12
NES: -2.12 FDR: 0.03
NES: 2.92 FDR: 0.0
NES: 2.35 FDR: 0.001
NES: -2.2 FDR: 0.002
NES: -2.05 FDR: 0.005
NES: 2.34 FDR: 0.0
NES: 2.65 FDR: 0.0
NES: -2.4 FDR: 0.00
NES: -1.95 FDR: 0.02

Figure 9: **Top down and upregulated genes and pathways in wt vs Evi2a KO samples**. RNA-seq data was analyzed using volcano plot function in "Galaxy" (https://usegalaxy.org) and gene set enrichment analysis (GSEA, Subramanian, Tamayo, et al. 2005, PNAS, Mootha, Lindgren, et al. 2003, Nat Genet). A) Volcano plots show differentially expressed genes between day 4 wt vs Evi2a KO, day 5 wt vs Evi2a KO and day 6 wt vs Evi2a KO. The 30 top most statistically significant genes were highlighted. Significance threshold was set to p-value < 0.01, log2(FC) threshold was set to FC > |1|. Each blue dot indicates a downregulated gene in wt vs KO, each red dot an upregulated gene in wt vs KO and each grey dot a not significantly (sig) deregulated gene. B) GSEA of day 4 wt vs KO cells, day 5 wt vs KO cells and day 6 wt vs KO cells. Input data included all differentially expressed genes with p-value (adj) < 0.1. NES = normalized enrichment score, FDR = false discovery rate.

2.1.3 Epithelial to mesenchymal transition pathway is the most differentially regulated pathway between wt and Evi2a KO cells

In order to gain a better insight into which pathways were deregulated we made use of the program ingenuity pathway analysis (IPA). IPA provided detailed analysis of deregulated canonical pathways, activated or inhibited master regulators and signal transduction cascades. IPA also applied algorithms to give a probability score of, for example developing a certain disease or developmental dysfunctions. By performing a so-called core analysis, we wanted to get a comprehensive overview of all deregulated pathways that were affected by the Evi2a KO. Figure 10 displays the top 15 most deregulated pathways between wt and Evi2a KO on each day of differentiation. Of note, this type of analysis does not include any information on up or downregulation of affected pathways.

The most deregulated pathways between wt and Evi2a KO cells on day 4 regarded early embryonic development such as EMT pathway, wnt signaling and axonal signaling. We observed that the EMT pathway was deregulated on all three days of analysis. EMT is a crucial step during normal development when cells leave a cellular bond to migrate to different locations, as seen in mesoderm fromation[113]. Nanog and wnt/ß-catenin signaling are also crucial developmental pathways and were highly deregulated between wt and Evi2a KO cells on day 4 and 5. When concentrating on the most deregulated pathways on day 5 controversies in deregulated signaling pathways were observed. On the one hand the wnt/ß catenin signaling pathway was still deregulated together with the pathway for embryonic stem cell pluripotency but on the other hand more downstream pathways such as leukocyte extravasation signaling or cardiac signaling were also deregulated. On day 6 of differentiation analysis, we again observed the deregulation of the embryonic stem cell pluripotency pathway and axonal signaling but also the deregulation of more downstream pathways which are involved in blood and inflammatory signaling, for example the thrombin signaling pathway[115] and the leukocyte extravasation signaling pathway. Since no information about up or downregulated pathways was displayed, we can only speculate which pathways might be up- or down- regulated based on our hypothesis that Evi2a KO cells

remained in a rather undifferentiated state whereas wt cells proceeded in the developmental process.

In summary, we observed a wide range of pathways that were deregulated. Beginning with deregulated EMT pathway and wnt/ß catenin signaling that are crucial early on during development[6] up to more specified pathways such as leukocyte extravasation signaling and thrombin signaling.

We also performed comparison analyses, an implemented tool in IPA, to identify the differences in the most deregulated canonical pathways between differentiated wt and Evi2a KO cells (Figure 11 A). The advantage of this analysis was that we could directly capture if the exact same pathway was active or inactive at a specific day of analysis. The EMT pathway, which was observed to be deregulated throughout the analyzed days when performing core analysis (Figure 10), was active on day 4 and inactive on day 5 and 6 of wt cells when performing comparison analysis, indicated by a positive and negative z-scores, respectively. The mouse embryonic stem cell pluripotency pathway showed a continuously decreased activation score from day 4 to day 6. Signaling pathways involved in proliferation (ERK/MAPK signaling), hematopoietic specification and differentiation such as the thrombin signaling and Tec kinase signaling pathway, exhibited a continuous increased in the activation score over time. We also performed comparison analysis focusing on deregulated canonical pathways in disease and development (Figure 11 B). Interestingly, day 4 showed activation of pathways associated with body development (development of body axis/of head/of body trunk/of abdomen), which were denoted inactive on day 5 and day 6 of analysis. This again, supported our hypothesis that Evi2a KO delayed not only hematopoietic development but also other fundamental developmental processes. However, as we frequently observed a deregulation of hematopoietic related pathways (aggregation of blood platelets, development of vasculature, cell movement of blood cells), this supported the findings that Evi2a is involved in regulating hematopoietic development and specification. Detailed lists indicating up and down regulation of the above-mentioned deregulated pathways involved in diseases and biological functions can be found in appendix section 10.2 (Figure 39).

In summary, by performing detailed pathway analysis we could strengthened our hypothesis that Evi2a is important already early on during development but also plays a role in early hematopoietic but especially in blood and platelet formation.

Top 15 most deregulated pathways between differentiated wt and Evi2a KO cells

Day 4

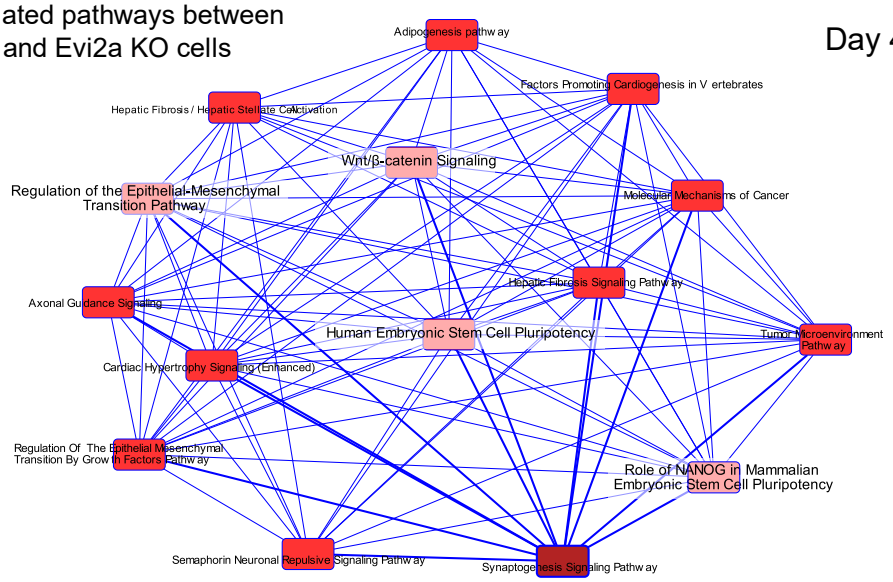

Day 5

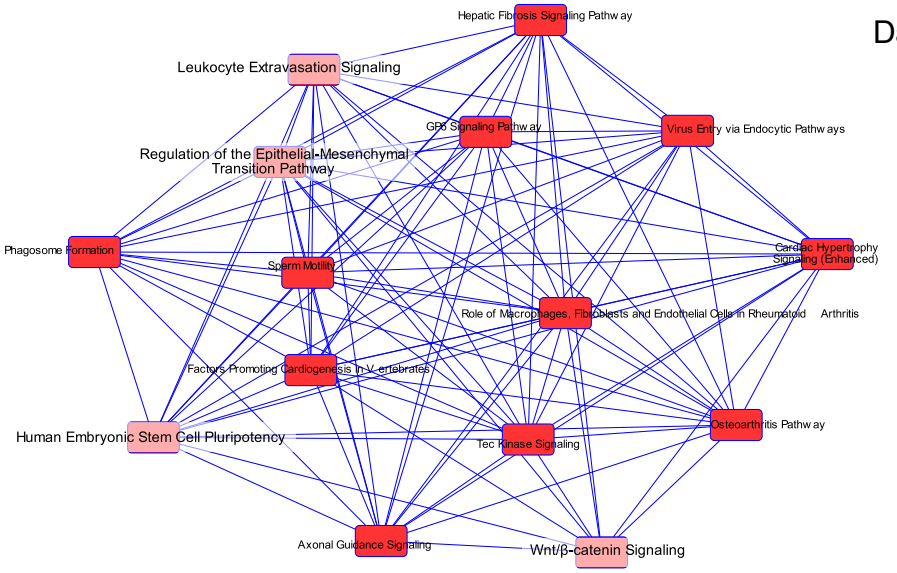

Day 6

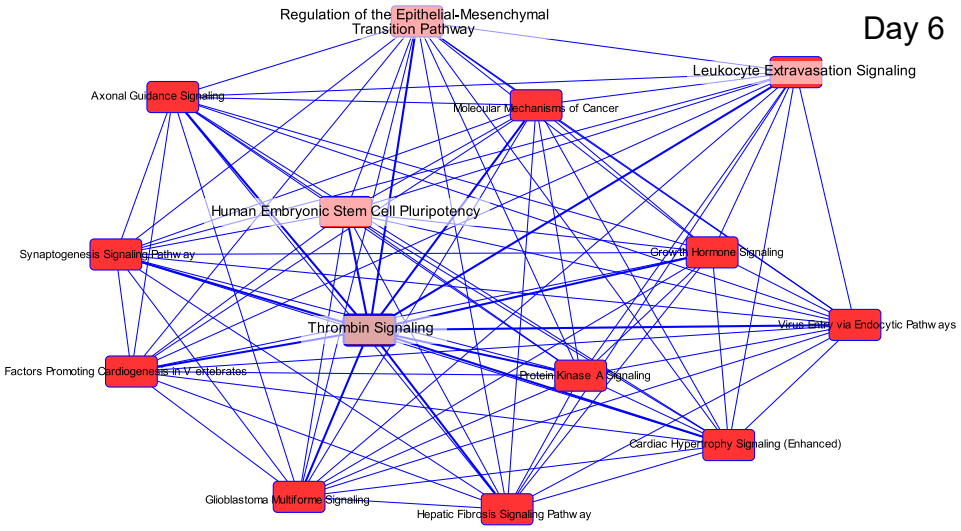

Figure 10: **Embryonic stem cell pluripotency pathway was deregulated between differentiated wt and Evi2a KO cells on day 4, day 5 and day 6.** The "core analysis" tool implemented in the ingenuity pathway analysis (IPA) software, was performed on differentially expressed genes between samples from wt day 4 vs Evi2a KO day 4, wt day 5 vs Evi2a KO day 5 and wt day 6 vs Evi2a KO day 6. Top 15 most deregulated canonical pathways of each time point are displayed. Blue line indicates a gene sets that is joined between pathways. Pathways relevant for hematopoietic specification are highlighted by a light red box.

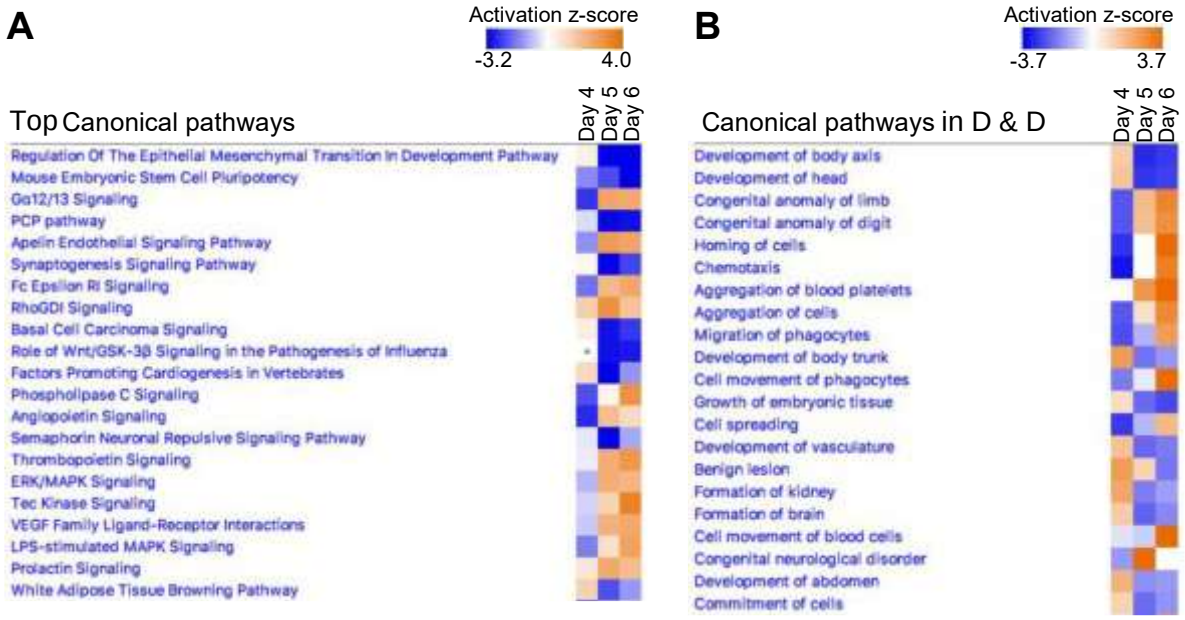

Figure 11: **IPA comparison analysis showing inactive and active pathways from wt vs Evi2a KO samples on day 4, day 5 and day 6 of differentiation.** IPA comparison analysis was performed on differentially expressed genes between cells from wt day 4 and Evi2a KO day 4, wt day 5 and Evi2a KO day 5, wt day 6 and Evi2a KO day 6. Blue color indicates a negative activation score (downregulated/non-active in wt cells), orange color indicates a positive activation z-score (upregulated/active in wt cells). A) Top most deregulated canonical pathways are shown. B) Top deregulated canonical pathways in development and disease (in D & D) are displayed.

2.2 Generation of a conditional Evi2a KO mouse model

Since we knew already from previous *in vitro* experiments that loss of Evi2a leads to a block in hematopoietic differentiation we wanted to investigate the functions of Evi2a *in vivo*. For this we aimed to generate an Evi2a KO mouse model.

A DNA vector was designed by Dr. Paul Kaschutnig such that the Evi2a coding sequence was flanked by cis arranged loxP sites (here referred to as Evi2a vector). With the support of the transgene service unit of the center for preclinical research core facility at the DKFZ, the Evi2a vector was transfected into Jm8a3 ESCs. Before microinjecting the transfected ESCs into embryonic day E3.5 blastocysts, we confirmed the insertion of the vector by PCR and sanger-sequencing. After confirming the presence of the flanked Evi2a gene in ESCs, these were injected into blastocysts and afterwards transferred into foster mothers, giving rise to brown (agouti) colored transgenic pups due to Jm8a3 cells expressing a dominant agouti gene[116]. To achieve germline transmission of the transgenic Evi2a flanked coding sequence we randomly selected 11 mice with 50% to 80% agouti fur color for further breeding with Ly5.1 mice. Due to the fact that the transgenic Evi2a gene was derived from an agouti background we could select for mice in the F1 generation with agouti fur color and be certain that these mice inherited the transgenic vector sequence.

In summary, we were able to achieve germline transmission by genetically modifying Jm8a3 ESCs, inserting these into E3.5 blastocysts from wt C57BL/6 mice, followed by the selection for agouti-colored mice and backcrossing to wt Ly5.1 mice.

2.2.1 Breeding strategy to globally delete Evi2a in mice

Since we successfully achieved germline transmission of the loxP flanked Evi2a vector (hereon referred to as Evi2a$^{wt/loxP\text{-}R}$ strain), we next aimed to generate an Evi2a KO mouse model. Figure 12 A-D schematically represents the required breeding steps. In brief, first the bacterial restriction cassette flanked by FRT sites had to be removed by crossing the Evi2a$^{wt/loxP\text{-}R}$ with a FLP deleter mouse. Next, these mice with a deleted resistance cassette (Evi2a$^{wt/loxP,FLP}$) were crossed to a CMV-cre recombinase expressing mouse strain to achieve ubiquitous deletion of Evi2a. These heterozygous Evi2a KO mice (Evi2a$^{wt/KO,\ Cre+}$) were then mated with a wt Ly5.1 strain to outbreed the cre recombinase. As a last step, we bred heterozygous Evi2a KO mice (Evi2a$^{wt/KO}$) to obtain homozygous Evi2a KO mice (Evi2a$^{KO/KO}$). Mendelian ratios indicated the probability of receiving the desired genotype displayed below in the breeding scheme (Figure 12). We performed extensive genotyping of each F1 generation to ensure the propagation of the correct phenotype.

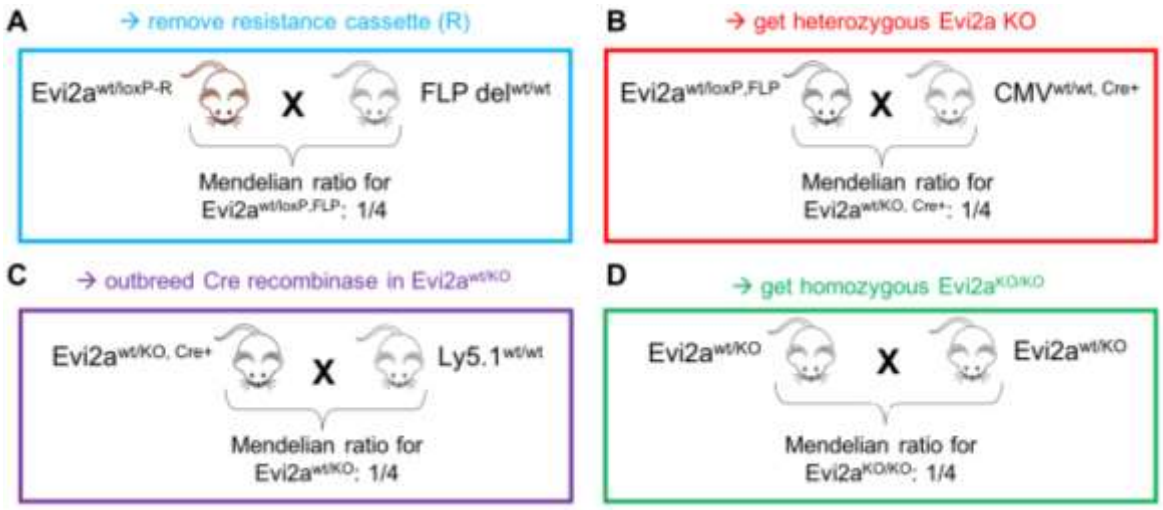

Figure 12: **Breeding strategy to obtain homozygous Evi2a KO mice.** A) Evi2a$^{wt/loxP\text{-}R}$ mice integrated the Evi2a vector construct into their germline. Brown color indicated their dominant agouti gene expression. These were crossed to FLP deleter mice and according to mendelian law ¼ of the offspring excised the antibiotic resistance cassette (R) and obtain heterozygous Evi2a$^{wt/loxP,FLP}$ mice. B) To delete Evi2a in all tissues Evi2a$^{wt/loxP,FLP}$ mice were crossed with a CMV-cre recombinase expressing mouse strain. According to mendelian law ¼ of the offspring excised the Evi2a gene, resulting in heterozygous Evi2a$^{wt/KO,Cre}$ mice. C) To remove the cre recombinase Evi2a$^{wt/KO,\ Cre+}$ mice were crossed with wt Ly5.1 mice. According to mendelian law ¼ of the offspring were heterozygous Evi2a$^{wt/KO}$. D) To obtain homozygous Evi2a$^{KO/KO}$ mice, heterozygous Evi2a$^{wt/KO}$ mice were crossed. According to mendelian law ¼ of the offspring showed a homozygous Evi2a deletion.

2.2.2 Heterozygous Evi2a KO mice are viable

To genotype transgenic Evi2a mice we made use of the resistance cassette for bacterial selection that was included in the vector construct. Even though it was cut out after FLP deletion, additional external base pairs remained which were targeted for the design of unique primers. Figure 13 A shows the section of the Evi2a vector that was recombined with the ESCs (see appendix section 10.3 for the whole vector map, Figure 40). Primer binding sites are indicated on the Evi2a vector section. Different primer combinations were tested to verify insertion of (i) complete Evi2a vector in Evi2a$^{wt/loxP\text{-}R}$ mice, (ii) FLP deletion of antibiotic resistance cassette in Evi2a$^{wt/loxP,FLP}$ mice and (iii) excision of loxP flanked Evi2a sites in Evi2a$^{wt/KO}$. Expected PCR fragment sizes are listed in Figure 13 B.

To verify insertion of the Evi2a vector we designed a forward primer (Pf) that bound to the homology arm (P8f) and reverse primer (Pr) that bound to the resistance cassette (P2r) resulting in a 4.2kb fragment size (Figure 13 C). Since P2r did not bind on the wt sequence nor on mice originating from a FLP deleter or CMV-cre breeding, no PCR band was expected for wt and loxP. Next, we designed primers such, that it would allow us to distinguish between mice with the full-length construct (loxP-R) and FLP deleted construct. We designed primers, P4f and P1r, that bound on the endogenous intron flanking the FRT enclosed restriction cassette (Figure 13 D). By including

loxP and FRT recombination sites approximately 100bp were added to the transgenic construct, hence a smaller PCR band was detected for wt mice than for FLP deleted transgenic mice (loxP). If the FLP deletion did not take place we obtained a 3kb fragment for the PCR with primers P4f and P1r. Additionally, we confirmed the FLP excision by using Primer P1f binding onto the loxP site which was placed in front of the FRT site together with P1r binding on the intron. With this primer combination (P1f and P1r) no PCR band from wt was expected (Figure 13 E). As a last step, we designed primers to verify the Evi2a KO. P32r bound downstream of the second loxP site located in the Evi2a exon. After FLP deletion the fragment size was 2.1kb and after CMV-cre excision the Evi2a KO genotype resulted in a fragment length of approximately 250bp. Since P1f did not bind on wt no band was detected for the wt control. However, as P1f was designed such that 50% of the primer sequence bound to the loxP site this could explain the unspecific band with approximately 250bp that was seen in PCR P1f and P32r (Figure 13 F).

A

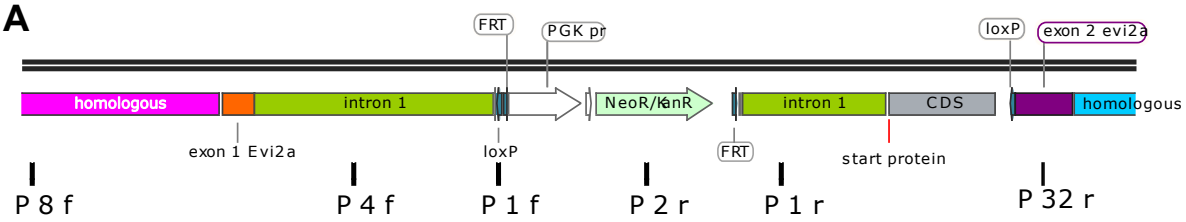

B

Expected band size / Primer combinations	WT	loxP-R (full construct)	loxP	KO
8 fwd – 2 rev	no band	4175 bp	no band	no band
4 fwd – 1 rev	1226 bp	2915 bp	1365 bp	no band
1 fwd – 1 rev	no band	1940 bp	356 bp	no band
1 fwd – 32 rev	no band	3701 bp	2117 bp	246 bp

C Primer 8 fwd - 2 rev

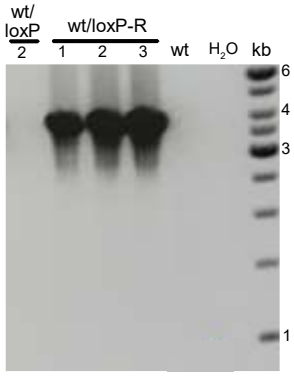

D Primer 4 fwd - 1 rev

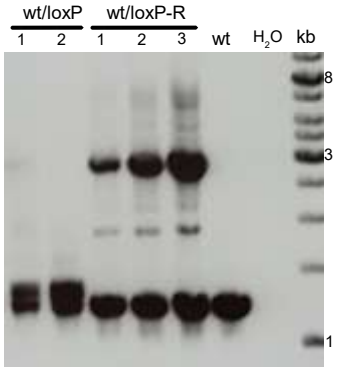

E Primer 1 fwd - 1 rev

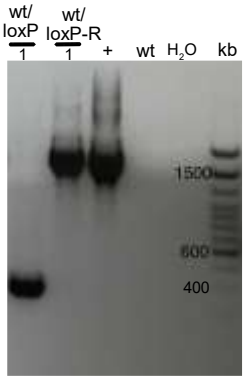

F Primer 1 fwd - 32 rev

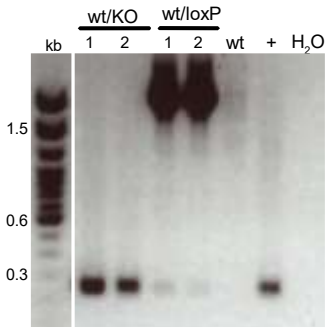

Figure 13: **Genotyping of Evi2a$^{wt/loxP,FLP-R}$ Evi2a$^{wt/loxP}$ and Evi2a$^{wt/KO}$ mice strains to validate germline transmission**. A) Schematic representation of the section from the Evi2a vector that was integrated into ESCs via homologous recombination. "Intron1" represents intron 27b of the Nf1 gene. Resistance cassette (neomycin and kanamycin resistance under control of the PGK promoter) was flanked by FRT sites and Evi2a coding sequence was flanked by loxP sites. Primer (P) binding sites and forward (f) or reverse (r) orientation are indicated below the sequence. CDS = coding sequence of Evi2a. B) Four different PCR reactions were carried out to determine the genotype of the mice. The table listed the expected fragment sizes in base pairs (bp) for each genetic background. C-F) Exemplary pictures from agarose gel of the PCR reactions, performed on purified DNA from indicated mouse models. Reference DNA sizes are indicated by the DNA ladder (kb). Numbers (1, 2, 3) indicates the mouse ID of the respective strain.

2.2.3 Hematopoietic parameters were normal in one-year old Evi2a$^{KO/wt}$ mice

After having characterized the genotype of mice we monitored the health status of heterozygous Evi2a$^{KO/wt}$ mice. Up until the point when the thesis was written 49 pups were born from several different Evi2a$^{KO/wt}$ breeding pairs. 36 pups were identified as heterozygous for Evi2a and 13 were identified as wt. Importantly, to date no homozygous Evi2a$^{KO/KO}$ mice have been obtained. Suggesting, that the potentially delayed Evi2a KO that we observed in the RNA seq analysis, could have detrimental effects *in vivo*, which might be embryonic lethality. In order to monitor hematologic parameters of heterozygous Evi2a$^{KO/wt}$ mice, peripheral blood from young and old heterozygous Evi2a$^{KO/wt}$ mice was analyzed for white blood cell counts, platelet counts, hemoglobin content and red blood cell counts (Figure 14 A-D, respectively). Control data from wt mice was generated by Dr. Bogeska and kindly provided as reference values. We could not observe any significant differences in PB parameters between wt and Evi2a$^{KO/wt}$ mice. Notably, most of the PB parameters were still within a normal range which was indicated by the grey background[117,118]. Interestingly, platelet counts increased with age (up to 36-week-old mice) but unfortunately, we only had two old, aged mice and were not able to verify the gradual increase in platelet counts further. However, it is known that platelet counts increase with age and we could confirm this on our data[119]. RBCs in 30-week-old wt mice were increased (12.5 ± 0.8 x 10^6 RBCs/µl) in comparison to 12-week-old mice (10.3 ± 0.1 x 10^6 RBCs/µl). However, RBC counts went back to a normal level, with 8.6 ± 1 x 10^6 RBCs/µl measured in 58-week-old wt mice. No change was measured in RBCs of Evi2a$^{KO/wt}$ mice. Next, we examined the bone marrow compartment and counted femur cellularity of Evi2a$^{KO/wt}$ mice (Figure 14 E). Femur counts from Evi2a$^{KO/wt}$ were similar to femur counts in wt mice (Figure 20 B and Figure 23 B), hence, within a normal range.

In summary, we were able to monitor heterozygous Evi2a$^{KO/wt}$ mice up until one year of age and did not observe any adverse hematopoietic blood parameters. Additionally, femur counts were also within a normal range. We had strong evidence to assume that a homozygous Evi2a deletion is embryonically lethal, in line with the *in vitro* differentiation data that suggested that Evi2a was essential for blood cell differentiation.

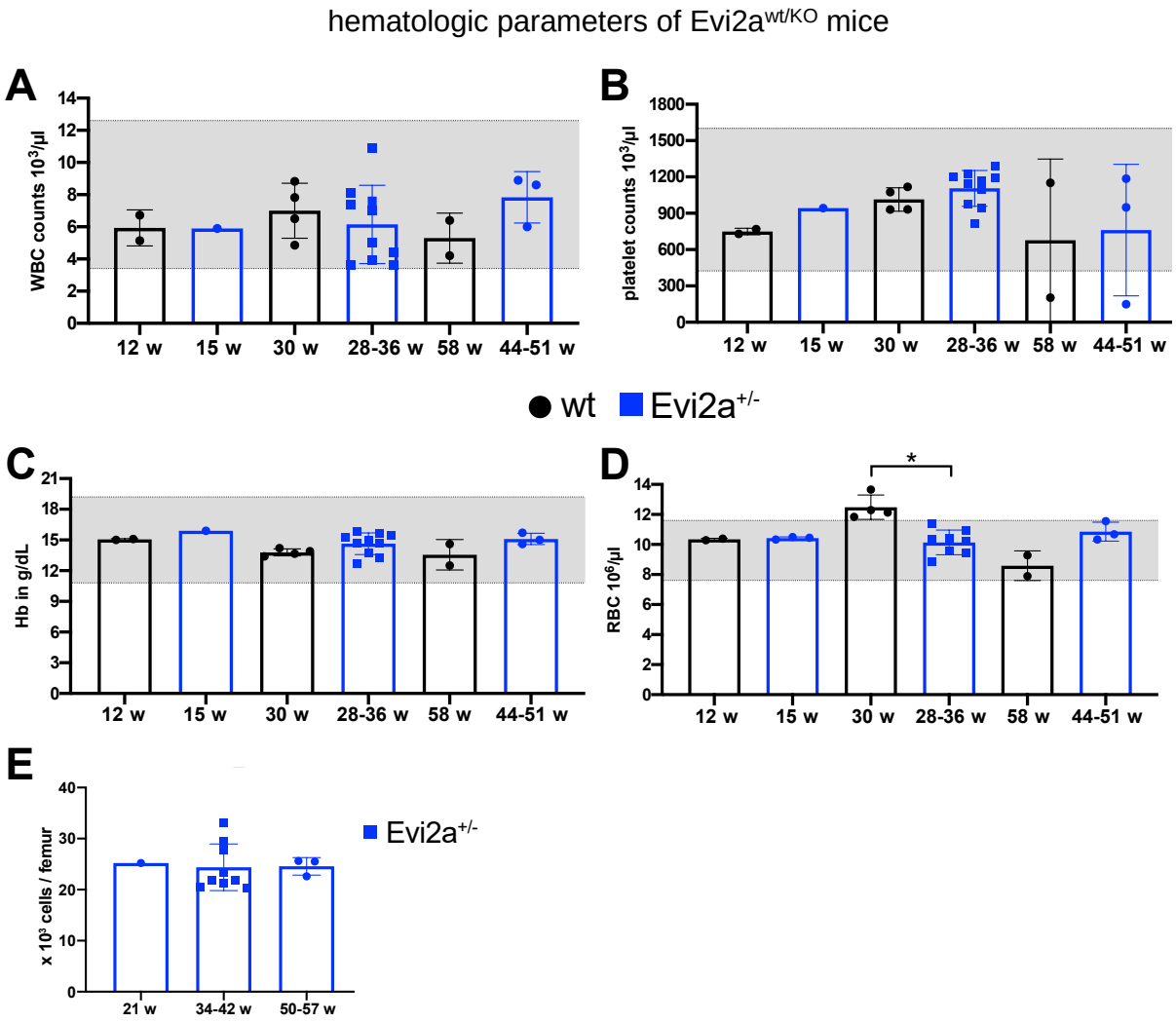

Figure 14: **Peripheral blood parameters of Evi2a$^{KO/wt}$ were in a normal range.** A-D) Peripheral blood was drawn from the vena facialis of Evi2a$^{KO/wt}$ mice of different age (w = week) and analyzed using an automated hematology analyzer (scil vet). Wt control mouse data was generously provided by Dr. Bogeska. Grey background indicates the normal range. E) Evi2a$^{KO/wt}$ mice were sacrificed, femurs flushed and counted.

2.2.4 Timed mating with heterozygous Evi2a KO mice

Since we did not obtain any homozygous Evi2a KO mice from our breedings, we hypothesized that homozygous Evi2a KO might be embryonically lethal. In order to test this hypothesis and identify at which time point the homozygous Evi2a deletion is embryonically lethal, we set up three timed matings each containing one male Evi2a$^{KO/wt}$ and one female Evi2a$^{KO/wt}$ mouse (see breeding scheme in Figure 12 D). We decided to sacrifice pregnant mice on day E10.5 as mature HSCs have not emerged yet but hematopoietic structures should have already formed. The AGM was clearly visible harboring the dorsal aorta (Figure 15). EHT has presumably already taken place around E9/E9.5[120,121]. Out of 17 embryos we observed one that was already degraded. Unfortunately, we could not obtain any cells for genotyping from this single embryo. Of the remaining 16 embryos

we isolated DNA and genotyping was performed by Theo Aurich. Only heterozygous Evi2a$^{KO/wt}$ embryos were identified. However, since we had no experience in isolating embryos, we assume that embryos were contaminated with maternal Evi2a$^{KO/wt}$ material and therefore we obtained only heterozygous results. This hypothesis is supported by the fact, that we also did not obtain any wt mice from the genotyped embryos.

In summary, up to now we do not know whether homozygous Evi2a deletion led to embryonic lethality. Since our embryo isolation was not very accurate, we have repeated the timed mating experiments but data was not available at the time of writing this thesis.

Figure 15: **Fully developed E10.5 embryos were obtained from the homozygous Evi2a$^{KO/KO}$ breeding setup**. Pregnant female mice were sacrificed, subsequently the uterine horn extracted, then decidua, amniotic sac and placenta were removed. The picture shows a representative embryo isolated on E10.5 and was viewed at 2x magnification. Picture was taken by Theo Aurich.

3 Results – Part two

In this part of the project, we wanted to evaluate the impact of repeated stimulation and activation of hematopoietic stem cells. It is already known that inflammation-induced activation of HSCs leads to their functional decline and to an increased risk of developing adverse or even malignant bone marrow compositional changes[44]. For the current line of investigation, we decided to use thrombopoietin (TPO) and the TPO mimetic Romiplostim (Rom) as stimulating agents, for several reasons. Firstly, TPO and Rom lead to HSC activation and proliferation[44,122], secondly their impact on HSCs is ambiguous and thirdly, TPO mimetics are used in the clinics. The ambiguity regarding TPO function is that TPO has been proposed to both maintain HSC quiescence while conversely promoting HSC expansion and self-renewal divisions[77,80].

By using a range of treatment regimens and different mouse models, we aimed to determine how repetitive TPO-induced activation impacts on hematopoietic stem cell function, and whether it leads to bone marrow failure or if mice show any other adverse side effects.

3.1 Increased platelet counts after single Romiplostim treatment

Based on the results of a previous study performed in our laboratory, we formulated our hypothesis that every HSC division reduces its functional potential to some degree and that perfect self-renewal divisions do not occur. In the previous study, the dsRNA mimetic polyI:C-induced HSC proliferation resulted in a progressive and irreversible decrease in HSC potency[62]. We therefore aimed to conduct our experiments in a similar way, in order that we could directly compare our results from the TPO and Rom experiments to previous studies carried out with polyI:C.

Before initiating experiments involving repeated Rom treatment, we first performed an empirical dose finding study to establish a dosage that would enforce HSC proliferation to a similar extent as that observed with polyI:C and recombinant murine TPO (in the following sections only referred to as TPO) (200µg/kg). We used four different Rom doses ranging from 5µg/kg to 375µg/kg per mouse and as a reference control for LT-HSC activation we used polyI:C (5mg/kg), phosphate-buffered saline (PBS) was used as a baseline control due to all reagents being dissolved in PBS. The injection with 5µg/kg Rom did not induce any HSC activation 24h after the treatment. In contrast, a single injection with 375µg/kg Rom led to a pronounced HSC activation which was much higher than observed after polyI:C-induced LT-HSC activation. After a single injection of 375µg/kg Rom nearly all (97% ± 0.2% of LT-HSCs) exited G0-phase of the cell cycle whereas only 22% ± 9% of polyI:C stimulated LT-HSCs exited the G0-phase (Figure 16). As we intended to compare the results

from this study to the previously conducted experiments with polyI:C, we only show the experiments conducted with 50µg/kg and 100µg/kg Rom in the following section.

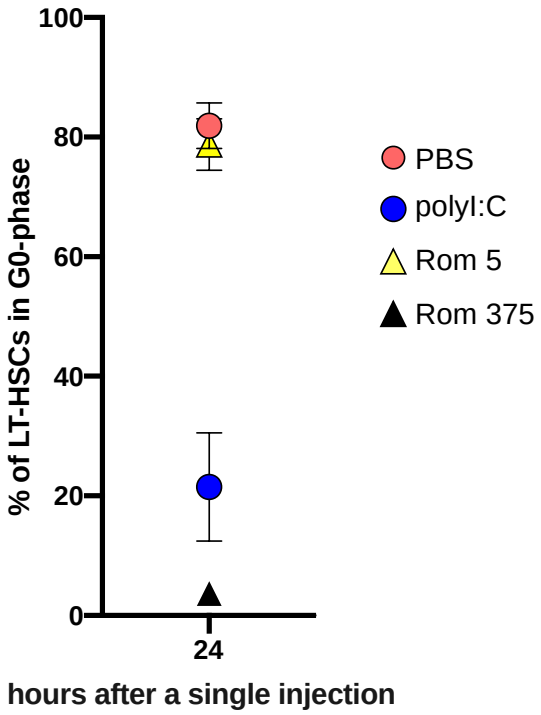

Figure 16: **High concentration of Romiplostim leads to activation of nearly all LT-HSCs**. Mice were injected once with either PBS (homeostatic control), polyI:C (positive control for activation), Rom 5µg/kg or Rom 375µ/kg and sacrificed 24h after the injection. BM was analyzed and stained for Ki67/Hoechst to examine cell cycle activity.

PBS and Rom: n=3, polyI:C: n=2. Since only two mice were treated with polyI:C we did not perform any statistical analysis.

Since Rom was developed to increase platelet counts in patients, we analyzed the capacity of Rom to induce platelet production in mice. Additionally, we also monitored white blood cell counts (WBCs), femur cellularity as well as absolute numbers of LT-HSCs in the bone marrow (BM). For the empirical dose finding study, mice were treated only once and hematologic parameters were observed every 24h up to 96h after the injection (Figure 17 A). Results from PBS treatment were used as reference and at 24h after the agonist injection the WBC counts decreased for all treatments However, WBC counts from Rom 50µg/kg and Rom 100µg/kg treated mice dropped the least and remained at a constant level throughout the time course at around 8 ± 1.2 x 10^3 WBCs/µl blood and 8.5 ± 1.5 x 10^3 WBCs/µl blood, respectively. In contrast, at 24h after the injection WBCs of TPO and polyI:C treated mice dropped to 6 ± 0.1 x 10^3 cells/µl and 1.5 ± 0.5 x 10^3 cells/µl, respectively. After 96h WBCs returned to levels within the normal range which is indicated by the gray background[117,118] (Figure 17 B). Platelet counts remained unchanged after polyI:C injection but rose upon Rom and TPO treatment (Figure 17 C). It can be noted that Rom

induced platelet production more efficiently than TPO, 1.4-fold higher platelet levels were measured at 96h after Rom 50µg/kg treatment and 1.6-fold at 96h after Rom 100µg/kg treatment. However, changes were neither significant throughout the time course nor 96h after the treatment.

Next, since Rom, polyI:C and TPO also affect the cells residing in the bone marrow, we measured femur cellularity. We observed that femur cellularity remained constant after Rom injection but was slightly increased after TPO treatment and stabilized at an elevated level. After TPO treatment we observed an average femur cellularity of 28 ± 2.7 x 10^6 cells/femur throughout the observed period, whereas we measured 23 ± 2.2 x 10^6 cells/femur for PBS control mice. 24h after polyI:C treatment femur cellularity decreased by 1.8-fold compared to PBS but turned back to control level over time. As such, femur cellularity changes were lost after 96h and no significant differences were observed (Figure 17 D). Exemplary FACS plots shown in Figure 17 E display the gating strategy for LT-HSCs. First, we excluded doublets and lineage positive cells (panels 2 and 4, respectively), then gated on Sca-1^+c-Kit^+ cells and subsequently on $CD150^+CD48^-$ HSCs, as seen in panel 6. We defined LT-HSCs in this thesis as $CD34^-$ HSCs. We were interested whether alterations in femur cellularity affected the absolute number of LT-HSCs. Absolute LT-HSC numbers remained constant upon polyI:C injection. Whereas after the Rom treatment LT-HSC counts increased but not to such a strong extent as after the TPO treatment. This effect was only temporary and 96h after the TPO treatment LT-HSC counts went back to a homeostatic level at approximately 1706 ± 826 LT-HSCs (Figure 17 F).

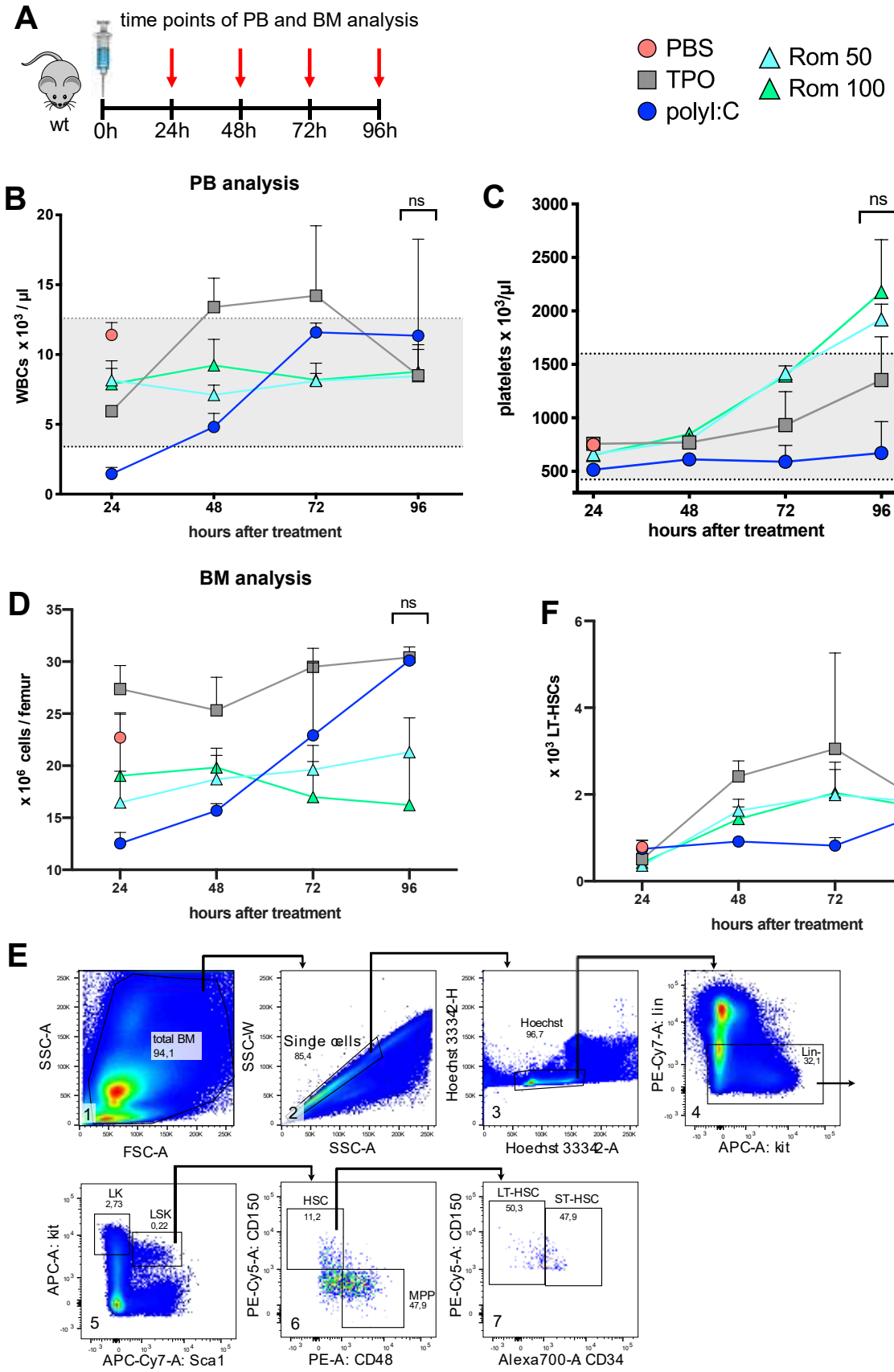
A
time points of PB and BM analysis
wt
0h
24h
48h
72h
96h
PBS
TPO
polyI:C
Rom 50
Rom 100
B
PB analysis
WBCs x 10³ / µl
hours after treatment
ns
C
platelets x 10³/µl
hours after treatment
ns
D
BM analysis
x 10⁶ cells / femur
hours after treatment
ns
F
x 10³ LT-HSCs
hours after treatment
ns
E
SSC-A
FSC-A
total BM
94,1
SSC-W
SSC-A
Singe cells
85,4
Hoechst 33342-H
Hoechst 33342-A
Hoechst
96,7
PE-Cy7-A: lin
APC-A: kit
Lin-
32,1
APC-A: kit
APC-Cy7-A: Sca1
LK
2,73
LSK
0,22
PE-Cy5-A: CD150
PE-A: CD48
HSC
11,2
MPP
47,9
PE-Cy5-A: CD150
Alexa700-A CD34
LT-HSC
50,3
ST-HSC
47,9

Figure 17: **Single Rom injection resulted in temporarily increased WBC, platelet and LT-HSC counts**. A) Mice were treated once with Rom, TPO, polyI:C or PBS. PB and BM parameters were monitored 24h, 48h, 72h and 96h after the injection. B) WBCs were monitored over time after a single injection with PBS, TPO, polyI:C or Rom. Grey background indicates the normal WBC range. C) Platelet counts were monitored over time after a single injection of the indicated treatment. Grey background indicates the normal platelet range. D) Exemplary FACS plots show the gating strategy for LT-HSCs (lineage$^-$Sca-1$^+$c-Kit$^+$CD150$^+$CD48$^-$CD34$^-$. Numbers on the bottom left and arrows indicate subsequent gating strategy. Numbers in the plot indicate percentage of parent population. E) BM cellularity was determined by counting flushed femur cells. F) LT-HSC numbers were calculated using femur counts and percentage of LT-HSCs of 20 mil stained and analyzed BM cells.

Data represents mean and error bars SD, ns: no statistical significance, Rom 50/Rom 100: 50µg/kg or 100µg/kg Rom injected PBS, polyI:C, TPO treatment: n=2, Rom treatment: n=3

Since platelets are produced by Megakaryocytes (MKs)[123], we next assessed whether we induced an increase in MKs after treatment. Therefore, BM cells were stained for MK markers CD41 and CD42d (Figure 18 A, panel 4). As MK polyploidy increases upon activation and upon an increased demand of platelets[124], we also stained MKs with Dapi to examine ploidy (Figure 18 A, panel 5). Surprisingly, at 24h after TPO or Rom injections we did not observe an increase in MK cells nor a change in MK ploidy (Figure 18 B-C) even though, as seen before, TPO and Rom activated MKs and produce platelets. However, at 24h after injection we also did not see an increase in platelet counts (Figure 17 C). Interestingly, at 24h after the polyI:C treatment we saw a 3.7-fold increase in MK percentage.

In summary, although Rom treatment led to a higher platelet production it did not affect other peripheral blood (PB) or bone marrow parameters. It should be noted that due to technical issues, we could not obtain three data points for all conditions, hence statistical analysis was not performed. These experiments should be repeated to enhance significance of the results. Nevertheless, we observed a small variability between the available data points which allowed us to draw preliminary conclusions.

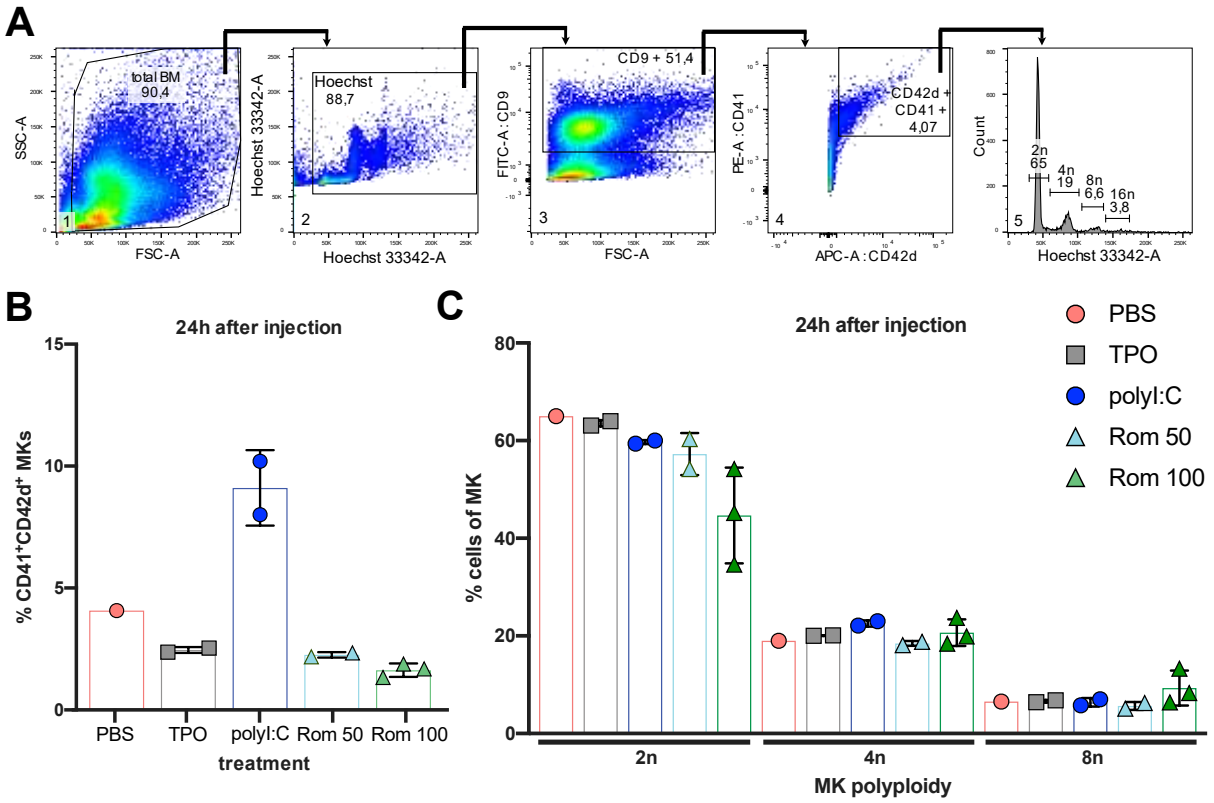

Figure 18: **Increase in megakaryocytes (MKs) in the BM 24h after polyI:C injection**. A) Representative FACS plots of MK staining from a PBS control mouse. BM cells were stained, fixed and flow cytometrically analyzed. Arrows and numbers on the bottom left indicate gating strategy. The third gate defines $CD9^+$ cells and fourth gate is set on mature $CD42d^+CD41^+$ MKs. To determine ploidy a histogram of Hoechst fluorescence was plotted, see panel 5. B) Percentage of $CD42d^+CD41^+$ cells of all $CD9^+$ cells was plotted, 24h after the injection. PBS: n=1, TPO, polyI:C, Rom 50µg/kg: n=2, Rom 100µg/kg: n=3. C) MK ploidy from all treatments was assessed 24h after the injection. PBS: n=1, TPO, polyI:C, Rom 50µg/kg: n=2, Rom 100µg/kg: n=3

Since only two data points were obtained, no statistical analysis was performed.

3.1.1 Romiplostim-induced LT-HSC activation was similar to TPO- or polyI:C-induced LT-HSC activation

After having examined PB and general BM parameters, cell cycle status of LT-HSCs was assessed next. wt mice were injected once with either Rom, TPO, polyI:C or PBS and the activation status of LT-HSCs was compared by determining percentage of cells in G0-phase. For this we stained BM cells from mice 24h, 48h, 72h and 96h after treatment for Ki67 expression (see Figure 17 A for treatment schedule). Ki67 is a protein that participates in ribosomal biogenesis and mitotic chromosome separation and has been shown to be upregulated in active phases of the cell cycle while being downregulated in quiescent (G0-phase) cells. Ki67 is typically used in combination with a DNA intercalating dye, such as Hoechst or Dapi, to detect cells in G0, G1 (2n chromosome set) and SG2M (4n chromosome set) phases[125]. The cell cycle gating strategy is shown in Figure 19 A in exemplary FACS plots from a PBS control mouse. Ki67 is plotted against Hoechst (or Dapi) and cells

in G0-phase can be found in the Ki67-negative fraction. Cells in G1-phase are Ki67-positive but have not increased their DNA content above 2n yet, whereas cells in SG2M phase have partially or fully duplicated their DNA and harbor DNA content ranging between >2n and 4n and express Ki67. The Ki67/Hoechst plot, highlighted in grey, shows LT-HSCs from a TPO treated mouse 24h after the injection. The majority of the cells were activated upon TPO treatment and 60% of LT-HSCs were in G1-phase and 18.5% in SG2M-phase. Figure 19 B shows the time course of LT-HSC activation after a single injection. Under homeostatic conditions most of the LT-HSCs remained in a quiescent state shown by 82% ± 4% of LT-HSCs in G0-phase. Activation induced by TPO or polyI:C exhibited a similar activation pattern with approximately 20% of LT-HSCs in G0-phase after 24h and 48h of injection (19.6% and 17.2% 24h and 48h after TPO treatment and 21.5% and 20.9% 24h and 48h after polyI:C treatment). LT-HSCs quickly returned to pre-treatment levels and after 72h approximately 70% were back in G0. At 96h after the injection majority of LT-HSCs had again reached their quiescent state and had left the active cell cycle. Treatment with 50µg/kg and 100µg/kg Rom concentrations led to a similar transient cell cycle activation of LT-HSCs. At 24h after the injection approximately 20% of LT-HSCs remained in G0 while at 48h post-injection already 40% of LT-HSCs were back in G0. After 72h, cells from mice stimulated with 50µg/kg Rom were back up to baseline with 79% ± 9% of LT-HSCs in G0 whereas only 57% ± 15% of LT-HSCs from 100µg/kg Rom treated mice were in G0-phase. 96h after the injection most cells had stopped cycling and returned to baseline. Since we only wanted to proceed with one Rom dose and in order to better decide which Rom concentration to use, we took a more detailed look at cell cycle results from TPO, Rom 50µg/kg and Rom 100µg/kg treated mice. No significant differences between the groups were detected. However, 72h after the injection double the percentage of cells from the Rom 100µg/kg group in comparison to the TPO or the Rom 50µg/kg group were still in SG2M phase (11.5% ± 2% and 5.5% ± 1%, respectively) (Figure 19 C). Hence, for further experiments we decided to use an intermediate dose of 75µg/kg Rom, as we can achieve a profound activation of LT-HSCs which was comparable to the activation capacity of TPO and polyI:C.

In summary, we were able to induce cycling of LT-HSCs using Rom and, with an appropriate treatment dosage, could faithfully reproduce a similar LT-HSC cell cycle activation response to that observed after TPO or polyI:C injections. For further Rom treatment experiments we used 75µg Rom per kg mouse weight.

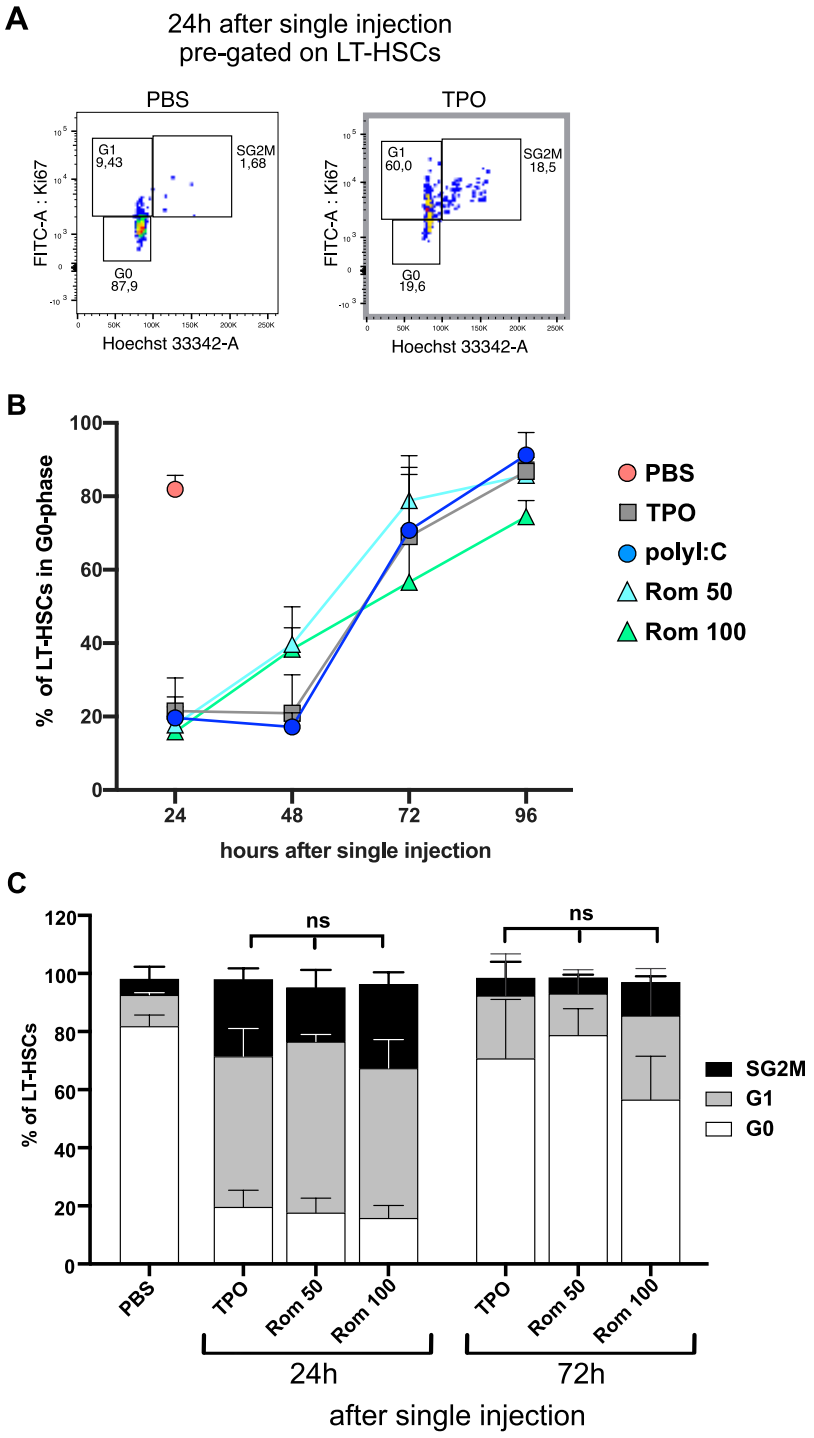

Figure 19: **Single Rom injection pushed hematopoietic stem cells into cycle.** A) Exemplary FACS plots from Ki67/Hoechst staining of total BM cells from PBS control mouse already pre-gated on LT-HSCs. Three different cell cycle phases (G0, G1, SG2M) can be distinguished. Exemplary plot on the right side was pre-gated on LT-HSCs 24h after TPO injection. B) Time course of LT-HSCs in G0-phase from different treatments. Mean % of LT-HSCs in G0-phase is shown. C) Different cell cycle phases of LT-HSCs from PBS control or TPO, 50µg/kg Rom and 100µg/kg Rom treated mice 24h and 72h after the injection. ns: no statistical significance.

PBS, TPO and polyI:C: n=2, all Rom treated mice: n=3.

3.2 Serial treatment of mice with Rom and TPO to investigate HSC exhaustion in a non-inflammatory setting

3.2.1 Repeated activation of HSCs with Rom does not lead to a functional decline of HSCs

Immune thrombocytopenic purpura (ITP) patients receive not only one treatment with the TPO mimetic Romiplostim but rather receive Rom for several weeks or even years in some cases. Most of the patients tolerate Rom treatment well, however, approximately 5% of patients showed an increase in reticulin in the BM[126]. Even though this condition was reversed after discontinuation of Rom treatment an increase in reticulin is often an indication for bone marrow fibrosis[127]. We aimed to investigate long-term treatment effects of Rom on blood and BM parameters of mice.

Of note, in the dose finding experiments described above, we observed a 2.6-fold increase in platelet counts 96h after a single Rom injection (Figure 17 C). Since we did not follow up on platelet levels further, we did not know whether platelet counts remained on a high level or returned to baseline levels. Due to the fact that we used healthy and not platelet-deficient mouse models, we decided to start with only a few injections of Rom treatment to not risk mice getting thrombocytosis after an extended Rom treatment. Since our group already had experience in serially treating mice, we applied the same treatment schedule which would also enable us to compare our experiments to previous serial LT-HSC activation experiments[44]. The treatment regimen consisted of two injections weekly for a period of four weeks followed by a four-week recovery period, which will be referred to as one round of treatment from now on. An additional one-week recovery period was added after one round (Figure 20 A). After one round no significant changes were detected in femur cellularity nor in LT-HSC counts (Figure 20 B-C). However, a slight increase in LT-HSC numbers in Rom treated mice was observed. On average we detected an approximately 1.8-fold increase of LT-HSC counts in Rom-treated wt mice and a 1.3-fold increase in LT-HSCs of Rom-treated UBC-GFP mice. However, since results were variable within one group, the difference in LT-HSCs counts were not statistically significant (in wt mice: p-value > 0.06, in UBC-GFP mice: p-value > 0.6).

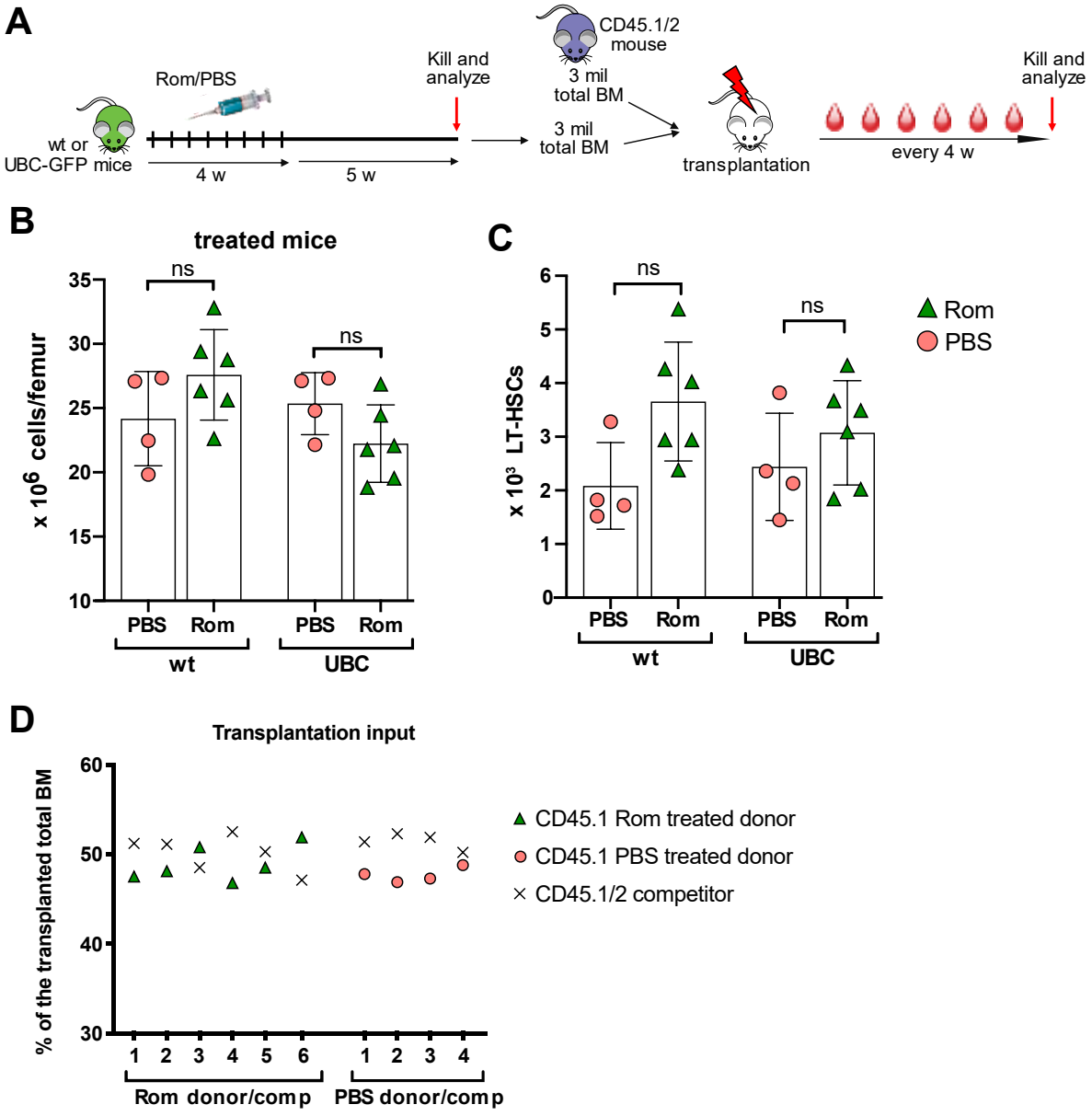

Figure 20: **No adverse effects of Romiplostim treatment on BM composition**. A) Treatment schedule is displayed. wt or UBC-GFP mice were treated with Romiplostim or PBS for one round: 2 injections weekly for four weeks with a subsequent recovery period of four weeks. One additional week of recovery was added. Donor bone marrow (BM) was isolated and transplanted together with 3 million (mil) total BM cells from CD45.1/2 competitor mice into lethally irradiated CD45.2 recipient mice. Recipient mice were bled every 4 weeks for in total 6 months. B) Femurs of PBS and Rom treated wt and UBC-GFP mice were flushed to assess femur cellularity. C) Absolute LT-HSC number per femur was determined after flow cytometric analysis of BM cells. D) Transplantation input was FACS analyzed and CD45.1 and CD45.1/2 proportion of the total input displayed as percentage. The analyzed input shown is from the competitive transplantation of UBC-GFP treated donors and CD45.1/2 competitors. Rom treated mice: n = 6, PBS treated donors: n = 4. ns = no statistical significance

As bone marrow or HSC transplantations are the gold standard to examine HSC function, we performed competitive transplantation assays in this experiment. A such, we mixed total BM cells from donor and competitors in a 1:1 ratio and transplanted it into lethally irradiated recipient mice (Figure 20 A). To be able to distinguish donor, competitor and recipient cells, we made use of the two isoforms of the pan-hematopoietic marker CD45. Treated donor mice expressed CD45.1, competitor cells expressed CD45.1 and CD45.2 (CD45.1/2) and recipients expressed CD45.2. By FACS analysis these populations could be easily distinguished. We FACS analyzed the transplantation input to be sure that a 1:1 ratio was achieved (Figure 20 D). After transplantation recipient mice were bled every four weeks for six months and CD45.1 chimerism was assessed in the blood via FACS analysis. Exemplary FACS plots, shown in Figure 21 A, indicate the gating strategy. Residual CD45.2 cells were observed in the blood (see panel 5) however, this proportion was usually small, on average less than 5% in our experiments, and excluded from the donor chimerism analysis. Panel 6 shows the gating for the CD45.1 donor chimerism. 12 weeks after transplantation donor chimerism in the wt treated Rom group (mean chimerism 57%) was higher than from the wt PBS treated control group (mean chimerism 39%) but did not prove to be significant (p-value > 0.1). 24 weeks after transplantation donor chimerism from wt mice was still similar (mean chimerism of 59% for wt Rom group, mean chimerism of 40% for wt PBS group, p-value > 0.06). We could observe a similar trend for CD45.1 chimerism from UBC-GFP treated mice, even though the overall chimerism from UBC-GFP was lower than that from wt mice. Of note, it has been shown before that UBC-GFP mice in general show decreased chimerism[103]. The huge variability in donor chimerism within the wt PBS control group, ranging from 12% to 64% chimerism was striking. We could not find a reason for this variability since the ratio from the transplantation input was almost 1:1 and the transplantation itself went well (Figure 20 D).

Since a myeloid bias is an indication for BM failure[44] and HSC dysfunction, we also stained blood for T-cell (CD4, CD8), B-cell (B220) and myeloid cell markers (CD11b and Gr-1). We first gated on the CD45.1^{+} cells (panel 6 in Figure 21 A) and subsequently examined the percentage of myeloid cells of the whole CD45.1 donor compartment (panel 7 in Figure 21 A). By comparing PBS to Rom samples, we can estimate whether the myeloid compartment is increased in Rom donors. No significant difference could be observed between PBS and Rom treated groups from wt or UBC-GFP donors (Figure 21 C). The use of the UBC-GFP mice enabled us to additionally assess platelet chimerism in CD45.2 recipients since platelets do not express CD45 on their surface. We also stained PB from UBC-GFP recipients for platelets 24 weeks after transplantation (Figure 21 D). Ter119-negative, CD41-positive and GFP-positive platelets (panel 5 in Figure 21 D) were used to determine donor chimerism. We could observe a slightly higher platelet contribution to the PB from Rom treated mice. However, the difference compared to the PBS control was not significant (p-value = 0.1, Figure 21 E). We could only record data from three mice of each group as one mouse died throughout the 24 weeks and two mice of the Rom cohort had to be excluded from

the experiment due to technical reasons. The genotype of these mice was falsely annotated as GFP^+, but only GFP^- cells were detected.

In summary, although Rom activated and induced cycling of LT-HSCs we did not see any adverse effects on the BM composition nor any engraftment defect nor any biased contribution to the PB compartments, as previously observed when using polyI:C[44] or 5-FU[128] as stimulating agent. On the contrary, we could observe a trend in both, wt and UBC-GFP donors, that serial Rom treatment conferred an engraftment advantage to the transplanted cells. In order to obtain statistical significance more datapoints should be added.

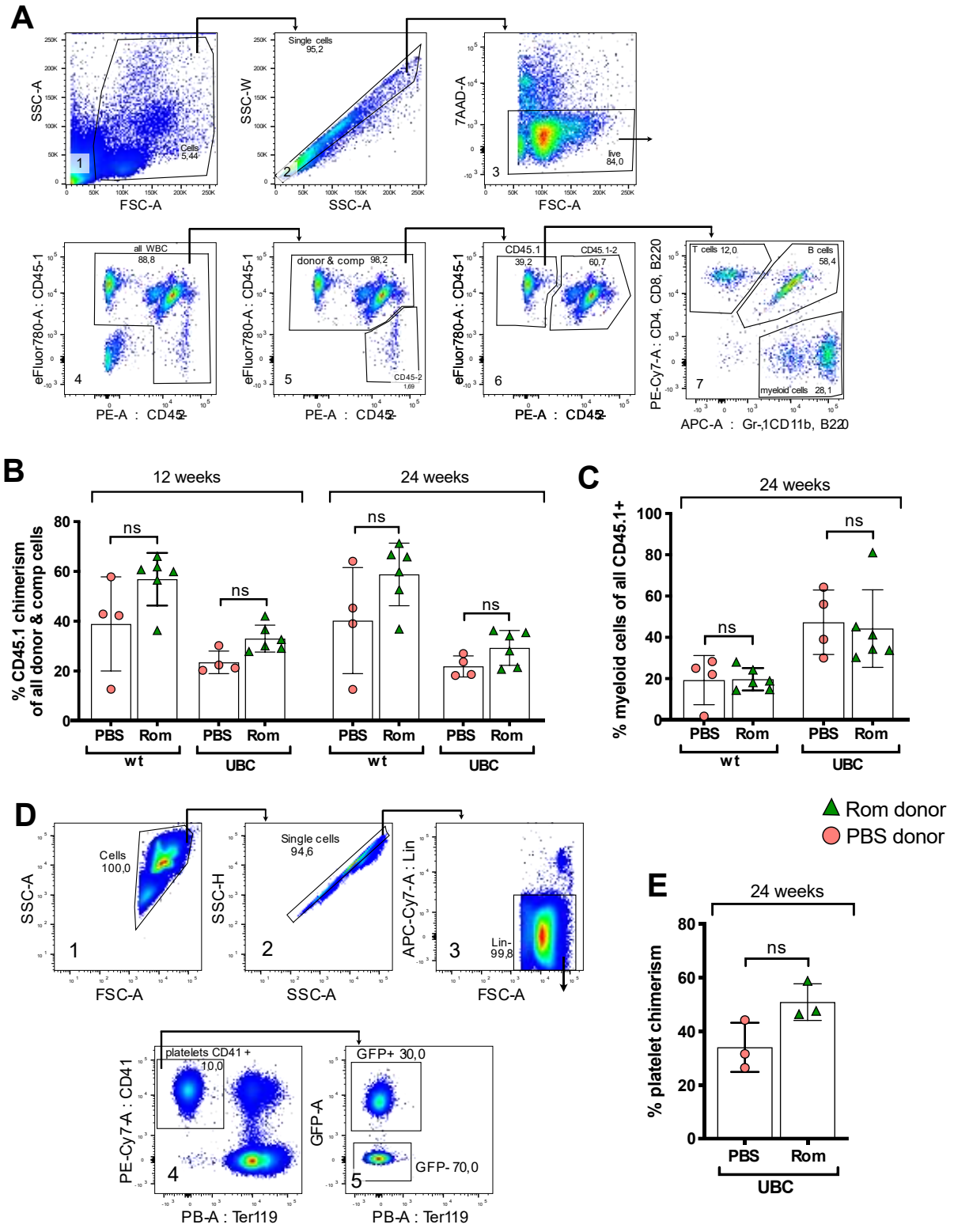
A
SSC-A
FSC-A
Cells 5,44
Single cells 95,2
SSC-W
SSC-A
7AAD-A
live 84,0
all WBC 88,8
eFluor780-A : CD45-1
PE-A : CD45-2
donor & comp 98,2
CD45-2 1,69
CD45.1 39,2
CD45.1-2 60,7
T cells 12,0
B cells 58,4
myeloid cells 28,1
PE-Cy7-A : CD4, CD8, B220
APC-A : Gr-1CD11b, B220
B
12 weeks
24 weeks
% CD45.1 chimerism of all donor & comp cells
ns
PBS
Rom
wt
UBC
C
24 weeks
% myeloid cells of all CD45.1+
D
Cells 100,0
Single cells 94,6
SSC-H
APC-Cy7-A : Lin
Lin- 99,8
platelets CD41 + 10,0
PE-Cy7-A : CD41
PB-A : Ter119
GFP+ 30,0
GFP-A
GFP- 70,0
Rom donor
PBS donor
E
24 weeks
% platelet chimerism

Figure 21: **Rom treatment did not lead to loss of HSC function.** A) Exemplary FACS plots of peripheral blood chimerism. Numbers on the bottom left and arrows indicate the sequence of gating strategy. Numbers next to the labeled population indicate the percentage. The sixth gate was used to assess the CD45.1 chimerism in peripheral blood of recipient mice. B) CD45.1 chimerism of wt and UBC-GFP donor mice 12 and 24 weeks after transplantation. Each symbol represents once mouse. C) Percentage of myeloid cells of the whole donor CD45.1 compartment, see 7th FACS panel. Rom treated mice: n = 6, PBS treated mice: n = 4. D) Exemplary FACS plots of platelet staining. SSC-A and FSC-A were set to logarithmic scale. Numbers on the bottom left indicate the sequence of gating and arrows indicate the parent population. Numbers next to the labeled population indicate the percentage of parent population. Fourth gate was set on platelets (CD41^{+}Ter119^{-}) and fifth panel shows GFP^{+} and GFP^{-} contribution to the platelets. E) Platelet chimerism 24 weeks after BM transplantation from PBS or Rom treated UBC-GFP mice. Rom and PBS treated mice: n = 3. Ns: no statistical significance

3.2.2 Mice stopped responding to the TPO mimetic Romiplostim

As we hypothesized that every division comes along with an increased risk of acquiring DNA mutations and a gradual decrease in HSC potential, we expected to see a decrease in engraftment of Rom treated donors due to the repetitive stimulation. Since we did not see an impaired engraftment of Rom treated mice over PBS treated mice (Figure 19 B), we were wondering whether mice still responded to the Rom treatment after several injections or whether Rom might be immunogenic in mice since it consists of a human Fc receptor. To examine this, we treated wt mice for two rounds with Rom or PBS, sacrificed mice 24h after the last injection and analyzed PB and BM parameters (Figure 22 A). Surprisingly, no change was observed in platelet counts (Figure 22 B) between PBS and Rom treated mice. We expected to see an approximately 2-fold increase in platelet counts since the second last injection was applied 72h before sacrificing mice. From the dose finding experiments we know that platelet levels were increased 72h after the injection (Figure 19 C). Additionally, when we stained BM for Ki67/Hoechst to examine cell cycle status 24h after the last (16th) injection, 88% ± 5.4% of LT-HSCs from Rom treated mice were in G0-phase (Figure 22 C), which is considered as homoestatic condition of the HSC pool[61]. Additionally, we could also no neither observe an increase nor a decrease in absolute LT-HSC numbers (Figure 22 D).

In summary, these findings support the theory that repeated Rom treatment led to an immunization of mice. Furthermore, this could explain why we did not see an HSC exhaustion phenotype after one round of treatment. Therefore, we continued with TPO to be able to activate HSCs in mice and to study the effects of repetitive stimulation of HSCs in a non-inflammatory setting.

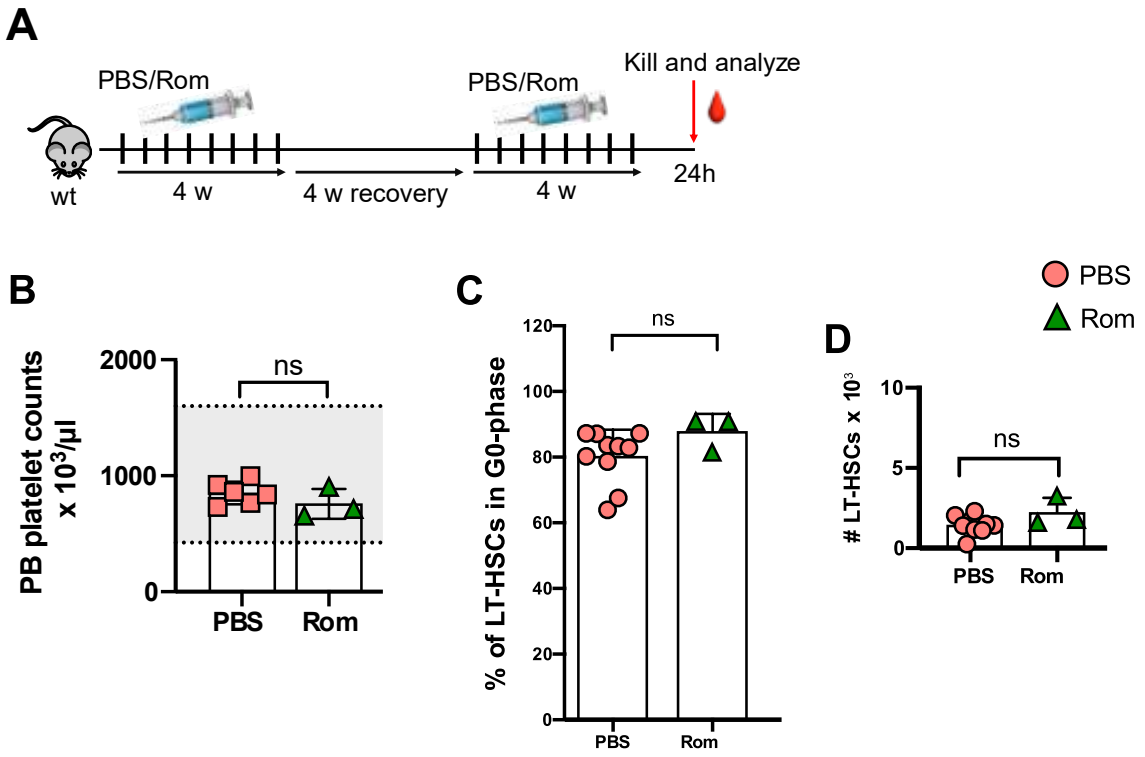

Figure 22: **Mice were unresponsive to Rom after serial treatment**. A) wt mice were treated with Rom for two treatment rounds. Already 24h after the last injection mice were sacrificed and PB and BM analyzed. B) Platelet counts were determined in PB. PBS treated mice: n = 6. C) BM was stained for Ki67/Hoechst to assess cell cycle activity and percentage of LT-HSCs in G0-phase are shown. PBS treated mice: n = 10, Rom: n = 3. D) BM was stained for LT-HSCs and absolute number of LT-HSCs per femur was assessed. PBS treated mice: n = 10, Rom treated mice: n = 3. ns = no statistical significance

3.2.3 Repeated activation of HSCs with TPO did not lead to their functional decline

In this section, we aimed to investigate LT-HSC exhaustion after a more extensive stimulation. Since we observed no adverse effects after one round of Rom treatment and hypothesized that mice were immunized against Rom, we treated mice for three rounds with TPO. Even though recombinant human (rh) TPO is not used in the clinics any more as it induces anti-TPO antibody formation, it served our purpose to repeatedly activate HSCs. We treated wt and UBC-GFP mice for three rounds with TPO (one round comprising two injections weekly for four weeks followed by a four-week recovery period) and after an additional one-week recovery period, mice were sacrificed and BM compartments were analyzed to detect any adverse side effects induced by serial TPO treatment (Figure 23 A). However, we could not detect any significant changes in BM cellularity between TPO and PBS treatment (Figure 23 B). Interestingly, we could observe a more than 3-fold increase in absolute LT-HSC numbers per femur in four out of the six TPO treated wt

mice. We also saw an approximately 3-fold increase in absolute LT-HSC numbers per femur in two out of the five TPO treated UBC-GFP mice (Figure 23 C). In order to determine differences in the progenitor populations, especially myeloid primed progenitors, we stained the BM for markers of oligopotent progenitors. Gating strategy and exemplary FACS plots can be found in Figure 23 D. Panel 5 shows an exemplary FACS plot of the gating strategy for common myeloid progenitors (CMP), megakaryocyte-erythroid progenitor (MEP) and granulocyte-monocyte progenitor (GMP) cells[41], which were derived from the $LS^{-}K$ BM population. We also included the CD55 marker (see panel 6) since $CD55^{+}$CMPs are biased towards MK production[129]. We did not observe any appreciable differences between PBS and TPO treatment in formation of the mentioned progenitor populations (Figure 23 E).

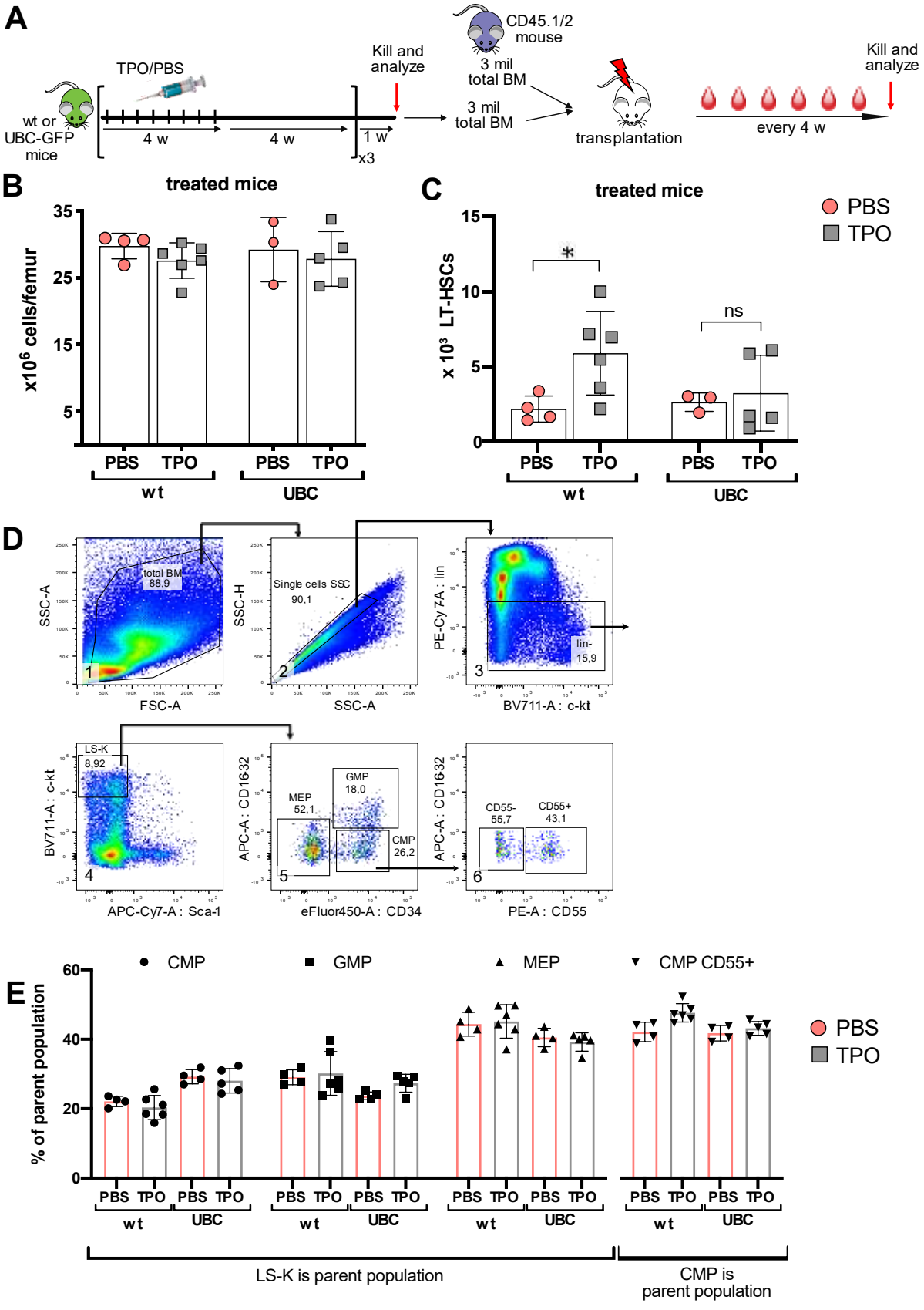
A
wt or UBC-GFP mice
TPO/PBS
4 w
4 w
1 w
x3
Kill and analyze
CD45.1/2 mouse
3 mil total BM
3 mil total BM
transplantation
Kill and analyze
every 4 w
B
treated mice
x10^6 cells/femur
PBS TPO PBS TPO
wt UBC
C
treated mice
x 10^3 LT-HSCs
*
ns
PBS TPO PBS TPO
wt UBC
PBS
TPO
D
total BM 88,9
Single cells SSC 90,1
lin- 15,9
LS-K 8,92
MEP 52,1
GMP 18,0
CMP 26,2
CD55- 55,7
CD55+ 43,1
SSC-A
FSC-A
SSC-H
SSC-A
PE-Cy7-A : lin
BV711-A : c-kt
BV711-A : c-kt
APC-Cy7-A : Sca-1
APC-A : CD16-32
eFluor450-A : CD34
APC-A : CD16-32
PE-A : CD55
E
CMP
GMP
MEP
CMP CD55+
% of parent population
PBS TPO PBS TPO PBS TPO PBS TPO PBS TPO PBS TPO PBS TPO PBS TPO
wt UBC wt UBC wt UBC wt UBC
LS-K is parent population
CMP is parent population
PBS
TPO

Figure 23: **TPO induced activation of LT-HSCs did not lead to loss of function.** A) Experimental outline of serial TPO treatment. wt or UBC-GFP mice were treated with TPO or PBS for three rounds, one round consisting of eight injections withing four weeks, followed by a four-week recovery period. Mice were sacrificed, BM was isolated and competitively transplanted with BM from CD45.1/2 mice in a 1:1 ratio into lethally irradiated CD45.2 recipient mice. Blood was drawn every four weeks from recipients over the next six months. B) Femur cellularity of PBS and TPO treated donor mice was determined. C) Absolute LT-HSC numbers per femur of PBS and TPO treated wt and UBC-GFP donor mice. D) Exemplary FACS plots of the progenitor staining. Arrows and numbers in the bottom left indicate subsequent gating strategy. E) Percentage of CMP, GMP and MEP is displayed as percentage of the LS-K population, see FACS panel 5. CMPs were further divided into $CD55^+$ and $CD55^-$, see FACS panel 6. Percentage of $CD55^+$ CMPs is displayed as percentage of all CMPs.

To assess HSC function, we again performed competitive transplantation assays after three rounds of treatment and transplanted three million (mil) total BM cells from treated donor mice together with three mil total BM cells from CD45.1/2 competitor mice into lethally irradiated CD45.2 recipient mice. Recipients were bled every four weeks after transplantation for a period of six months to assess donor chimerism in PB. Using UBC-GFP mice additionally allowed us to assess platelet chimerism from these donor mice (Figure 23 A). Mean PB donor chimerism has not much changed between 12 weeks and 24 weeks after competitive transplantation of PBS and TPO treated wt and UBC-GFP mice. At 24 weeks post-transplantation, PB chimerism from PBS and TPO treated wt mice was 32% and 27%, respectively, while in the UBC-GFP model mean donor chimerism from PBS and TPO treated mice was 34% and 27%, respectively (Figure 24 A). As previously reported, exhausted HSCs lose function over time resulting in an unfavorable change in PB composition towards the myeloid compartment[130]. At 24 weeks after transplantation, we stained PB from recipients for differentiated blood cells, but only the myeloid contribution to the whole CD45.1 donor compartment is shown. We could not detect a myeloid bias from TPO treated donors since myeloid contribution was similar between PBS and TPO treated mice (Figure 24 B). There might be a trend towards increased myeloid chimerism of TPO treated wt mice when compared to PBS treated mice, however, due to the heterogeneity of obtained results, differences did not manifest as statistically significant (p-value > 0.35). Furthermore, no significant difference in platelet chimerism from PBS and TPO treated mice was observed, neither 12 weeks (p-value > 0.9) nor 24 weeks (p-value > 0.9) after transplantation (Figure 24 C). Recipients were sacrificed six months after transplantation to analyze donor chimerism (Figure 23 A). When analyzing the BM chimerism, we were surprised to detect a slight increase in HSC engraftment without being significant, but observed a significant (p-value < 0.02) 1.8-fold increase in LT-HSC chimerism from TPO treated wt mice over PBS treated mice (Figure 24 D), although this did not approach the observed 3-fold increase in immunophenotypic LT-HSCs in the bone marrow of treated donor mice (Figure 23 C). However, as we carried out total BM transplantations and did not sort for a certain number of LT-HSCs, the absolute number of transplanted LT-HSCs was higher in TPO treated than PBS treated mice.

Of note, variability within the TPO UBC-GFP group increased from 12 weeks to 24 weeks after transplantation. Two mice in the TPO UBC-GFP group with the highest PB CD45.1 chimerism of 41% and 44%, also showed high CD45.1 BM chimerism of 74% and 81%, respectively. Only one of these mice was GFP positive and showed a high platelet chimerism of 41% (Figure 24 C). Interestingly, the mouse with the lowest platelet chimerism (19%) had the lowest PB chimerism (16%) and a low BM chimerism (22%). A similar correlation has been noticed in our group before during single cell transplantation experiments from UBC-GFP mice (unpublished data). The level of platelet chimerism robustly represented the level of BM engraftment. In other words, high platelet chimerism correlated with high BM chimerism. However, the exact mechanisms or signaling pathways which determine this correlative observation have to be further investigated and will be continued by a PhD student in the group.

In summary, after three rounds of TPO treatment (in total 24 injections) we saw no difference in the PB chimerism in cells derived from PBS or TPO donors. On the contrary, we observed an increase in HSC and LT-HSC engraftment from TPO treated donors. Interestingly, we already observed an increase in LT-HSC numbers in the donor mice undergoing three rounds of TPO (Figure 23 C). We assumed that by transplanting total BM we already had a higher proportion (cell number) of LT-HSCs in TPO treated donors, which could have led to an enhanced LT-HSC chimerism in the recipient mice.

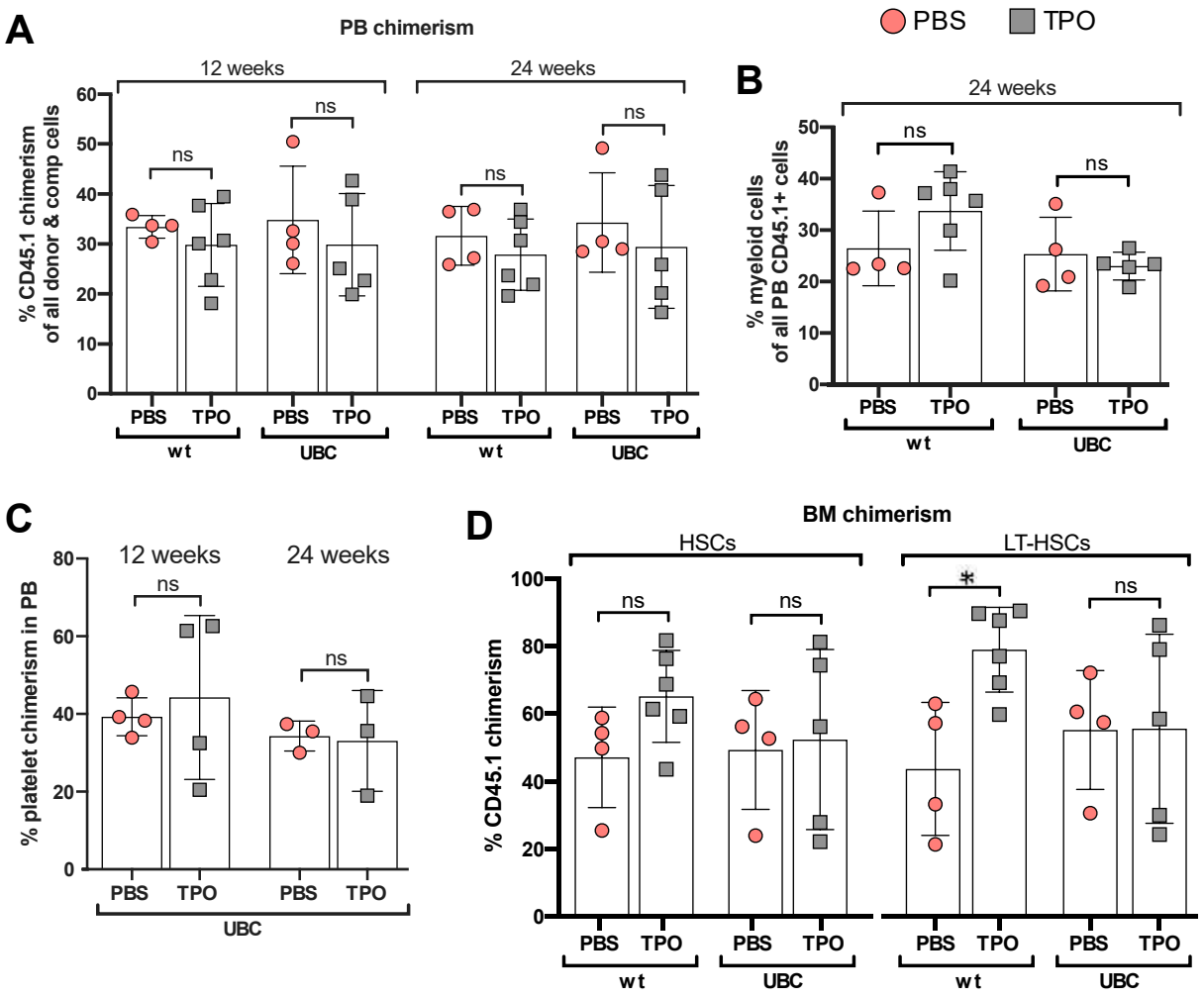

Figure 24: **TPO treatment of donors led to enhanced LT-HSC engraftment in recipients**. A) PB of recipient mice was stained for CD45 isoforms and chimerism was determined by flow cytometric analysis 12 and 24 weeks after transplantation. Each symbol represents one mouse. B) 24 weeks after transplantation PB was stained for myeloid cells (CD11b and Gr-1). Percentage of myeloid contribution to CD45.1 compartment is displayed. C) Platelet chimerism was determined from UBC-GFP treated donor mice 12 and 24 weeks after transplantation. D) Recipient mice were sacrificed 24 weeks after transplantation and CD45.1 chimerism in the HSC compartment (LSK, $CD150^{+}CD48^{-}$) and LT-HSC compartment (HSC $CD34^{-}$) was determined. ns: no statistical significance.

3.2.4 LT-HSCs did not respond to TPO stimulus after several injections

In the previous experiments we did not observe any signs of HSC exhaustion or HSC loss of function after serial TPO treatment. Knowing that rhTPO was immunogenic after long-term treatment in patients, we wanted to see if mice still responded to the TPO stimulus after our long-term treatment experiments. In order to be sure that LT-HSCs were activated, we again performed cell cycle analyses. In the case that mice did not respond to the induced stimulation, we would not see any upregulation of cell cycle activity.

Wt mice were again treated for three rounds with TPO but this time mice were already sacrificed 24h after the last injection (Figure 25 A). When analyzing platelet counts in PB of these mice, we observed a huge variation ranging from 378×10^3 to 2687×10^3 platelets/µl blood. Since we obtained these heterogeneous platelet counts no statistical significance was observed (Figure 25 B). Interestingly, we observed a slight drop in femur cellularity that was not significant (p-value > 0.05). Adding more data points would be helpful to see if the trend manifests as significant (Figure 25 C). Cell cycle activation was again analyzed by Ki67/Hoechst staining at 24h after the last injection of three rounds of TPO treatment. Obtained results were again very heterogeneous. Two mice showed high LT-HSC cell cycle activity (19% and 15% of LT-HSCs in G0-phase) whereas most of the mice showed low proliferation of LT-HSCs (on average 68% of LT-HSCs in G0-phase). Since in most cases LT-HSCs did not show any cell cycle activation (Figure 25 D), we concluded that mice might have become unresponsive to TPO after several injections. The reason why TPO mimetics were developed was due to the fact that patients treated with rhTPO started to develop antibodies against the endogenous as well as the rhTPO[91]. We might have induced the same effect in our mice and due to using a recombinant protein, created an immune reaction against TPO over time. Albeit mice were largely unresponsive to the TPO stimulation, we observed a robust 5.5-fold increase in absolute LT-HSC numbers per femur after serial TPO treatment (Figure 25 E) (average number of LT-HSCs after three rounds of TPO treatment: 7829 ± 5200 cells).

For this experiment we also stained BM for progenitor populations (GMP, MEP, CMP and CD55+/- CMP) to analyze if there is a bias in the appearance of certain myeloid primed progenitors. In the previous experiment a five-week recovery period was included after the last injection, after which we did not see any differences between TPO and PBS treated mice (Figure 23 E). We assumed that if there was a difference it could have been normalized during this five-week recovery. However, even 24h after the last injection no difference between PBS and TPO in the percentage of progenitor populations in the BM was observed (Figure 25 F).

In summary, although LT-HSCs did not proliferate and exhibit activation after several treatment rounds, we could detect a consistent increase in LT-HSC numbers after three rounds of TPO treatment. However, as we aimed to examine HSC exhaustion after repeated activation by a non-

inflammatory stimulant, we decided to only continue with one round of TPO treatment instead of three. As we assumed that it takes more than one round to immunize mice against TPO.

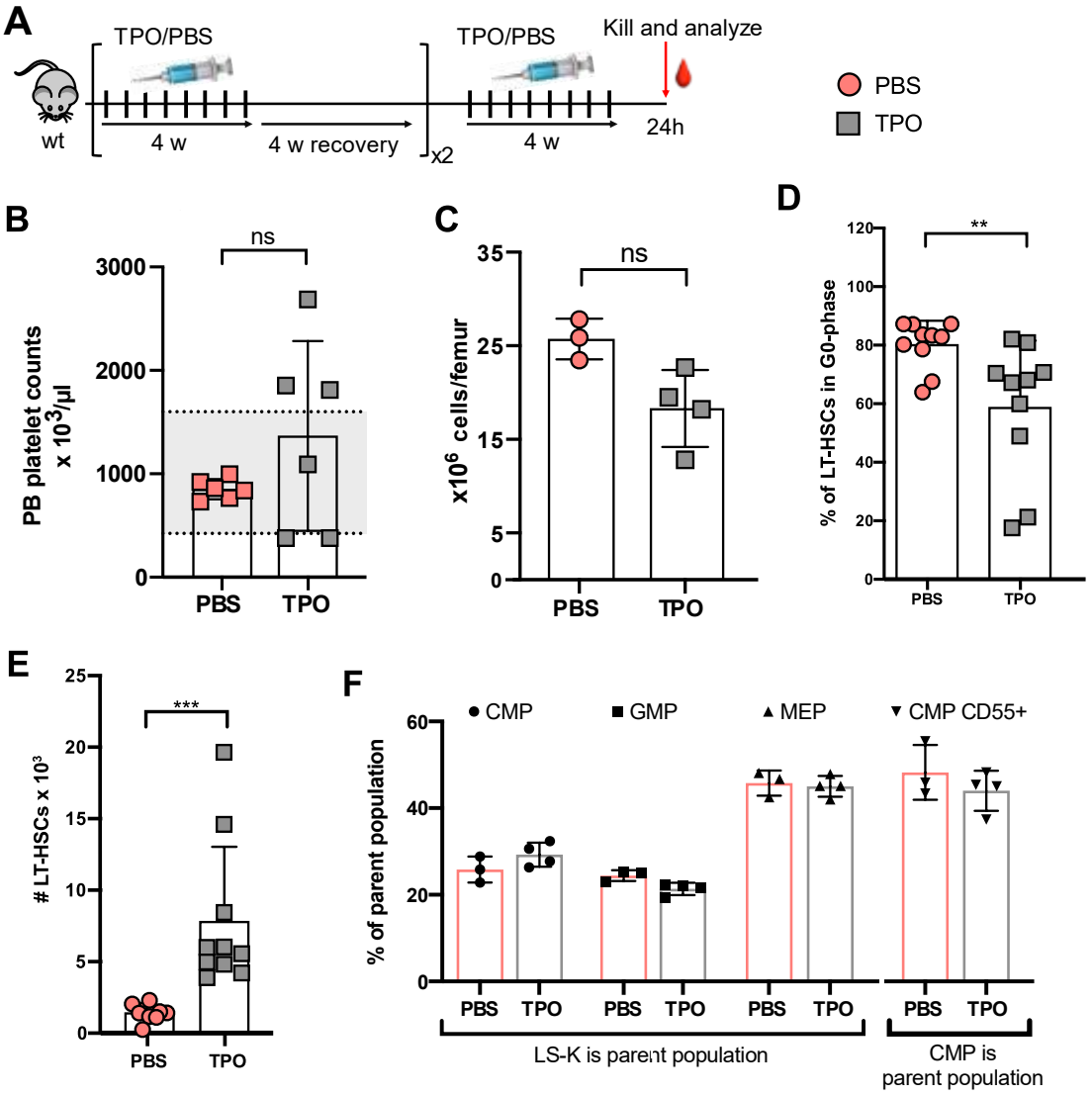

Figure 25: **Consecutive TPO treatment might have induced desensitization over time.** A) Treatment scheme for repeated HSC activation with TPO. wt mice were treated for three rounds. At 24h after the last injection, blood as drawn and mice sacrificed. BM was isolated and stained for Ki67/Hoechst. B) PB was analyzed using a hematology analyzer. Platelet counts/µl blood are shown. Grey background indicates the normal platelet range. PBS treated mice: n = 6, TPO treated mice: n = 6. C) Flushed femur cells were counted and displayed as femur cellularity in million cells/femur. PBS: n = 3, TPO: n = 4. D) Percentage of LT-HSCs in the quiescent G0-phase of the cell cycle 24h after the last injection. Each mouse is represented by a symbol, PBS: n = 10, TPO: n = 10. E) Absolute number of LT-HSCs per femur. Each mouse is represented by a symbol, PBS: n = 10, TPO: n = 10. F) BM was also stained for oligopotent progenitors. CMP, GMP and MEP are displayed as percentage of the LS-K compartment, CD55+ CMPs are displayed as percentage of the whole CMP compartment.

3.3 TPO treated Fanca$^{-/-}$ mice showed reduced engraftment potential

In the past, TPO mimetics have only been used to treat thrombocytopenic ITP or cancer patients but recently, TPO mimetics are also used to treat anemic and in general cytopenic Fanconi anemia patients to increase the number of differentiated hematopoietic cells in the peripheral blood (ClinicalTrials.gov Identifier: NCT03957694 and NCT03206086, https://clinicaltrials.gov/ct2/home). The Fanconi anemia pathway is involved in the homologous DNA repair mechanism and upon deletion or missense mutation of one of the Fanconi complex genes, the risk of DNA misrepair is increased. Experiments with Fanconi anemia KO mice (Fanca$^{-/-}$) showed that additional stress by for example injecting a viral dsRNA mimetic (polyI:C) into these mice had detrimental effects, such that Fanca$^{-/-}$ mice developed a bone marrow failure phenotype[44]. As we were strongly interested in the clinical approaches of TPO and TPO mimetics and observed an increase in the HSC pool of TPO treated wt mice (Figure 25 E) we wanted to find out if repeated TPO stimulation might not only have a beneficial effect on the PB counts (as observed in patients) but also on BM parameters. Likewise, to the study with polyI:C, we injected Fanca$^{-/-}$ mice for one round with TPO (Figure 26 A). After analyzing the PB of TPO treated Fanca$^{-/-}$ mice, we observed a significant increase in WBC counts ($8.7 \pm 0.9 \times 10^3$ WBCs/µl blood for PBS and $12.5 \pm 1.6 \times 10^3$ WBCs/µl blood for TPO, p-value < 0.001), a significant reduction in RBC counts (p-value < 0.02) but no change in platelet counts after (Figure 26 B). We could discern a tendency towards increased femur cellularity after TPO treatment however, differences (1.2-fold difference) were not significant between PBS and TPO groups (Figure 26 C). Likewise, LT-HSC counts were comparable between the two groups (Figure 26 D).

In summary, although we observed an increase in WBCs, our results do not support the clinical application which aims to increase all differentiated blood cells. In contrast, we observed a significant decrease in RBCs. The increase in WBCs in our experiment is rather concerning since the counts are above the normal range. This could indicate an emerging BM abnormality. To manifest this assumption and to test for BM attrition we conducted competitive BM transplantations.

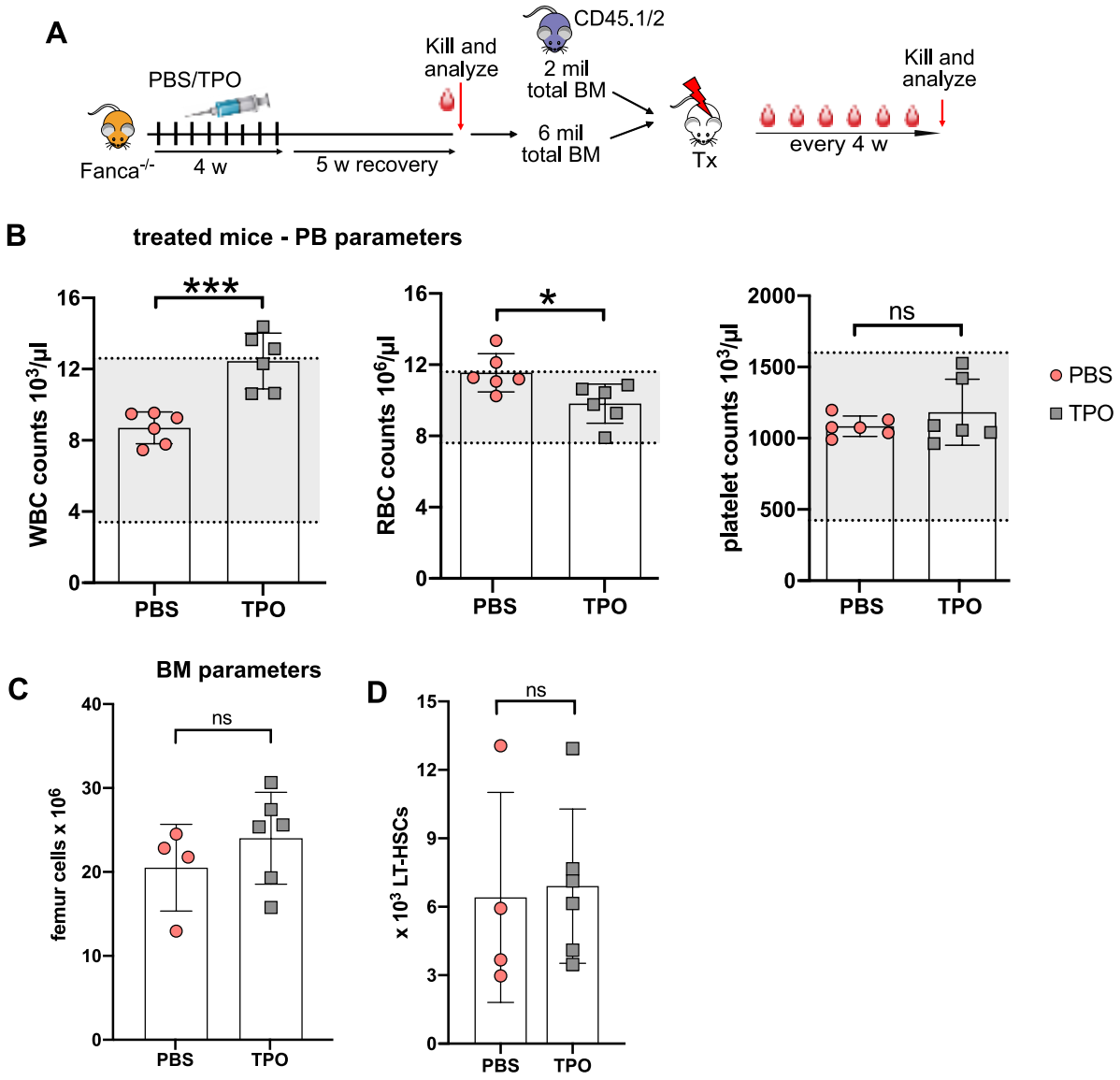

Figure 26: **Repeated TPO treatment increased WBC counts in Fanca$^{-/-}$ mice.** A) Schematic outline of experimental workflow. Fanca$^{-/-}$ mice were treated for one round with TPO or PBS, two injections per week for four weeks followed by a four- plus one-week recovery period, then sacrificed to analyze PB and BM. Total BM from Fanca$^{-/-}$ donor mice was transplanted together with total BM from CD45.1/2 mice in a 3:1 ratio into lethally irradiated CD45.2 recipients. Recipients were bled every four weeks for a period of six months to monitor engraftment. B) PB of treated Fanca$^{-/-}$ mice was analyzed. PBS and TPO treated mice: n = 6. C) Femur cellularity was determined by counting flushed femur cells. D) BM was stained for LT-HSCs to calculate absolute LT-HSC numbers per femur.

To determine and monitor CD45.1 chimerism after competitive transplantation, recipient mice were bled approximately every four weeks (Figure 26 A). Although it seemed that cells derived from TPO treated donor mice led to higher CD45.1 engraftment in the blood, these results did not prove to be statistically significant (Figure 27 A). Since we previously saw an increase in leukocytes in TPO treated Fanca$^{-/-}$ mice, we stained PB from recipients for T-, B- and myeloid cells to monitor lineage output from the transplanted cells. As it is known that PB of mice with BM failure syndrome or exhausted and non-functional HSCs show a myeloid bias, we hypothesized that PB chimerism from TPO treated Fanca$^{-/-}$ mice is biased towards myeloid cells. However, 26 weeks post-transplantation we could not observe any bias in lineage contribution from TPO treated donors to the whole CD45.1 PB compartment (Figure 27 B). When we stained BM from recipient mice for CD45 isoforms to determine CD45.1 chimerism in hematopoietic stem and progenitor cells (Lin^{-}Sca-1^{+}c-Kit^{+}), we observed that half of the PBS recipient cohort (3 out of 6 mice) and one out of six from the TPO cohort showed more than 70% CD45.2 chimerism (Figure 27 C). It is not unusual that residual CD45.2 cells remain. However, the CD45.2 leftover is estimated to be below 10%. If irradiation was insufficient and recipient BM was not completely destroyed, this can negatively influence the engraftment potential of transplanted cells. Since BM engraftment of Fanca$^{-/-}$ mice was in general low and we could not detect any HSC engraftment from some Fanca$^{-/-}$ mice, we decided to assess donor chimerism on LSK cells (Figure 27 D). Surprisingly, we did see a significant decrease in CD45.1 chimerism from TPO donors. Suggesting that TPO treatment negatively affected HSCs leading to impaired engraftment. Displaying PB and BM chimerism from PBS and TPO treated mice next to each other clearly highlighted that there was no difference in PB chimerism between PBS and TPO groups but a distinct difference in BM chimerism (Figure 27 E).

In summary, *in vivo* functional assays showed that reconstitution ability of cells derived from serially TPO treated mice was decreased. However, a decrease of PB chimerism from TPO treated donors was not observed. In order to claim that TPO-induced cycling leads to a functional impairment of HSCs from Fanca$^{-/-}$ rather than a rescue of BM failure, secondary transplantations could be carried out. Moreover, recipient mice could be monitored for up to one year in order to observe if PB donor chimerism from TPO treated donor mice further increases over time or gradually decreases, since we observed a significantly decreased BM chimerism.

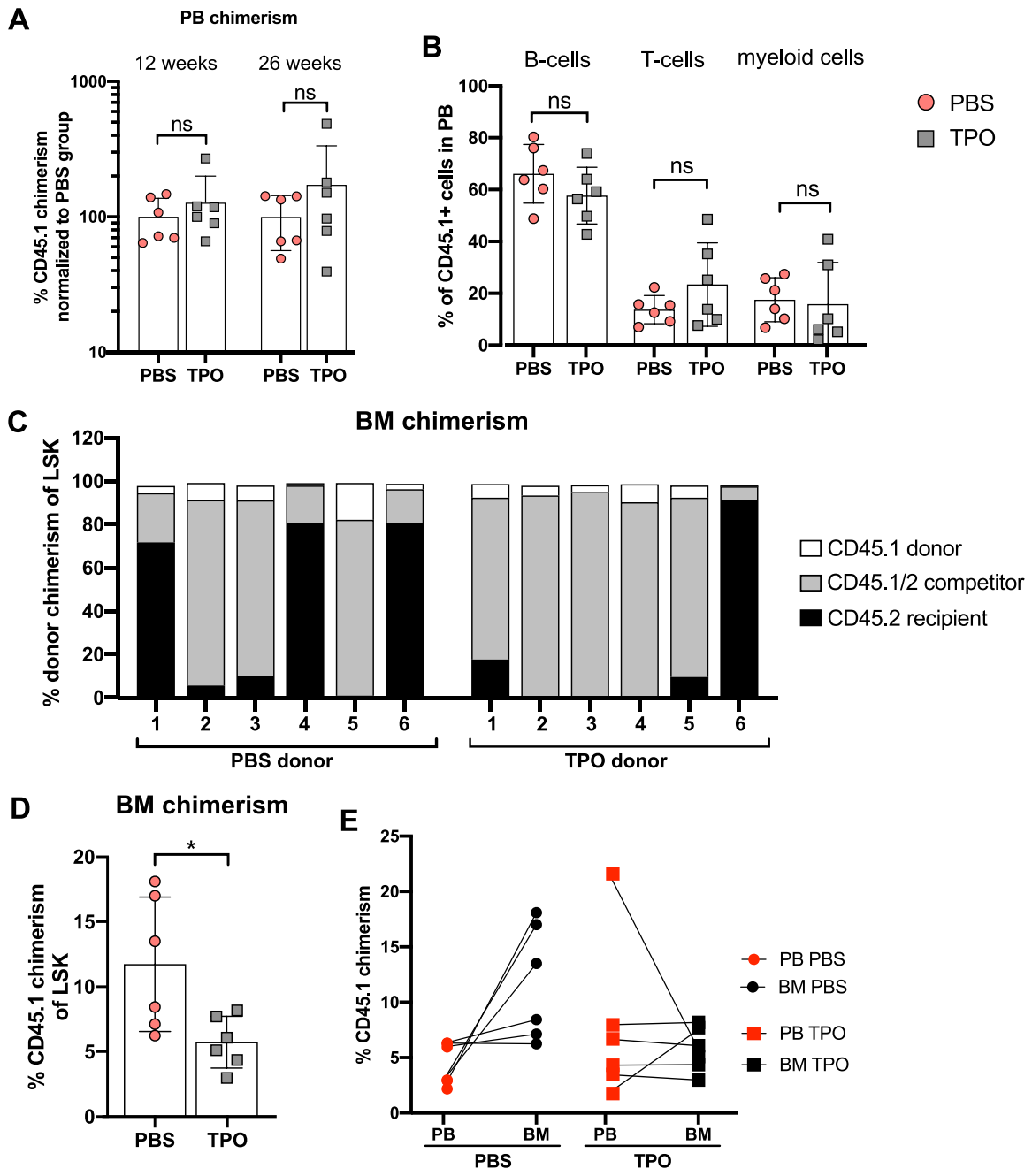

Figure 27: **TPO treatment reduced BM engraftment**. A) Recipients were bled repeatedly after transplantation and PB was stained for CD45 isoforms to distinguish donor, competitor and recipient cells. CD45.1 engraftment from PBS and TPO treated donors was normalized to the average PBS engraftment. B) 26 weeks after transplantation PB was also stained for B-, T- and myeloid cell markers and contribution of each lineage to the whole CD45.1 donor compartment is displayed. Each symbol represents one mouse. C) Mice were sacrificed 26 weeks after transplantation and BM was stained for CD45 isoforms. Each bar represents the percentages of donor, competitor and recipient BM cells from a single mouse. D) Contribution of CD45.1+ cells to the LSK compartment, CD45.2+ cells were previously excluded. E) PB and BM chimerism from PBS and TPO donors was displayed adjacent to each other. Lines connect PB and BM chimerism from the same mouse.

3.4 Tracking divisional history of LT-HSCs using a label retention mouse model

The Scl-tTA-H2B-GFP mouse model here referred to as a label-retaining cell (LRC) mouse model, was developed to examine differences between dormant (d) and active (a) LT-HSCs[61]. Under homeostatic conditions mice express a GFP-labeled Histone 2B molecule (H2B) under the scl promoter (additionally under the control of a tetracycline (tet) repression element) which is expressed in the hematopoietic compartment. If mice are treated with doxycycline (dox) H2B-GFP expression is stopped (chase is started) due to dox blocking the tet responsive element and inhibiting expression. With each cell division residual H2B-GFP is split between the daughter cells leading to GFP dilution. Hence remaining GFP-levels can be used to distinguish between dHSCs and aHSCs based on the amount of cell divisions the phenotypic HSCs underwent. We used this mouse model to decipher differences in the potency of phenotypic label-retaining (LR) and non-LR LT-HSCs having a lower or higher proliferative history, respectively.

3.4.1 Reduction of label retaining LT-HSCs after TPO treatment

In this section we examined the difference in engraftment capacity of LT-HSCs that cycled more often (non-LR LT-HSCs) due to induced activation and LT-HSCs that remained in a dormant state throughout the treatment (LR LT-HSCs). We included polyI:C since we knew that repeated polyI:C led to a robust activation of the HSC pool and used it as positive control for TPO-induced activation.

The dox chase was started one week prior to the first injection. LRC mice were treated for one round with PBS, polyI:C or TPO and were sacrificed after a total chase of 70 days (Figure 28 A). PB of treated LRC mice was analyzed and already PBS treated LRC mice showed a high basal level of WBCs (12.6 ± 4 x 10^3 WBCs/µl blood) (Figure 28 B) in comparison to wt (C57BL/6) mice (Figure 14 A, black bars). No difference was observed five weeks after the last injection between the TPO and polyI:C treatments (polyI:C: 14 ± 5. x 10^3WBCs/µl, TPO: 13 ± 4 x 10^3WBCs/µl). Again, we observed consistently high platelet level after TPO treatment (Figure 28 C) but no change in femur cellularity (Figure 28 D). To assess label loss after one round of treatment, we first examined the proportion of GFP^+ (LR) LT-HSCs as shown in exemplary FACS plots in Figure 28 E. Percentage of LR LT-HSCs was similar after polyI:C and TPO treatment, 63% ± 17% and 62% ± 15% of LR LT-HSCs, respectively, but significantly reduced in comparison to LR LT-HSCs from BPS treated mice (Figure 28 F). Even though the percentage of LR LT-HSCs was almost the same in polyI:C and TPO treatment, there was a small decrease in the average GFP MFI of TPO treated cells, which did not turn out to be statistically significant (p-value > 0.2). Mean GFP MFI of polyI:C treated LT-HSCs was 34 ± 13 whereas mean GFP MFI from TPO treated LT-HSCs was 23 ± 14 (Figure 28 G).

Concluding, by examining label dilution of LT-HSCs we could verify that TPO-induced cycling of LT-HSCs occurred in a similar way to that of polyI:C treatment and both stimulated LT-HSCs consistently. Mice responded to TPO treatment well considering that five weeks after the last injection, platelet counts were still elevated. Of note, the TPO treatment-induced reduction of GFP label in LT-HSCs that was similar to the polyI:C-induced reduction, confirmed our previous assumption that TPO was not immunogenic after one round of treatment.

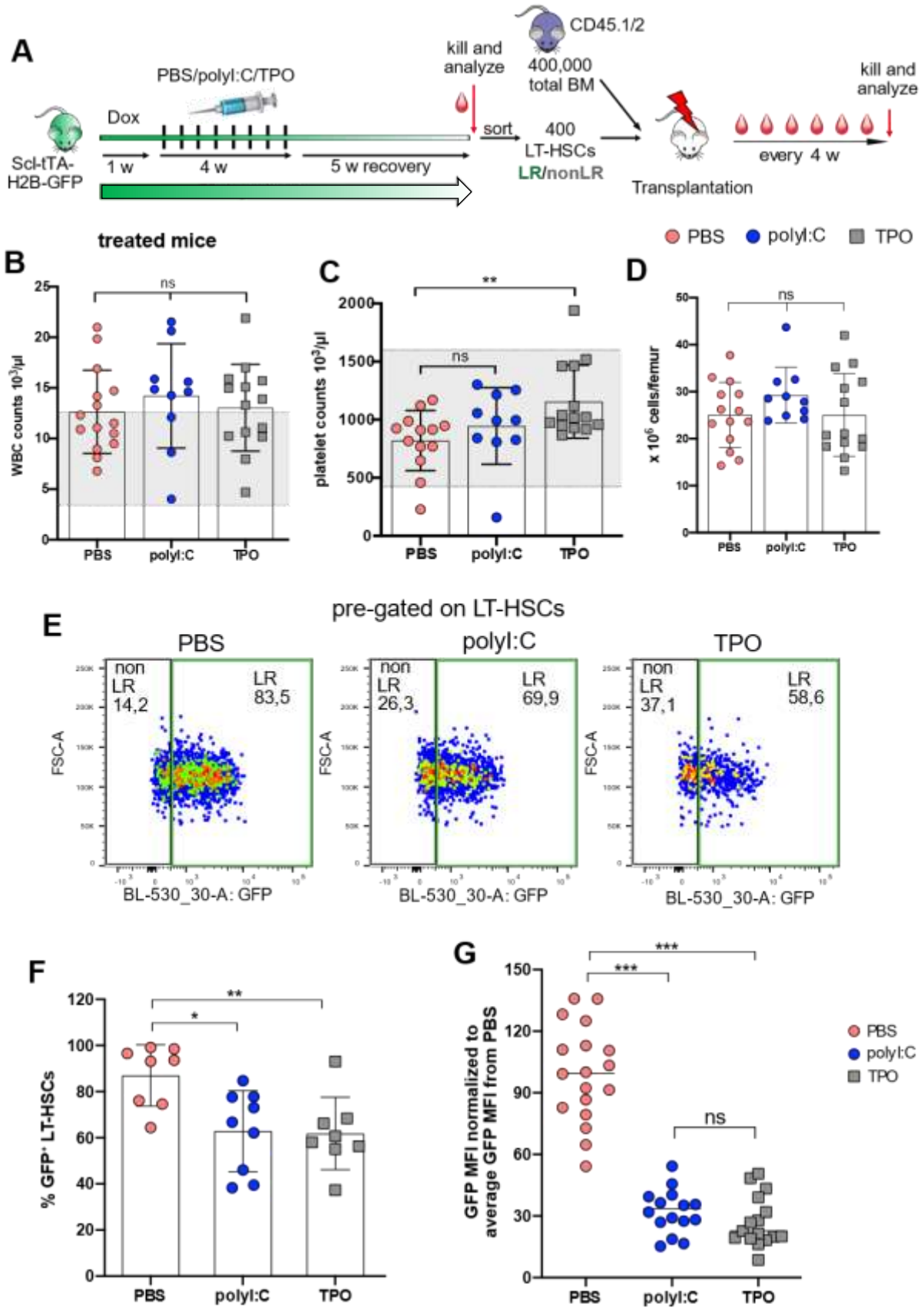
A
PBS/polyI:C/TPO
Dox
Scl-tTA-H2B-GFP
1 w
4 w
5 w recovery
kill and analyze
sort
CD45.1/2
400,000 total BM
400 LT-HSCs LR/nonLR
Transplantation
kill and analyze
every 4 w
treated mice
PBS
polyI:C
TPO
B
WBC counts 10³/µl
ns
C
platelet counts 10³/µl
**
ns
D
x 10⁶ cells/femur
ns
E
pre-gated on LT-HSCs
PBS
polyI:C
TPO
non LR 14,2
LR 83,5
non LR 26,3
LR 69,9
non LR 37,1
LR 58,6
FSC-A
BL-530_30-A: GFP
F
% GFP⁺ LT-HSCs
**
*
G
GFP MFI normalized to average GFP MFI from PBS
***
***
ns

Figure 28: **Strong reduction of GFP label after serial polyI:C and TPO treatment but not after PBS treatment**. A) Experimental setup. Dox treatment started one week before LRC mice (Scl-tTA-H2B-GFP) were treated for one round with PBS, polyI:C or TPO (eight injections within four weeks). After a total recovery period of five weeks, mice were sacrificed and PB and BM were analyzed. 400 LR LT-HSCs or 400 non-LR LT-HSCs were sorted and transplanted together with 400,000 total BM from CD45.1/2 mice into lethally irradiated CD45.2 recipients which were bled every four weeks after transplantation for a period of six months. B-C) PB from treated LRC mice was analyzed and WBCs and platelet counts are shown. D) Femurs were isolated, flushed and subsequently counted. E) Total BM was stained for LT-HSCs to determine GFP label loss. Exemplary FACS plots display GFP intensity in LT-HSCs. The non-LR (GFP^-) gate was set according to the H2B-GFP negative control. F) Percentage of label-retaining (GFP^+) LT-HSCs. PBS mice: n = 8, polyI:C mice: n = 9, TPO mice: n = 8. G) Mean fluorescence intensity of LT-HSCs from PBS, polyI:C and TPO mice was normalized to the average MFI of the PBS group and average GFP MFI from PBS group was set to 100.

3.4.2 Non-LRCs from TPO treated mice did not show any engraftment defects

To assess the performance of LR and non-LR LT-HSCs, we carried out transplantation assays and determined donor chimerism in PB and BM 24 weeks post-transplantation (Figure 28 A). By reason of previous findings from Wilson *et al*.[61], we expected to see a reduced engraftment potential of non-LR LT-HSCs, due to their increased proliferation background. Our results confirmed these findings and non-LR LT-HSCs from PBS and polyI:C treated mice showed a significant reduction in PB CD45.1 chimerism, whereas no difference between PB chimerism from LR or non-LR LT-HSCs of TPO treated mice was observed (Figure 29 A). In contrast to PB, we did not see significant differences in BM CD45.1 chimerism between PBS, polyI:C or TPO treated donors (Figure 29 B). However, we can observe a trend that BM engraftment from non-LR LT-HSCs from PBS and polyI:C treated mice is slightly impaired compared to BM engraftment of the LR LT-HSCs. Due to the outliers in the PBS non-LR group and the five out of ten mice with low CD45.1 chimerism in the polyI:C LRC group the difference was probably not statistically significant. For the TPO groups we could not observe any trend. It should be remarked that the obtained results from PB and BM chimerism were in general very heterogeneous. We again displayed PB and BM chimerism from the same mouse adjacent to each other to see if a high PB chimerism correlated with a high BM chimerism (Figure 29 C-D). However, we did not detect a significantly increased BM over PB chimerism or vice versa. We saw a minor increased BM over PB chimerism from transplanted TPO treated non-LR LT-HSCs. To keep it simple, only a few representative samples were shown here.

In summary, we observed a functional impairment of non-LR LT-HSCs derived from PBS and polyI:C treatment but could not identify this phenotype in TPO treated mice. However, a general issue with the LRC mouse model is the heterogeneity within mice of the same group.

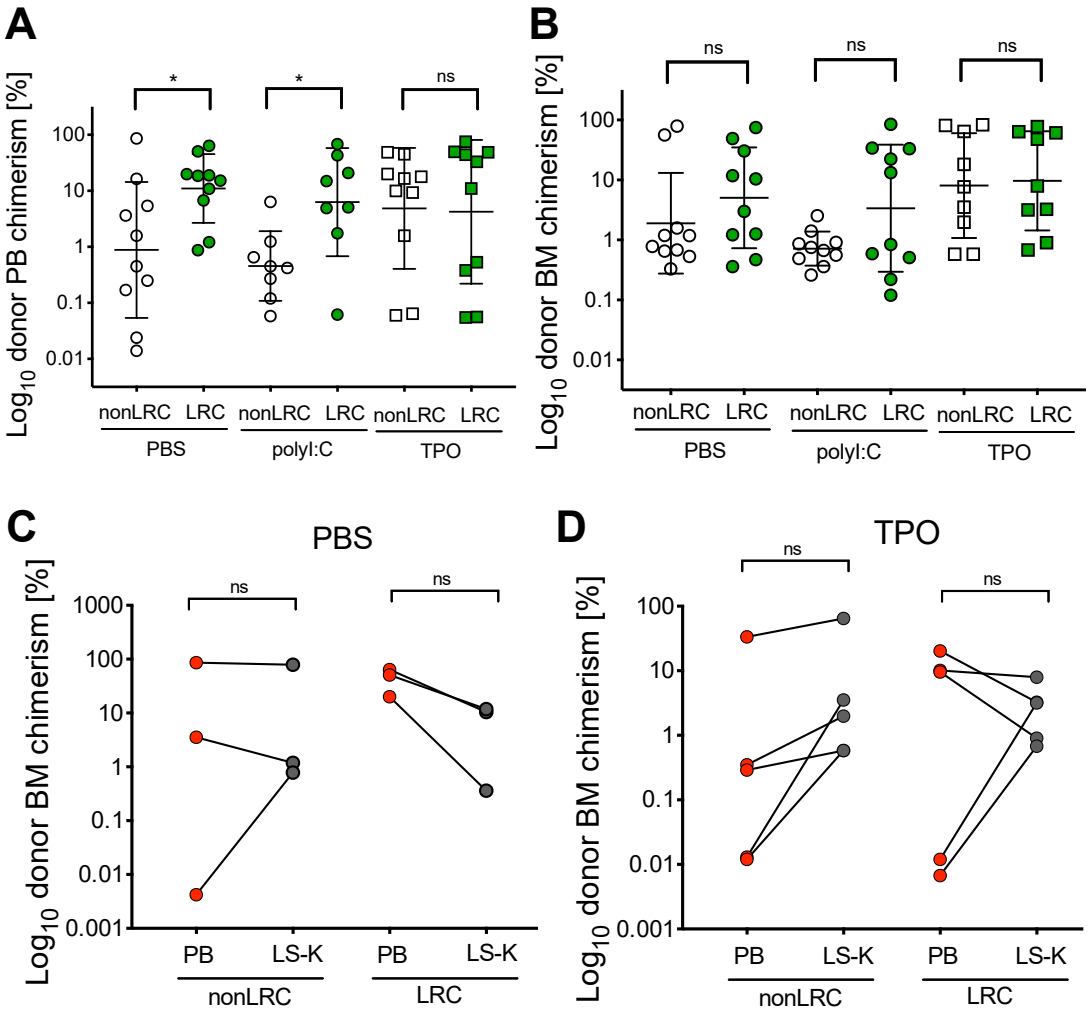

Figure 29: **Non-LR LT-HSCs from PBS and polyI:C but not from TPO treated mice led to reduced PB chimerism.** A-B) From each treated mouse 400 LR and 400 non-LR LT-HSCs were separately transplanted into lethally irradiated CD45.2 recipient mice together with 400,000 CD45.1/2 total BM cells. 24 weeks after transplantation PB and BM chimerism was analyzed by staining for CD45.1 and CD45.2. C-D) A representative selection was made to display PB and BM (measured on LS-K) chimerism from the same recipient mouse adjacent to each other. Lines connect the PB and BM chimerism from the same mouse.

3.5 *In vitro* differentiation potential after TPO treatment

3.5.1 Increased clonogenicity but decreased proliferation potential after TPO treatment

In addition to the *in vivo* functional assessment of HSCs, we evaluated HSC function *in vitro* by conducting colony forming assays. This assay allowed us to identify a possible differentiation bias, such as a myeloid bias that was often observed in aged or exhausted LT-HSCs, or a presumable megakaryocytic lineage bias after TPO treatment. With this assay we assessed the (i) proliferation capacity of LT-HSCs by counting all of the live cells each colony consisted of and the (ii) clonogenicity (colony forming potential) by counting how many colonies formed after a certain amount of individually sorted LT-HSCs. In brief, single LT-HSCs from three rounds treated PBS and TPO wt mice or one round treated Fanca$^{-/-}$ or LRC mice were sorted into differentiation medium in 96 well plates (Figure 30 A-C). Plates were kept for two weeks under low oxygen conditions (5% O_2), after which colonies were formed and identified manually. We only considered it a colony when more than 100 cells per well were manually counted. A representative myeloid biased colony (Figure 30 D) and megakaryocytic colony (Figure 30 E) are shown. These colonies were then FACS analyzed to determine their actual size (number of live cells/colony) and their differentiation output. It was important to incorporate a live/dead marker into the staining panel since after 14 days of *in vitro* culture, debris and dead cells accumulated. In this *in vitro* differentiation assay only myeloid (my), erythroid (ery) and megakaryocytic (MK) cells could be formed (Figure 30 F).

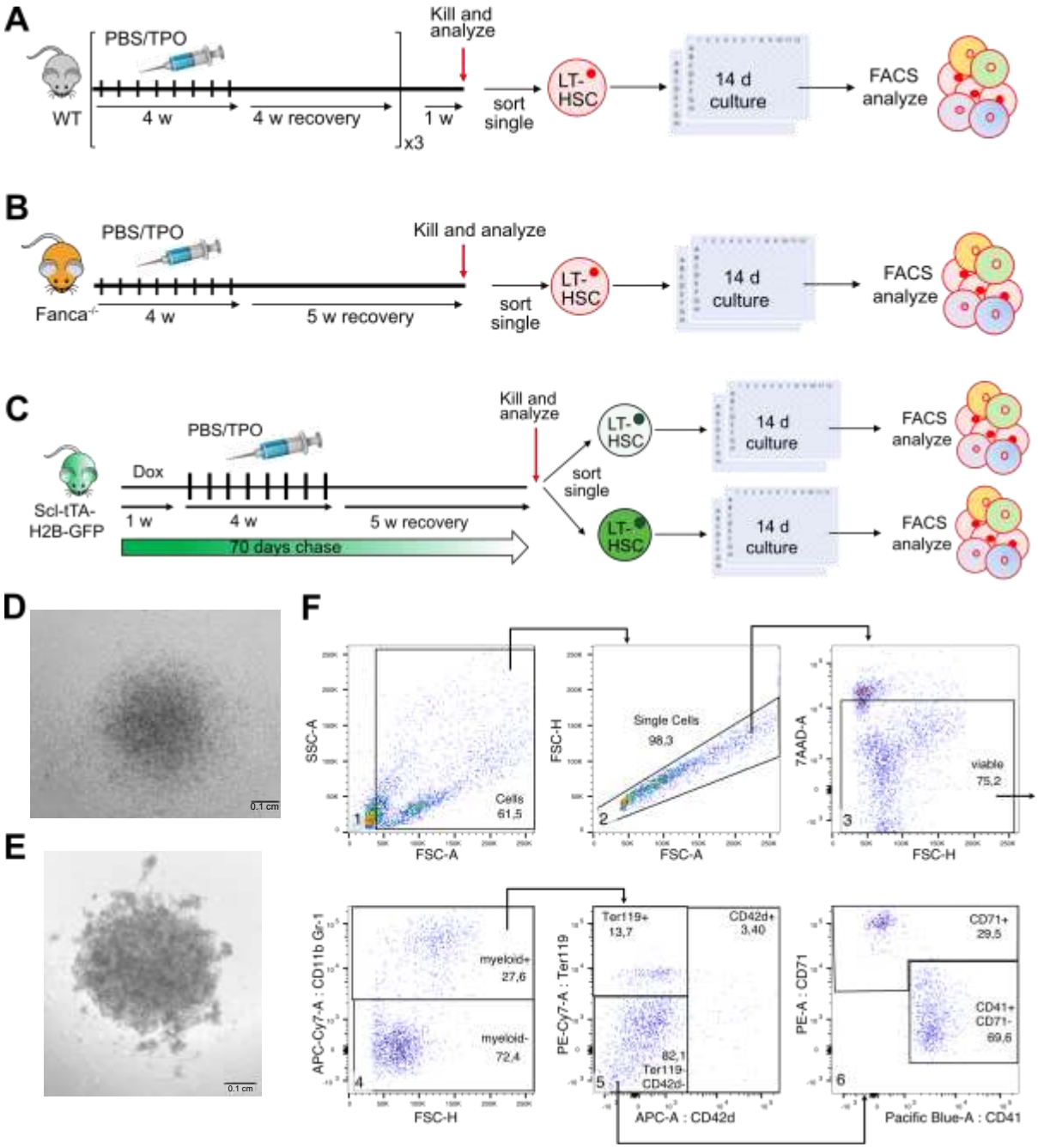

Figure 30: **Overview of performed *in vitro* colony differentiation assays**. Mice were treated with PBS or TPO and after a total of 5 weeks after the last injection, mice were sacrificed. BM was isolated and stained to subsequently sort single LT-HSCs from one mouse into two 96 well plates. After 14 days incubation at 5% O_2, 37°C and 5% CO_2 the formed colonies were counted and colony size as well as differentiation output was determined by flow cytometric analysis. A) wt mice were treated for three rounds. B) Fanca$^{-/-}$ mice were treated for one round. C) LRC mice (Scl-tTA-H2B-GFP) were put on dox for 70 days and in parallel treated for one round. Single LR and non-LR LT-HSCs were sorted separately and for each condition two 96 well plates were sorted. D) A typical myeloid biased colony derived from a single LT-HSC of a PBS treated wt mouse, viewed at 40x magnification. E) A typical megakaryocytic biased colony derived from a single LT-HSC of a TPO treated wt mouse, viewed at 40x magnification. F) Exemplary FACS plots of a multilineage colony derived from a sorted single LT-HSC from a PBS control wt mouse. Numbers at the bottom left and arrows indicate subsequent gating strategy. First three gates were set to determine single live cells. The fourth panel distinguished myeloid positive and negative cells. Myeloid negative cells were further divided into mature erythroid cells (Ter119^{+}), mature MK cells (CD42d^{+}) and double negative cells. The sixth panel was used to distinguish immature erythroid cells (CD71^{+}) and immature MK cells (CD41^{+}).

For each mouse and condition, two 96-well plates were sorted meaning that a maximum of 192 colonies could be obtained. Two independent colony assay experiments were carried out from LRC mice, referred to as LRC1 and LRC2. Colony forming potential from single LR LT-HSCs sorted cells was comparable between PBS and TPO treatments. On average we obtained similar number of colonies form PBS and TPO treated LR LT-HSCs, 125 colonies from PBS group and 121 colonies from TPO treated group (Table 1). In contrast, when evaluating colony formation potential from non-LR LT-HSCs, a significant difference between PBS and TPO treated cells was noted. After performing two LRC colony assay experiments, we measured on average only 66 colonies from PBS non-LR LT-HSCs whereas we counted on average an 1.6-fold increase in colonies from TPO treated non-LR LT-HSCs (= 108 colonies). After inspecting all plates from wt and Fanca$^{-/-}$, we observed an approximately 10% increase in colony formation potential from TPO treated wt and Fanca$^{-/-}$ mice, compared to colonies from the respective PBS treated mice.

In summary, TPO treated cells seemed to have a higher colony forming potential and surprisingly, TPO treated non-LR LT-HSCs were only slightly impaired in their colony forming potential, whereas PBS treated non-LR LT-HSCs showed a profound impairment to form colonies.

Table 1: **Overview of counted colonies from each condition: PBS and TPO treatment of LRC, wt and Fanca$^{-/-}$ mice**. Two independent colony forming experiments were carried out with LRC mice (LRC1 and LRC2), one colony forming experiment was carried out with wt and Fanca$^{-/-}$ mice. Two plates were used for analysis and numbers indicate average number of colonies formed per mouse.

Average # of analyzed colonies/192 sorted LT-HSCs per mouse	PBS			TPO		
	Colonies/ LRCs	Colonies/ non-LRCs	Mice/ treatment	Colonies/ LRCs	Colonies/ non-LRCs	Mice/ treatment
LRC 1	118.7	21	3	110	75.7	3
LRC 2	131.8	110.3	4	132.8	141	4
wt mice	82.5		4	91.5		6
Fanca$^{-/-}$ mice	94.2		5	110.8		6

3.5.2 Increase in megakaryocytic colonies after TPO treatment

We not only analyzed the number of colonies formed but also the size of each colony and their differentiation output since it is known that exhausted HSCs from both humans and mice show a myeloid bias[131,132]. In our *in vitro* colony differentiation assays, we only assessed myeloid (my), erythroid (ery) and megakaryocytic (mk) lineage output. In order to assess lymphoid output, co-culture with OP9 stromal cells is required[133]. Since the dispersion of the colony sizes was large, it should be noted that we used the Median to estimate the overall colony size of the respective condition and that the variation was given by the Median Absolute Deviation. This applies to the whole *in vitro* colony assay section.

Despite obtaining a higher number of colonies from TPO treated LT-HSCs (Table 1), the overall size (number of cells/colony) was significantly reduced (Figure 31 A). The median of the colony size derived from PBS treated wt mice was 1386 ± 705 cells whereas the median of colonies derived from TPO treated wt mice was significantly reduced and only 871 ± 781 cells/colony were counted. We observed this significant decrease in colony size also between PBS and TPO treated LT-HSCs from Fanca$^{-/-}$ mice. Colony size from PBS treated Fanca$^{-/-}$ mice was 1299 ± 849 cells, whereas colony size from TPO treated Fanca$^{-/-}$ mice was slightly reduced to 1085 ± 665 cells/colony (Figure 31 B). In order to easily analyze and evaluate the lineage output of a colony an R pipeline was developed by Dr. Holland-Letz and Dr. Bogeska. It was developed such, that a colony would be classified either as a monolineage, bilineage or multilineage colony depending on the differentiation output of every cell within a single colony. Displaying colony counts from all mono-, bi- and multilineage classified colonies would give us an overview which kind of biased or predetermined LT-HSC was affected by the TPO treatment. After three rounds TPO treatment LT-HSCs from wt mice giving rise to mono- and bilineage output were negatively affected by the TPO stimuli and impaired in their proliferation potential. In contrast, the clonogenic potential from LT-HSCs that gave rise to multilineage colonies was not affected by the TPO treatment and we could not observe a significant difference in colony size between PBS and TPO treatment (p-value > 0.4) (Figure 31 C). From Fanca$^{-/-}$ treated mice we only observed a decrease in proliferation capacity of monolineage biased LT-HSCs (see appendix section 10.3, Figure 41).

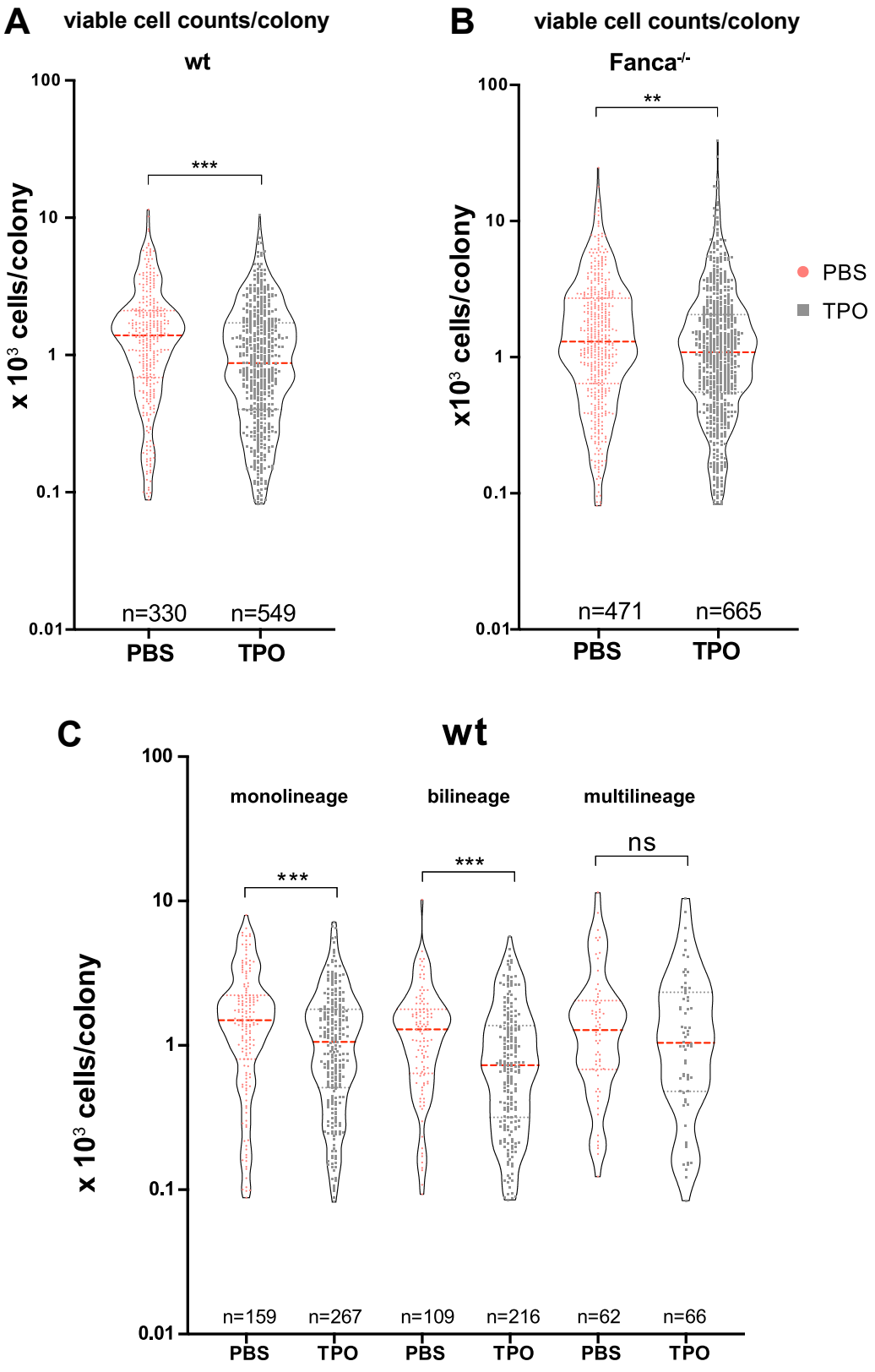

Figure 31: **Repeated TPO treatment resulted in the formation of smaller colonies.** A-B) Colony size from PBS or TPO treated wt or Fanca$^{-/-}$ LT-HSCs was assessed by flow cytometric analysis. n = number of acquired colonies. The red dashed line shows the median. C) Detailed colony output is shown for colonies derived from treated wt mice. Depending on the differentiation output of the cells derived from a single sorted LT-HSC, the colony lineage was determined. Colonies were defined as mono, bi- or multilineage. Colony size is displayed as cells/colony and depicted as violin plot. n= indicates the number of colonies assigned to each lineage output. The red dashed line shows the median.

Colony output was also depicted in pie charts. This allowed us to examine the specific lineage output, for example the percentage of myeloid, erythroid or megakaryocytic of all the monolineage colonies. To keep it simple, mono- (Figure 32 A), and bi- or multilineage (Figure 32 B) output was displayed separately. Approximately 50% of all the analyzed colonies from PBS or TPO treated wt showed a monolineage output. 48% (159 colonies out of total 330 colonies) of all colonies from PBS and 48% (267 out of 549 colonies) of all colonies from TPO treated wt mice gave rise to a monolineage output. We could observe a similar percentage of monolineage colonies out of all analyzed colonies for PBS and TPO treated Fanca$^{-/-}$ mice, 51% and 47%, respectively. First, we concentrated on the changes in MK colonies after TPO treatment of wt and Fanca$^{-/-}$ mice. We observed an increase in MK colonies after TPO treatment in both wt mice (5% MK colonies from PBS, 15% MK colonies from TPO treatment) and Fanca$^{-/-}$ mice (9.9% MK colonies from PBS, 12.9% MK colonies from TPO treatment). At the same time, we observed a decrease in erythroid colonies in both wt mice (6.5% Ery colonies from PBS, 1.9% Ery colonies form TPO treatment) and Fanca$^{-/-}$ mice (12% Ery colonies from PBS, 9.8% Ery colonies from TPO treatment). The proportion of myeloid colonies did was hardly not affected by the TPO treatment, neither in wt nor Fanca$^{-/-}$. We could observe a similar change for PBS and TPO colonies from Fanca$^{-/-}$ mice showing an increase in MK and a decrease in erythroid colonies, however, the increase in MK and decrease in erythroid colonies was more subdued in Fanca$^{-/-}$ mice as compared to wt mice (Figure 32 A). The most significant change was observed in bilineage output between PBS and TPO treated LT-HSCs from wt mice. We observed an 18% increase in the myeloid-megakaryocytic (My-MK) colonies from TPO treated mice and at the same time a 13% decrease of multilineage colonies. We could not observe any difference in the bi- and multilineage output between cells from PBS and TPO treated Fanca$^{-/-}$ mice.

In summary, we could not confirm the results obtained from the *in vivo* functional assay of wt treated mice, since in the *in vitro* assay we observed a significant decrease in proliferation capacity. Since we did not assess MK output after transplantation and could not assess lymphoid output in this *in vitro* assay, we cannot compare the lineage contribution. However, our results were in line with previous data, that TPO-induced activation of LT-HSCs leads to MK activation[134] as we saw an increase in the megakaryocytic lineage output in this *in vitro* differentiation assay of LT-HSCs from TPO treated mice. In the functional *in vivo* assay from Fanca$^{-/-}$ mice we saw a decrease in BM chimerism from TPO treated mice. Our *in vitro* assay confirmed these findings as we also observed a decrease in colony size from TPO treated LT-HSCs.

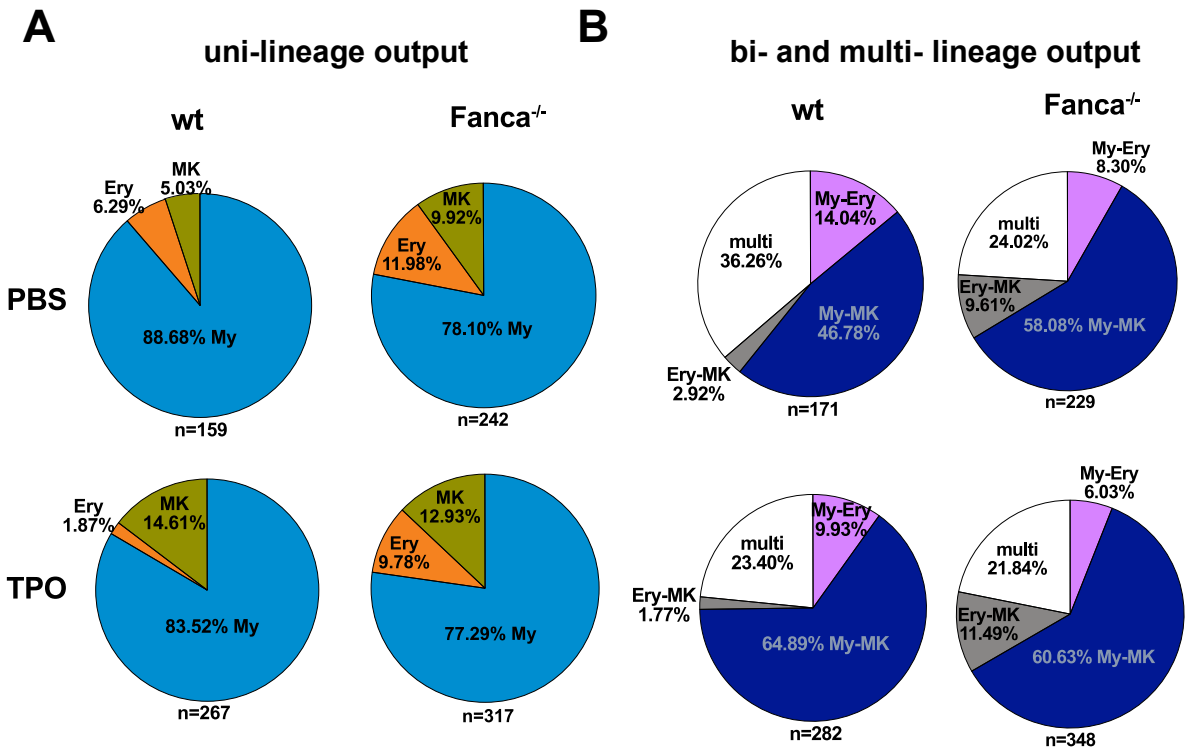

Figure 32: **TPO treatment induced a megakaryocytic differentiation bias**. A) Pie chart shows the mean percentage of defined megakaryocytic (MK, CD41$^+$ and CD42d$^+$ cells), erythroid (Ery, Ter119$^+$ and CD71$^+$ cells) and myeloid colonies (My, CD11b$^+$ and Gr-1$^+$ cells) of all measured mono (uni-) lineage colonies. n = total number of all analyzed monolineage colonies. B) Pie chart shows the mean percentage of defined myeloid-erythroid (My-Ery), myeloid-megakaryocytic (My-MK), erythroid-megakaryocytic (Ery-MK) and multilineage colonies of all measured bi- and multilineage colonies. n = total number of all multi- and bilineage colonies.

3.5.3 Non-LR LT-HSCs showed reduced colony forming potential

Due to the previously observed heterogeneity between LRC mice we performed the colony assay from three independent LRC treatment experiments. However, from one experiment we obtained less than 100 colonies for each condition due to an unknown reason and therefore had to exclude it. The results from the two remaining experiments (LRC1 and LRC2) were not consistent across experimental repeats, hence they are shown separately in the following section.

In order to address functional differences between LRC and non-LRCs, we *in vitro* differentiated single LR and non-LR LT-HSCs and analyzed their proliferation capacity as well as the differentiation output by flow cytometry (Figure 30 C). When comparing colony sizes between colonies derived from PBS treated LR and non-LR LT-HSCs in the LRC1 experiment, we only observed a slight reduction in colony size (1152 ± 834 cells/colony from PBS LR LT-HSCs colonies, 1064 ± 861 cells/colony from PBS non-LR LT-HSCs) but results were not statistically significant. Since we pre-selected colonies for FACS analysis and were dependent on a specific size (> 100 cells) we might have introduced a bias towards the bigger colonies. However, we observed a 5.7-

fold reduction in the absolute number of colonies formed between LR and non-LR LT-HSCs from PBS treated mice (356 and 63 colonies, respectively). Surprisingly, colonies from TPO stimulated non-LR LT-HSCs were significantly (p-value < 0.001) bigger in size than colonies derived from TPO treated LR LT-HSCs. We did not expect this, since we hypothesized that non-LR LT-HSCs which had already undergone several cell divisions, would be exhausted and show a decrease in proliferation capacity. Moreover, we did not observe a significant difference (p-value > 0.25) in colony size between non-LR LT-HSC colonies from PBS and TPO treated mice, but due to the fact that only 63 colonies were analyzed from PBS non-LR LT-HSCs this could be the reason that results did not prove to be statistically significant (Figure 33 A). In the second experiment (LRC2), we observed a significant reduction in colony size between LR LT-HSCs and non-LR LT-HSCs from each treatment. These results are in line with our hypothesis, but contradictory to the findings we observed in LRC1 for LR and non-LR LT-HSC colonies from TPO treated mice. Nevertheless, we can conclude from this analysis that TPO treatment did not induce a proliferation defect since the differences between the colony size derived from PBS and TPO treated LR LT-HSCs colonies and the colonies derived from PBS and TPO treated non-LR LT-HSCs did not show significant differences (Figure 33 B).

Next, we again depicted the mature hematopoietic lineage contribution to all the monolineage colonies as pie charts (pie chart on the left side = LRC1 experiment; pie chart on the right side = LRC2 experiment) (Figure 33 C-D). Figure 33 C shows the difference in monolineage output between colonies from PBS and TPO treated LR LT-HSCs. The common feature between LRC1 and LRC2 is that after TPO treatment the proportion of monolineage MK colonies decreased whereas we observe a parallel increase in Ery colonies in LRC1 and an increase in My colonies in LRC2. Figure 33 D shows the difference in monolineage output between colonies from PBS and TPO treated non-LR LT-HSCs. Interestingly, the lineage output from TPO treated non-LR LT-HSCs did not resemble the lineage distribution from PBS treated non-LR LT-HSCs but rather the lineage output of the colonies from the TPO treated LR-LT-HSCs shown in Figure 33 C. Concluding, TPO treatment did not induce a change in monolineage output between colonies from LR and non-LR LT-HSCs as seen for PBS treated LR and non-LR LT-HSCs.

As a next step, we depicted the mature hematopoietic lineage contribution to all the bi- and multilineage colonies as pie charts (pie chart on the left side = LRC1 experiment; pie chart on the right side = LRC2 experiment) (Figure 33 E-F). Figure 33 E shows the difference in bi- and multilineage output between colonies from PBS and TPO treated LR LT-HSCs. The common feature between LRC1 and LRC2 is that after TPO treatment the proportion of Ery-MK colonies increased the most (3.2-fold in LRC1, 1.4-fold in LRC2) upon all the smaller changes in proportion. Figure 33 F shows the difference in bi- and multilineage output between colonies from PBS and TPO treated non-LR LT-HSCs. No major differences could be observed in the lineage output from TPO treated non-LR LT-HSCs and PBS treated non-LR LT-HSCs. Interestingly, when comparing the lineage output of the colonies from the PBS and TPO treated LR-LT-HSCs shown in Figure 33 D, it stood

out that, again, the lineage output from LR and non-LR LT-HSCs from TPO treated mice was similar whereas differences in the lineage output between LR and non-LR LT-HSCs from PBS treated mice were be observed (especially in the Ery-MK compartment: 4.4-fold increase in LRC1 and 1.9-fold increase in LRC2 between colonies from LR and non-LR LT-HSCs from PBS mice).

In summary, we confirmed our previous findings from the wt and Fanca$^{-/-}$ experiments (Figure 31), that TPO enhanced clonogenicity and that repeated TPO treatment did not lead to a myeloid bias as it was often observed from exhausted HSCs[44]. Particularly it was interesting that colonies from TPO treated non-LR LT-HSCs resembled a similar differentiation outcome as colonies from LR LT-HSCs. These results were in line with previous *in vivo* data where we also did not observe any lineage bias or reduced donor chimerism from TPO treated non-LR LT-HSCs compared to TPO treated LR LT-HSCs (Figure 29 A-B).

This *in vitro* differentiation assay holds great potential to assess HSC function, however, the inconsistencies observed between the LRC experiments makes interpretation of the results challenging. As this assay is very sensitive to changes in oxygen concentration and the commonly used hypoxic incubator is frequently opened, this leads to short-term increase in oxygen concentration. It was observed before that increase in oxygen leads to a formation of bigger colonies and hence biases the experiments (this was seen in an experiment where the hypoxic incubator broke). After the incubation time of 14 days the medium of big colonies is already completely used but (shift to yellow-orange color of the pH indicator in the medium). This can have a negative impact on the viability of cells. For the next in vitro colony differentiation assay it would be advisable to shorten the incubation time to for example 10 days to improve the reproducibility of the data.

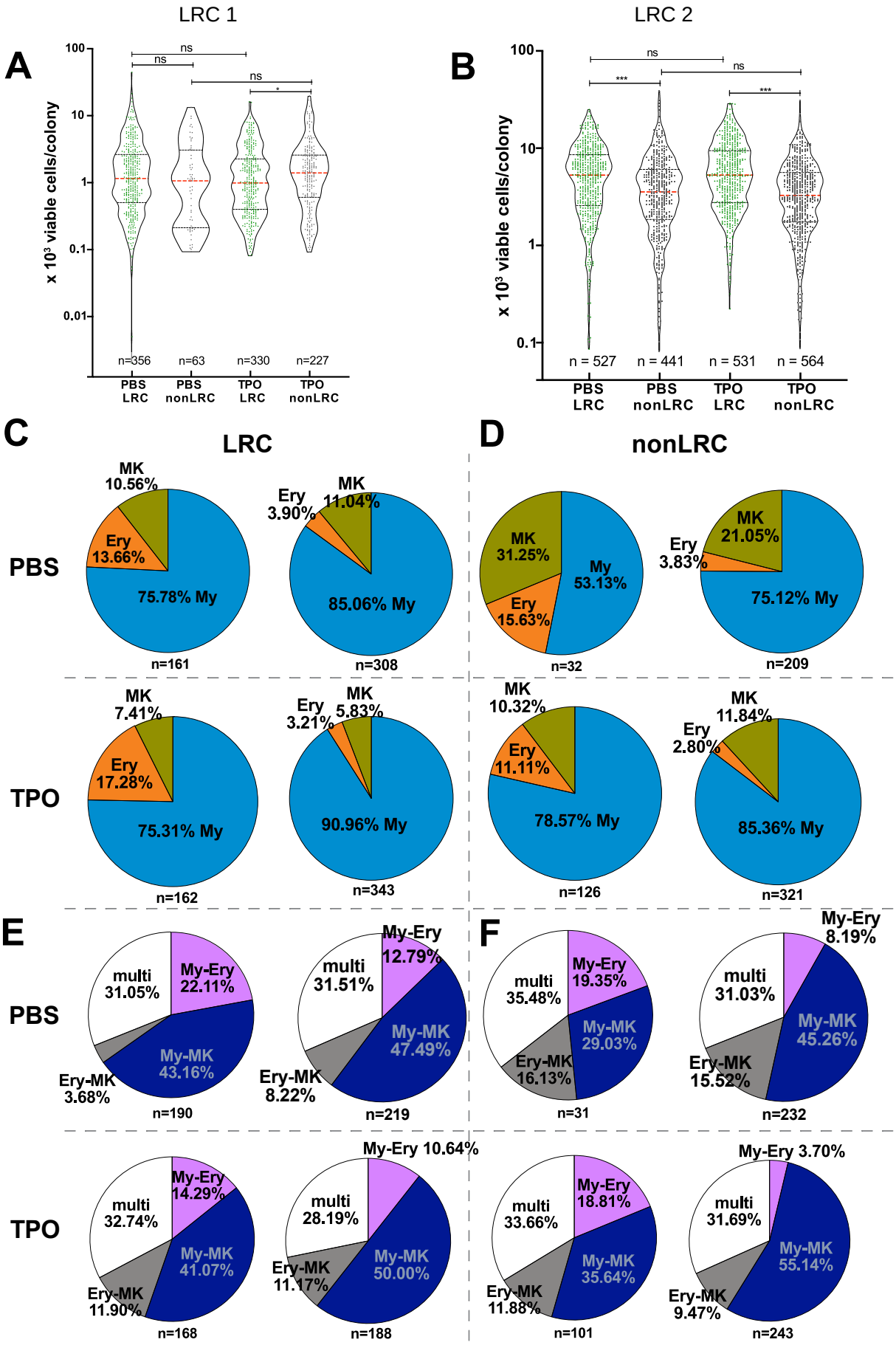
LRC 1
LRC 2
A
B
x 10³ viable cells/colony
ns
*
***
n=356
n=63
n=330
n=227
n = 527
n = 441
n = 531
n = 564
PBS LRC
PBS nonLRC
TPO LRC
TPO nonLRC
C
LRC
D
nonLRC
PBS
TPO
MK 10.56%
Ery 13.66%
75.78% My
n=161
Ery 3.90%
MK 11.04%
85.06% My
n=308
MK 31.25%
My 53.13%
Ery 15.63%
n=32
Ery 3.83%
MK 21.05%
75.12% My
n=209
MK 7.41%
Ery 17.28%
75.31% My
n=162
Ery 3.21%
MK 5.83%
90.96% My
n=343
MK 10.32%
Ery 11.11%
78.57% My
n=126
Ery 2.80%
MK 11.84%
85.36% My
n=321
E
F
multi 31.05%
My-Ery 22.11%
My-MK 43.16%
Ery-MK 3.68%
n=190
multi 31.51%
My-Ery 12.79%
My-MK 47.49%
Ery-MK 8.22%
n=219
multi 35.48%
My-Ery 19.35%
My-MK 29.03%
Ery-MK 16.13%
n=31
multi 31.03%
My-Ery 8.19%
My-MK 45.26%
Ery-MK 15.52%
n=232
multi 32.74%
My-Ery 14.29%
My-MK 41.07%
Ery-MK 11.90%
n=168
My-Ery 10.64%
multi 28.19%
My-MK 50.00%
Ery-MK 11.17%
n=188
multi 33.66%
My-Ery 18.81%
My-MK 35.64%
Ery-MK 11.88%
n=101
My-Ery 3.70%
multi 31.69%
My-MK 55.14%
Ery-MK 9.47%
n=243

Figure 33: **LR and non-LR LT-HSCs from TPO treatment displayed a similar lineage output.** A-B) Colony size displayed as number of cells per colony derived from a single LR or non-LR LT-HSC was assessed by flow cytometric analysis. n = number of acquired colonies. A) shows results from experiment 1 (LRC1) and B) shows results from experiment 2 (LRC2). C-D) Pie charts depict percentage of myeloid, erythroid and megakaryocytic differentiation output of all defined monolineage colonies from either LR or non-LR LT-HSCs from the respective experiment. Left pie chart represents results from LRC1, right pie chart represents results from LRC2. n = total number of all analyzed monolineage colonies. MK = megakaryocytic colony ($CD41^+$ and $CD42d^+$ cells), Ery = erythroid colony ($Ter119^+$ and $CD71^+$ cells), My = myeloid colony ($CD11b^+$ and $Gr\text{-}1^+$ cells). E-F) Pie charts depict percentage of myeloid-erythroid, myeloid-megakaryocytic, erythroid-megakaryocytic and multilineage differentiation output of all defined bi- and multilineage colonies from either LR or non-LR LT-HSCs from the respective experiment. Left pie chart shows LRC1, right pie chart shows LRC2 results. n = total number of all analyzed bi- and multilineage colonies.

3.6 Rag2 KO mice responded to serial TPO stimulation

From the above-mentioned LRC experiments and our *in vitro* data we know that one round of TPO treatment pushes HSCs into cycle and has an impact on their signaling processes indicated by an increased LT-HSCs pool and does not show any signs of reduced lineage potential. Since these were interesting findings, we wanted to pursue an extended TPO treatment. However, as we cannot use wt mice due to TPO being immunogenic after several rounds, we used the Rag2 KO mouse model. These mice harbor a mutation in the Rag2 protein which is involved in the VDJ recombination of B- and T-cell receptors. Therefore, maturation of B- and T- cell receptors is incomplete within these mice resulting in impaired immune responses[106]. We assumed that by using an immunodeficient mouse model (Rag2 KO), no immune response should be induced after three treatment rounds of TPO. First, we wanted to verify that Rag2 KO LT-HSCs still responded to the TPO stimulus after three rounds and set up the same experiment as described in Figure 25 A to examine LT-HSC cycling 24h after the 24^{th} injection. Additionally, we took a PB sample before (Day 0) and 24h after the last injection of each treatment round to monitor PB parameters (Figure 34 A-C). Since we knew that mice responded to a single injection, we included two Rag2 KO mice which received only a single TPO or PBS injection as controls for cell cycle activation. As expected, WBC counts were below the normal range due to the lack of mature B- and T- cells in Rag2 KO mice. RBC counts from both PBS and TPO treated mice were within a normal range. Also, platelet counts were within a normal range before the treatment but steadily increased with every TPO treatment round until platelet levels were doubled after three rounds ($1234 \times 10^3 \pm 190$ platelets/µl blood in PBS, $2472 \times 10^3 \pm 270$ platelets/µl blood after three rounds of TPO). In line with previous data, 24h after a single injection platelet levels did not rise.

Similar to previous data, we sacrificed mice 24h after the last injection of round three and observed an increase in absolute LT-HSC numbers after three rounds of treatment in Rag2 KO mice (Figure 34 D). These mice showed an eight-fold increase in LT-HSC counts after TPO treatment

compared to PBS control. When analyzing the cell cycle of LT-HSCs using Ki67/Hoechst, only 26% ± 8% of LT-HSCs remained in G0-phase, which was comparable to the activation induced after a single injection with 19% ± 2% of LT-HSCs being in G0-phase (Figure 34 E). Due to mice still responding to TPO treatment after three rounds, we expected a reduction in femur counts. Reduction of femur cellularity often comes along with HSC exhaustion which is not only a hallmark of aging but also an indicator of an increased risk to develop BM disorders[47]. Past experiments that have been conducted with polyI:C showed that LT-HSCs from mice which responded to the polyI:C stimulus after three rounds showed reduced femur cellularity[44,45]. When we measured femur cellularity in Rag2 KO mice after three rounds of TPO treatment we found a significant reduction (1.7-fold decrease) in cell numbers per femur compared to results from PBS treated mice (Figure 34 F). In order to find out if LT-HSCs were exhausted hence, functionally impaired, we set up another cohort of Rag2 KO mice. These mice were also treated with three rounds of TPO and we performed competitive transplantation assays to asses HSC function. Since these are long-term experiments and the endpoint is scheduled for July 2021, results from this experiment are not presented in this thesis.

In summary, when treating Rag2 KO mice for three rounds with TPO, an increase in platelet counts and LT-HSC numbers was observed. Furthermore, we have reason to speculate that repeated TPO treatment led to HSC exhaustion as we observed a drastic decrease in femur cellularity. However, this has to be verified by functional assays such as competitive transplantations.

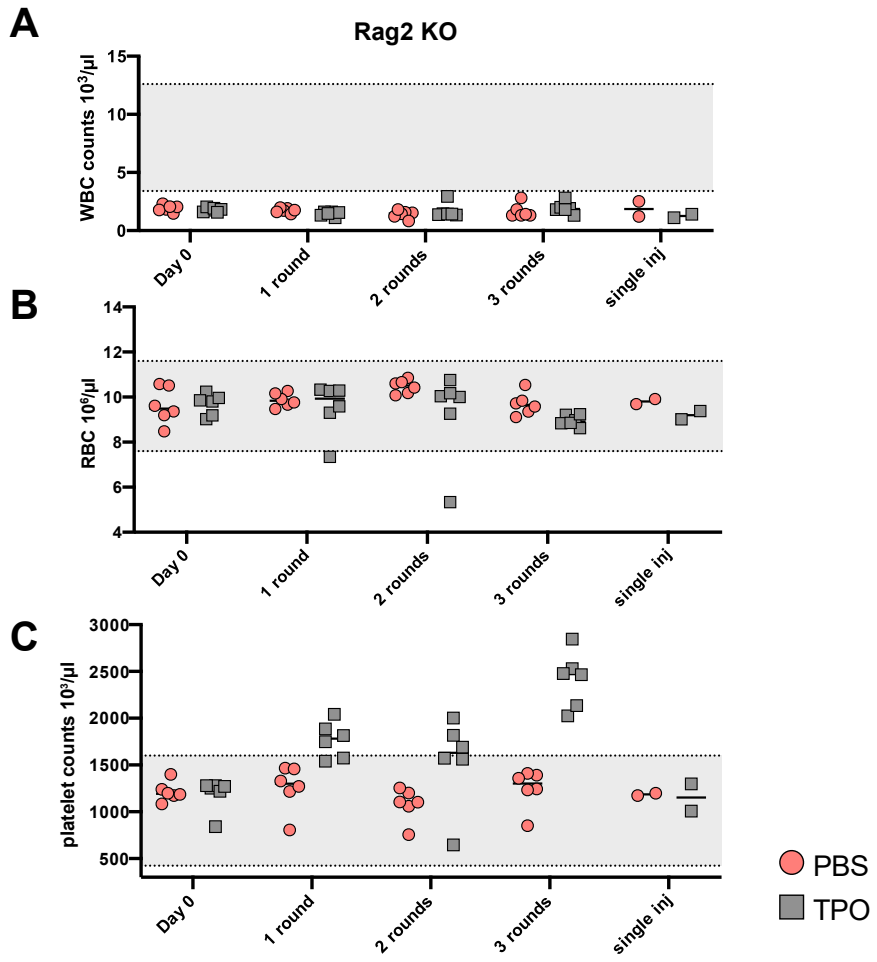
A
Rag2 KO
WBC counts 10³/µl
15
10
5
0
Day 0
1 round
2 rounds
3 rounds
single inj
B
RBC 10⁶/µl
14
12
10
8
6
4
Day 0
1 round
2 rounds
3 rounds
single inj
C
platelet counts 10³/µl
3000
2500
2000
1500
1000
500
Day 0
1 round
2 rounds
3 rounds
single inj
PBS
TPO

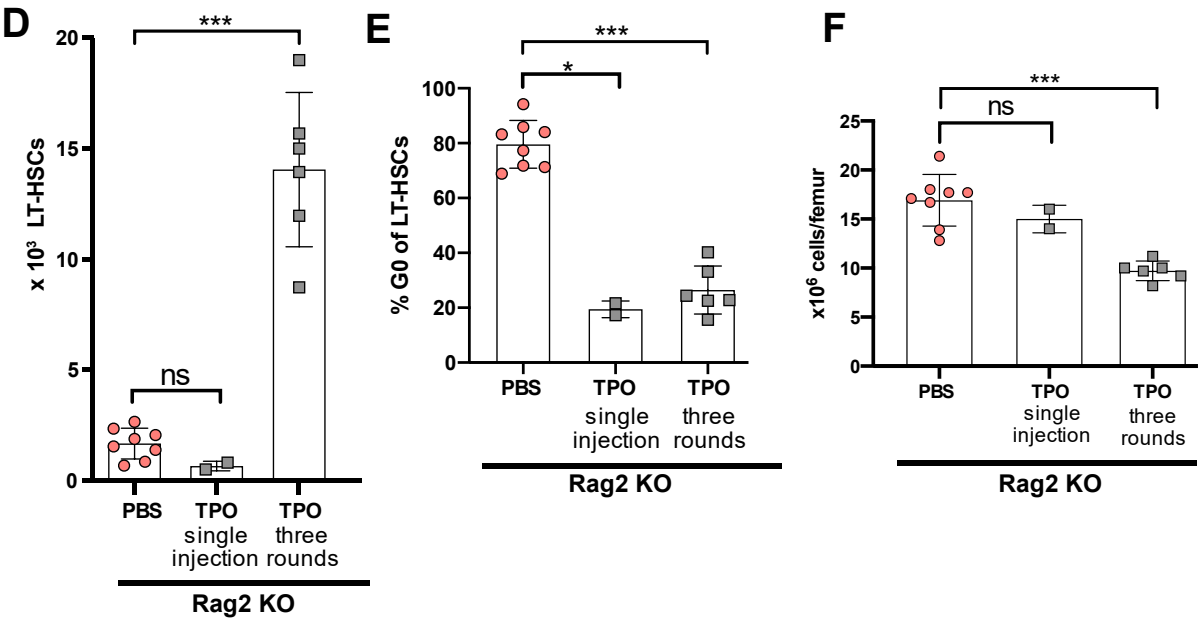
D
x 10³ LT-HSCs
20
15
10
5
0
***
ns
PBS
TPO single injection
TPO three rounds
Rag2 KO
E
% G0 of LT-HSCs
100
80
60
40
20
0
***
*
PBS
TPO single injection
TPO three rounds
Rag2 KO
F
x10⁶ cells/femur
25
20
15
10
5
0
***
ns
PBS
TPO single injection
TPO three rounds
Rag2 KO

Figure 34: **After three rounds of TPO treatment LT-HSCs from Rag2 KO mice showed robust cell cycle activity.** A-C) Rag2 KO mice were treated for three rounds with TPO and PBS. PB blood was collected from Rag2 KO mice before the treatment started (Day 0) and 24h after every treatment round as well as from mice treated only once with TPO or PBS (single inj). PB was analyzed with a hematology analyzer. WBC, RBC and platelet counts are shown. For three treatment rounds n = 6 mice were used for single injection n = 2 mice were used. D-F) At 24h after the last injection of round three or after a single injection, mice were sacrificed, BM isolated and subsequently stained for LT-HSCs and Ki67/Hoechst and analyzed. Absolute numbers of LT-HSCs were determined. D) Absolute number of LT-HSCs per femur was determined. E) Percentages of LT-HSCs in G0-phase are displayed. F) Femur cellularity of treated Rag2 KO mice was assessed.

4 Discussion – part one

In this part we focused on hematopoietic development. There are still many open questions regarding hematopoietic specification, which cell type is the first to emerge during hematopoietic development and how to best reconstruct hematopoietic development *in vitro*. Our lab has optimized an *in vitro* differentiation protocol[32] and established an experimental workflow which enabled identifying markers during endothelial to hematopoietic transition (EHT)[26]. EHT is a critical step in the hematopoietic specification process and describes the emergence of the first hematopoietic cell. During previous experiments Evi2a was identified to be highly upregulated during EHT and *in vitro* differentiation experiments showed that Evi2a KO ESCs were impaired in their ability to form hematopoietic cells.

In this study we investigated the role of the largely uncharacterized ecotropic viral integration site 2a (Evi2a) protein during hematopoietic specification. By performing differential gene expression analysis on RNA seq data of differentiated Hoxb4^{+} Evi2a KO and Hoxb4^{+} wt cells we aimed to find out about deregulated pathways upon Evi2a KO. We aimed to delineate deregulated pathways upon Evi2a KO during hematopoietic specification to in turn appreciate the importance of Evi2a during development. Furthermore, we also addressed the function of Evi2a *in vivo* by generating an Evi2a KO mouse model.

4.1 Developmental hematopoiesis

As mentioned before the exact mechanisms of hematopoietic specification are still a matter of debate. Starting already at the point which could mark the hematopoietic precursor cell. Hematopoietic cells have been shown to derive form an endothelial precursor which has both hematopoietic and endothelial potential. However, two possible cell types or cellular structures are considered to be the common endothelial-hematopoietic precursor: the hemangioblast and the hemogenic endothelium[2,135]. It is still not fully understood if the hemangioblast is a true cell that can actually be isolated or rather represents a precursor cell emerging at the end of the primitive streak and beginning of mesoderm formation, harboring hematopoietic and endothelial fate[136]. However, it was suggested that the hemangioblast is Flk1 (Kdr)-positive[135] and only capable of forming primitive erythroid cells and does not contribute to formation of definitive hematopoietic cells[7]. In order to resolve the function of the hemangioblast, early murine embryos could be dissected and highly sensitive methods like single cell sequencing or spatial transcriptomics could be applied to obtain further information regarding emerging endothelial-hematopoietic precursors. The hemogenic endothelium in contrast is more defined than the hemangioblast and is widely accepted to be the precursor of definitive hematopoietic cells.

However, also the HE is not exactly defined by CSM expression or a specific location. K. Hirschi presented data that HE emerges in the YS[8]. A detailed study by Hou *et al*. suggested that HE emerges at E9.5 mainly from the ventral side of the DA. They specified HE cells as $CD44^+$ $Neurl3^{+}$[11]. CD44 has been reported before to be present on hemogenic cells[137] and thus, represents a potential marker for identifying HE.

One reason for the seemingly controversial findings could be that hematopoietic development takes place in different sites and to different time points. Dzierzak and Bigas reviewed the complexity of the hematopoietic development[138]. Hematopoietic specification does not only take place in the ventral side of the DA but also in the extraembryonic YS and the placenta. During an early developmental stage, all of these tissues show endothelial characteristics. Hence, it is difficult to depict which cell the origin of the hematopoietic system is. Of note, another level of complexity might be added by the already established blood circulation at around E8.25. HE or pre-mature hematopoietic cells can easily migrate from one to another location. Hence, it could be that hematopoietic development starts at different sites but the origin cell was the same[138,139].

Once EHT is executed, first definitive hematopoietic cells are detected and identified by CSM expression of hematopoietic markers such as c-kit, CD45, CD41 and EPCR (CD201) or by transcription factor expression such as Runx1, Erg, Fli1 and Gata2 at E11.5 in the AGM. The knowledge of advanced hematopoietic development increases from this point onwards mainly due to the rise in generated cells[138,140,23].

4.1.1 Hematopoietic development *in vitro*

Since isolating and propagating the first hematopoietic stem cell holds great therapeutic potential the interest in resolving hematopoietic specification to simulate hematopoietic development *in vitro* is high. The young, non-exhausted and unbiased HSCs arising during development, could be transplanted into patients with BM failure syndrome or patients with hematopoietic malignancies to replace the diseased hematopoietic system with a healthy one[12,141]. However, it is not as trivial as it sounds since developmental processes are highly dynamic and involve different cell types and structures, which presents major obstacles to reconstruct hematopoietic specification *in vitro*. The fact that not all signaling processes of hematopoietic development are uncovered adds on to the difficulty of finding appropriate culture conditions. Progress has been made and in 2008 Pearson *et al*. established an *in vitro* protocol that robustly generated brachyury-positive mesoderm[32]. In our group, using this protocol, we also showed the generation of $c\text{-}Kit^{+}CD41^{+}$ hematopoietic cells. However, when we co-cultured these hematopoietic cells on OP9 cells to induce B cell formation we hardly obtained mature B-cells. This showed that even though cells can be pushed by exogenous factors into a certain differentiation pathway and phenotypically appear as hematopoietic cells this does not mean that fully functional cells were generated. A few years later

Teichweyde *et al*. tried to overcome this issue of generating non-functional cells, by inherently changing the cells and overexpressed Hoxb4 in ESCs. This led to hemogenic endothelial formation and robust $CD41^{+}CD45^{+}$ hematopoietic cell expansion *in vitro*[23]. A more recent study by Elahi *et al*. considered the dynamic processes during development and established a protocol to transiently knock out ARS2 an RNA binding protein. This to some extent enhanced the expansion of $Sca\text{-}1^{+}EPCR^{+}$ hematopoietic cells[142]. However, mimicking the dynamic processes during development will remain a major obstacle in *in vitro* cell culture.

The most promising studies of *in vitro* HSC generation have been published in 2017 in nature. The group of Rafii and Daley transduced several transcription factors into $CD34^{+}$ HE cells or murine endothelial cells, respectively, and showed engraftment after transplantation of *in vitro* generated HSCs. Additionally, in both studies even secondary transplantations could be performed, but overall donor chimerism and immune responses were low. Moreover, both studies also compared the transcriptome between *in vitro* generated and *in vivo* isolated cells and could identify similar expression patterns of hematopoietic transcription factors. Drawbacks of both studies are that viral transductions leading to integration of foreign DNA, pose a risk of developing anomalies. Performing DNA methylation analysis to compare the epigenome would have added additional information whether generated HSCs do not only phenotypically but also intrinsically display true HSC characteristics[34,35]. Thus, some optimizations of culture conditions have to be performed, these studies hold great potential in developing not only murine HSCs but hopefully soon human HSCs *in vitro*.

In recent years, more sensitive techniques like single cell sequencing or spatial transcriptomics were developed and huge progress was made in examining unperturbed hematopoietic development *in vivo*. Many transcription factors or cells surface receptors have been identified. Even though these studies often lack functional data this knowledge can still help to understand hematopoietic development and advance the design of *in vitro* protocols.

4.1.2 Hoxb4 as early hematopoietic marker

A big challenge is the isolation of the precursors of the first hematopoietic stem cell since the exact characteristics of this cell are not known yet. However, it is known that hematopoietic cells derive form an endothelial precursor. Some genes have been identified that were already expressed in endothelial cells and retained their expression throughout the formation of definitive hematopoietic cells. Generation of reporter mouse models to monitor gene expression of this specific gene, allows to isolate cells along the endothelial to hematopoietic specification *in vivo* and *in vitro*. As an example, the homeobox protein Hoxb4 is expressed early during development and was shown to lead to hematopoietic expansion when overexpressed in ESCs[143]. A Hoxb4-YFP reporter mouse model verified early Hoxb4 expression in AGM and high Hoxb4 expression in FL

and adult HSCs[24]. In a previous study conducted in our group, a Hoxb4-YFP expressing reporter ESC line was developed in order to differentiate these to hematopoietic cells and due to Hoxb4-YFP expression we were able to sort emerging hematopoietic precursors. It was shown that Hoxb4-YFP$^+$ cells were in a transitional state and expressed both endothelial (Flk1, Ve-Cadherin) and hematopoietic (CD41, c-Kit, Aa4.1) CSM. By sorting and performing microarray analysis on three different cell types: (i) immature endothelial Hoxb4$^-$ cells (ii) Hoxb4$^+$ Aa4.1$^+$ transitional cells (iii) definitive hematopoietic cells Hoxb4$^-$CD41$^+$, the group found out that several cell surface proteins were specifically expressed on the Hoxb4$^+$Aa4.1$^+$ population. Amongst them was Evi2a. When knocking out Evi2a in ESCs followed by *in vitro* differentiation of Evi2a KO ESCs to hematopoietic cells, it was observed that Evi2a KO cells were impaired in their hematopoietic differentiation potential. Interestingly, the Evi2a KO cells still expressed Hoxb4 but could not generate CD41$^+$c-Kit$^+$ hematopoietic cells[26] indicating that pre-mature hematopoietic programs can be activated but differentiation would not precede.

4.2 Evi2a – a cell surface marker with uncharacterized function

Not much was known about the Evi2a gene except that it (i) is a likely spot for viral integration, (ii) encodes for a cell surface receptor, (iii) is located within an intron of the Nf1 gene[28] and (iv) upregulated in some leukemic cell lines[31]. Remarkably, upon KO hematopoietic development was clearly impaired. Interesting parallels can be drawn to the well described ecotropic viral integration protein 1 (Evi1/Mecom). The transcription factor Evi1 is crucial for hematopoietic development. However, de-regulation of Evi1 in adult hematopoietic cells leads to Evi1 overexpression and induces a malignant transformation, which in the worst case can stimulate leukemia[144]. Similarly, the transcription factor Runx1 also crucial for hematopoietic development leads to formation of leukemia when mutated[21,145]. We assumed that Evi2a could have similar characteristics that it is crucial for hematopoietic development but when mutated or overexpressed leading to the onset of malignant phenotypes.

We aimed to identify the role of Evi2a in developmental signaling pathways and performed RNA seq and differential gene expression analysis on Hoxb4$^+$ wt and Hoxb4$^+$ Evi2a KO cells on three consecutive days after *in vitro* hematopoietic differentiation.

4.2.1 Evi2a during developmental hematopoiesis *in vitro*

Previous studies performed by Dr. Paul Kaschutnig addressed the question which markers to use to identify cells undergoing EHT. It was postulated that Evi2a is crucial for hematopoietic development *in vitro*. The difficulty of studying Evi2a is, that it has not been well investigated during development so far and e.g., no antibodies were developed to detect its presence. It was only mentioned in a study from Zeng *et al*. where it was observed as one of the top ten markers being upregulated in lymphoid differentiation[29].

In this thesis, we focused more broadly on Evi2a and its role during early development. Our study suggested that Evi2a might already play a role in the early hematopoietic specification process since we only detected early endothelial-hematopoietic cells ($Flk1^{+}Hoxb4^{+}$) upon *in vitro* differentiation of Evi2a KO cells. Upon Evi2a KO and subsequent differentiation of these cells a profound defect in hematopoietic specification was observed. After performing PC analysis, it was striking that Evi2a KO cells from day 6 clustered closely with wt cells from day 5 suggesting that Evi2a delayed the differentiation process (Figure 8 B). This hypothesis was supported by the fact that c-Kit expression was also delayed. c-Kit was highly expressed in wt cells on day 4 whereas it was upregulated in Evi2a KO cells on day 5 (Figure 8 D). Interestingly, Evi2a KO cells were still able to express Runx1, a transcription factor known to be required for EHT initiation[21].

Upregulation of Cdh2 and Cdh11 (mesoderm specification) as well as downregulation of Gdf3 (a pluripotency marker) in wt cells on day 4 indicated that Evi2a KO cells remained in a rather undifferentiated state after 4 days of *in vitro* differentiation. Evi2a KO cells have probably not reached a mesodermal state yet. Furthermore, volcano plot analysis revealed that mature hematopoietic markers such as Gypa (erythroid marker)[25] and Csf2rb (lymphoid marker)[146] were overexpressed on day 5 and day 6 in wt cells indicating that wt cells advanced in their development. In contrast, Chd3, Cdx2 and Wnt5a were downregulated in wt cells on day 6 concluding that these were upregulated in Evi2a KO day 6. Chd3 and Cdx2 are involved in the formation of trophectoderm[110] and Wnt5a, amongst other functions, induces mesoderm formation[7]. This data supports the hypothesis that Evi2a KO cells were delayed in their developmental process and that Evi2a is already involved in mesoderm formation or differentiation. Mesoderm formation depends on EMT. At the end of the primitive streak when gastrulation starts cells need to leave their cellular bond to be able to migrate to a different location. This process is an essential incident during gastrulation and mesoderm formation. GSEA reinforces the previous observations that Evi2a KO leads to impaired mesodermal formation since EMT was enriched in wt cells day on 4 but only enriched in Evi2a KO cells on day 5. Hedgehog signaling is a crucial signaling axis in EHT[111], hence, it is usually expressed early on during development. Hedgehog signaling was already enriched in wt cells on day 4 whereas it was only enriched in Evi2a KO cells on day 6.

By additionally performing IPA analysis we confirmed the previous trend that Evi2a KO delayed development but is still able to induce hemogenic endothelium formation. Of note, IPA analysis revealed that not only downstream processes involved in hematopoietic specification were deregulated or delayed upon Evi2a KO but that the delay in signaling was already apparent at the level of pluripotent state. IPA core analysis revealed that Nanog expression and stem cell pluripotency signaling were deregulated on day 4 and day 5. It should be noted that we only examined a short developmental window ranging from early EHT to early hematopoietic development which hampers the interpretation whether Evi2a KO cells were only delayed in their hematopoietic formation potential. Examining Evi2a KO cells during earlier time points would probably resolve if Evi2a KO leads to impaired mesoderm formation. Additionally, differentiated cells could be stained for the mesodermal marker brachyury and flow cytometrically analyzed.

A disadvantage of performing RNA seq on bulk samples from a highly heterogeneous and probably profoundly dynamic cell population is that smaller differences between cells or cell types get lost. Implementing single cell sequencing would allow to perform pseudotime analysis and get a more detailed idea of the differentiation process. We also never continued *in vitro* differentiation of wt and Evi2a KO cells beyond day 6 to inspect if Evi2a KO cells caught up in hematopoietic development or if they stayed at an immature phenotype with hardly any hematopoietic characteristics. Since we saw an upregulation of Hoxa10 in Evi2a KO cells on day 6 (Figure 9 A), this this could support the delay in the hematopoietic specification rather than a complete impairment of hematopoietic differentiation. Hoxa10 is a known regulator for HSPC development[147].

For further studies on this data set it would be advisable to compare Evi2a KO cells on day 5 with wt cells on day 4 as well as Evi2a KO cells on day 6 and wt cells on day 5. If differences in gene expression are less pronounced between these samples that would underpin our hypothesis of Evi2a KO delaying embryonic development. Since we were very restricted in our differentiation model by inducing hematopoietic specification, we could only make an assumption about the function of Evi2a in development. Recently, it has been shown by Wang *et al*. that Evi2a is involved in prefrontal cortex development. The human protein atlas database (https://www.proteinatlas.org/ENSG00000126860-EVI2A) also reports high expression of Evi2a in brain and neuronal tissue. Considering this information, the hypothesis that Evi2a KO delays not only hematopoietic development but already fundamental developmental processes can be formed.

In this study we did not specifically address which genes or pathways are upstream or downstream of Evi2a but rather only examined deregulated pathways. We observed that Runx1 was upregulated in Evi2a KO cells on day 6 (Figure 8 D) but it would be interesting to see if Evi2a is also still upregulated upon Runx1 KO, as Runx1 is crucial for generating blood cells[148]. As example, Runx1 KO ESCs could be *in vitro* differentiated and Evi2a expression could be analyzed on day 4, 5 and 6. This would clarify if Evi2a might be dependent on Runx1.

4.2.2 Functional analysis of Evi2a *in vivo*

By generating a KO mouse model, we wanted to analyze the importance and function of Evi2a *in vivo*. We successfully established heterozygous Evi2a KO mice and showed that heterozygous Evi2a KO did not negatively impact the survival of adult mice. Peripheral blood parameters of up to one-year old Evi2a$^{wt/KO}$ mice were in a normal range (Figure 14). This also excluded a putative haploinsufficiency which was, for example observed upon heterozygous Gata2 KO[149].

When generating homozygous Evi2a KO mice, we were not successful. On the one hand it could be that homozygous Evi2a KO is embryonically lethal, on the other hand it could be that when the Evi2a vector was introduced into the ESCs, the recombination took place only with one allele of the sister chromatids. Hence, the KO could be induced on only one allele and the second allele would still have the wt Evi2a sequence. Monoallelic integrations are frequently observed after transfection. In order to achieve bi-allelic integration heterozygous KO cells can be targeted again to induce the KO on the residual allele. Furthermore, methods such as the CRISPR/Cas9 technique have been developed to specifically induce KO on both alleles[150].

We addressed the question to which time point Evi2a KO is embryonically lethal by setting up timed matings and aimed to look for defective hematopoiesis. Embryos were examined phenotypically by microscopy and molecularly by genotyping. Primers were designed such that the presence (wt) of absence (KO) of the Evi2a gene could be detected. So far, we only analyzed pups at E10.5. Genotyping of these pups uncovered that all 16 pups were heterozygous for Evi2a. There might be two reasons why we obtained only heterozygous mice: The first reason could be a technical issue. The isolated embryos could have been contaminated with maternal cells. Since isolating pups requires some practice and we did it the first time this could have led to a poor quality of the embryo isolation. This hypothesis would be supported by the fact that we also did not detect any wt embryos, which would be expected according to the mendelian law. The second reason could be that pups died before E10.5. Since hedgehog signaling was affected this could support the hypothesis that Evi2a signaling might already be crucial for AGM formation and embryos could have died as early as E8[111]. For the next timed mating set up we should rather take a look at E7.5 or E8.5 when mesoderm is established and hematopoietic and endothelial precursors such as hemangioblast and hemogenic endothelium can be detected.

5 Discussion – Part two

Hematopoietic stem cells are crucial for healthy blood production throughout the entire lifetime of an organism. Under homeostatic conditions, most of the HSCs are in a dormant state in the so-called niche of the bone marrow. However, in aged humans it has been observed that peripheral blood composition is out of balance, including a frequently observed myeloid bias and a subsequently high risk of acquiring severe bone marrow diseases[68]. The question that still remains is, which events or circumstances lead to or induce these changes in PB composition over time. That being said, taking a closer look at the HSC compartment may provide us with some answers as it is the likely origin of the adverse blood production.

It was suggested that stress, in particular inflammatory stress, regularly pushes HSCs into cycle, leading to an increased risk of acquiring DNA mutations, which may result in aberrant signaling that could lead to uncontrolled proliferation[44,151]. Many studies have already investigated the concept of HSC exhaustion using inflammatory agents. This HSCs stimulation resulted in a dysfunction in blood production as well as adverse BM composition[152,45]. We made use of two agonists that activate HSCs but would not induce an inflammatory response, to see if stressed HSCs also exhibit this exhaustion phenotype after repeated non-inflammatory stimulation.

In this part we were interested in how repeated stress and recurrent activation of hematopoietic stem cells affected their function and whether there were a few remaining dormant and fully potent HSCs that resided in the bone marrow throughout the challenging events.

5.1 Implementation of our work into known literature

5.1.1 Exhaustion of HSCs upon serial activation

Amongst all blood cancers, myeloid leukemias (acute and chronic myeloid leukemias) are the most prevalent. The risk of developing a myeloid leukemia is highest in people older than 70 years[69]. Even though a leukemic incidence is often correlated to mutated genes, the question remains whether this mutation was acquired during inaccurate DNA replication in HSCs due to induced proliferation stress or whether it was induced by for example, environmental and exogenous agents. It was assumed that repeated exit out of dormancy over an individual´s lifetime leads to an accumulation of DNA mutations in HSCs and subsequently to the development of (pre-) malignant diseases. On the other hand, dysfunctional HSCs might also just be lost by for example, undergoing apoptosis which would lead to BM failure syndromes[83]. In this work we concentrated on consequences of induced proliferative stress on the hematopoietic system.

The concept of HSC exhaustion that we examined in this thesis was based on several studies. Initially, it was found that under normal circumstances, the HSC pool increases with age, but at the same time phenotypic HSCs display a loss-of-function in transplantation assays, as well as a myeloid bias and impaired lymphoid repopulation potential. The same effects, HSC loss-of-function and increased DNA damage, were also observed after recurrent replication stress induced by either G-CSF, IFN alpha or the dsRNA mimetic polyI:C. HSC function was analyzed by transplantation assays and likewise, a lower donor engraftment from agonist treated mice in comparison to control treatment was identified. Additionally, these studies also confirmed the myeloid lineage bias along with a reduced lymphoid potential of serially activated HSCs[152,45,44]. In the field it was hypothesized that aged HSCs divided more often than young HSCs. Hence, the increased replication stress led to an increase in DNA damage resulting in aberrant HSC function[151]. However, HSCs as all cells in general can repair (induced) DNA damage by either homologous recombination (HR) or non-homologous end joining (NHEJ) repair, whereas NHEJ is preferred in non-dividing HSCs[153]. However, with age and under constant stress also DNA damage response pathway and DNA repair machinery decrease in accuracy and DNA damages cannot be repaired sufficiently any more[47].

In the aforementioned studies, inflammatory agonists were used to stimulate and push HSCs into cycle. Thereupon, we set to investigate whether a non-inflammatory stress inducing agent would lead to the same loss-of-function phenotype, as if HSCs were activated in a non-inflammatory manner. We chose thrombopoietin (TPO) as an activating agent since the TPO receptor Mpl is expressed directly on HSCs and is able to push HSCs into cycle. Moreover, Mpl receptor agonists are used in the clinics.

5.1.2 TPO: good or bad for hematopoietic stem cells

TPO is an interesting molecule to study since its impact on HSCs is not yet completely clear and its effects are a subject of controversial discussions. Namely, even though TPO activates HSCs and leads to their exit of dormancy, it has been speculated that TPO-induced activation does not lead to HSC exhaustion but rather to HSC self-renewal. Self-renewal is defined by a symmetric cell division, where the daughter cell harbors the same potential as the mother cell. It was shown that TPO mimetic stimulated HSCs divided several times but could still engraft after secondary transplantation whereas control cells that divided naturally, did not engraft after secondary transplantations. In the mentioned study the conclusion was that TPO mimetic-induced proliferation led to self-renewal. However, it seemed that the majority of the transplanted cells from TPO mimetic treated mice gave rise to an increased myeloid proportion in the donor compartment. However, the lineage output was not further examined in the study from Kovtonyuk *et al*.[80].

In contrast to the previous study, it has been observed that TPO is required to keep HSCs in a quiescent and dormant state. The following points summarize the main findings of two studies by Yoshihara *et al*. and Quian *et al*. from 2007: (i) TPO signaling upregulated ß-1 integrin expression and increased adherence to stromal cells in co-culture experiments concluding, that TPO is required to keep HSCs in the quiescent niche. (ii) The TPO receptor Mpl is highly expressed on $CD34^-$LSKs and after keeping these cells in TPO-containing culture medium, they showed an upregulation of the negative cell cycle regulator Cdkn1c. Concluding that TPO stimulation led to upregulation of cell cycle inhibitors. (iii) Additionally, both Mpl^+LSKs and Mpl^+CD34^-LSKs led to higher engraftment after transplantation than their Mpl^- controls suggesting that cells that can respond to TPO retain a higher potential than cells that cannot respond to TPO signaling[77]. (iv) $TPO^{-/-}$ and $MPL^{-/-}$ mice have significantly decreased HSC numbers and $TPO^{-/-}$ HSCs show increased proliferation indicating that TPO and TPO signaling are required for a normal and functional HSC pool[76].

All of the above-mentioned studies examined TPO signaling in a very specific and isolated setting. However, TPO regulation is very complex and acts on different levels. On one hand TPO leads to MK and platelet activation but on the other hand MKs and platelets internalize TPO. Suggesting that there are feedback loops between MKs and peripheral platelet counts likely leading to fluctuating TPO levels in the blood plasma[91]. Since $TPO^{-/-}$ mice show increased HSC cycling and have reduced platelet levels[76] it could alternatively be interpreted such that not the lack of TPO-induced HSC cycling but decreased platelet numbers led to HSC activation. However, this hypothesis would have to be validated experimentally.

In our experiments, we did not measure TPO concentrations to monitor potential fluctuating levels and also did not measure platelet counts withing the scope of one treatment round. But from the dose finding experiments (Figure 17 C) we known that platelet levels increased between 48h and 72h after the injection. In our three round treatment schedule (Figure 20) we applied the second injection 48h after the first one meaning that platelet levels were still within a normal range, so the TPO from the second injection should still have the same effect than the first TPO injection. We assumed that the same amount of the injected TPO reached the LT-HSCs after the second injection. However, from the previous dose finding experiments we know that platelet levels are approximately 1.7-fold higher after 96h. In the three round experiments, the third injection is applied 120h after the second injection and platelet levels were probably still elevated. In conclusion, most of the injected TPO from the third injection might have been internalized by the platelets leaving probably less TPO to activate HSCs. But since we saw a robust increase in platelet counts even after a five-week recovery period, we know that platelet levels remained high at some point during the treatment regimen. Additionally, from the LRC mouse model we know that HSCs were sufficiently activated after one round of TPO treatment as the GFP label loss in TPO and polyI:C treated mice was almost identical (Figure 28).

In 2013 de Laval *et al*. reported that TPO stimulation increased non-homologous end joining (NHEJ) repair pathway. They showed that irradiation-induced DNA damage was prevented by administering TPO to mice shortly before the irradiation process[81]. However, in a study from Mohrin *et al*. it was shown that activation of HSCs prior to exposure to irradiation had a favorable outcome since DNA repair pathways had already been activated due to the previously administered stimulating agent[153]. It is well known that DNA damages accumulate in quiescent HSCs and eventually get repaired once the cell is activated. In the study from Beerman *et al*. the stimulation was secondary since they used 5-FU as *in vivo* and cell culture as *in vitro* stimulant to activate DNA repair mechanisms in old, dormant HSCs[154]. It remains to be elucidated whether only TPO led to this beneficial effect in the first study or whether any other stimulating agent would have had the same effect. After interpreting these studies, it suggests that the agonist that leads to HSCs activation is of minor importance. Due to the induced cycling prior to mutagenic stimulation, cells were better prepared as DNA repair programs have already been upregulated.

Since the mode of action of TPO is diverse we monitored platelet and WBC counts, femur cellularity and LT-HSC counts in our experiments. By doing so, we wanted to ensure that we have an overall assessment of the TPO effect on the peripheral blood and bone marrow. In addition, some of the above mentioned studies also suggested that TPO acts on progenitor cells[77,153]. Thus, we stained BM for oligopotent progenitors like CMPs, GMPs and MEPs. We did not detect any significant differences in the above-mentioned populations between PBS and TPO treatment.

One of the well described signaling pathways that are activated upon TPO signaling via its receptor Mpl is the JAK2/STAT5 pathway. Mpl activates Jak2 signaling which, when constitutively active, is one of the leading drivers of myeloproliferative neoplasms (MPNs)[155]. By constantly activating this signaling pathway via repetitive TPO injections, we could have potentially paved the way for the development of diseases like polycythemia vera (PV) or essential thrombocythemia (ET)[156] in the treated mice. However, since all measured PB parameters were within a normal range and mice did not exhibit any signs of pain or stress from the external appearance, we cannot claim that we induced a pre-malignant MPN phenotype. In order to look for adverse BM composition we could stain BM sections and examine these for abnormal composition or increased reticulin.

5.1.3 Defined LT-HSCs are already biased

In this and also other studies, a myeloid lineage bias in the PB compartment is considered to be a sign for HSCs being exhausted, aged or dysfunctional[49]. However, depending on how HSCs or LT-HSCs are phenotypically defined, a bias might already be introduced. The phenotypic definition of (LT-) HSCs can have an impact on the observed lineage outcome in the transplantation or *in vitro* differentiation assay. For sure, the most potent HSCs are quiescent. In addition to previous studies, this has recently been confirmed by Pietras *et al*. where they found that EPCR is a marker of

quiescent cells and that LSK SLAM CD34$^-$ EPCR$^+$ cells outperform the LSK SLAM CD34$^-$ EPCR$^-$ cells[157]. In our study, we did not include EPCR, but used the LRC mouse model to define the quiescent and more potent LT-HSCs within the phenotypic LT-HSC pool. However, even this potent cell population shows some cycling activity under homeostatic conditions shown by gradual loss of GFP label over time[61].

Here, we defined our LT-HSCs as CD34$^-$ HSCs (HSCs defined as: lin$^-$Sca-1$^+$c-kit$^+$CD150$^+$CD48$^-$)[44] and claimed that the LT-HSCs were expanded upon treatment. However, since the LT-HSCs pool is a very heterogeneous population we should have included further markers to define and understand which type of LT-HSCs were expanded. Using for example Flt3 (CD135/Flk2), known to be expressed on lymphoid primed HSPCs and lymphoid primed sub-fractions of LT-HSCs, would resolve if only lymphoid biased LT-HSCs were expanded[55].

Likewise, including the cell surface marker CD41, CD9, MPL or vWF (von Willebrand factor) could have helped us to more precisely define whether the whole LT-HSCs pool or only a very specific subset of LT-HSCs have been expanded upon serial TPO treatment. For instance, CD41 positive LT-HSCs have been studied extensively as this HSC sub-fraction is increased during aging but still confers high overall engraftment efficacy and high platelet engraftment. On the other hand this population also showed a myeloid bias in transplantation assays which was probably expected since it marked an increased pool of aged HSCs[119,43,158]. Since we also mimic an aging phenotype in our study by repeatedly stimulating HSCs and observe a subsequent increase in the LT-HSCs pool, it could be that this CD41$^+$LT-HSC population was specifically propagated instead of the whole LT-HSCs pool. Concluding, TPO treatment might not have induced self-renewal but rather accelerated aging.

In addition to CD41, vWF or MPL both known to be expressed in MK and platelet primed LT-HSCs, represent interesting candidates to investigate the potential biases in phenotypic LT-HSC pool upon serial TPO treatment[57]. However, because we did not include further markers in our staining panel, we cannot be sure whether TPO treatment increased the whole phenotypic LT-HSC pool or only a sub-fraction. Since we used total bone marrow for competitive transplantations, we avoided introducing a bias by sorting for specific HSCs. Nonetheless, we should sort a specific number of HSCs next time after serial TPO treatment, to avoid transplanting a higher proportion of HSCs within the whole BM. As we saw a significant increase in absolute LT-HSC numbers after serial TPO treatment (Figure 34 D). For the future experiments when using the LRC mouse model, and LR and non-LR LT-HSCs are sorted and subsequently transplanted, we could consider including Flt3 as an additional marker to exclude an inherent lymphoid bias.

5.1.4 Clinical significance of this study

The TPO mimetics Eltrombopag and Romiplostim were developed in order to induce an increase in platelet counts in patients with chronical or iatrogenically-induced reduction of platelet counts. Since the TPO receptor Mpl is not only present on megakaryocytes and platelets but also present on HSCs, this induced severe side effects in patients after long-term treatment[127] . Eltrombopag is a small molecule and specifically binds to the intermembrane region of the Mpl receptor. The advantage of using a small molecule as drug is that it does not have any protein components and thus is not immunogenic. However, the Eltrombopag binding region differs in one amino acid between mice and human and thus, cannot be used in mice. During the course of this study a genetically modified mouse model expressing the transmembrane part of the human Mpl receptor in mice was developed to allow studying the effects of Eltrombopag in more detail[159].

In this study we focused on Romiplostim. Romiplostim binds to the extracellular part of the TPO receptor and this binding motif is conserved between mouse and human. The only downside of using Romiplostim is that it is fused to a human Fc receptor part which likely induces an immune reaction in the treated mice and as such, is not suitable for long-term studies in a mouse model[160]. The clinical significance of our study may not be immediate especially considering that we (i) immunized the mice (ii) used TPO as a stimulating agent to push HSCs into cycle to eventually exhaust HSCs (iii) and did not use TPO as a therapeutic agent since we were treating healthy wt mice. However, our results contribute to the understanding of basic molecular adult stem cell biology which is of utter importance for development of suitable therapeutic options.

Patients with Fanconi anemia show peripheral blood cytopenia and are treated with Rom to increase the overall amount of differentiated peripheral blood cells. In our study, we also examined the effect of repeated TPO treatment on Fanca$^{-/-}$ mice. We treated Fanca$^{-/-}$ mice for one round and observed an increase in WBCs, but no increase in erythrocytes or platelets. Additionally, we rather obtained an increased number of phenotypic LT-HSCs after TPO treatment, even though this increase did not show to be significant. However, it should be noted that Fanca$^{-/-}$ mice did not show any signs of anemia or any reduced BM cell counts under homeostatic conditions. The genetic Fanconi$^{-/-}$ model should be further optimized in order to obtain the Fanconi anemia phenotype which can then be treated. That is, these mice would first need to be challenged to induce stress in the hematopoietic system which would then induce an adverse phenotype. After having induced an Fanconi anemia phenotype, the TPO treatment should be repeated to see if the Fanconi anemia symptoms can be mitigated.

Although we did not detect any significant changes in femur cellularity and LT-HSC numbers after TPO treatment in Fanca$^{-/-}$ donor mice, it was concerning that WBCs were significantly increased and out of the normal range which could indicate the possible onset of leukemia. Additionally, it was also concerning that upon transplantation TPO treated cells showed a significantly reduced

BM chimerism implying a possible HSC exhaustion phenotype. It can be concluded that in our setting TPO negatively affected engraftment efficacy of Fanca$^{-/-}$ donor cells in recipient BM, although overall PB engraftment and contribution to differentiated PB cells and the progenitor compartment was not affected. At the moment it is not entirely clear how to translate this knowledge into the clinics but it should be considered to closely monitor peripheral blood and BM parameters of Fanconi anemia patients during Rom treatment.

5.1.5 Caveats of using mouse models

When studying hematopoietic stem cells, there is hardly no way around using mouse models as no other reliable and robust protocols to propagate functional HSCs *in vitro* are available. HSCs are very much dependent on their BM niche to stay in a quiescent state. Although a few protocols have been developed to keep HSCs in cell culture for a short period while still maintaining HSC function, it is not possible to keep cells alive for more than 57 days[99,100]. The caveat of these protocols is that HSCs, which usually try to prevent proliferation, are pushed to cycle under cell culture conditions. Additionally, since we want to examine the effects of extensive TPO treatment we would not be able to get robust results from *in vitro* experiments, considering that TPO is a crucial component of HSC cell culture. The TPO concentrations used in the two published protocols (one from Kobayashi *et al*., one from Wilkinson *et al*.) varies dramatically. There is a 1000-fold difference (0.1ng/ml TPO and 100ng/ml TPO, respectively) in the recommended TPO concentration for HSC cell culture. However, both protocols claim to have developed a system where functional HSCs can be cultured and expanded. With regards to TPO it is tricky to draw a clear conclusion from these *in vitro* experiments. The question remains whether HSCs are kept in quiescence or are expanded/undergo self-renewal due to the presence of TPO. Therefore, mouse models are still used to examine HSC function.

However, using mouse models also has some pitfalls. When carrying out transplantation assays, recipient mice are myeloablated by 10Gy total body irradiation (TBI), which not only destroys the host bone marrow and immune system, but affects all of the cells in the body. In particular, the destroyed BM niche/BM environment should be mentioned since LT-HSCs are dependent on a functional niche to develop to their full potential[161]. Transplanting cells into such an environment adds additional stress and as TBI does not always work perfectly (see Figure 27 C), this could lead to experimental biases. That being said, competitive transplantations after conditioning recipient mice by TBI, are still the gold standard to test for hematopoietic function *in vivo*.

Since TPO induces platelet formation, it was of interest for us to monitor platelet chimerism after transplantation to determine whether repeated TPO stimulation to produce platelets also manifested after transplantation. Since platelets do not express CD45 we needed to use other models to monitor platelet chimerism, for example the UBC-GFP mouse model. These mice

express GFP under the human ubiquitin C (UBC) promoter, which is active in every cell so even platelets retain the GFP label. However, this model has an inherent engraftment defect resulting in a general lower donor chimerism. Additionally, a myeloid bias upon transplantation has been observed with these mice[103]. Thus, when using this mouse model, it must be noted that a decrease in donor chimerism does not necessarily prove a loss of function.

As we pushed HSCs into cycle, we were interested in monitoring the amount of cell divisions. Since we sorted cells and aimed to characterize the cells after the induced proliferation the BrdU labeling method could not be used. To analyze label loss of BrdU marked cells, these have to be fixed and as such, cannot be used for downstream experiments. Therefore, we used the label retaining mouse model (Sc-tTA-H2B-GFP) in order to measure how much cells cycled (based on the label retention), as well as sort cells for follow up experiments. Since LRC mice were treated for 70 days with the antibiotic dox to stop the expression of the H2B-GFP label, the gut microbiome was partially depleted. Seeing as the gut microbiome is part of the immune system its impact and indirect effects on the whole hematopoietic system should not be neglected. It was shown that antibiotic treatment of mice led to an upregulation of inflammatory cytokines which in our case means an activation of HSCs and additional stress for the mice[162].

In our study, dox was applied to mice via drinking water and as dox is very bitter it, was mixed with 20g sucrose/L water. The side effects of a high sucrose/sugar intake are an increase in weight and the development of a fatty liver, which negatively impacts on the general health of mice. Both conditions were observed in our chased mice, thus it was especially important in these experiments to have the PBS control so we would be sure that observed differences between the conditions were due to the induced agonist treatment alone. The combination of prolonged antibiotic treatment and high sugar diet could explain the high label dilution (up to 40% GFP-label loss) in some PBS mice. We also speculate that already the dox and sugar treatment might lead to a general lower engraftment efficacy than would be achieved with normal PBS wt mice. We only got an average BM chimerism from PBS LRC mice of 5% ± 24%. This, of course, cannot be compared to our competitive transplantation experiments, but when we transplanted 3mil total BM cells from PBS treated wt mice we transplant approximately 100 LT-HSCs and achieved a donor chimerism of approximately 32% on average.

We also used a diseased mouse model, the Fanca$^{-/-}$ mouse model. Although the genetic defect is present, only upon challenge does the Fanconi anemia disease show up. Due to the fact that laboratory mice are housed under strictly controlled specific pathogen free (SPF) conditions, their immune system is hardly ever challenged by a normal variety of bacteria or pathogens.

In our case, using the Rag2 KO mouse model was convenient since we did not introduce an immune reaction with repetitive TPO treatment, which we nicely showed by a uniformly high upregulation of Ki67 in LT-HSCs 24h after the 24th injection (three rounds, see Figure 34 E). We were also interested in functional hematopoiesis and wanted to examine whether we could

observe a myeloid bias in these mice. Since the Rag2 KO mice already have a myeloid bias as no functional B- or T- cells are produced[106], the results obtained from this model have to be interpreted carefully. Additionally, femur cellularity under homeostatic conditions in Rag2 KO mice was approximately 1.5-fold reduced in comparison to wt mice. This was not surprising, but did indicate that Rag2 KO mice do not have a normal BM composition, already under homeostatic conditions.

5.2 Relevance of our work in the context of the field

5.2.1 Overcompensation of WBC after sudden decrease due to treatment

Upon a single TPO or polyI:C injection WBCs decreased to only approximately 5.5 $x10^3$ WBC/µl blood and 2 $x10^3$ WBC/µl blood, respectively. After 48h and 72h, we noted an overproduction of WBCs in the blood. The same phenomenon was observed for femur cellularity after polyI:C treatment. After an initial drop of femur counts, we saw a temporary overproduction in femur cells. This overcompensation after a cellular depletion has been previously observed in our lab. Importantly, this myeloablation robustly activates HSCs to proliferate in order to replenish the depleted cells as fast as possible. After cell replenishment, the hematopoietic system normalizes again to homeostatic levels.

5.2.2 Increased MK percentage after treatment

A 2.2-fold increase of MK cells was observed after polyI:C treatment but not after TPO treatment (Figure 18 B). Initially we were surprised by this result but after careful consideration we noted that the concept of emergency megakaryopoiesis could explain this observation[71]. During acute infection, platelets are a crucial component to fight pathogens since together with neutrophils they form a so-called neutrophil extracellular trap (NET). These NETs lead to a significant decrease in platelet counts, which activates an emergency megakaryopoiesis program, and directs the differentiation of HSCs into MKs during the acute infection phase, resulting in a large increase in MKs. HSCs respond to this high demand of platelets and more importantly, the body tries to avoid a life-threatening thrombocytopenia.

Rom is very effective at increasing platelets, but *in vitro* experiments comparing the efficacy of inducing MK proliferation between TPO and Rom showed that Rom is less effective in inducing MK proliferation. In the referred to experiments, an increase in MKs after TPO treatment was only observed after eight days of culturing lin^- BM cells in TPO containing medium[163]. Since we only

have data from 24h after TPO and Rom treatment, and platelet counts only start to rise in TPO or Rom treated mice 72h after the injection, we can only speculate that MK numbers likely increase between 48h to 72h after a single TPO injection, if at all.

According to the classical hematopoietic hierarchy, CMPs are precursors to MEPs and GMPs, which are responsible for the formation of myeloid cells and MKs. We also investigated hematopoietic progenitors in the BM, specifically focusing on $CD55^{+}$ CMPs as these have been identified as megakaryocytic primed[129]. However, after three rounds of treatment, we did not observe any difference in the progenitor populations between TPO and PBS treated mice. Therefore, if there was an increase in any progenitor population, this would have only been transiently present shortly after the treatment.

5.2.3 Ki67 to assess cycling of HSCs

Ki67 is often used to analyze cell cycle phases (G0, G1 and SG2M) however, it might not be the best marker to use since it is gradually expressed until it accumulates in S-phase and afterwards only gradually degraded. Thus, cells that exit cell cycle can still express Ki67[164]. In our study we defined Ki67 positive cells as cycling, but due to the beforementioned caveat of Ki67, this could have been an overestimation. Other methods should be taken into consideration to reliably conclude that LT-HSCs are actively cycling.

BrdU labeling is another method that is often used to distinguish cell cycle phases. BrdU can be injected and is incorporated into all actively cycling cells. However, since BrdU is toxic the injection itself might induce an activation of quiescent HSCs[64]. As such, results obtained after BrdU injections should be interpreted carefully. Hence, labeling cycling cells with BrdU can also lead to an overestimation of cells in cycle during homeostasis. We did not use BrdU labeling in our mice for two reasons. Firstly, cells have to be fixed in order to stain for BrdU, which would not allow further experiments with these cells and secondly, BrdU only labels the majority of dormant cells, but not all of them. Since BrdU is usually administered to mice for 13 to 14 days it only labels cells that have divided during this time period[61]. If cells did not cycle within these two weeks and are thus true dormant cells, these dormant cells would not be labeled with BrdU.

Additionally, there are better, more intrinsically regulated cell cycle proteins to reliably assess proliferating cells. Proteins like Mcm4 and Mcm6 are tightly regulated and used to identify cells in mitosis or early G1 phase. Furthermore, Mcm4 and Mcm6 are crucial for cell cycle progression whereas Ki67 does not play a major role in cell cycle initiation and continuation. To assess cell cycle, cells can also be stained for (i) phosphorylated histone H3 (pH3) which is exclusively present in M-phase or (ii) proliferating cell nuclear antigen (PCNA) that can be only detected in S-phase[165,151].

A snapshot of cell cycle activity can also be examined by using Fucci mice. These mice are designed such that at the start of S-phase cells appear yellow whereas cells in G1 phase are red and cells in G2M phase are green. The cell cycle status of a single cell can easily be determined by flow cytometry and cells can be propagated afterwards[166]. However, considering that we were not only interested in cell cycle status to a specific time point but also in the whole proliferative history of a cell, we chose to use of the LRC mouse model for our study. As mentioned before there might be some obstacles using this label retention mouse model but it would still give us a reliable estimate whether a cell has cycled more often than another cell by inspecting its residual GFP intensity after chase.

5.2.4 Observed heterogeneity between mice after transplantation

For some of our experiments, especially the TPO treated experiments and those from using the LRC mice, we observed a large heterogeneity not only within the same experiment but also within different experiments even though we used inbred mice. However, a certain amount of heterogeneity will always be observed considering that inbred mice are individual animals with their own characteristics. A heterogeneity is already induced from birth onwards depending on where the mouse embryo lay in the uterus and when smaller differences in imprinting occur[167]. Nonetheless, these inherent differences are usually expected to be quite small. Since there is no official recommendation, we would assume that a variation of 10% to 15% from average is still within a normal range. In some of the presented experiments, we noted variations of up to 400%, for example in the engraftment potential between LRC PBS mice (Figure 29B). This was extreme, however, when using irradiation to myeloablate recipient mice, irradiation does not always occur to the exact same extent in every mouse. This would introduce a bias in the engraftment efficacy between mice considering the transplanted cells would have to compete with the residual recipient cells for colonizing the BM niche. After all, transplantation experiments are complex and involve various different steps that could all influence the outcome. Therefore, after competitive transplantations we analyze the transplantation input via flow cytometry to make sure we mixed the cells in the desired ratio (1:1 or 1:3). Additionally, if the transplantation itself was flawed these recipient mice were excluded from the analysis.

For the LR and non-LR LT-HSC functional analysis, we decided to transplant 400 sorted cells to obtain a good representation of the HSC pool. Since both LR and non-LR LT-HSCs are rare populations, we set the GFP gates rather generous to obtain enough cells within each population. However, since we hypothesize that potency decreases with every single division, we should have rather been more specific with the GFP-positive and GFP-negative gate to reduce the potential heterogeneity within one population (in this specific example with 400% heterogeneity: LR LT-HSCs).

5.2.5 Increase in LT-HSCs numbers after TPO and Rom treatment

For nearly all experiments that included serial TPO or TPO mimetic treatment we observed an increase in phenotypic LT-HSCs numbers. Wt, UBC-GFP and Rag2 KO mice were treated with either one or three rounds of TPO or TPO mimetic and after a five-week recovery period we observed an increase in LT-HSCs numbers. These result fit with the theory that TPO leads to self-renewing divisions of HSCs. Additionally, we did not observe any impaired engraftment or any lineage bias from TPO or Rom treated wt and UBC-GFP mice. Suggesting that their potency, that is their ability to give rise to differentiated blood cells, is not affected. However, since we carried out competitive transplantations with total BM, the absolute number of LT-HSCs that were transplanted after TPO treatment was higher than that of PBS controls. This could have compensated for the loss of potential of a single HSC. To examine the potency of LT-HSCs after TPO treatment, transplantation of a specific number of sorted LT-HSCs would be required.

As LT-HSCs are very dependent on their surrounding niche, the questions arouse whether TPO injections alone would lead to an increase in the HSC pool or whether the cells in the BM niche also reacted to the TPO stimuli and subsequently created an environment that was advantageous for the propagation of LT-HSCs. In order to investigate these changes and spatial organization of cells in the BM niche further, spatial transcriptomic experiments together with single cell sequencing and BM microscopy could be conducted to see which, if any, cells might be affected by TPO treatment[168].

It is known that G-CSF injections lead to HSC migration and extramedullary hematopoietic organs play an important role in maintaining blood production[169]. That being said, during this project, we only focused on LT-HSCs in the bone marrow and did not check for changes in niche composition or extramedullary hematopoiesis in for example, the liver or spleen. Since we did not examine the spleen and liver we do not know if the extensive TPO treatment only leads to an increase in phenotypic HSCs in the BM or whether it could potentially lead to an increase in HSC numbers in extramedullary hematopoietic organs.

5.2.6 Issue of immunizing mice with Rom and TPO

The fact that Rom was immunogenic in mice was, after all, not such a big surprise seeing as Rom has a human fc receptor part attached for stabilization[91] and repeated injection of a foreign material/protein is the ideal way to elicit an immune response in a recipient[170].

TPO mimetics have been developed because rhTPO induces an immune response in patients. Since we did not see LT-HSC activation in our experiments after three rounds of TPO treatment (Figure 25 C), we speculated that similarly to patients treated with rhTPO our mice were immunized. Even though we made sure to purchase the animal-free TPO it could still be that bacterial contents remained or that a small tag from the recombinant expression vector was still attached to the rmTPO. However, on the webpage of Peprotech (https://www.peprotech.com/de/recombinant-murine-tpo-2) we could not find any information about residual contaminations. An enzyme-linked immunosorbent assay (ELISA) could have been done to verify antibody formation against TPO. However, the tricky part would be to find the right epitope of murine antibodies that would bind to the assay since we can only speculate that we induced an immune response against the TPO protein and not any other protein/antigen that was injected in parallel with the TPO.

When we examined cell cycle activity 24h after three rounds of TPO treatment, we observed upregulated cycling in some mice. Considering that an immune reaction induced by the repetitive injecting of TPO might have resulted in a cytokine storm, this could have consequently led to HSC proliferation and upregulated Ki67[171]. So, the activation that we see after three rounds of TPO treatment (Figure 25 D) might not be due to the TPO injection itself but rather due to the allergic reaction that followed afterwards. Although we observed this immunization issue, we still thought that it is valid to use TPO for one round since it takes several rounds of (TPO) treatments to induce an immunization. Using the Rag2 KO mice would overcome the issue of immunization after serial treatment rounds. Unfortunately, at the time of writing this thesis we did not have transplantation output from TPO treated Rag2 transplanted mice. Since we saw a significant decrease in BM cellularity after three rounds of TPO treatment it would be interesting to see if this resulted in an HSC loss of function.

5.2.7 *In vitro* differentiation of HSCs

We assessed LT-HSC function not only *in vivo* but also *in vitro*. The colony assay would give us information about lineage output, as well as proliferation capacity of the LT-HSCs. One disadvantage of this specific assay it is that only myeloid, erythroid and megakaryocytic lineage output can be analyzed. In order to differentiate HSCs to lymphoid cells, a co-culture with OP9 stromal cells for B-cell differentiation and co-culture with OP9-DL1 cells for T-cell differentiation would be required[56].

Even though the colony assay was performed with three different mouse strains (wt, Fanca$^{-/-}$ and LRC), we robustly observed an increase in established colonies/absolute colony number and a smaller colony size (less cell counts/colony) from TPO treated cells. This increase in clonogenicity (ability to form colonies) was not expected. We can only speculate that TPO treatment led to a reduced susceptibility to stress caused by the procedure of isolating, staining and sorting cells.

Since it has been shown that TPO upregulates NHEJ repair mechanisms, TPO treated cells could be better prepared to repair DNA damages induced by any kind of stress.

Recently, it was suggested that HSCs can form an epigenetic memory based on their experiences[172]. This concept of a HSC memory has been theorized before, when researchers showed that HSCs which have been previously exposed to a stimulus respond faster or in a more efficient way, when later exposed to that same stimulus again[173]. In our case, a LT-HSC that has been repeatedly exposed to supranatural concentrations of TPO could have learned how to react to this repeated TPO signal. When this LT-HSC is then put in cell culture where again a supranatural TPO concentration prevails, it can immediately react to this environmental change and start a certain signaling program, in our case possibly a self-renewal program. This could confer an advantage to TPO-treated LT-HSCs cultured in the TPO-containing *in vitro* medium.

We were initially surprised by the high myeloid bias in monolineage colonies from PBS treated wt mice. Knowing that with age there is a myeloid bias it is highly likely that this result can be related to the age of mice. That being said, as these mice underwent three treatment rounds the average age of these mice was 220 days (approximately 32 weeks) and since we do not have any colony assay data from younger mice to compare, we cannot be sure that the proportion of myeloid colonies would be smaller in younger mice. This colony assay is very useful in terms of examining clonogenicity and differentiation. However, it is also a very sensitive assay. Only small changes in oxygen concentration can result in big differences. The cells are usually kept at only 5% O_2 to mimic low oxygen concentrations in the bone marrow. However, if these cells are kept under higher or fluctuating oxygen concentrations, this leads to increased stress and increased cycling resulting in the formation of bigger colonies. Since the incubator was heavily used by other lab members, oxygen concentration was highly variable and could explain differences between experiments. Since it is known that different oxygen concentrations can lead to differences in HSC differentiation, apoptotic signaling and other related signaling pathways that are critical in the differentiation outcome of HSCs. One example is the formation of erythrocytes, under low oxygen concentrations an increase in RBCs was observed in *in vitro* cell culture[174].

In summary, our results showed that TPO has a great potential to be used to phenotypically expand HSCs. Even though we did not see any signs of HSC exhaustion in or experiment, DNA damages should be examined before being too enthusiastic about a potential self-renewing effect of TPO. If TPO is studied further, especially in a disease setting, mouse models should be selected carefully to be able to transfer results obtained from murine studies to human patients.

6 Conclusion and Outlook

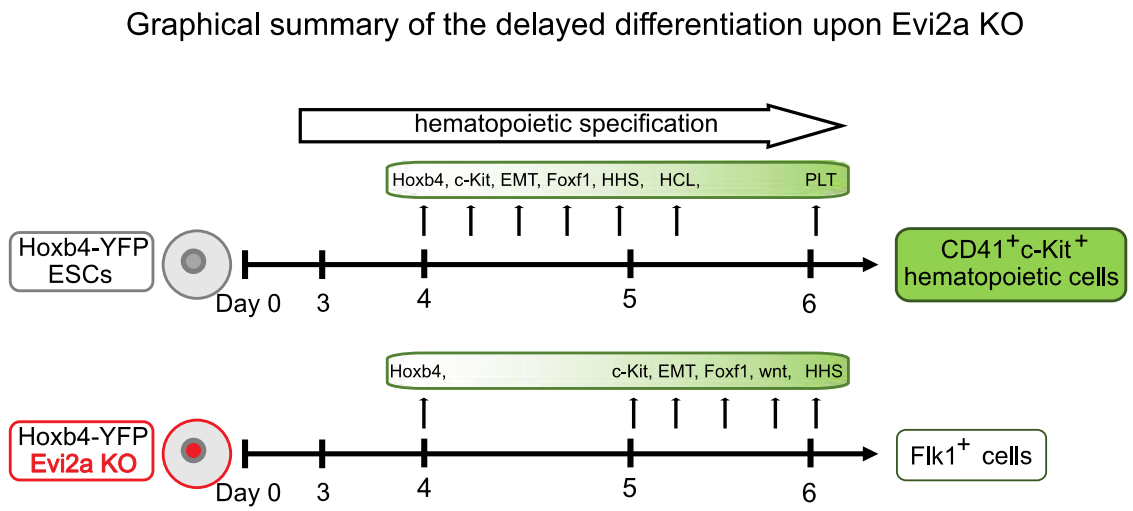

Figure 35: **Evi2a KO delayed hematopoietic differentiation.** Summary of differential gene expression analysis of differentiated wt vs Evi2a KO cells. wt Hoxb4-YFP ESCs and Evi2a KO ESCs were *in vitro* differentiated and Hoxb4^{+} cells were sorted on day 4, 5 and 6. Subsequently, RNA was isolated and cDNA libraries submitted for sequencing. Transcriptome analysis resulted in the hypothesis that Evi2a KO delayed the hematopoietic differentiation shown by delayed expression of signaling pathways or transcription factors in Evi2a KO cells. After six days of in vitro differentiation Evi2a KO cells still displayed an endothelial phenotype (Flk1+) and hematopoietic CD41+ c-Kit+ cells were not obtained. EMT = endothelial to mesenchymal transition, HHS = hedgehog signaling, HCL = hematopoietic cell lineage signaling, PLT = aggregation of blood platelet signaling, wnt = wnt/ß catenin signaling

Our aim of project one was to decipher the signaling processes that Evi2a is involved in. By performing transcriptome analysis, we uncovered that Evi2a KO delayed hematopoietic differentiation. Interestingly, we detected that genes involved in early developmental processes such as mesoderm formation were also delayed in Evi2a KO cells (Figure 35). In summary, Evi2a is probably not only involved in hematopoietic specification. Even though it was initially found to be differentially expressed during EHT, this does not exclude an important function of Evi2a during earlier developmental processes. Additionally, since it was shown that Evi2a is upregulated in neuronal tissue, it could also play a role in brain development. If Evi2a is additionally crucial for neuronal development, this could also be an explanation why we did not detect homozygous Evi2a KO embryos at E10.5.

To dissect the role of Evi2a in hematopoietic development, we plan to cross heterozygous Evi2a$^{loxP/loxP}$ with mice that express the cre-recombinase under the VE-Cadherin or the Vav1 promoter. This enables us to excise Evi2a at E7.5 and E12.5, respectively, during development and to examine at which time point Evi2a KO is lethal during hematopoietic development. As a next step, we also aim to examine Evi2a in the context of leukemia. We first want to define Evi2a high and low expressing leukemic cell lines and to then perform shRNA knockdown of Evi2a or Evi2a

overexpression in these cell lines, respectively. Additionally, to elucidate if Evi2a alone is able to transform cells, we aim to isolate primary HSPCs, transfect these with an Evi2a overexpression construct and perform replating assays. By performing the two above mentioned experiments, we aim to answer the question whether Evi2a is crucial for the onset and maintenance of a leukemic phenotype.

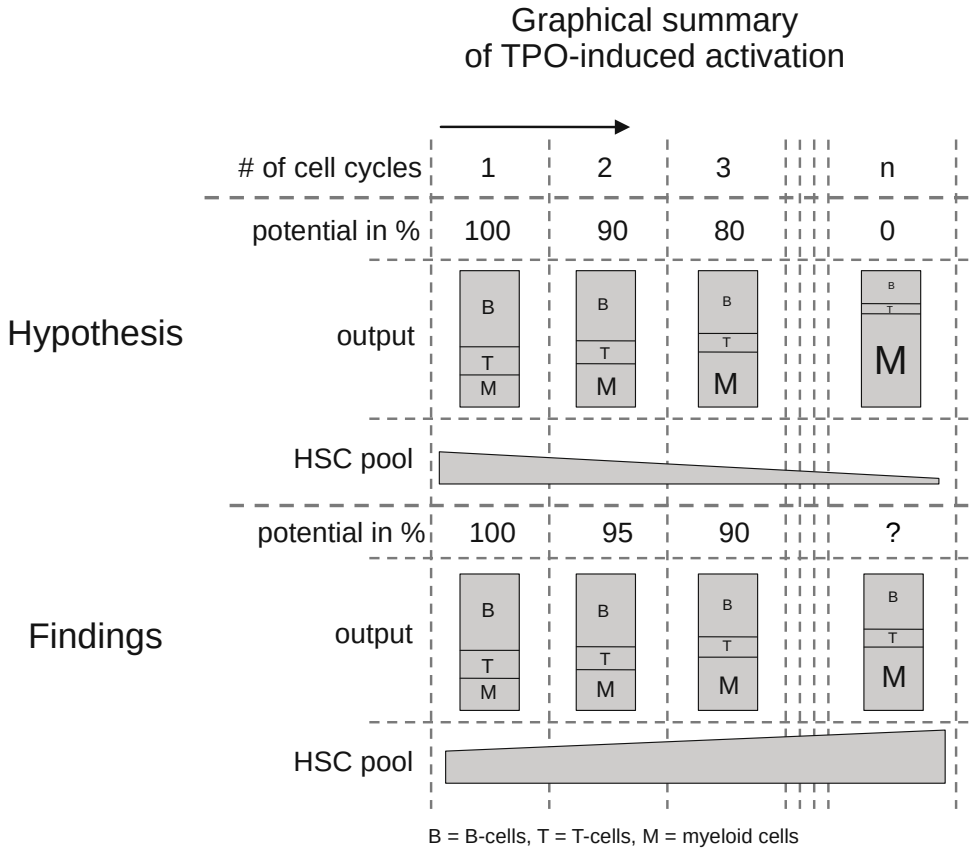

Figure 36: **Graphical summary of our hypothesis and findings.** The hypothesis was that with every cell division LT-HSCs lose potential, myeloid bias increases and the overall size of the phenotypic HSC pool decreases. The findings after TPO treatment were that potential did not decrease as would have been expected and no significant lineage bias was observed. An increase in phenotypic LT-HSCs was found.

Our aim of the second part was to study HSCs under stress and examine HSC exhaustion in a non-inflammatory setting. Our hypothesis was that every cell division leads to increased DNA damage and hence to HSC exhaustion which leads to a reduced engraftment potential. However, we could not confirm our hypothesis (Figure 36) and can conclude that TPO might not be the best agonist to study serial HSC exhaustion since we observed a possible immunization of mice against TPO. Our results also do not convince us that TPO induces self-renewal divisions, if self-renewal is defined as not losing potency and giving rise to an equal lineage output. Nevertheless, we saw an

increased HSC pool after TPO treatment and TPO seems to act on a lot of different levels and can potentially propagate phenotypic HSCs. However, similar to the saying “the dose makes the poison”, it might just be a matter of concentration that is healthy and beneficial for HSCs/patients without doing harm.

The clinical aspect we touched in our study has to be taken with care since we used healthy mice (not thrombocytopenic mice) and the Fanca$^{-/-}$ mice themselves did not show any symptoms. Furthermore, the Rom concentration we used for mice (75µg/kg) is much higher than Rom concentrations used to treat patients which start out with 1µg/kg body weight. Nevertheless, it is interesting to see that also Rom induced an increase in HSC pool and mice tolerated this high concentration well. Still pending are the results from the three round TPO treatment of Rag2 KO mice. The BM of these mice was competitively transplanted into recipients to examine HSC function after serial TPO treatment. Since the Rag2 KO mice did not have a functional adaptive immune system we did not induce immunization against TPO.

For future experiments to examine HSC exhaustion in a non-inflammatory setting, it would be suitable to use other agonists than TPO which can either have a direct effect on HSCs such as CD41-induced activation. CD41 is expressed on HSCs and by injecting an anti-CD41 antibody HSCs can be activated and at the same time anti-CD41 antibody binding leads to depletion of platelets adding additional stress to HSCs and pushing them into cycle[119]. Another indirect method to stress the system would be to disrupt the day and night rhythm of mice. It was shown that melatonin injections indirectly activate HSCs. This could be another non-inflammatory activation to examine how HSCs respond to different types of non-inflammatory stress[175]. However, when examining HSC function, it is also interesting whether any sustained epigenetic or methylation marks are altered or certain differentiation programs are constitutively upregulated upon repeated stimulation[176,177]. This could be examined by performing transcriptome and methylome analysis of the isolated HSCs.

To be sure that LT-HSCs are still functional and do not have any intrinsic lineage bias after repeated TPO treatment single cell transplants could be carried out. By performing competitive and bulk-sorted cell transplantations, the individual loss of potential of a single LT-HSC might have been compensated by the fact that many other LT-HSCs also contributed to the PB compartment, which in summary led to a normal and healthy peripheral blood composition. Spatial transcriptomics and combined microscopy methods could further help to identify where LT-HSCs reside in the BM. The surrounding niche (sinusoidal, endosteal or non-vascular) could already indicate whether LT-HSCs retained their function and potential. Additionally, to control for any (deleterious) DNA mutations single cell sequencing could be carried out to assess mutations and SNV burden that are induced by serial treatment. It can also give an insight into mutations in, for example leukemic divers like DNTM3a, or Tet2 to see if it induced activation increased DNA damage.

7 Materials and Methods

7.1 Animal experiments

All animal treatments have been approved by the Regierungspräsidium Karlsruhe. Approval number for TPO and Romiplostim experiments: G-117-17 and G-269-17; for Evi2a experiments: G-187-16 and G-15-19. Organ sampling was documented on DFKZ-357 license. All mice were housed under specific pathogen free conditions (SPF) in individually ventilated cages (ICV) at the DKFZ within the facilities of the ZPF core facility.

C57BL/6J (CD45.2) were obtained from Janvier labs in France, all other animal models (Fanca$^{-/-}$, Scl-tTA-H2B-GFP, UBC-GFP, C57BL/6J-Ly5.1 (CD45.1), B6-CD45.1/J x B6-CD45.2/J (CD45.1/2) and all Evi2a strains) were bred at the DKFZ ZPF core facility. Breeding and genotyping of mice was included on licenses Z-173I02, EP-Z-173I02 and A-23/17 and genotyping was carried out by all lab members of the Milsom group and done according to established standardized protocols. Mice were at least 8 weeks old at the start of the experiments.

7.1.1 Injections and treatments

Recombinant murine TPO (#AF-315-14, Peprotech) was dissolved in sterile PBS to a stock concentration of 1g/ml. Final working concentration was 0.02 µg/ml and 200µl (4µg TPO) were injected intraperitoneal (i.p.) into a 20g mouse. Stock concentrations were kept at -80°C.

Nplate® (Romiplostim) was generously provided by Amgen Inc. California, USA, for research purposes (Master Material and Funding Agreement between DKFZ and Amgen from August 2018). Romiplostim was dissolved in PBS and stock solutions were stored at -80°C and prepared such that 200µl were injected i.p. into a 20g mouse.

Injections with Rom, TPO, polyI:C or PBS were done on day 1, 3, 8, 10, 15, 17, 22 and 24. Day 1 indicating the start of the experiment. Mice were exposed to two injections within 48h then a recovery period was given. Only 120h after the second injection the third would follow and the same pattern was repeated for in total four weeks until mice received eight injections followed by a four-week recovery period. This scheme was described as one round in this thesis. Mice were injected with up to three rounds, so a total of 24 injections were applied.

Scl-tTA-H2B-GFP (LRC) mice were treated with doxycycline (dox) containing water one week prior to start of injections. Doxycycline (2g/1L) was mixed with sucrose (20g/1L) and dissolved in

autoclaved water. Dox water was exchanged weekly by the animal care takers of the respective mouse facility.

24h (max. 48h) prior to transplantation mice were irradiated with a lethal dose of two times 500 Rad (5Gy) from a cesium-137 irradiation source. To prevent bacterial infections mice received Sulfamethoxazol/Trimethoprim (90mg/kg/day) drinking water for three weeks after the irradiation. For transplantation mice were shortly exposed to an infrared light source and a solution of 200µl PBS containing cells was injected intravenously (iv) into the tail vein. Mice were closely monitored daily by the animal care takers. If mice showed any signs of pain or more than 20% weight loss or if an endpoint criterion was met mice were sacrificed.

Mice were bled by puncture of the facial vein (vena facialis) and max. 150µl peripheral blood was collected into EDTA-containing blood tubes. Peripheral blood parameters were determined using a Hemavet 950FS hematology analyzer (Drew Scientific) or a scil Vet abc Plus (scil animal care company GmbH). 30µl blood were aliquoted for flow cytometric staining.

7.1.2 Bone marrow collection and lineage depletion

For smaller experiments (Romiplostim time course, end point analysis or test stainings) mice were sacrificed by cervical dislocation, organs were checked for any anomalies and legs were separated. Flesh, tendons and ligaments were removed from tibias, femurs and hips. Both femurs were flushed into 2ml PBS/2% FCS, filtered through a 35µm filter and a 30µl aliquot was taken to analyze femur counts. Hips were additionally flushed into the same tube and another aliquot was taken to analyze the total BM counts. Appropriate aliquots for different stainings were taken and spun down to be resuspended in the respective antibody master mix.

For bigger experiments (LRC experiments) mice were sacrificed by cervical dislocation and all bones including spine, femurs, tibias, hips, sternum and humeri were collected. Liver and spleen were collected for histology. Both femurs were flushed into 2 ml PBS or PBS/2% FCS, filtered through a 35µm filter and femur counts were analyzed using the hematology analyzers. For total BM transplantation (3 mil total BM from wt and UBC-GFP mice and 6 mil total BM from Fanca$^{-/-}$ mice) were aliquoted. For plain flow cytometric analysis aliquots (8 mil for progenitor staining, 30 mil for HSC and Ki67 staining) were taken. Residual bones were crushed in RPMI and filtered through a 40µm cell strainer. Cells were sedimented at 1500rpm for 5min at 4°C, supernatant was discarded, cells counted and approximately 350µl biotinylated lineage antibody mix (112µl/1x10^8 cells) added. After 40min incubation on the rotor at 4°C cells were washed with PBS and magnetic beads were added (1ml beads/1x10^8 cells). To deplete the lineage positive cells the falcon tube containing cells and bead mixture was placed into a magnetic rack. Supernatant was transferred to a tube in a second magnetic rack and the supernatant was collected in a 50ml falcon tube. Beads

were washed twice and collected lineage depleted solution (in total 21ml) was spun down to be resuspended in LT-HSC LRC antibody master mix.

All master mixes were prepared with PBS/2% FCS, if not stated otherwise.

Table 2: Master mix composition of antibody staining for LT-HSCs and progenitors.

Bone marrow analysis master mix	**LT-HSCs without GFP**	**LT-HSCs with GFP**	**Progenitors without GFP**	**Progenitors with GFP**
Lin	PE-Cy7	PE-Cy7	PE-Cy7	PE-Cy7
Streptavidin		PE-Cy7		
c-Kit	BV711	BV711	APC or BV711	BV711
Sca-1	APC-Cy7	APC-Cy7	APC-Cy7	APC-Cy7
CD150	PE-Cy5	PE-Cy5		
CD48	PE or PacBlue	PE		
CD34	FITC	eF450	FITC	eF450
CD135	PE			
CD16/32			eF450 or APC	APC
CD55			PE	PE
GOI (gene of interest)		GFP		GFP

7.1.3 Sort and flow cytometry analysis

Flow cytometry machines LSR and LSRFortessa as well as fluorescence activated cell sorting (FACS) machines Aria and Aria Fusion were maintained and kindly set up (frequency node, drop delay and stream trajectory) by the DKFZ flow cytometric core facility staff. BD FACSDiva™ software was installed on all machines. Data analysis was done using FlowJo™ v10. All sorts were carried out using the 100µm nozzle at a max. speed of 4000 events/sec. Compensation was done prior to analysis and single stains were prepared with oneComp eBeads.

Master mixes were freshly prepared in PBS/2% FCS and kept at 4°C in the dark until usage. Incubation was carried out for 30-40min and cells were washed with PBS after staining. Cells were resuspended in an appropriate amount of PBS/2% FCS and if necessary 7AAD was added prior to measurement to distinguish live and dead cells.

For the LRC experiments bulk sorts were carried out: 580 cells were sorted into 1.5ml tubes containing 400µl StemSpan. Single cell sorts were performed for colony assays and a single cell was sorted into one well of a 96 well plate containing 150µl differentiation medium.

7.1.4 Supportive/competitive bone marrow

Total bone marrow cells from two B6-CD45.1/J x B6-CD45.2/J (CD45.1/2) mice were used as competitor and/or supportive cells. Mice were sacrificed by cervical dislocation and legs were isolated. Tibias were flushed separately to determine the CD45.1/2 surface marker expression, femurs and hips were flushed into sterile PBS and cell number was determined.

CD45.1/2 competitor staining master mix was added to the flushed tibias and incubated for 30min at 4°C in the dark. RBCs were lysed by addition of 1ml ACK lysis buffer and incubated for 10min at room temperature. Cells were centrifuged at 2500rpm (270g) for 5min and pellet was resuspended in 200µl PBS/2% FCS containing 5µg/ml 7AAD. No compensation was needed for FC analysis.

The respective number of cells (for competitor experiments 2 mil or 3 mil total BM cells, for supportive experiments 400,000 total BM cells) was added to the previously sorted or isolated cells from the donor mice, spun down at 2500rpm (270g) for 5min in a table top centrifuge. Pellet was resuspended in 200µl PBS and kept on ice until transplantation.

Table 3: Antibody panel for competitor staining.

CD45.1/2 competitor master mix	
CD45.1	PacBlue
CD45.2	A700
Live/dead	7AAD

7.1.5 Fixation of BM cells for Ki67 and MK staining

30 mil total BM cells were used for Ki67 staining and 5 mil BM cells for MK staining. 30 mil BM cells were stained in 300µl Ki67 master mix, 5 mil cells were stained in 200µl MK master mix. For both stainings the DNA dyes DAPI or Hoechst were initially excluded and for the Ki67 staining the intracellular marker Ki67 was also initially excluded. Cells were incubated at 4°C in the dark on ice. 1ml ACK lysis solution was added and incubated for another 10min at room temperature. Cells were spun down at 4°C, 2500rpm (270g), 5min in a table top centrifuge and washed twice with 1ml PBS/2% FCS. 300µl BD Fixation solution was added to 30 mil cells and 100µl BD Fixation solution to 5 mil cells and incubated for 20min on ice in the dark. Two washing steps with 1ml of diluted BD Perm/Wash buffer followed.

Cells for the Ki67 staining were resuspended in Ki67 antibody-Perm/Wash solution and incubated over night at 4°C in the dark. Ki67 antibody was washed off with 1ml diluted Perm/Wash buffer.

MK stained cells were directly washed once with 1ml diluted Perm/Wash and cells from both stainings (MK and Ki67) were incubated for 10min in 1ug/ml DAPI- or Hoechst-Perm/Wash solution. 30 mil and 5 mil cells were washed once with PBS and resuspended in 350µl or 200µl PBS/2% FCS, respectively.

Table 4: Antibody panel for Ki67 staining.

Ki67 master mix	**no GFP**	**with GFP**
Lin	PE-Cy7	A700
c-Kit (CD117)	APC or BV711	APC or BV711
Sca-1	APC-Cy7	APC-Cy7
CD150	PE-Cy5	PE-Cy5
CD48	PE	PE
CD34	A700	
GOI		GFP
Ki67	FITC	PE-Cy7
DNA	DAPI/Hoechst	DAPI/Hoechst

Table 5: Antibody panel for megakaryocyte (MK) staining.

MK master mix	
CD9	FITC
CD41	PE
CD42d	APC
DNA	Hoechst

7.1.6 Regular blood analysis

Mice were bled every four to eight weeks after transplantation and/or shortly before death to monitor the general health status of the mice by analyzing the blood using the peripheral blood analyzer. To assess B-cell, T-cell and myeloid cell (BTM) chimerism 30µl blood were mixed with 70µl of master mix and incubated for 30min at 4°C. Red blood cell lysis followed by adding of 1ml ACK lysis buffer. After 10min incubation at room temperature cells were spun down (2500rpm, 5min in a table top centrifuge), washed with 1ml PBS/2% FCS and resuspended in 200µl PBS/2% FCS with or without 7AAD depending on the staining.

For platelet analysis 3µl peripheral blood were stained with 50µl platelet master mix and incubated for 30min at 4°C in the dark. 1ml PBS/2% FCS was added and cells were kept on ice and covered until FC measurement.

Table 6: Antibody panel for regular peripheral blood analysis and CD45 chimerism analysis.

Regular blood analysis – BTM master mix	**no chimerism**	**with chimerism and GFP**	**with chimerism**
CD11b	APC	APC	APC
Gr1	APC	PE	PE
B220	APC, PE-Cy7	APC-Cy7	APC-Cy7
CD4	PE-Cy7	PE-Cy5	FITC
CD8	PE-Cy7	PE-Cy7	PE-Cy7
GOI	GFP	GFP	
CD45.1		eF450	eF450
CD45.2		A700	A700
Live/dead	7AAD		

Table 7: Antibody panel for platelet staining.

Platelet master mix	
CD4	APC-Cy7
CD8	APC-Cy7
CD11b	APC-Cy7
Gr-1	APC-Cy7
B220	APC-Cy7
Ter119	PacBlue/ eF450
CD41	PE-Cy7
CD71	PE
GOI	GFP

7.1.7 *In vitro* colony assay

Single LT-HSCs were sorted into a well of a 96 round bottom well plate (Greiner) containing 150µl *in vitro* HSC differentiation medium, see components below. Cytokines were reconstituted in appropriate amount of cytokine reconstitution buffer, aliquoted and stored at -80°C . Cells were kept at low oxygen conditions (5% O_2, at 37°C, 5% CO_2) for two weeks and formed colonies were first assessed microscopically to determine the size (approximate cell number) of each colony. Too small colonies (< 100 cells) were excluded from the flow cytometric analysis. Colony assay master mix was added to each colony (> ~ 100 cells), thoroughly mixed and incubated on ice for 30min in the dark. To wash the colonies 70µl PBS was added and plates were spun down at 1500rpm (270g) at 4°C for 5min. supernatant was carefully removed leaving approximately 20-30µl and colonies were resuspended in 80µl PBS/2% FCS containing 5µg/ml 7AAD. Plates were kept in the dark and

on ice until measurement with the high throughput sampler (HTS) system reader of the LSRFortessa. HTS settings were as follows:

Table 8: Settings for high throughput sampler (HTS) analysis using the LRSFortessa of stained colonies

HTS adjustments	**settings**
Throughput mode	standard
Sample flow rate	3µl/sec
Sample volume	80µl
Mixing volume and frequency	50µl, 3 times
Mixing speed	200µl/sec
Washing volume	800µl
Events to record	set to maximum

Table 9: Medium composition of *in vitro* HSC differentiation medium for single cell colony assay.

In vitro differentiation medium Components	**Final concentration**	**Stock concentration**	**Volume for 100ml Medium in µl**
Penicillin/Streptomycin	1%		1000
L-Glutamin	1%		1000
rhFlt3 ligand	10 ng/mL	100 ng/uL	10
rm SCF	50 ng/mL	100 ng/uL	50
rm TPO	10 ng/mL	100 ng/uL	10
rm IL-3	5 ng/mL	100 ng/uL	5
rm IL-11	10 ng/mL	100 ng/uL	10
rh EPO	0.3 IU/mL	1 IU/uL	30
rm IL-7	22.2 ng/mL	100 ng/uL	22

Table 10: Antibody panel for colony staining.

Colony assay master mix	
CD42d	APC
CD41	PacBlue
CD11b, Gr-1	APC-Cy7
CD71	PE
Ter119	PE-Cy7
Live/dead	7AAD

Table 11: Components of the cytokine reconstitution buffer.

Cytokine reconstitution buffer	Volume in ml
2% BSA	5
1M HEPES	1
PBS	94

7.1.8 Colony assay analysis in RStudio

The colonies were FACS analyzed with flow jo and counts were extracted. Mono-, bi- and multilineage colony output analysis was done in RStudio version 1.3.1093. The R code was developed and written by Dr. Tim Holland-Letz and Dr. Ruzhica Bogeska, optimizations were added by Dr. Ana-Matea Mikecin Drazic.

```
dat.B <- read.csv("dat.B as example.csv",sep=',', row.names=NULL, stringsAsFactors=FALSE)
dat.B <- subset(dat.B, count >=80)
dat.B$sum <- dat.B$Myeloid + dat.B$CD71 + dat.B$Ter119 + dat.B$CD41 + dat.B$CD42
dat.B$etd <- dat.B$CD71+dat.B$Ter119
dat.B$mgk <- dat.B$CD41+dat.B$CD42
dat.B$perc.My <- (dat.B$Myeloid/dat.B$sum)*100  #
dat.B$perc.etd <- (dat.B$etd/dat.B$sum)*100
dat.B$perc.mgk <- (dat.B$mgk/dat.B$sum)*100
dat.B <- dat.B[complete.cases(dat.B), ]
dat.B1<-dat.B[,c(11:13)]
norm.B<-
cbind(100*dat.B1[,1]/max(dat.B1[,1]),100*dat.B1[,2]/max(dat.B1[,2]),100*dat.B1[,3]/max(dat.B
1[,3]))
su<-norm.B[,1]+norm.B[,2]+norm.B[,3]
normnorm.B<-cbind(norm.B[,1]/su,norm.B[,2]/su,norm.B[,3]/su)

colnames(normnorm.B)<-c('% Myeloid','% Erythroid','% Megakaryocytic')
l.B<-length(normnorm.B[,1])
p <-
cbind(rep(1,l.B),rep(0,l.B),rep(0,l.B),rep(0.6,l.B),rep(0,l.B),rep(0,l.B),rep(0.5,l.B),rep(0.5,l.B),rep(0.
5,l.B),rep(0,l.B),rep(0,l.B),rep(0.5,l.B),rep(0.333,l.B),rep(0.333,l.B))

#these clusters are set according to vector above
    #1- myeloid [(1,l) and (0,l)],
    #2- ery [(0,l) and (0.6,l)],
    #3- mega [(0,l) and (0,l)],
    #4- mye + ery [(0.5,l) and (0.5,l)],
```

```
    #5- mye + mega [(0.5,l) and (0,l)],
    #6- ery + meg [(0,l) and (0.5,l)],
    #7- multilineage [(0.333,l) and (0.333,l)]

# calculate distance (dev) between every cell and every group center:

dev.B<-cbind(sqrt(apply((normnorm.B[,1:2]-p[,1:2])^2,1,sum)),sqrt(apply((normnorm.B[,1:2]-
p[,3:4])^2,1,sum)),sqrt(apply((normnorm.B[,1:2]-
p[,5:6])^2,1,sum)),sqrt(apply((normnorm.B[,1:2]-
p[,7:8])^2,1,sum)),sqrt(apply((normnorm.B[,1:2]-
p[,9:10])^2,1,sum)),sqrt(apply((normnorm.B[,1:2]-
p[,11:12])^2,1,sum)),sqrt(apply((normnorm.B[,1:2]-p[,13:14])^2,1,sum)))
groups.B<-array(0,l.B)
for (i in 1:l.B){groups.B[i]<-(dev.B[i,]==min(dev.B[i,]))%*%c(1:7)}
jpeg(filename = "example data B.jpeg")
normnorm.B.plot <-
plot(normnorm.B[,1],normnorm.B[,2],col=groups.B,xlab='Myeloid',ylab='Erythroid')
plot.normnorm.B.plot <-
plot(normnorm.B[,1],normnorm.B[,2],col=groups.B,xlab='Myeloid',ylab='Erythroid')
dev.off()

#extract data for violin plots and for pie charts

dat.B.counts <- dat.B[,c(2)]
write.table(dat.B.counts, file=”save as dat.B counts.csv”, sep=";")
counts.B <- data.frame(dat.B$counts)
counts.B["group"] <- "control"
colnames(counts.B)<-c("counts","group")
dat.groups.B <- cbind(dat.B, groups.B)
dat.groups.BB<-dat.groups.B[,c(2,14)]
colnames(dat.groups.BB)<-c("counts","group")

#mono lineage

mono.B <- subset(dat.groups.BB, groups.B <=3, select = c(counts))
mono.all.col <- merge(data.frame(mono.C, row.names=NULL), data.frame(mono.B,
row.names=NULL), by = 0, all = TRUE)
write.table(mono.all.col, file="dat.B monolineage counts.csv", sep=";")

#bi lineage

bi.B <- subset(dat.groups.BB, groups.B >3 & groups.B <7, select = c(counts))
bi.all.col <- merge(data.frame(bi.C, row.names=NULL), data.frame(bi.B, row.names=NULL), by =
```

```
0, all = TRUE)
bi.all.col <- bi.all.col[,c(2,3)]
colnames(bi.all.col)<-c("Control","Treatment")
write.table(bi.all.col, file="dat.B bilineage counts.csv", sep=";")

#multi lineage

multi.B <- subset(dat.groups.BB, groups.B >=7, select = c(counts))
multi.all.col <- merge(data.frame(multi.C, row.names=NULL), data.frame(multi.B,
row.names=NULL), by = 0, all = TRUE)
multi.all.col <- multi.all.col[,c(2,3)]
colnames(multi.all.col)<-c("Control","Treatment")
write.table(multi.all.col, file="dat.B multilineage counts.csv", sep=";")
```

7.2 Evi2a *in vitro* and *in vivo* experiments

A lot of work and effort has been done in the lab to be able to study the effect of certain cell surface markers on hematopoietic differentiation as well as groundwork to generate a conditional KO mouse model. This project was taken over and continued from a previous PhD student.

7.2.1 Evi2a genotyping

Ear tags were either collected from animal care takers or from Julia Knoch, Melanie Ball or Marleen Büchler-Schäff. DNA was isolated using the DNeasy Blood and Tissue Kit from Qiagen. In brief, tissue was incubated in ATL buffer and Proteinase K for approximately 3h at 56°C. When the ear tag was completely lysed buffer AL was added and thoroughly mixed. EtOH was added and the lysis solution was pipetted onto a spin column. Column was washed twice and DNA was eluted in 100µl H_2O. Buffers and columns were provided with the kit.

PCR reactions were optimized and worked best using the Kapa2G 2x master mix, however, for some PCR reactions the Phusion polymerase or the Genaxxon master mix were used. In order to confirm the sequence PCR products were purified and submitted to be sequenced by eurofins (https://www.eurofins.de). Sequences were analyzed using SnapGene viewer.

Table 12: Components of master mixes for genotyping PCRS.

Polymerase chain reaction for Evi2a genotyping	Phusion Volume in µl	Genaxxon Volume in µl	Kapa2G Volume in µl	Qiagen Long Range PCR Volume in µl
5x Phusion HF buffer	5			
2x Genaxxon MM		12.5		
LongRange PCR buffer				2.5
2x Kapa2G MM			12.5	
dNTPs 10mM	0.5			1.25
Primer fwd 10µM	1.25	1	1.25	1
Primer rev 10µM	1.25	1	1.25	1
H2O	15.75	9	9	18.55
Polymerase/Enzyme mix	0.25			0.2
DNA	1	1.5	1	0.5

Table 13: PCR program details for different genotyping PCRs.

PCR reaction	PCR steps	Temperature in °C / time in sec	Number of cycles
Primer 4 fwd Primer 1 rev	Initial denaturation	93 / 180	
	Denaturation	93 / 10	35
	Annealing	63.5 / 30	
	Elongation	68 / 180	
	Final extension	68 / 60	
Primer 8 fwd Primer 2 rev	Initial denaturation	93 / 180	
	Denaturation	93 / 15	35
	Annealing	64-62 / 30	
	Elongation	68 / 300	
	Final extension	68 / 60	
Primer 1 fwd Primer 1 rev	Initial denaturation	95 / 600	
	Denaturation	95 / 30	32
	Annealing	60.5 / 30	
	Elongation	72 / 130	
	Final extension	72 / 300	

Primer 1 fwd **Primer 32 rev**	Initial denaturation	95 / 600	
	Denaturation	95 / 30	32
	Annealing	62 / 30	
	Elongation	72 / 130	
	Final extension	72 / 300	

Primers were designed using the "Primer-BLAST" tool from NCBI Bethesda MD, USA (https://www.ncbi.nlm.nih.gov/tools/primer-blast/) and Primer3Plus[178] (http://www.bioinformatics.nl/cgi-bin/primer3plus/primer3plus.cgi/).

Table 14: List of primer sequences.

Primer name	Binding site	5´ - 3´ sequence
1 fwd	loxP site 1	GGCCGCATAACTTCGTATAATGT
1 rev	Exon2 Evi2a wt	ACAGTGCTTCTCTCAACCAGAAC
2 rev	Kan resistance	ATGATGGATACTTTCTCGGCAG
4 fwd	Intron1 Evi2a	GTAGGAAAGGACGGACACTTCT
8 fwd	endogenous Evi2a locus	AGTAAGAATCAAGGAGGCTGTGG
32 rev	Evi2a exon 2	CATTGGGAATTTGACATCTGC

7.2.2 Embryoid body differentiation

The embryoid body (EB) differentiation protocol was developed by Dr. Paul Kaschutnig and adapted from Pearson *et al*. 2008[32]. $7.5x10^4$ ESCs (after MEF depletion) were transferred to EB medium-containing ultra-low attachment cell culture flasks (7ml for a T25 flask) and incubated for 60h at 5% O_2, 5% CO_2, 37°C. Activin A, BMP4, FGF2 and VEGF (each cytokine with a final concentration of 5ng/ml) were added and another 60h incubation followed. On day 5 supernatant was collected, spun down to remove dead cells and conditioned medium was returned to the flask. After another 24h incubation cells were harvested on day 6. First, EBs were washed twice with PBS (EBs settled down by gravity) then incubated for 20min at 37°C in dissociation enzyme mix (10mg/ml Collagenase type IV, 20mg/ml Hyaluronidase type II, 40,000U/ml Deoxyribonuclease type I and II). EBs were mechanically separated to obtain a single cell suspension and washed with PBS. Cells were spun down at 1500rpm (270g) for 5min at 4°C and resuspended in either MM for staining or resuspended in PBS/2% FCS with 5µg/ml 7AAD for sorting.

Table 15: Staining panel for EB differentiation and sort of cells for RNA seq.

EB differentiation	FACS analysis	Staining for RNA seq analysis
c-Kit	APC-Cy7	
CD41	PE-Cy7	
CD144	PE	
CD309 (Flk-1)	Biotin	eF450
SAV	PacBlue	
CD93 (AA4.1)	APC	
Hoxb4	YFP	YFP
Live/dead		7AAD

Table 16: Cell culture medium composition of normal ESC medium and EB differentiation medium.

Medium components	ESC medium, final concentration	EB Medium, final concentration
DMEM Knockout	500ml - all other volumes	
IMDM		500ml – all other volumes
ESC FCS	10%	
FCS		15%
Pen/Strep	1%	1%
L-Glutamine	1%	1%
CHIR99021	3µM	
PD032591	1µM	
non-essential AA	1%	
ß-mercaptoethanol	0.1%	
Ascorbic acid		50µg/ml
MTG		4.5mM
Holotransferrin		200µg/ml
PFHM		5%
LIF	1000U/ml	

7.2.3 RNA isolation, library prep and RNA sequencing

Wt and Evi2a KO ESCs, three clones for each cell line, were differentiated according to the EB differentiation protocol. For RNA isolation at least 1000 Hoxb4-YFP$^+$ cells were sorted into RLT+ buffer on day 4, 5 and 6 of EB differentiation and directly processed according to the manufacturer´s protocol of the RNeasy Micro Plus Kit. In brief, cells were homogenized by vortexing and run through a QIAshredder spin column to shear DNA. The lysate was run through a gDNA eliminator column, the flow through was precipitated and transferred to an RNeasy MinElute spin column. After in total three washing steps, RNA was eluted in 14µl sterile H_2O. Sample preparation was done together with Wenjun Chang.

To generate cDNA the SMART-Seq v4 Ultra Low Input RNA kit was used. In brief, 3ng RNA were used for the first strand cDNA generation and mixed with primers and enzymes provided by the kit. An amplification step of nine PCR cycles followed using the SeqAmp reagents from the kit. AMPure XP beads were used to purify and wash the generated cDNA. 17µl cDNA was eluted and concentration was measured using the Qubit™ system. cDNA (total of 16µl) was sheared using the Covaris M220 with the 55µl microtubes. Settings were adjusted as follows: Peak Incident Power (W) to 75, Duty Factor to 10%, 200 Cycles per burst, 160 sec treatment time, temperature to 20°C. The resulting fragment size was approximately 250bp.

The NEBNext Chip-Seq kit was used for library preparation and the NEBNext Multiplex oligos for Illumina was used to multiplex the libraries in order to be able to use 6 samples on one lane. The sheared cDNA was used for the library prep according to the manufacturer´s protocol. In brief, end repair of sheared cDNA was done using the green buffers, followed by dA-tailing using the yellow kit components. Adaptor ligation was done using the red components and finally a PCR (15 cycles) was performed to amplify the products. The washing and purification steps in between were again performed using the AMPure XP beads. Quality of libraries was checked using the bioanalyzer High Sensitivity DNA chip from Agilent. Libraries were handed over to the high throughput sequencing unit of the Genomics and Proteomics core facility of the DKFZ and sequenced on a HiSeq 4000 as Single-Read 50bp.

Table 17: After RNA was isolated, cDNA was generated followed by library preparation for RNA-Seq. Samples were multiplexed in order to be able to run several samples on one lane. The table shows the multiplexing using i5 and i7 primers, provided by the NEBNext Multiplex Oligos for Illumina kit.

	i5 Primer			
i7 Primer		i501 – lane 1	i502 – lane 2	i503 – lane 3
	i701	Sample #3 (12.09.)	Sample #1 (20.09.)	Sample #10 (1.10.)
	i702	Sample #6 (12.09.)	Sample #2 (20.09.)	Sample #11 (1.10.)
	i703	Sample #15 (12.09.)	Sample #5 (20.09.)	Sample #13 (1.10.)
	i704	Sample #9 (20.09.)	Sample #7 (20.09.)	Sample #14 (1.10.)
	i705	Sample #12 (20.09.)	Sample #4 (1.10.)	Sample #16 (1.10.)
	i706	Sample #18 (20.09.)	Sample #8 (1.10.)	Sample #18 (1.10.)

Table 18: Prepared libraries that were submitted to the core facility to be sequenced. C0, C1, C14 referring to three different wt ESC clones, KO4, KO5 and KO8 referring to three different Evi2a KO clones.

Sample Name	Cell type (wt or Evi2a KO)	Day of isolation
EB-diff-1	C0	D4
EB-diff-2	C0	D5
EB-diff-3	C0	D6
EB-diff-4	C1	D4
EB-diff-5	C1	D5
EB-diff-6	C1	D6
EB-diff-7	C14	D4
EB-diff-8	C14	D5
EB-diff-9	C14	D6
EB-diff-10	KO4	D4
EB-diff-11	KO4	D5
EB-diff-12	KO4	D6
EB-diff-13	KO5	D4
EB-diff-14	KO5	D5
EB-diff-15	KO5	D6
EB-diff-16	KO8	D4
EB-diff-17	KO8	D5
EB-diff-18	KO8	D6

7.2.4 Bioinformatical analysis

Quality control and mapping/aligning of genes was performed by the Genomics and Proteomics core facility. Downstream analysis was performed using “Galaxy” an open source, web-based platform for computational/bioinformatical research and analysis (https://galaxyproject.org). Read counts and read lengths were extracted from BAM files using “featureCounts” function in Galaxy. Next, DESeq2 was performed to get differentially expressed genes (p-value (adj), log2(FC)),

normalized read counts and principal component analysis plots. To annotate genes the core facility generously provided a mouse reference genome (description: evidence-based annotation of the mouse genome (GRCm38), version M12 (Ensembl 87), provider: GENCODE) as gff file which was then concatenated with the DESeq2 output data using “Annotate DESeq2/DEXSeq output tables”. Volcano plots were also generated in galaxy using the “Volcano plot” function.

Gene set enrichment analysis (GSEA) was performed on a pre-selected dataset with a p-value adj <0.1. following parameters were set for enrichment analysis:

Gene set enrichment analysis settings

Required/Basic/Advanced fields	**-**	**Setting**
Number of permutations	-	1000 (default)
Gene set database Gene matrix (from website)	-	h.all.v7.2.symbols.gmt (Hallmarks), c2.cp.biocarta.v7.2symbols.gmt (curated), c2.cp.kegg.v7.2.symbols.gmt (curated), c2.cp.reactome.v7.2.symbols.gmt (curated), c7.all.v7.2.symbols.gmt(Immunologic signatures)
Phenotype labels	-	wt vs KO
Collapse/Remap to gene symbols	-	Collapse (default)
Permutation type	-	gene_set (default)
Enrichment statistic	-	Weighted (default)
Metric for ranking genes	-	Signal2Noise (default)
Gene list sorting mode	-	Real (default)
Gene list ordering mode	-	Ascending
Max size: exclude larger sets	-	500 (default)
Min size: exclude smaller sets	-	15 (default)
Collapsing mode for probe sets -> 1 gene	-	Median_of_probes (default)
Normalization mode	-	Meandiv (default)
Randomization mode	-	No_balance (default)
Create GCT files	-	False (default)
Create SVG plot images	-	False (default)
Omit features with no symbol match	-	True (default)
Make detailed gene set report	-	True (default)
Median for class metrics	-	False (default)
Number of markers	-	100 (default)

Plot graphs for the top sets of each phenotype	-	30
Seed for permutation	-	Timestamp (default)
Save random ranked lists	-	False (default)
Make a zipped file with all reports	-	False (default)

IPA analysis was performed on differentially expressed genes.

Ingenuity pathway analysis settings

Required field/options	**-**	**Setting**
Core analysis type	-	Expression analysis
Measurement type	-	Expr Log Ratio
Reference set	-	Ingenuity Knowledge base (genes only) (default)
Network interaction & Causal networks	-	Default
Node types	-	All selected (default)
Data sources	-	All selected (default)
Confidence	-	Experimentally observed
Species	-	Mouse
Tissues and cell lines	-	All selected (default)
Mutation	-	Functional effect, inheritance. Mode, translation impact, zygosity, wild type
Cutoffs: log2(FC)	-	-0.58 (down), 0.58 (up)
p-adj	-	0.01

Table 19: List of bioinformatical tools used for RNA seq analysis.

Bioinformatical tool/tutorial	citation
Galaxy version 20.09	https://usegalaxy.org
featureCounts	Liao, Y., Smyth, G. K., & Shi, W. (2013). featureCounts: an efficient general purpose program for assigning sequence reads to genomic features. Bioinformatics, 30(7)
DESeq2	Love, M. I., Huber, W., & Anders, S. (2014). Moderated estimation of fold change and dispersion for RNA-seq data with DESeq2. Genome Biology, 15(12)
Reference-based RNA-seq data analysis	Bérénice Batut, Mallory Freeberg, Mo Heydarian, Anika Erxleben, Pavankumar Videm, Clemens Blank, Maria Doyle, Nicola Soranzo, Peter van Heusden
GSEA version 4.1.0	Subramanian, Tamayo, *et al*. (2005, PNAS 102, 15545-15550) Mootha, Lindgren, *et al*. (2003, Nat Genet 34, 267-273) http://www.gsea-msigdb.org/gsea/index.jsp
IPA version 01-16 (01-16)	Qiagen, free access via DKFZ license

7.3 Statistical analysis

Statistical analyses as well as graphs were generated with GraphPad Prism version 8.3. Data is shown as mean value with error bars for standard deviation (SD) and statistical test were done using unpaired nonparametric, two-tailed t-tests. Significant results were marked with “ns” if $P > 0.05$, with “*” if P value is $0.05 > P > 0.01$, “**” if P value is $0.01 > P > 0.001$ and “***” if $P < 0.001$, if not indicated differently. Statistical analysis was only performed when at least three data points were available.

7.4 Use of published figures

In order to be able to use or modify figures from published studies, the permission was obtained via the “Copyright Clearance Centre RightsLink®”. http://www.copyright.com

7.5 List of reagents and consumables

Most of the materials, reagents and consumables were ordered centrally by the department or Hi-STEM. All basic, standard labware (e.g. pipet tips, vortexer, tubes, table top centrifuge, etc.) is not listed in the following table. Only specific kits, antibodies, solutions, consumables that go beyond the standard lab equipment are listed.

Table 20: List of materials and reagents used.

Antibody/reagent/buffer/ consumable	Fluorochrome/ clone	Ordering number	company
7-aminoactinomycin D (7-AAD)		A1310	Life Technologies
B220 (CD45R) IgG2a, k	RA3-6B2	553086	BD Pharmingen
CD144 (V-Cadherin)	APC Alexa Fluor 647/BV13		BioLegend
CD144 (V-Cadherin)	PE/11D.41		BD
CD309 (Flk1)	Avas12a1		eBioscience
CD34 Monoclonal	RAM34	48-0341-82	eBioscience
CD42d	APC/1C2	17-0421-82	eBioscience
CD5 (Ly-1) Biotin IgG2a, k	53-6.7	553019	BD Pharmingen
CD55	PE/RIKO-3	131803	BioLegend
CD71 (Transferrin Receptor)	PE/RI721714	12-0711-83	eBioscience
CD8a (Ly-2), IgG2a, k	53-6.7	553029	BD Pharmingen
CD9	FITC/eBioKMC8	11-0091-82	eBioscience
CD93 (AA4.1)	APC/AA4.1	17-5892-82	eBioscience
Centrifuge 5424 R			Eppendorf
Centrifuge; Medifuge, Standard, Heraeus			Thermo Fisher
DAPI Solution 1mg/ml		62248	Thermo Fisher
Gr-1 (Ly-6G), IgG2b, k	RB6-8C5	553125	BD Pharmingen
ESGRO recombinant mouse LIF		ESG1106	Merck-Millipore

Mac-1 (CD11b), IgG2b, k	M1/70	553309	BD Pharmingen
Ter-119 (Ly-76), IgG2b, k	TER-119	553672	BD Pharmingen
100 bp ladder		15628-050	Thermo Fisher
ACK lysing buffer		10-548E	Lonza
AMPure XP		A63881	Beckman Coulter
BD Cytofix/Cytoperm™ Fixation/Permeablization Kit		554714	BD Biosciences
DMEM Knockout		10829018	Gibco
DNeasy Blood and Tissue kit		69506	Qiagen
Doxycycline hydrate		D9891	Sigma
DynabedsTM M-280 Streptavidin		11206D	Invitrogen
EmbryoMax ES Cell qualified FCS		ES-009-B	Merck
Falcon 5ml round bottom polystyrene tube with cell strainer cap		352235	Corning
FACS AriaFusion™ cell sorter			BD
FACS Aria™ cell sorter			BD
FCS		26140079	Gibco
Genaxxon red Taq MM2x		M3029	BioScience
Gene Ruler 1kb DNA ladder		SM0312	Thermo Scientific
Gr96 well cell culture plate U bottom		650180	Greiner Bio-one
High Sensitivity DNA Analysis		5067-4626	Agilent
IL7 rec. Murine		217-17-10	PeproTech
IMDM		21980065	LifeTechnologies
KAPA2G robust HS RM		KK5702	Sigma
LongRange PCR kit		206402	Qiagen
LSRFortessa™ with HTS			BD
LSRFortessa™			BD
LSR™			BD

microvette 500µl collection tube EDTA		NC9990563	Sarstedt Inc
NEBNext CHIP-Seq Library Prep Master Mix Set for Illumina		E6240S	NEB
NEBNext Multiplex Oligos for Illumina (Dual Index Primers Set 1)		E7600	NEB
OneComp eBeads™ Compensation Beads		01-1111-42	Invitrogen
PBS		D8537-500ML	Sigma
Penicillin/Streptomycin solution		P4458	Sigma
Pipettes: 1000µl, 200µl, 100µl, 20µl, 10µl, 2.5µl		Eppendorf Research® plus	Eppendorf
Phusion High-Fidelity DNA Polymerase		M0530L	NEB
Qubit™ dsDNA HS Assay Kit		Q32851	ThermoFisher/Invitrogen
RNA 6000 Nano Kit		5067-1511	Agilent
RNeasy Plus Micro Kit		74034	Qiagen
RPMI1640 Medium		11875093	Gibco
SCF rec. Murine		250-03-100	PeproTech
SMART-Seq® v4 Ultra Low Input RNA kit		634889	Takara
StemSpan SFEM		9560	StemCell
sucrose		S0389-500G	Sigma
Ultra-low attachment cell culture flasks		CLS3815	Corning
ZEISS Primovert Cell and Tissue Culture Microscope			Carl Zeiss Microscopy
QIAquick PCR Purification Kit (250)		28106	Qiagen

8 Acknowledgements and contributions

I couldn't have done all this work without the support of so many people.

First of all, I would like to thank my supervisor **Dr. Michael Milsom** for giving me the opportunity to do my PhD in his lab, especially since I did not have any background knowledge regarding the hematopoietic system. Thank you, Mick, for giving me two amazing and challenging projects. I really enjoyed working on both of them, learned so much and could develop myself further during the last years. I really appreciate the time and effort you spend to support me, teach me and guide me through the PhD, especially during the year 2020.

Thank you, **Prof. Dr. Ingrid Lohmann**, **Prof. Dr. Ursula Klingmüller** and **Prof. Dr. med. Daniel Nowak** for being part of my defense committee. Moreover, I would like to thank Ursula and **Prof. Dr. Ute Modlich** for their scientific input and discussions during my TAC meetings.

Many thanks to **Mick**, **Megan**, **Matea**, **Theo** and **Alina** for proof-reading (parts) of my thesis. I am deeply grateful for all your comments, critique and suggestions.

Next, I would like to say a big thank you to the **Milsom group** including all former and current members and all internship students that contributed to such an amazing lab life. Thank you, **Paul Kaschutnig**, for passing on a great project that I was able to continue working on. Thank you **Julius Gräsel**, **Sina Stäble**, **Jens Langstein**, **Natasha Anstee**, **Yolanda (Wenjun) Chang**, **Mariana Coelho**, **Ruzhica Bogeska**, **Ana-Matea Mikecin-Drazic**, **Susanne Lux**, **Megan Druce**, **Jeyan Jayarajan**, **Esther Rodriguez Correa**, **Fenia Fotopoulou**, **Theo Aurich**, **Melanie Ball** and **Julia Knoch** for all the experimental and scientific contribution and support during my PhD. Thank you everyone for creating such a motivating atmosphere, for sharing countless coffee breaks and for making the early morning preps actually fun. I am especially grateful for the constant support from Melanie and Julia during all the experiments but also for taking care of mouse colonies and input during trouble shooting.

A huge thank you goes to the "**MaMaRu experimental group**". Thank you **Matea** and **Ruzhi** for making the LRC experiments fun, for staying awake during all the long-night sorts, for just everything that I could learn from you and experience with you.

Another big thank you goes to the people that I shared the "aquarium" with during my time in the lab. Thank you for all the scientific discussions but also all the laughter we shared in this little space.

I would like to thank my amazing master student **Yolanda** for her dedication to her thesis project. Working with you was great and on top of that you really pushed the Evi2a project forward. Thank you for carrying out all the differentiation experiments needed to perform the RNA-seq analysis.

In addition, I also want to thank **Prof. Dr. Andreas Trumpp** and all **Hi-STEM** members for creating such an inspiring, motivating and encouraging environment. I highly appreciated working in a surrounding with such talented and cooperative people. I want to acknowledge **Dr. Marc Thier**, **Dr. Elisa Donato** and **Dr. Paula Werner** for their help and support in the scope of the Evi2a project. Thank you **Shubhankar Sood** for being such a lovely person and always happy to discuss science or any other topic of life.

At this point, I also want to thank the department of **Prof. Dr. Peter Lichter** and especially **Laura Llao Cid** for handing me the Rag2 KO mice.

Next, I would like to thank the **DKFZ core facilitie**s for support. Especially the **Center for Preclinical Research** for taking care of mice, for help with generating the mouse model and for support during TVA submissions. The **Information Technology (ZDV)** unit for help with creating and retrieving backup data and for solving any other technical issue. The **Flow cytometry** unit for maintaining and setting up FACS machines. The **Genomics and Proteomics** as well as the **Omics IT and Data Management Core Facility** for support in submitting libraries as well as performing RNA sequencing and RNA analysis.

Moreover, I truly want to thank the "DKFZ-Mädels" **Andrea**, **Anka**, **Dani**, **Julia**, **Mone**, **Nina**, **Sabrina** and **Sophie** for a great journey so far. I am so grateful that we went through this together and enjoyed all the on-site meetings, virtual meetings and sport sessions.

I would also like to thank **all my friends** from the bottom of my heart. Thank you for always being there for me, listening to me, standing by me and supporting me even during difficult times. Most of all, thank you for your great understanding that I sometimes had too little time. I am probably repeating myself, but I am so grateful for your friendship.

Außerdem möchte ich meinen **Eltern Annerose und Martin** und meiner **Schwester Kristin** von Herzen danken. Danke, dass ihr immer für mich da seid, mich immer in allem unterstützt und ich immer auf Euch zählen kann. Vielen Dank für euer unendliches Verständnis und eure Geduld mit mir, ohne Euch hätte ich das alles nie geschafft.

Marc, die Zeilen reichen nicht aus, um Dir zu sagen, wie dankbar ich für deine Unterstützung bin und wie glücklich ich mich schätzen kann, dich zu haben. Danke, dass du immer an meiner Seite bist!

9 List of figures, tables and abbreviations

List of figures

List of tables

List of abbreviations

A700	-	Alexa700
AGM	-	aorta-gonad-mesonephros region
BM	-	bone marrow
BMP4	-	Bone morphogenetic protein 4
CMPs	-	common myeloid progenitors $Lin^-Sca\text{-}1^+c\text{-}kit^-CD16/32^-CD34^+$
CSM	-	cell surface marker
DA	-	dorsal aorta
DNA/RNA	-	deoxyribonucleic acid/ribonucleic acid
dox/tet	-	doxycycline/tetracycline
EB	-	embryoid body
EHT	-	epithelial to hematopoietic transition
EMT	-	epithelial to mesenchymal transition
ESCs	-	embryonic stem cells
Evi2a/b	-	Ecotropic viral integration site 2a/b
FACS/FC	-	fluorescence-activated cell sorting/flow cytometry
FCS	-	fetal calf serum
FGF	-	fibroblast growth factor
FL	-	fetal liver
FSC-A/FSA-H	-	forward scatter area/forward scatter height
GFP/YFP	-	green fluorescent protein/yellow fluorescent protein
GMPs	-	granulocyte/monocyte Progenitors
GOI	-	gene of interest
GSEA	-	gene set enrichment analysis
h	-	hour(s)
HSCs	-	hematopoietic stem cells, (in this thesis: $Lin^-Sca\text{-}1^+c\text{-}kit^+CD150^+CD48^-$)

HSPCs	-	hematopoietic stem and progenitor cells
HTS	-	high throughput sampler
IACs	-	intra-aortic clusters
IL	-	interleukin
IPA	-	ingenuity pathway analysis
(h)iPSCs	-	(human) induced pluripotent stem cells
ITP	-	immune thrombocytopenia
iv/ip	-	intravenous/intraperitoneal
IVC	-	individually ventilated cages
Lin	-	lineage cells (in this thesis: CD4, CD8, CD11b, Gr-1, B220, Ter119)
LRC	-	label retaining cells, cells from the scl-tTA-H2B-GFP mouse model
LT-HSCs	-	long-term HSCs (in this thesis: $Lin^-Sca\text{-}1^+c\text{-}kit^+CD150^+CD48^-CD34^-$)
max	-	maximum
MEF	-	murine embryonic fibroblasts
MEPs	-	megakaryocyte-erythroid Progenitor
mil	-	million
MKs	-	megakaryocytes
ml	-	milliliter
MM	-	master mix (for stainings)
Mpl	-	myeloproliferative leukemia protein
MPPs	-	multipotent progenitor cells
NET	-	neutrophil extracellular trap
PB	-	peripheral blood
PLTs	-	platelets
polyI:C	-	polyinosinic:polycytidylic acid
RBCs	-	red blood cells
Rom	-	Romiplostim (Nplate®)
rpm	-	rounds per minute
SAV	-	Streptavidin
seq	-	sequencing
SPF	-	specific pathogen free
SSC-A/SSC-H	-	side scatter area/side scatter height
ST-HSCs	-	short-term HSCs (in this thesis: $Lin^-Sca\text{-}1^+c\text{-}kit^+CD150^+CD48^-CD34^+$)
TBI	-	total body irradiation
tg		transgene
TPO (rm/rh)	-	thrombopoietin (recombinant murine/recombinant human)
UBC	-	human ubiquitin C promoter
VEGF	-	Vascular Endothelial Growth Factor
WBCs	-	white blood cells
wt	-	wild type (in this thesis: C57BL/6J mice or non-transgenic cells)
µl	-	microliter

9 List of figures, tables and abbreviations

10 Appendix

Additional figures and information.

10.1 Quality of RNA isolation and cDNA libraries

This section supports Figure 8. Quality of isolated RNA was measured using the Bioanalyzer (Agilent) and the appropriate RNA kit.

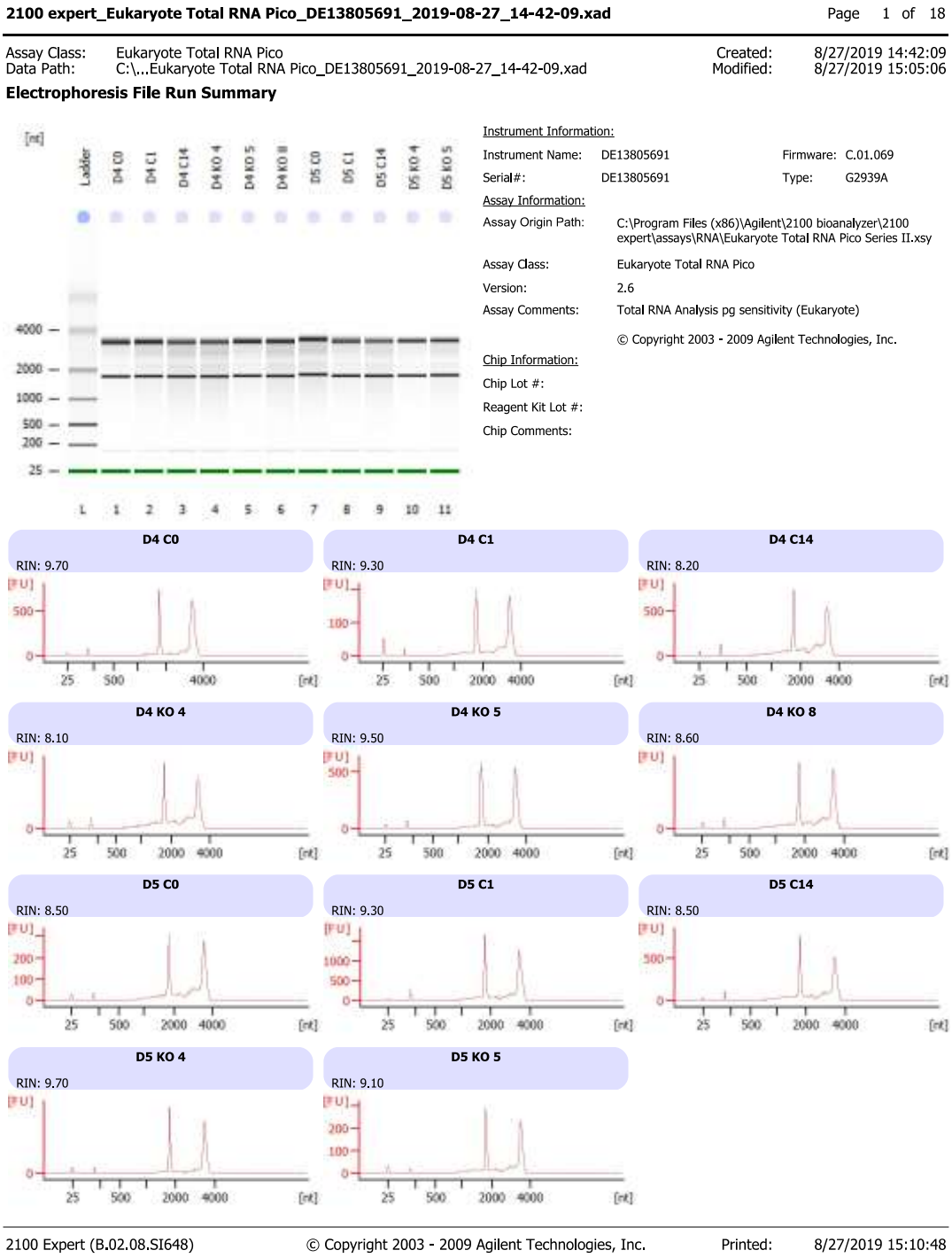

Figure 37: **Bioanalyzer results from isolated RNA**.

Qualitiy of cDNA libraries was controlled using the Bioanalyzer (Agilent) and the appropriate DNA kit.

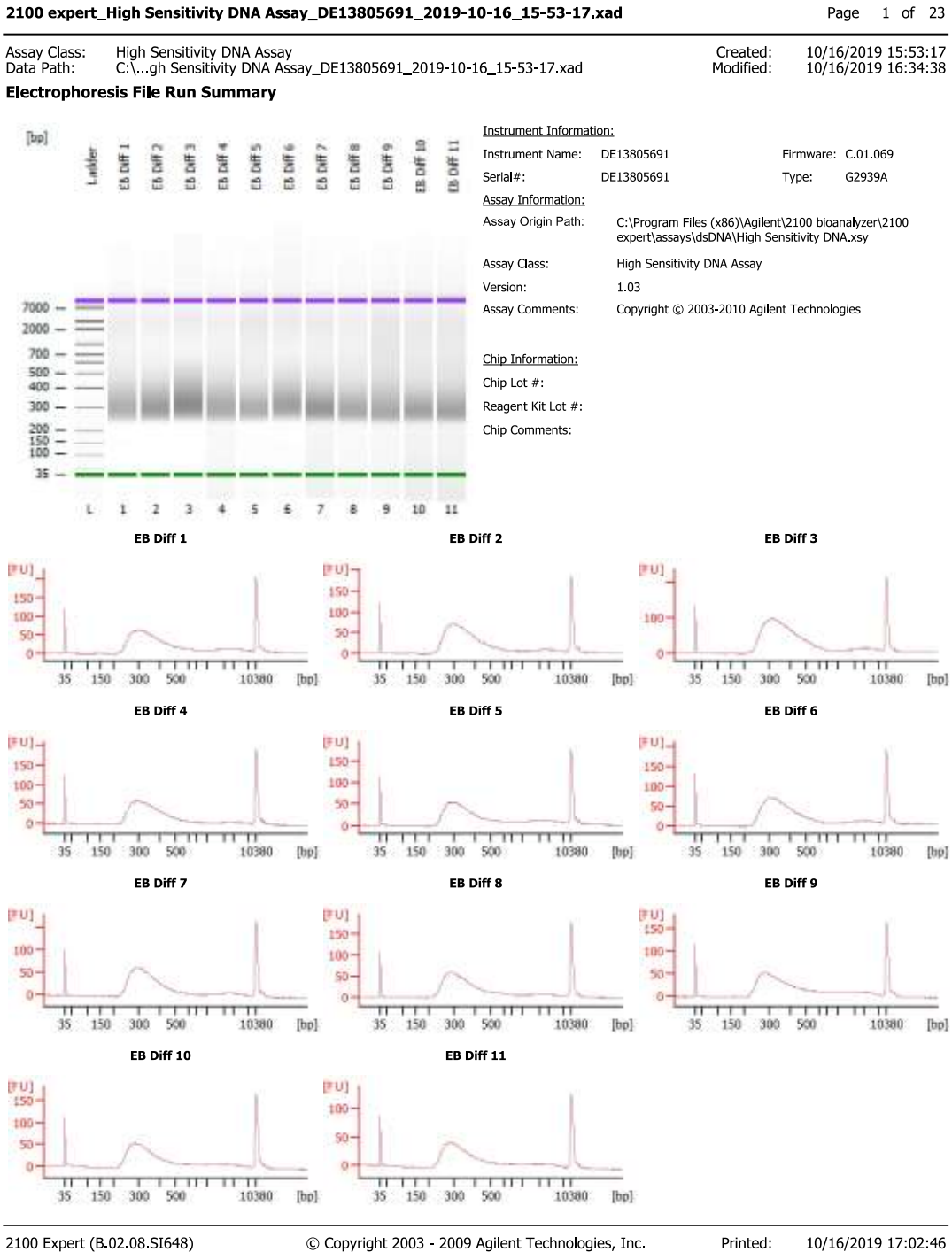

Figure 38: **Bioanalyzer results from RNA libraries.**

10.2 List of deregulated pathways from IPA core analysis

This section supports Figure 10.Ingenuity pathway analysis (IPA) was used to analyze RNA seq data. A so-called core analysis was performed to identify pathways and functions that were deregulated between differentiated wt and Evi2a KO cells.

Diseases and Bio Functions for My Projects->eb-diff-2->Galaxy646-pval_IPA_D4_2 - 2021-01-30 06:44 PM					
Categories	Functions	p-Value	Predicted Ac	Activation z-	# Molecules
Cardiovascular System Development and Function	development	9.92E-33		1.527	341
Embryonic Development, Organismal Development	development	4.44E-31	Increased	2.503	418
Cardiovascular System Development and Function, Organismal Devel	angiogenesis	1.84E-29		1.589	293
Cellular Movement	cell movement	6.41E-29		-0.235	503
Cellular Assembly and Organization, Cellular Function and Maintenan	organization	1.12E-27		-0.558	351
Cellular Movement	migration	1.97E-27		0.01	444
Cellular Assembly and Organization, Cellular Function and Maintenan	organization	1.91E-25		-0.558	365
Cellular Assembly and Organization, Cellular Function and Maintenan	organization	6.14E-25		-0.3	312
Cardiovascular System Development and Function, Organismal Devel	vasculogenesis	5.48E-23		1.385	226
Organismal Development	morphology	6.43E-23			508
Cell Morphology, Cellular Assembly and Organization, Cellular Functic	formation	7.42E-22		-0.614	253
Embryonic Development, Organismal Development	development	9.58E-22		1.294	354
Organismal Survival	organismal death	2.07E-21		-0.554	675
Organismal Survival	morbidity or mortality	2.18E-21		-0.613	683
Organismal Development	abnormal morphology	1.39E-20			441
Cardiovascular System Development and Function	morphology	4.35E-20			271
Respiratory System Development and Function	development	1.58E-19		1.094	139
Digestive System Development and Function	development	4.06E-19		1.839	111
Digestive System Development and Function	development	5.98E-19	Increased	2.184	150
Embryonic Development, Organismal Development	development	6.42E-19		1.514	325
Cardiovascular System Development and Function	morphogenesis	7.28E-19		0.896	95
Cardiovascular System Development and Function, Embryonic Develo	cardiogenesis	8.70E-19		0.913	182
Cellular Development, Cellular Growth and Proliferation, Nervous Sys	development	5.09E-18		0.776	237
Cell Morphology, Cellular Development, Cellular Growth and Prolifera	morphogenesis	9.85E-18		0.123	186
Cancer, Organismal Injury and Abnormalities	solid tumor	2.26E-17		1.68	403
Cell Morphology, Cellular Assembly and Organization, Cellular Develo	neuritogenesis	2.46E-17		0.123	183
Organismal Development	development	3.08E-17		1.677	320
Embryonic Development, Organismal Development	development	3.25E-17		1.946	206
Tissue Morphology	quantity	3.66E-17		1.021	549
Embryonic Development, Organ Development, Organismal Developm	formation	2.49E-16		1.094	119
Tissue Development	growth	4.90E-16		0.19	166
Tissue Development	development	5.02E-16		1.148	125
Cardiovascular System Development and Function, Embryonic Develo	morphogenesis	1.05E-15		1.387	72
Cardiovascular Disease, Cardiovascular System Development and Fun	abnormal morphology	1.15E-15			229
Organismal Development, Organismal Injury and Abnormalities	abnormal morphology	1.64E-15			249
Diseases and Bio Functions for My Projects->eb-diff-2->Galaxy647-pval_IPA_D5 - 2021-01-30 07:05 PM					
Categories	Functions	p-Value	Predicted Ac	Activation z-	# Molecules
Cardiovascular System Development and Function	development	2.27E-34	Decreased	-2.227	372
Organismal Development	morphology	1.59E-30			583
Cardiovascular System Development and Function, Organismal Devel	angiogenesis	3.39E-28	Decreased	-2.18	312
Embryonic Development, Organismal Development	development	1.38E-27	Decreased	-3.129	404
Organismal Development	morphology	2.54E-27			385
Organismal Development	abnormal morphology	3.07E-27			506
Organismal Survival	organismal death	4.45E-26	Increased	4.589	760
Organismal Survival	morbidity or mortality	7.64E-26	Increased	4.615	768
Embryonic Development, Organismal Development	development	8.58E-25	Decreased	-2.058	431
Organismal Development, Organismal Injury and Abnormalities	abnormal morphology	1.21E-24			336
Organismal Development, Organismal Injury and Abnormalities	abnormal morphology	2.98E-23			296
Cardiovascular System Development and Function	morphology	7.81E-23			302
Cellular Movement	cell movement	1.84E-22	Decreased	-2.276	521
Embryonic Development, Organismal Development	patterning	2.22E-22			73
Cardiovascular System Development and Function	morphogenesis	3.55E-22		-1.277	107
Cardiovascular System Development and Function, Embryonic Develo	morphogenesis	3.57E-22			87
Embryonic Development, Organismal Development	patterning	1.10E-21			64
Cardiovascular Disease, Cardiovascular System Development and Fun	abnormal morphology	3.82E-21			266
Cardiovascular System Development and Function, Embryonic Develo	cardiogenesis	4.85E-21		-1.049	202
Cellular Assembly and Organization, Cellular Function and Maintenan	organization	5.48E-21	Decreased	-2.984	357
Connective Tissue Development and Function, Skeletal and Muscular	morphology	1.23E-20			233
Cellular Movement	migration	1.84E-20		-1.548	455
Cardiovascular System Development and Function, Organismal Devel	vasculogenesis	4.45E-20		-1.587	235
Embryonic Development, Organismal Development	development	8.62E-20	Decreased	-2.943	356
Cellular Assembly and Organization, Cellular Function and Maintenan	organization	1.56E-19	Decreased	-2.984	374
Connective Tissue Development and Function, Connective Tissue Diso	abnormal morphology	6.23E-19			175
Nervous System Development and Function	morphology	8.35E-19			350
Cellular Assembly and Organization, Cellular Function and Maintenan	organization	1.20E-18	Decreased	-2.666	316
Cardiovascular Disease, Cardiovascular System Development and Fun	abnormal morphology	1.35E-17			223
Cardiovascular System Development and Function, Organ Morphology	morphology	1.42E-17			245
Nervous System Development and Function, Neurological Disease	abnormal morphology	7.71E-17			291
Tissue Morphology	quantity	9.29E-17	Decreased	-2.055	598
Developmental Disorder	dysgenesis	1.05E-16	Increased	3.013	187
Developmental Disorder	aplasia or hypoplasia	1.73E-16	Increased	2.796	185
Cellular Development, Tissue Development	differentiation	2.04E-16		1.341	117
Organismal Survival	perinatal death	2.45E-16	Increased	3.926	190

Diseases and Bio Functions for My Projects->eb-diff-2->Galaxy649-pval_IPA_D6 - 2021-01-30 07:09 PM					
Categories	Functions	p-Value	Predicted Ac	Activation z-	# Molecules
Cellular Movement	migration	6.32E-37	Increased	2.401	392
Cardiovascular System Development and Function	development	1.75E-35		-1.931	291
Cellular Movement	cell movement	3.04E-35	Increased	2.288	431
Cardiovascular System Development and Function, Organismal Devel	angiogenesis	4.44E-35		-1.931	258
Cardiovascular System Development and Function, Organismal Devel	vasculogenesis	2.94E-31	Decreased	-2.148	208
Embryonic Development, Organismal Development	development	3.86E-26	Decreased	-2.893	304
Embryonic Development, Organismal Development	development	2.24E-25		-1.529	328
Tissue Morphology	quantity	4.47E-25	Decreased	-2.139	474
Cellular Assembly and Organization, Cellular Function and Maintenan	organization	4.53E-23		0.079	277
Cellular Assembly and Organization, Cellular Function and Maintenan	organization	2.63E-22		0.079	291
Cellular Movement	cell movement	2.97E-22	Increased	4.042	238
Cellular Movement, Immune Cell Trafficking	migration	9.19E-22	Increased	4.206	235
Embryonic Development, Organismal Development	patterning	1.53E-21			54
Embryonic Development, Organismal Development	development	1.08E-20	Decreased	-2.795	272
Embryonic Development, Organismal Development	morphogenesis	2.13E-20		-1.086	92
Cellular Assembly and Organization, Cellular Function and Maintenan	organization	2.14E-20		0.617	245
Organismal Development	morphology	3.69E-20			402
Cellular Movement, Hematological System Development and Functio	cell movement	1.24E-19	Increased	3.908	209
Organismal Development	abnormal morphology	2.35E-19			354
Organismal Development	morphology	4.32E-19			269
Embryonic Development, Organismal Development	patterning	4.64E-19			57
Organismal Survival	organismal death	8.35E-19	Increased	3.442	531
Nervous System Development and Function	morphology	9.12E-19			264
Organismal Survival	morbidity or mortality	9.60E-19	Increased	3.578	537
Cardiovascular System Development and Function	morphogenesis	1.99E-18		-1.022	81
Digestive System Development and Function	development	3.98E-18		-1.117	93
Hematological System Development and Function, Tissue Morphology	quantity	1.07E-17		-0.013	294
Cardiovascular System Development and Function, Embryonic Develo	cardiogenesis	1.53E-17		-1.101	149
Cell-To-Cell Signaling and Interaction	aggregation	2.70E-17	Increased	2.975	79
Cell Death and Survival	necrosis	8.16E-17		1.457	402
Organismal Development, Organismal Injury and Abnormalities	abnormal morphology	1.01E-16			233
Inflammatory Response	inflammation	1.08E-16		-0.213	254
Hematological System Development and Function, Tissue Morphology	quantity	1.15E-16		0.453	265
Cancer, Organismal Injury and Abnormalities	cancer	1.19E-16		-0.258	343
Connective Tissue Development and Function, Connective Tissue Diso	abnormal morphology	1.63E-16			131
Cancer, Organismal Injury and Abnormalities	solid tumor	2.30E-16		-1.369	323

Figure 39: **IPA core analysis results from differential gene expression of differentiated wt vs Evi2a KO cells**. Top deregulated pathways and functions are shown.

10.3 Vector map of the Evi2a vector

This section supports Figure 13.

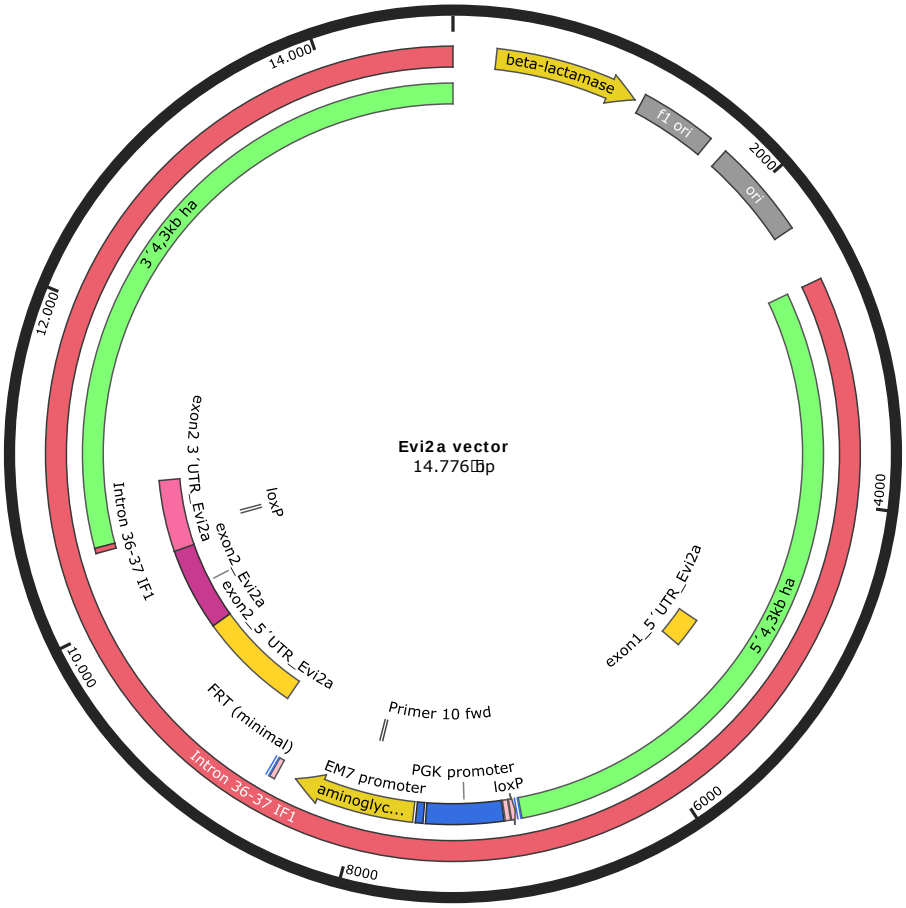

Figure 40: **Evi2a vector map**. The vector contains bacterial characteristics (such a sori) and eukaryotic NF1 and Evi2a sequence. 5´ and 3´ homology arms were added to ensure correct recombination within the genome. The Evi2a CDS (coding sequence) is flanked by loxP sites and resistance caasette necessary for bacterial cloning is flanked by FRT sites. Vector map was created with SnapGene®

10.4 Counts of mono-, bi- and multilineage colonies from wt and Fanca$^{-/-}$ mice

Fanca$^{-/-}$ mice were treated for one round with TPO and PBS (see Figure 30 A). Mice were sacrificed, single LT-HSCs sorted and colonies were FACS analyzed. Mono-, bi- and multilineage output was determined based on a developed R pipeline by Dr. Holland-Letz and Dr. Bogeska. Each dot in the violin plot represents one colony.

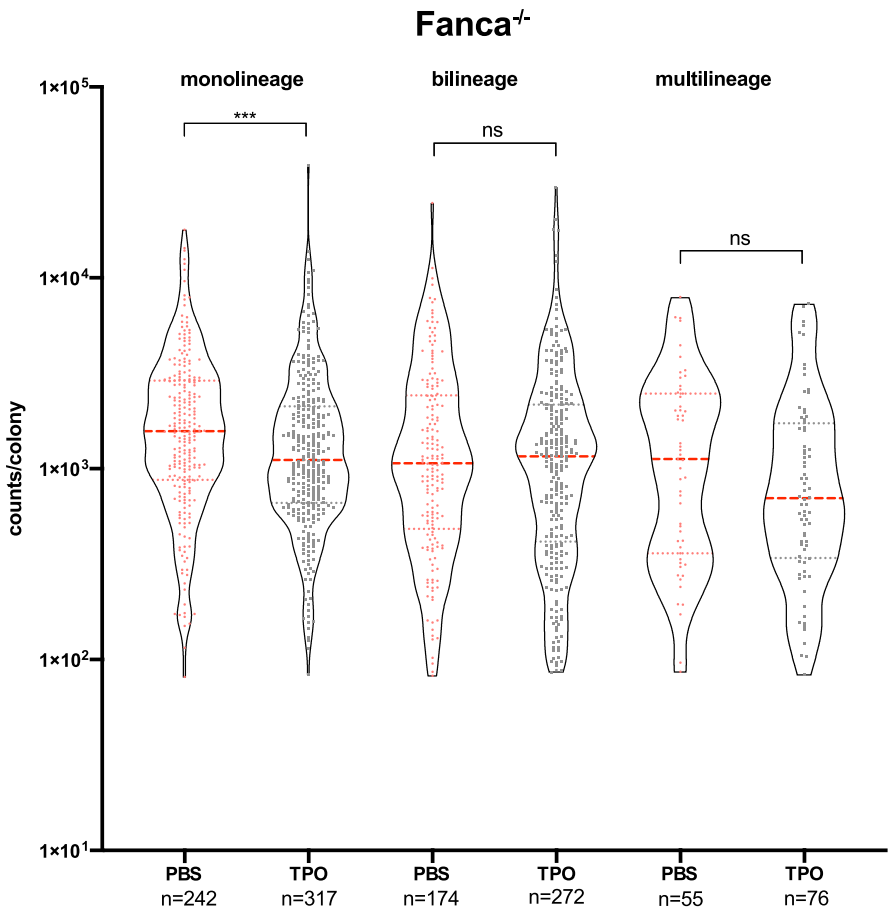

Figure 41: **Lineage output of every single colony displayed as a violin plot.** Results are shown from Fanca$^{-/-}$ treated mice. Dashed red line indicates the median.

11 References

1. Luis TC, Killmann NMB, Staal FJT. Signal transduction pathways regulating hematopoietic stem cell biology: Introduction to a series of Spotlight Reviews. *Leukemia*. 2012;26(1):86-90. doi:10.1038/leu.2011.260

2. Stefanska M, Batta K, Patel R, Florkowska M, Kouskoff V, Lacaud G. Primitive erythrocytes are generated from hemogenic endothelial cells. *Sci Rep*. 2017;7:6401. doi:10.1038/s41598-017-06627-9

3. Taylor E, Taoudi S, Medvinsky A. Hematopoietic stem cell activity in the aorta-gonad-mesonephros region enhances after mid-day 11 of mouse development. *Int J Dev Biol*. 2010;54:1055-1060. doi:10.1387/ijdb.103152et

4. Lee L, Ghorbanian Y, Wang W, et al. LYVE1 Marks the Divergence of Yolk Sac Definitive Hemogenic Endothelium from the Primitive Erythroid Lineage. *Cell Rep*. 2016;17(9):2286-2298. doi:10.1016/j.celrep.2016.10.080

5. Boisset J, Cappellen W Van, Andrieu-Soler C, Galjart N, Dzierzak E, Robin C. In vivo imaging of haematopoietic cells emerging from the mouse aortic endothelium. *Nature*. 2010;464:116-120. doi:10.1038/nature08764

6. Lancrin C, Sroczynska P, Ferreras C, Kouskoff V. Blood cell generation from the hemangioblast. *J Mol Med*. 2010;88:167-172. doi:10.1007/s00109-009-0554-0

7. Choi KD, Vodyanik MA, Togarrati PP, et al. Identification of the Hemogenic Endothelial Progenitor and Its Direct Precursor in Human Pluripotent Stem Cell Differentiation Cultures. *Cell Rep*. 2012;2:553-567. doi:10.1016/j.celrep.2012.08.002

8. Hirschi KK. Hemogenic endothelium during development and beyond. *Blood*. 2012;119(21):4823-4828. doi:10.1182/blood-2011-12-353466.

9. Huber TL, Kouskoff V, Fehling HJ, Palis J. Haemangioblast commitment is initiated in the primitive streak of the mouse embryo. 2004;432(December):625-630. doi:10.1038/nature03131.1.

10. Dzierzak E, Speck NA. Of lineage and legacy - the development of mammalian hematopoietic stem cells. *Nat Immunol*. 2008;9:129-136. doi:10.1038/ni1560.Of

11. Hou S, Li Z, Zheng X, et al. Embryonic endothelial evolution towards first hematopoietic stem cells revealed by single-cell transcriptomic and functional analyses. *Cell Res*. 2020;(December 2019). doi:10.1038/s41422-020-0300-2

12. Mikkola HKA, Orkin SH. The journey of developing hematopoietic stem cells. *Development*. 2006;133:3733-3744. doi:10.1242/dev.02568

13. Yoder MC. Inducing definitive hematopoiesis in a dish. *Nat Biotechnol*. 2014;32(6):539-541. doi:10.1038/nbt.2929

14. Gritz E, Hirschi KK. Specification and function of hemogenic endothelium during embryogenesis. *Cell Mol Life Sci*. 2016;73(8):1547-1567. doi:10.1007/s00018-016-

2134-0

15. Ganuza M, Hall T, Finkelstein D, Chabot A, Kang G, McKinney-Freeman S. Lifelong haematopoiesis is established by hundreds of precursors throughout mammalian ontogeny. *Nat Cell Biol*. 2017;19(10):1153-1163. doi:10.1038/ncb3607

16. Ganuza M, Hall T, Obeng EA, McKinney-Freeman S. Clones assemble! The clonal complexity of blood during ontogeny and disease. *Exp Hematol*. 2020;83:35-47. doi:10.1016/j.exphem.2020.01.009

17. Ottersbach K. Endothelial-to-haematopoietic transition: An update on the process of making blood. *Biochem Soc Trans*. 2019;47(2):591-601. doi:10.1042/BST20180320

18. Rafii S, Kloss CC, Butler JM, et al. Human ESC-derived hemogenic endothelial cells undergo distinct waves of endothelial to hematopoietic transition. *Blood*. 2013;121:770-780. doi:10.1182/blood-2012-07-444208.There

19. Lancrin C, Sroczynska P, Stephenson C, Allen T, Kouskoff V, Lacaud G. The haemangioblast generates haematopoietic cells through a haemogenic endothelium stage. *Nature*. 2009;457(7231):892-895. doi:10.1038/nature07679

20. Eich C, Arlt J, Vink CS, et al. In vivo single cell analysis reveals Gata2 dynamics in cells transitioning to hematopoietic fate. *J Exp Med*. 2017;215(1):233-248. doi:10.1084/jem.20170807

21. Chen MJ, Yokomizo T, Zeigler BM, Dzierzak E, Speck NA. Runx1 is required for the endothelial to haematopoietic cell transition but not thereafter. *Nature*. 2009;457(7231):887-891. doi:10.1038/nature07619

22. Chen MJ, Rocha EL da, Cahan P, et al. Transcriptome Dynamics of Hematopoietic Stem Cell Formation Revealed Using a Combinatorial Runx1 and Ly6a Reporter System. *Stem Cell Reports*. 2020;14:1-16. doi:10.1016/j.stemcr.2018.04.001

23. Teichweyde N, Kasperidus L, Carotta S, et al. Hoxb4 promotes Hemogenic Endothelium Formation without Perturbing Endothelial Cell Development. *Stem Cell Reports*. 2018;10:875-889. doi:10.1016/j.stemcr.2018.01.009

24. Hills D, Gribi R, Ure J, et al. Hoxb4-YFP reporter mouse model: A novel tool for tracking HSC development and studying the role of Hoxb4 in hematopoiesis. *Blood*. 2011;117(13):3521-3528. doi:10.1182/blood-2009-12-253989

25. Crosse EI, Gordon-Keylock S, Rybtsov S, et al. Multi-layered Spatial Transcriptomics Identify Secretory Factors Promoting Human Hematopoietic Stem Cell Development. *Cell Stem Cell*. 2020;27:1-18. doi:10.1016/j.stem.2020.08.004

26. Kaschutnig P. HSCs - A journey from development to aging. Published online 2016.

27. Blaydes SM, Kogan SC, Truong B-TH, et al. Retroviral Integration at the Epi1 Locus Cooperates with Nf1 Gene Loss in the Progression to Acute Myeloid Leukemia. *J Virol*. 2001;75(19):9427-9434. doi:10.1128/jvi.75.19.9427-9434.2001

28. Largaespada DA, Shaughnessy JD, Jenkins NA, Copeland NG. Retroviral integration at the Evi-2 locus in BXH-2 myeloid leukemia cell lines disrupts Nf1 expression without changes in steady-state Ras-GTP levels. *J Virol*. 1995;69(8):5095-5102. papers3://publication/uuid/76FD7D0D-B91D-49D5-A998-25A6A098E399

29. Zeng Y, He J, Bai Z, et al. Tracing the first hematopoietic stem cell generation in human embryo by single-cell RNA sequencing. *Cell Res*. 2019;29:881-894. doi:10.1038/s41422-019-0228-6

30. Gentles AJ, Plevritis SK, Majeti R, Alizadeh AA. Association of a leukemic stem cell gene expression signature with clinical outcomes in acute myeloid leukemia. *JAMA - J Am Med Assoc*. 2010;304(24):2706-2715. doi:10.1001/jama.2010.1862

31. Rücker FG, Sander S, Döhner K, Döhner H, Pollack JR, Bullinger L. Molecular profiling reveals myeloid leukemia cell lines to be faithful model systems characterized by distinct genomic aberrations. *Leukemia*. 2006;20(6):994-1001. doi:10.1038/sj.leu.2404235

32. Pearson S, Sroczynska P, Lacaud G, Kouskoff V. The stepwise specification of embryonic stem cells to hematopoietic fate is driven by sequential exposure to Bmp4, activin A, bFGF and VEGF. *Development*. 2008;135:1525-1535. doi:10.1242/dev.011767

33. Vo LT, Daley GQ. De novo generation of HSCs from somatic and pluripotent stem cell sources. *Blood*. 2015;125:2641-2648. doi:10.1182/blood-2014-10-570234

34. Sugimura R, Jha DK, Han A, et al. Haematopoietic stem and progenitor cells from human pluripotent stem cells. *Nature*. 2017;545:432-438. doi:10.1038/nature22370

35. Lis R, Karrasch CC, Poulos MG, et al. Conversion of adult endothelium to immunocompetent haematopoietic stem cells. *Nature*. Published online 2017. doi:10.1038/nature22326

36. Ho D, Quake SR, McCabe ERB, et al. Enabling Technologies for Personalized and Precision Medicine. *Trends Biotechnol*. 2020;38:497-518. doi:10.1016/j.tibtech.2019.12.021

37. Wattanapanitch M. Recent updates on induced pluripotent stem cells in hematological disorders. *Stem Cells Int*. 2019;2019:1-15. doi:10.1155/2019/5171032

38. Yamanaka S, Takahashi K, Okita K, Nakagawa M. Induction of pluripotent stem cells from fibroblast cultures. *Nat Protoc*. 2007;2(12):3081-3089. doi:10.1038/nprot.2007.418

39. Blaser BW, Zon LI. Making HSCs In Vitro: Don't Forget the Hemogenic Endothelium. *Blood*. 2018;132(13):1372-1379. doi:10.1182/blood-2018-04-784140

40. Daniel MG, Pereira C-F, Lemischka IR, Moore K a. Making a Hematopoietic Stem Cell. *Trends Cell Biol*. 2016;26(3):202-214. doi:10.1016/j.tcb.2015.10.002

41. Wang LD, Wagers AJ. Dynamic niches in the origination and differentiation of haematopoietic stem cells. *Nat Rev Mol Cell Biol*. 2011;12(10):643-655. doi:10.1038/nrm3184

42. Orkin SH, Zon LI. Hematopoiesis: An Evolving Paradigm for Stem Cell Biology. *Cell*. Published online 2008. doi:10.1016/j.cell.2008.01.025

43. Yamamoto R, Morita Y, Ooehara J, et al. Clonal Analysis Unveils Self-Renewing Lineage-Restricted Progenitors Generated Directly from Hematopoietic Stem Cells. *Cell*. 2013;154(5):1112-1126. doi:10.1016/j.cell.2013.08.007

44. Walter D, Lier A, Geiselhart A, Thalheimer F, Huntscha S, Sobotta M. Exit from Dormancy Provokes DNA-damaged-induced attrition in Haematopoietic Stem Cells. *Nature*. 2015;520:549-552. doi:10.1038/nature14131

45. Essers MAG, Offner S, Blanco-Bose WE, et al. IFNα activates dormant haematopoietic stem cells in vivo. *Nature*. 2009;458(7240):904-908. doi:10.1038/nature07815

46. Fuchs A, Monlish DA, Ghosh S, et al. Trauma Induces Emergency Hematopoiesis through IL-1/MyD88–Dependent Production of G-CSF. *J Immunol*. 2019;202:3020-3032. doi:10.4049/jimmunol.1801456

47. López-Otín C, Blasco MA, Partridge L, Serrano M, Kroemer G. The hallmarks of aging. *Cell*. 2013;153(6):1194. doi:10.1016/j.cell.2013.05.039

48. Hanahan D, Weinberg RA. Hallmarks of cancer: The next generation. *Cell*. 2011;144(5):646-674. doi:10.1016/j.cell.2011.02.013

49. Haas S, Trumpp A, Milsom MD. Causes and Consequences of Hematopoietic Stem Cell Heterogeneity. *Cell Stem Cell*. 2018;22(5):627-638. doi:10.1016/j.stem.2018.04.003

50. Velten L, Haas SF, Raffel S, et al. Human haematopoietic stem cell lineage commitment is a continuous process. *Nat Cell Biol*. 2017;19:271-281. doi:10.1038/ncb3493

51. Camargo FD, Chambers SM, Drew E, McNagny KM, Goodell MA. Hematopoietic stem cells do not engraft with absolute efficiencies. *Blood*. 2006;107:501-507. doi:10.1182/blood-2005-02-0655

52. Rodriguez-Fraticelli AE, Wolock SL, Weinreb CS, et al. Clonal analysis of lineage fate in native haematopoiesis. *Nature*. 2018;553:212-216. doi:10.1038/nature25168

53. Subramaniam A, Talkhoncheh SM, Magnusson M, Larsson J. Endothelial protein C receptor (EPCR) expression marks human fetal liver hematopoietic stem cells. *Haematologica*. 2019;104:898-901.

54. Laurenti E, Göttgens B. From haematopoietic stem cells to complex differentiation landscapes. *Nature*. 2018;553:418-426. doi:10.1038/nature25022

55. Mooney CJ, Cunningham A, Tsapogas P, Toellner KM, Brown G. Selective expression of Flt3 within the mouse hematopoietic stem cell compartment. *Int J Mol Sci*. 2017;18:1-19. doi:10.3390/ijms18051037

56. Adolfsson J, Månsson R, Buza-Vidas N, et al. Identification of Flt3+ lympho-myeloid stem cells lacking erythro-megakaryocytic potential: A revised road map for adult blood lineage commitment. *Cell*. 2005;121(2):295-306. doi:10.1016/j.cell.2005.02.013

57. Sanjuan-Pla A, Macaulay IC, Jensen CT, et al. Platelet-biased stem cells reside at the apex of the haematopoietic stem-cell hierarchy. *Nature*. 2013;502(7470):232-236. doi:10.1038/nature12495

58. Cho IJ, Lui PP, Obajdin J, et al. Mechanisms, Hallmarks, and Implications of Stem Cell Quiescence. *Stem Cell Reports*. 2019;12:1190-1200. doi:10.1016/j.stemcr.2019.05.012

59. Tümpel S, Rudolph KL. Quiescence : Good and Bad of Stem Cell Aging. *Trends Cell Biol*. Published online 2019:1-14. doi:10.1016/j.tcb.2019.05.002

60. Challen GA, Goodell MA. Promiscuous expression of H2B-GFP transgene in hematopoietic stem cells. *PLoS One*. 2008;3:1-9. doi:10.1371/journal.pone.0002357

61. Wilson A, Laurenti E, Oser G, et al. Hematopoietic Stem Cells Reversibly Switch from Dormancy to Self-Renewal during Homeostasis and Repair. *Cell*. 2008;135(6):1118-1129. doi:10.1016/j.cell.2008.10.048

62. Bogeska R, Kaschutnig P, Fawaz M, et al. Hematopoietic stem cells fail to regenerate following inflammatory challenge. *bioRxiv*. Published online 2020:1-50.

63. Saçma M, Pospiech J, Bogeska R, et al. Haematopoietic stem cells in perisinusoidal niches are protected from ageing. *Nat Cell Biol*. 2019;21:1309-1320. doi:10.1038/s41556-019-0418-y

64. Trumpp A, Essers M, Wilson A. Awakening dormant haematopoietic stem cells. *Nat Rev Immunol*. 2010;10:201-209. doi:10.1038/nri2726

65. Boulais P, Frenette P. Making sense of hematopoietic stem cell niches. *Blood*. 2015;125(17):2621-2630. doi:10.1182/blood-2014-09-570192.

66. Boyer SW, Rajendiran S, Beaudin AE, et al. Clonal and Quantitative In Vivo Assessment of Hematopoietic Stem Cell Differentiation Reveals Strong Erythroid Potential of Multipotent Cells. *Stem Cell Reports*. 2019;12:801-815. doi:10.1016/j.stemcr.2019.02.007

67. Kovtonyuk L V, Fritsch K, Feng X, Manz MG, Takizawa H. Inflamm-Aging of Hematopoiesis, Hematopoietic Stem Cells and the Bone Marrow Microenvironment. *Front Immunol*. 2016;7(November):1-13. doi:10.3389/fimmu.2016.00502

68. Moehrle BM, Geiger H. Aging of hematopoietic stem cells: DNA damage and mutations? *Exp Hematol*. 2016;44(10):895-901. doi:10.1016/j.exphem.2016.06.253

69. Siegel RL, Miller KD, Jemal A. Cancer statistics, 2019. *CA Cancer J Clin*. 2019;69:7-34. doi:10.3322/caac.21551

70. Takizawa H, Fritsch K, Kovtonyuk L V., et al. Pathogen-Induced TLR4-TRIF Innate Immune Signaling in Hematopoietic Stem Cells Promotes Proliferation but Reduces Competitive Fitness. *Cell Stem Cell*. 2017;21:225-240.e5. doi:10.1016/j.stem.2017.06.013

71. Haas S, Hansson J, Klimmeck D, et al. Inflammation-Induced Emergency Megakaryopoiesis Driven by Hematopoietic Stem Cell-like Megakaryocyte Progenitors. *Cell Stem Cell*. 2015;17(4):422-434. doi:10.1016/j.stem.2015.07.007

72. Petit-Cocault L, Volle-Challier C, Fleury M, Peault B, Souyri M. Dual role of Mpl receptor during the establishment of definitive hematopoiesis. *Development*. 2007;134(16):3031-3040. doi:10.1242/dev.001818

73. De Graaf CA, Metcalf D. Thrombopoietin and hematopoietic stem cells. *Cell Cycle*. 2011;10:1582-1589. doi:10.4161/cc.10.10.15619

74. Decker M, Leslie J, Liu Q, Ding L. Hepatic thrombopoietin is required for bone marrow hematopoietic stem cell maintenance. *Science (80-)*. 2018;360(6384):106-110. doi:10.1126/science.aap8861

75. Murone M, Carpenter D, de Sauvage F. Hematopoietic Deficiencies in c-mpl and TPO Knockout Mice. *Stem Cells*. 1998;16:1-6.

76. Qian H, Buza-Vidas N, Hyland CD, et al. Critical Role of Thrombopoietin in Maintaining Adult Quiescent Hematopoietic Stem Cells. *Cell Stem Cell*. 2007;1(6):671-684. doi:10.1016/j.stem.2007.10.008

77. Yoshihara H, Arai F, Hosokawa K, et al. Thrombopoietin/MPL Signaling Regulates Hematopoietic Stem Cell Quiescence and Interaction with the Osteoblastic Niche. *Cell Stem Cell*. 2007;1(6):685-697. doi:10.1016/j.stem.2007.10.020

78. Umemoto T, Yamato M, Ishihara J, et al. Integrin-αvβ3 regulates thrombopoietin-mediated maintenance of hematopoietic stem cells. *Blood*. 2012;119(1):83-94. doi:10.1182/blood-2011-02-335430

79. Fox N, Priestley G, Papyannopoulou T, Kaushansky K. Thrombopoietin expands hematopoietic stem cells after transplantation. *J Clin …*. 2002;110(3):389-394. doi:10.1172/JCI200215430.Introduction

80. Kovtonyuk L V, Manz MG, Takizawa H. Enhanced thrombopoietin but not G-CSF receptor stimulation induces self-renewing hematopoietic stem cell divisions in vivo. *Blood*. 2016;127(25):blood-2015-09-669929. doi:10.1182/blood-2015-09-669929

81. De Laval B, Pawlikowska P, Petit-Cocault L, et al. Thrombopoietin-increased DNA-PK-dependent DNA repair limits hematopoietic stem and progenitor cell mutagenesis in response to DNA damage. *Cell Stem Cell*. Published online 2013. doi:10.1016/j.stem.2012.10.012

82. Laval D, Pawlikowska P, Barbieri D, et al. Thrombopoietin promotes NHEJ DNA repair in hematopoietic stem cells through speci fi c activation of Erk and NF- k B pathways and their. *Blood*. 2014;123(4):509-519. doi:10.1182/blood-2013-07-515874.B.d.L.

83. Moehrle BM, Nattamai K, Brown A, et al. Stem Cell-Specific Mechanisms Ensure Genomic Fidelity within HSCs and upon Aging of HSCs. *CellReports*. 2015;13:2412-2424. doi:10.1016/j.celrep.2015.11.030

84. Schepers H, Wierenga ATJ, Vellenga E, Schuringa JJ, Transducer S. STAT5-mediated self-renewal of normal hematopoietic and leukemic stem cells. *JAK-STAT*. 2012;1(1):13-22.

85. Wei Z, Liu HT. MAPK signal pathways in the regulation of cell proliferation in mammalian cells. *Cell Res*. 2002;12(1):9-18. doi:10.1038/sj.cr.7290105

86. Bhat FA, Advani J, Khan AA, et al. A network map of thrombopoietin signaling. *J Cell Commun Signal*. 2018;12:737-743. doi:10.1007/s12079-018-0480-4

87. Kohlscheen S, Wintterle S, Schwarzer A, et al. Inhibition of thrombopoietin/Mpl signaling in adult hematopoiesis identifies new candidates for hematopoietic stem cell maintenance. *PLoS One*. 2015;10(7):1-23. doi:10.1371/journal.pone.0131866

88. Skoda RC, Duek A, Grisouard J. Pathogenesis of myeloproliferative neoplasms. *Exp Hematol*. 2015;43:599-608. doi:10.1016/j.exphem.2015.06.007

89. Varghese LN, Defour JP, Pecquet C, Constantinescu SN. The thrombopoietin receptor: Structural basis of traffic and activation by ligand, mutations, agonists, and mutated

calreticulin. *Front Endocrinol (Lausanne)*. 2017;8(MAR):1-13. doi:10.3389/fendo.2017.00059

90. Grinfeld J, Nangalia J, Green AR. Molecular determinants of pathogenesis and clinical phenotype in myeloproliferative neoplasms. *Haematologica*. 2017;102:7-17. doi:10.3324/haematol.2014.113845

91. Kuter DJ. The biology of thrombopoietin and thrombopoietin receptor agonists. *Prog Hematol*. 2013;98:10-23. doi:10.1007/s12185-013-1382-0

92. Siegal D, Crowther M, Cuker A. Thrombopoietin Receptor Agonists in Primary ITP. *Semin Hematol*. 2013;50(1):18-21. doi:10.1038/jid.2014.371

93. Kuter DJ. Thrombopoietin and Thrombopoietin Mimetics in the Treatment of Thrombocytopenia. *Annu Rev Med*. 2009;60(1):193-206. doi:10.1146/annurev.med.60.042307.181154

94. Hitchcock IS, Kaushansky K. Thrombopoietin from beginning to end. *Br J Haematol*. 2014;165(2):259-268. doi:10.1111/bjh.12772

95. Ghanima W, Cooper N, Rodeghiero F, Godeau B, Bussel JB. Thrombopoietin receptor agonists: Ten years later. *Haematologica*. 2019;104(6):1112-1123. doi:10.3324/haematol.2018.212845

96. MacArthur Clark J. The 3Rs in research: A contemporary approach to replacement, reduction and refinement. *Br J Nutr*. 2018;120:1-7. doi:10.1017/S0007114517002227

97. Wu Q, Liu J, Wang X, et al. Organ-on-a-chip: Recent breakthroughs and future prospects. *Biomed Eng Online*. 2020;19:1-19. doi:10.1186/s12938-020-0752-0

98. Giralt S, Bishop MR. Principles and overview of allogeneic hematopoietic stem cell transplantation. *Physiol Behav*. 2009;144:1-20. doi:10.1007/978-0-387-78580-6

99. Wilkinson AC, Ishida R, Kikuchi M, et al. Long-term ex vivo haematopoietic-stem-cell expansion allows nonconditioned transplantation. *Nature*. 2019;571:117-121. doi:10.1038/s41586-019-1244-x

100. Kobayashi H, Morikawa T, Okinaga A, et al. Environmental Optimization Enables Maintenance of Quiescent Hematopoietic Stem Cells Ex Vivo. *Cell Rep*. 2019;28(1):145-158.e9. doi:10.1016/j.celrep.2019.06.008

101. Kieusseian A, de la Grange PB, Burlen-Defranoux O, Godin I, Cumano A. Immature hematopoietic stem cells undergo maturation in the fetal liver. *Development*. 2012;139(19):3521-3530. doi:10.1242/dev.079210

102. Eaves CJ. Hematopoietic stem cells: Concepts, definitions, and the new reality. *Blood*. 2015;125(17):2605-2613. doi:10.1182/blood-2014-12-570200

103. Faltusová K, Szikszai K, Molík M, et al. Stem Cell Defect in Ubiquitin-Green Fluorescent Protein Mice Facilitates Engraftment of Lymphoid-Primed Hematopoietic Stem Cells. *Stem Cells*. 2018;36(8):1237-1248. doi:10.1002/stem.2828

104. Walden H, Deans AJ. The Fanconi Anemia DNA Repair Pathway: Structural and Functional Insights into a Complex Disorder. *Annu Rev Biophys*. 2014;43:257-278. doi:10.1146/annurev-biophys-051013-022737

105. Kaschutnig P, Bogeska R, Walter D, Lier A, Huntscha S, Milsom MD. The Fanconi anemia pathway is required for efficient repair of stress-induced DNA damage in haematopoietic stem cells. *Cell Cycle*. 2015;14(17):2734-2742. doi:10.1080/15384101.2015.1068474

106. Shinkai Y, Rathbun G, Oltz EM, et al. RAG-2-Deficient Mice Lack Mature Lymphocytes Owing to Inability to Initiate V(D)J Rearrangement. *Cell*. 1992;68:855-867.

107. Niwa H, Toyooka Y, Shimosato D, et al. Interaction between Oct3/4 and Cdx2 determines trophectoderm differentiation. *Cell*. 2005;123(5):917-929. doi:10.1016/j.cell.2005.08.040

108. Marcelo KL, Sills TM, Coskun S, et al. Hemogenic endothelial cell specification requires c-Kit, notch signaling, and p27-mediated cell-cycle control. *Dev Cell*. 2013;27(5):504-515. doi:10.1016/j.devcel.2013.11.004

109. Alimperti S, Andreadis ST. CDH2 and CDH11 act as regulators of stem cell fate decisions. *Stem Cell Res*. 2015;14(3):270-282. doi:10.1016/j.scr.2015.02.002

110. Saiz N, Plusa B. Early cell fate decisions in the mouse embryo. *Reproduction*. 2013;145:65-80. doi:10.1530/REP-12-0381

111. Kim PG, Albacker CE, Lu YF, et al. Signaling axis involving Hedgehog, Notch, and Scl promotes the embryonic endothelial-to-hematopoietic transition. *Proc Natl Acad Sci U S A*. 2013;110(2). doi:10.1073/pnas.1214361110

112. Engert S, Burtscher I, Liao WP, Dulev S, Schotta G, Lickert H. Wnt/β-catenin signalling regulates Sox17 expression and is essential for organizer and endoderm formation in the mouse. *Dev*. 2013;140(15):3128-3138. doi:10.1242/dev.088765

113. Lindsley RC, Gill JG, Kyba M, Murphy TL, Murphy KM. Canonical Wnt signaling is required for development of embryonic stem cell-derived mesoderm. *Development*. 2006;133(19):3787-3796. doi:10.1242/dev.02551

114. Dongre A, Weinberg RA. New insights into the mechanisms of epithelial–mesenchymal transition and implications for cancer. *Nat Rev Mol Cell Biol*. 2019;20(February):69-84. doi:10.1038/s41580-018-0080-4

115. Arora P, Ricks TK, Trejo JA. Protease-activated receptor signalling, endocytic sorting and dysregulation in cancer. *J Cell Sci*. 2007;120(6):921-928. doi:10.1242/jcs.03409

116. Pettitt SJ, Liang Q, Rairdan XY, et al. Agouti C57BL/6N embryonic stem cells for mouse genetic resources. *Nat Methods*. 2009;6(7):493-495. doi:10.1038/nmeth.1342

117. Connell KEO, Mikkola AM, Stepanek AM, et al. Practical Murine Hematopathology : A Comparative Review and Implications for Research. *Comp Med*. 2015;65(2):96-113.

118. Wirth-Dzieciolowska E, Karaszewska J, Kazimiera P, Smolińska M, Gajewska M. Selected peripheral blood cell parameters in twelve inbred strains of laboratory mice. *Anim Sci Pap Reports*. 2009;27(1):69-77.

119. Gekas C, Graf T. CD41 expression marks myeloid-biased adult hematopoietic stem cells and increases with age. *Blood*. 2013;121(22):4463-4472. doi:10.1182/blood-2012-09-457929

120. Taoudi S, Medvinsky A. Functional identification of the hematopoietic stem cell niche in the ventral domain of the embryonic dorsal aorta. *PNAS*. 2007;104(22):9399-9403. doi:10.1073/pnas.0700984104

121. Koch U, Lehal R, Radtke F. Stem cells living with a Notch. *Dev*. 2013;140(4):689-704. doi:10.1242/dev.080614

122. Kovtonyuk L V, Manz MG, Takizawa H. Enhanced thrombopoietin but not G-CSF receptor stimulation induces self-renewing hematopoietic stem cell divisions in vivo. *Blood*. 2016;127(25):blood-2015-09-669929. doi:10.1182/blood-2015-09-669929

123. Pluthero FG, Kahr WHA. The birth and death of platelets in health and disease. *Physiology*. 2018;33(3):225-234. doi:10.1152/physiol.00005.2018

124. Mazzi S, Lordier L, Debili N, Raslova H, Vainchenker W. Megakaryocyte and polyploidization. *Exp Hematol*. 2018;57:1-13. doi:10.1016/j.exphem.2017.10.001

125. Szade K, Bukowska-Strakova K, Zukowska M, Jozkowicz A, Dulak J. Analysis of cell cycle status of murine hematopoietic stem cells. *Methods Mol Biol*. Published online 2016:91-99. doi:10.1007/7651_2016_361

126. Janssens A, Rodeghiero F, Anderson D, et al. Changes in bone marrow morphology in adults receiving romiplostim for the treatment of thrombocytopenia associated with primary immune thrombocytopenia. *Ann Hematol*. 2016;95(7):1077-1087. doi:10.1007/s00277-016-2682-2

127. Kuter DJ, Mufti GJ, Bain BJ, Hasserjian RP, Davis W, Rutstein M. Evaluation of bone marrow reticulin formation in chronic immune thrombocytopenia patients treated with romiplostim. *Blood*. 2009;114(18):3748-3756. doi:10.1182/blood-2009-05-224766

128. Brenet F, Kermani P, Spektor R, Rafii S, Scandura JM. Tgfβ restores hematopoietic homeostasis after myelosuppressive chemotherapy. *J Exp Med*. 2013;210(3):623-639. doi:10.1084/jem.20121610

129. Guo G, Luc S, Marco E, et al. Mapping cellular hierarchy by single-cell analysis of the cell surface repertoire. *Cell Stem Cell*. 2013;13:492-505. doi:10.1016/j.stem.2013.07.017

130. Beerman I, Bhattacharya D, Zandi S, et al. Functionally distinct hematopoietic stem cells modulate hematopoietic lineage potential during aging by a mechanism of clonal expansion. *Proc Natl Acad Sci U S A*. 2010;107(12):5465-5470. doi:10.1073/pnas.1000834107

131. Pang WW, Price EA, Sahoo D, et al. Human bone marrow hematopoietic stem cells are increased in frequency and myeloid-biased with age. *Proc Natl Acad Sci U S A*. 2011;108(50):20012-20017. doi:10.1073/pnas.1116110108

132. Cho RH, Sieburg HB, Muller-Sieburg CE. A new mechanism for the aging of hematopoietic stem cells: Aging changes the clonal composition of the stem cell compartment but not individual stem cells. *Blood*. 2008;111(12):5553-5561. doi:10.1182/blood-2007-11-123547

133. Schmitt TM, Zúñiga-Pflücker JC. Induction of T cell development from hematopoietic

progenitor cells by delta-like-1 in vitro. *Immunity*. 2002;17(6):749-756. doi:10.1016/S1074-7613(02)00474-0

134. Nakamura-Ishizu A, Matsumura T, Stumpf PS, et al. Thrombopoietin Metabolically Primes Hematopoietic Stem Cells to Megakaryocyte-Lineage Differentiation. *Cell Rep*. 2018;25(7):1772-1785.e6. doi:10.1016/j.celrep.2018.10.059

135. Lacaud G, Kouskoff V. Hemangioblast, hemogenic endothelium, and primitive versus definitive hematopoiesis. *Exp Hematol*. 2017;49:19-24. doi:10.1016/j.exphem.2016.12.009

136. Amaya E. The hemangioblast: A state of competence. *Blood*. 2013;122:3853-3854. doi:10.1182/blood-2013-10-533075

137. Garcia-Alegria E, Menegatti S, Fadlullah MZH, Menendez P, Lacaud G, Kouskoff V. Early Human Hemogenic Endothelium Generates Primitive and Definitive Hematopoiesis in vitro. *Stem Cell Reports*. 2018;11:1-14. doi:10.1016/j.stemcr.2018.09.013

138. Dzierzak E, Bigas A. Blood Development: Hematopoietic Stem Cell Dependence and Independence. *Cell Stem Cell*. 2018;22:639-651. doi:10.1016/j.stem.2018.04.015

139. McGrath KE, Frame JM, Fegan KH, et al. Distinct Sources of Hematopoietic Progenitors Emerge before HSCs and Provide Functional Blood Cells in the Mammalian Embryo. *Cell Rep*. 2015;11(12):1892-1904. doi:10.1016/j.celrep.2015.05.036

140. Baron CS, Kester L, Klaus A, et al. Single-cell Transcriptomics Reveal the Dynamic of Haematopoietic Stem Cell Production in the Aorta. *Nat Commun*. 2018;9:1-15. doi:10.1038/s41467-018-04893-3

141. Lerou PH, Daley GQ. Therapeutic potential of embryonic stem cells. *Blood Rev*. 2005;19:321-331. doi:10.1016/j.blre.2005.01.005

142. Elahi S, Holling GA, Stablewski AB, Olejniczak SH. Improved hematopoietic differentiation of mouse embryonic stem cells through manipulation of the RNA binding protein ARS2. *Stem Cell Res*. 2020;43:1-6. doi:10.1016/j.scr.2020.101710

143. Kyba M, Perlingeiro RCR, Daley GQ. HoxB4 Confers Definitive Lymphoid-Myeloid Engraftment Potential on Embryonic Stem Cell and Yolk Sac Hematopoietic Progenitors. *Cell*. 2002;109:29-37.

144. Goyama S, Yamamoto G, Shimabe M, et al. Evi-1 Is a Critical Regulator for Hematopoietic Stem Cells and Transformed Leukemic Cells. *Cell Stem Cell*. 2008;3:207-220. doi:10.1016/j.stem.2008.06.002

145. Bellissimo DC, Speck NA. RUNX1 mutations in inherited and sporadic leukemia. *Front Cell Dev Biol*. 2017;5:1-11. doi:10.3389/fcell.2017.00111

146. Watanabe-Smith K, Tognon C, Tyner JW, Meijerink JPP, Druker BJ, Agarwal A. Discovery of functional characteriyation of a germline, CSF2RB-activating mutation in leukemia. *Leukemia*. 2016;30:1950-1953. doi:10.1038/leu.2016.95.Discovery

147. Magnusson M, Brun ACM, Miyake N, et al. HOXA10 is a critical regulator for hematopoietic stem cells and erythroid/megakaryocyte development. *Blood*. 2007;109:3687-3696. doi:10.1182/blood-2006-10-054676

148. Yzaguirre AD, Howell ED, Li Y, Liu Z, Speck NA. Runx1 is sufficient for blood cell formation from non-hemogenic endothelial cells in vivo only during early embryogenesis. *Development*. 2018;145. doi:10.1242/dev.158162

149. de Pater E, Kaimakis P, Vink CS, et al. Gata2 is required for HSC generation and survival. *J Exp Med*. 2013;210:2843-2850. doi:10.1084/jem.20130751

150. Idoko-Akoh A, Taylor L, Sang HM, McGrew MJ. High fidelity CRISPR/Cas9 increases precise monoallelic and biallelic editing events in primordial germ cells. *Sci Rep*. 2018;8:1-14. doi:10.1038/s41598-018-33244-x

151. Flach J, Bakker ST, Mohrin M, et al. Replication stress is a potent driver of functional decline in ageing haematopoietic stem cells. *Nature*. 2014;512:198-202. doi:10.1038/nature13619

152. Morrison SJ, Wright DE, Weissman IL. Cyclophosphamide/granulocyte colony-stimulating factor induces hematopoietic stem cells to proliferate prior to mobilization. *PNAS*. 1997;94:1908-1913. doi:10.1073/pnas.94.5.1908

153. Mohrin M, Bourke E, Alexander D, et al. Hematopoietic stem cell quiescence promotes error-prone DNA repair and mutagenesis. *Cell Stem Cell*. 2010;7:174-185. doi:10.1016/j.stem.2010.06.014

154. Beerman I, Seita J, Inlay MA, Weissman IL, Rossi DJ. Quiescent hematopoietic stem cells accumulate DNA damage during aging that is repaired upon entry into cell cycle. *Cell Stem Cell*. 2014;15:37-50. doi:10.1016/j.stem.2014.04.016

155. Kaushansky K. Thrombopoietin and its Receptor in Normal and Neoplastic Hematopoiesis. *Thromb J*. 2016;14:23-26. doi:10.1186/s12959-016-0095-z

156. Kota J, Caceres N, Constantinescu SN. Aberrant signal transduction pathways in myeloproliferative neoplasms. *Leukemia*. 2008;22:1828-1840. doi:10.1038/leu.2008.236

157. Rabe JL, Hernandez G, Chavez JS, Mills TS, Nerlov C, Pietras EM. CD34 and EPCR coordinately enrich functional murine hematopoietic stem cells under normal and inflammatory conditions. *Exp Hematol*. 2020;81:1-15. doi:10.1016/j.exphem.2019.12.003

158. Bernitz JM, Kim HS, MacArthur B, Sieburg H, Moore K. Hematopoietic Stem Cells Count and Remember Self-Renewal Divisions. *Cell*. 2016;167(5):1296-1309.e10. doi:10.1016/j.cell.2016.10.022

159. Yoshida H, Yamada H, Nogami W, et al. Development of a new knock-in mouse model and evaluation of pharmacological activities of lusutrombopag, a novel, nonpeptidyl small-molecule agonist of the human thrombopoietin receptor c-Mpl. *Exp Hematol*. 2018;59:30-39.e2. doi:10.1016/j.exphem.2017.12.005

160. Newland A. Thrombopoietin Receptor Agonists in the Treatment of Thrombocytopenia. *Curr Opin Hematol*. 2009;16:357-364. doi:10.1097/MOH.0b013e32832e06e4

161. Shen H, Yu H, Liang PH, et al. An acute negative bystander effect of γ-irradiated recipients on transplanted hematopoietic stem cells. *Blood*. 2012;119(15):3629-3637.

doi:10.1182/blood-2011-08-373621

162. Sun L, Zhang X, Zhang Y, et al. Antibiotic-induced disruption of gut microbiota alters local metabolomes and immune responses. *Front Cell Infect Microbiol*. 2019;9:1-13. doi:10.3389/fcimb.2019.00099

163. Rommel MGE, Hoerster K, Milde C, et al. Signaling properties of murine MPL and MPLmutants after stimulation with thrombopoietin and romiplostim. *Exp Hematol*. Published online 2020. doi:10.1016/j.exphem.2020.04.006

164. Miller I, Min M, Yang C, et al. Ki67 is a Graded Rather than a Binary Marker of Proliferation versus Quiescence. *Cell Rep*. 2018;24(5):1105-1112.e5. doi:10.1016/j.celrep.2018.06.110

165. Romar GA, Kupper TS, Divito SJ. Research Techniques Made Simple : Techniques to Assess Cell Proliferation. Published online 2016:1-7. doi:10.1016/j.jid.2015.11.020

166. Sakaue-Sawano A, Kurokawa H, Morimura T, et al. Visualizing Spatiotemporal Dynamics of Multicellular Cell-Cycle Progression. *Cell*. 2008;132:487-498. doi:10.1016/j.cell.2007.12.033

167. Lathe R. The individuality of mice. *Genes, Brain Behav*. 2004;3:317-327. doi:10.1111/j.1601-183X.2004.00083.x

168. Baccin C, Al-Sabah J, Velten L, et al. Combined single-cell and spatial transcriptomics reveals the molecular, cellular and spatial bone marrow niche organization. *Biorxiv*. Published online 2019:718395. doi:10.1038/s41556-019-0439-6

169. Mendt M, Cardier JE. Role of SDF-1 (CXCL12) in regulating hematopoietic stem and progenitor cells traffic into the liver during extramedullary hematopoiesis induced by G-CSF, AMD3100 and PHZ. *Cytokine*. 2015;76(2):214-221. doi:10.1016/j.cyto.2015.05.004

170. Marshall JS, Warrington R, Watson W, Kim HL. An introduction to immunology and immunopathology. *Allergy, Asthma Clin Immunol*. 2018;14:5-14. doi:10.1186/s13223-018-0278-1

171. Fischer KD, Agrawal DK. Hematopoietic stem and progenitor cells in inflammation and allergy. *Front Immunol*. 2013;4(DEC):1-9. doi:10.3389/fimmu.2013.00428

172. de Laval B, Maurizio J, Kandalla PK, et al. C/EBPβ-Dependent Epigenetic Memory Induces Trained Immunity in Hematopoietic Stem Cells. *Cell Stem Cell*. Published online 2020:1-18. doi:10.1016/j.stem.2020.01.017

173. Mann M, Mehta A, de Boer CG, et al. Heterogeneous Responses of Hematopoietic Stem Cells to Inflammatory Stimuli Are Altered with Age. *Cell Rep*. 2018;25(11):2992-3005.e5. doi:10.1016/j.celrep.2018.11.056

174. Vlaski M, Lafarge X, Chevaleyre J, Duchez P, Boiron JM, Ivanovic Z. Low oxygen concentration as a general physiologic regulator of erythropoiesis beyond the EPO-related downstream tuning and a tool for the optimization of red blood cell production ex vivo. *Exp Hematol*. 2009;37:573-584. doi:10.1016/j.exphem.2009.01.007

175. Golan K, Kumari A, Kollet O, et al. Daily Onset of Light and Darkness Differentially

Controls Hematopoietic Stem Cell Differentiation and Maintenance. *Cell Stem Cell*. 2018;23(4):572-585.e7. doi:10.1016/j.stem.2018.08.002

176. Field AE, Robertson NA, Wang T, Havas A, Ideker T, Adams PD. DNA Methylation Clocks in Aging: Categories, Causes, and Consequences. *Mol Cell*. 2018;71(6):882-895. doi:10.1016/j.molcel.2018.08.008

177. Bell CG, Lowe R, Adams PD, et al. DNA methylation aging clocks: Challenges and recommendations. *Genome Biol*. 2019;20(1):1-24. doi:10.1186/s13059-019-1824-y

178. Rozen S, Skaletsky H. Primer3 on the WWW for General Users and for Biologist Programmers In: *Methods Mol Biol*. 2000;132(1):365-386. http://dx.doi.org/10.1385/1-59259-192-2:365